KINETICS OF ADSORPTION AND REDOX PROCESSES ON IRON AND MANGANESE OXIDES: REACTIONS OF AS(III) AND SE(IV) AT GOETHITE AND BIRNESSITE SURFACES

Thesis by

Michael James Scott

In Partial Fulfillment of the Requirements

for the Degree of

Doctor of Philosophy

California Institute of Technology

Pasadena, California

1991

(Submitted September 26, 1990)

Dedicated to

the loves of my life

Wendy Sue

and

Caitlin Marie

ACKNOWLEDGMENTS

I wish to thank my advisor Professor James Morgan for his latitude in his guidance and support. Without it, this typical Scott project would have never matured into a typical Morgan thesis. I would also like to thank Professors Michael Hoffmann, Norman Brooks, Clair Patterson, and George Rossman for their scientific encouragement and for serving on my examination committees. Also, I would like to acknowledge Dr. Alan Stone of Johns Hopkins University for providing the computer code framework which made the kinetic modeling possible.

I would like to gratefully acknowledge the financial support of the initial portion of my research by the Andrew W. Mellon Foundation. Also, the research on which this report is based was financed in part by the United States Department of the Interior, Geological Survey, through the State Water Resources Research Institute, Project No. 14-08-0001-G1550, and by the University of California Water Resources Center, Project UCAL-WRC-W-22605-89(03). Contents of this publication do not necessarily reflect the views and policies of the U.S. Department of Interior, nor does mention of trade names or commercial products constitute their endorsement or recommendation for used by the U.S. Government.

I would like to thank the friendly and generous staff of Keck Laboratories--Elaine Granger, Joan Matthews, Sandy Brooks, and Fran Matzen--and the Environmental Engineering librarians--Rayma Harrison and Gunilla Hastrup--for always making time for me and, especially, for Caitlin. I would like to express my

appreciation for all their assistance and friendship in the classroom, laboratory, ball fields, and, in general, my life from 1985 to 1990 to Yigal Erel, Kevin Power, Nick Bauer, Julie Kern, David Wheeler, Bruce Daube, Jr., Jeff Collett, Bill Munger, Bob Arnold, Theresa Fall, Tom DiChristina, the Waterbugs, David James, Claudius Kormann, Kit Yin Ng, Liyuan Liang, Mark Schlautman, Sandy Elliot, Howell Yee, Natasha Kotronarou, Stan Grant, Jeremy Semrau, Annmarie Eldering, and Russell Mau.

Finally, I would like to acknowledge the encouragement and support given to me by family and friends, without which I could have never reached this point in my life. And most of all, I would like to simply say to Wendy, "Thanks for your love--it makes everything worthwhile."

ABSTRACT

Selenium and arsenic are naturally-occurring, non-metallic elements with complex chemical and biological behavior in aquatic environments. In this study, rates and mechanisms of adsorption, desorption, and electron transfer reactions involving selenium and arsenic oxyanions and two naturally occurring metal oxides, goethite (α-FeOOH) and birnessite (δ-MnO_2), have been investigated. Adsorption of Se(IV), As(III), and As(V) on goethite and of Se(IV) and As(III) on birnessite occurs within a time scale of minutes. Equilibrium is achieved within a few hours. Adsorption behavior can be described accurately with a surface complexation model.

Goethite does not oxidize Se(IV) or As(III) in solution at pH 4 and above. However, redox products (Mn(II), Se(VI), As(V)) are observed when Se(IV) or As(III) is added to aqueous suspensions of birnessite. In the arsenite-birnessite system, the rate of As(V) appearance in solution is equal to the rate of As(III) disappearance from solution while the appearance of Mn(II) in solution is slightly slower. In the selenite-birnessite system, uptake of Se(IV) occurs in minutes. Extent of adsorption decreases with increasing pH. The appearance of measurable Se(VI) occurs slowly (time scale of days to weeks) and is a function of adsorbed selenite. This indicates that the rate of selenite oxidation by birnessite is limited by the rate of electron transfer. Rate data from both arsenic and selenium redox systems are successfully described by a reversible four-step kinetic model that accounts for adsorption of the reduced species, electron-transfer, release of the oxidized species, and release of reduced Mn(II).

The data suggest that iron oxides provide an adsorptive sink for mobile Se and As oxyanions, while manganese oxides play a major role in accelerating the oxidation of Se(IV) and As(III). Results on the rates of key chemical processes affecting selenium and arsenic should be useful in understanding complex geochemical cycles and in finding solutions to problems in pollutant transport and accumulation in water-sediment systems.

TABLE OF CONTENTS

LIST OF TABLES

LIST OF FIGURES

Chapter 1

INTRODUCTION AND MOTIVATION

1.1 Introduction

Arsenic and selenium are naturally occurring non-metallic elements with complex biological and chemical properties. Selenium is an essential trace nutrient for most organisms and both elements are generally considered toxic at elevated levels. A common feature is that both elements exist in multiple oxidation states in aquatic systems. Aqueous arsenic species exist in the oxidation states As(III) and As(V), while aqueous selenium species are found in the oxidation states Se(IV) and Se(VI). Adsorption onto metal oxides and oxidation of reduced forms are two major reactions that control the fates of arsenic and selenium.

The focus of this dissertation is to demonstrate experimentally that redox-active metal oxide surfaces play an active role in determining the environmental behavior of arsenic and selenium. The rates and mechanisms of adsorption and oxidation-reduction were studied to determine the dependence on pH, temperature, dissolved and major particulate minerals, and oxidation-reduction status. The experimental results prove useful in defining time scales for the adsorption of both oxidation states of each element and the oxidation of reduced arsenic and selenium in aquatic environments. The time scales of conversion of harmful elements are of fundamental importance in the prediction of exposure levels for human populations through ground and surface waters and for ecosystem biota through sediments and overlying waters.

1.2 Arsenic and Selenium in the Environment

1.2.1 Geologic Sources of Arsenic and Selenium

The original source of arsenic and selenium in the environment is the molten magma beneath the earth's crust. The elements reach the surface primarily by vulcanism as metallic arsenides and selenides associated with igneous mineral deposits (Rosenfeld and Beath, 1964). Table 1.1 gives selected arsenic and selenium concentrations in various materials and aqueous systems.

Arsenic is ubiquitous in the environment as a result of weathering of igneous rocks and geothermal activity. Sedimentary rocks generally contain higher arsenic concentrations than igneous and metamorphic rocks. High arsenic concentrations (50-48,000 μg/l) in groundwater in the western United States have been associated with gold, pyrite, and uranium ore mining areas, geothermal areas and basin-fill deposits (Welch et al., 1988).

In most cases selenium is highly dispersed and in low concentrations in geologic deposits. The exceptions are rocks of igneous and volcanic origin and sedimentary rocks, where geological and biological forces have increased selenium concentration. Sediments of the Cretaceous period are particularly rich in selenium. High levels of selenium in shales, carbonaceous material in sandstones and phosphate rocks may be largely the result of bioconcentration (Bainbridge et al., 1988).

1.2.2 Accumulation in Aquatic Systems

Widespread accumulation of arsenic and selenium has occurred most recently due to the use of arsenical pesticides, mining and processing of sulfide and uranium

Table 1.1: As and Se concentrations in various materials and aqueous systems

Material	As (mg/kg)[1]	Se(mg/kg)[2]
Earth's crust	1.5-2.0	0.05
Granite	1.5	0.01-0.05
Limestone	1.7	0.03-0.10
Sandstone	2.0	< 0.05
Shales	14.5	0.6
Phosphate Rocks	22.6	1-300
Soils	<0.1-97	---
Seleniferous	---	1-80
Coal	13	0.1-4.3

Aqueous Systems	As (µg/l)[3]	Se (µg/l)[2]
Rivers	0.2-264	0.46-10.65
Mississippi	---	0.14
Amazon	---	0.21
Colorado	---	< 10 (pH 6.1-6.9) 10-400 (pH 7.8-8.2)
Lake Michigan	0.5-2.4	0.8-10
Seawater	0.15-6.0	0.09
Kesterson Area Groundwater[4]	2 (max 82)	11 (max 42,000)
EPA Water Quality Standards		
Drinking Water	50	10
Irrigation Water	100	20
Hazardous Waste	5000	1000

(1) NRC, 1977; (2) McNeal & Balistrieri, 1989; (3) Welch et al., 1989;
(4) Presser and Barnes, 1984; (1 µg/l As = 13.4 nM; 1 µg/l Se = 12.7 nM)

ores, burning of fossil fuels, and irrigation and drainage of newly developed arid and semi-acid agricultural lands. Contamination of Kesterson National Wildlife Reservoir (NWR) in the San Joaquin Valley, California is perhaps the best known example of a selenium accumulation problem in an ecosystem. Other areas identified as having irrigation-induced contamination problems (selenium and other inorganic salts) include the Salton Sea and Tulare Lake in California; Stillwater NWR, Nevada; Middle Green River, Utah; and Kendrick Water Reclamation Project, Wyoming (NRC, 1989). Well-known examples of arsenic contamination are the ecosystems of Puget Sound, Washington (Crecelius et al., 1975), the Menominee River, Wisconsin (Anderson et al., 1978), Whitewood Creek, South Dakota (Fuller and Davis, 1989), and the creeks around the Blackbird Mining District, Idaho (Mok and Wai, 1989).

The serious problems at Kesterson NWR resulted from a combination of natural geological factors and human influences. The soils of the western portion of the San Joaquin Valley, derived from Cretaceous marine sediments, have naturally high selenium content. Because this is an area with low rainfall, the soils do not release substantial amounts of selenium into the environment until they are irrigated. Irrigation releases soluble forms of selenium into the soil water which then enters surface waters and shallow groundwaters through cropland drainage systems, irrigation tailwaters, and deep percolation into groundwater.

1.2.3 Environmental Chemistry

The complex chemistries of arsenic and selenium in the environment are a result of their multiple oxidation states and active surface adsorption properties.

Arsenic and selenium are both stable as inorganic oxyanions (e.g., arsenite, arsenate, selenite, selenate) in oxidized states and as anthropogenic or microbially-produced organic compounds in reduced states. Arsenic as arsenate is similar to phosphate in its acid-base properties and affinity for mineral surfaces, but arsenic differs from phosphorus because of its multiple inorganic oxidation states. Selenium is analogous to sulfur in chemical properties, but there are notable differences. Even though selenic acid is a strong acid and selenate has the same adsorption characteristics as sulfate, selenate is a stronger oxidant than sulfate, though not necessarily a kinetically fast oxidant. Also, Se(IV) is much less volatile and can exist at greater redox potentials than S(IV). Selenide (Se(-II)) exists in reducing environments as a foul-smelling, poisonous gas, hydrogen selenide (H_2Se) and as metal selenides. Although it is a weak acid, aqueous H_2Se is a much stronger acid and is more poisonous than hydrogen sulfide (H_2S). Metal selenides tend to be found in metal sulfide ores (e.g., Fe, Cu, Pb), and tend to be very insoluble (Elrashidi et al., 1987). A qualitative guide in studies of the environmental behavior of arsenic and selenium is the application of analogous environmental chemistries of phosphorus and sulfur.

In most natural systems, arsenic and selenium are primarily found in oxidized forms as inorganic oxyanions. The oxyanions exhibit various degrees of affinity for metal oxide surfaces in heterogeneous systems. The limited studies of such systems suggest that selenite, arsenite, and arsenate are all strongly bonded to metal oxide surfaces whereas selenate is only weakly adsorbed. The extent of adsorption of all

of the oxyanions is greatly affected by solution variables (i.e., pH, temperature, competing anions).

1.3 Motivation of this Study

Thermodynamic calculations dictate that, at equilibrium, arsenate and selenate are the stable forms of arsenic and selenium in oxic systems, while in anoxic systems, arsenite and selenite are the stable forms. For example, in oxic seawater (pH 8.3, pE 12.5), the arsenate/arsenite concentration ratio should be approximately 10^{15}. However, several studies have reported arsenate/arsenite concentration ratios of only 15 to 250 in oxic seawater (Andreae, 1979; Peterson and Carpenter, 1983). Similar observations have been reported about the selenate/selenite concentration ratio. These results suggest that the reduction-oxidation process between oxidation states is not at equilibrium, and thus, is kinetically inhibited. Recent investigations have reported that most natural aquatic redox systems are far from equilibrium and that energetically-favored redox reactions are slow processes (Lindberg and Runnells, 1984). Lack of chemical equilibrium in most redox systems makes a kinetic description necessary. Information concerning the rate of As amd Se redox reactions in solution or on surfaces is lacking and specific rate constants are generally unknown. The rates of reactions need to be established in order to properly assess the importance of redox reactions on the distribution of arsenic and selenium in aquatic systems.

Although dissolved oxygen is a primary oxidant in natural systems, studies have shown that as a result of slow oxidation kinetics some reduced species of redox-

active elements are stable in oxic homogeneous solutions. However, the rate of reaction between dissolved oxygen and reduced species increases dramatically in heterogeneous systems (Wehrli, 1990; Eary and Schramke, 1990). A growing number of fundamental kinetic studies of redox systems exist that suggest oxide minerals play an important role, either as catalysts or as direct reactants. The systems that have been examined consist of reduced species of first-row transition metals (V, Cr, Mn, Fe, Co, and Cu) with hydrous oxides of iron, manganese, aluminum and titanium (Wehrli, 1987; Eary and Rai, 1987; Sung and Morgan, 1980, 1981; Crowther et al., 1983; Davies and Morgan, 1989).

1.4 Scope and Objectives

The geochemical behavior of arsenic and selenium in aquatic systems is poorly understood. The purpose of this research is to study the dynamics of arsenic and selenium interactions in water-sediment systems. There are several key questions that this dissertation attempts to address:

(i) What chemical reactions control the geochemical distribution of the two oxidation states of both arsenic and selenium in aquatic systems and how does the distribution vary as the chemical and physical conditions of the system vary?

(ii) In what types of environmental systems is the transport of arsenic and selenium favored?

(iii) What is the role of metal oxides in aquatic systems that contain arsenic and selenium?

(iv) Assuming that, as a result of their energetics and naturally occurring

concentrations, the probable oxidants of As(III) and Se(IV) in groundwater systems are dissolved oxygen, manganese oxides, and iron oxides (the latter for As(III) only), what are the rates of reaction among the oxidants and reduced species? Which oxidants are kinetically fast and provide the dominant pathway for oxidation of As(III) and Se(IV)?

(v) How is the rate of reaction affected by changes in pH, temperature, ionic strength, and concentration of reactants?

(vi) What are the essential steps in the mechanism of oxidation by metal oxides, and which of these steps is rate-determining?, and

(vii) If As(III) and Se(IV) can be oxidized by metal oxides, are the rates and mechanisms comparable for both elements, and how do the mechanisms for these nonmetallic elements compare with the heterogeneous oxidation rates and mechanisms of transitional metals such as iron, chromium, manganese, and vanadium?

The environmental chemistries of arsenic and selenium are reviewed in Chapter 2, with an emphasis on the thermodynamic properties and adsorption behavior of the elements in aqueous systems. Chapter 3 is concerned with the preparation of iron and manganese oxides and characterization of the surface properties of each mineral. The rates and mechanisms of adsorption and desorption of arsenic and selenium oxyanions on iron and manganese oxides are presented and discussed in Chapter 4. Chapter 5 examines the processes involved in the oxidation of As(III) and Se(IV) by manganese oxides. Factors influencing rates of

transformation, including pH, temperature, dissolved oxygen, and the concentration of competitive bivalent cations are examined. Chapter 6 concludes with a discussion of the implications of the experimental results for geochemical systems. Topics discussed are the rates of redox transformations in aquatic systems, the role of metal oxides in the environmental distribution of arsenic and selenium, and the determination of redox potentials of metal oxide surfaces.

Chapter 2

GEOCHEMISTRY OF ARSENIC AND SELENIUM SYSTEMS

2.1 Introduction

The solution of environmental problems associated with arsenic and selenium in aquatic systems requires an understanding of the complex chemistry of these elements. The principles and processes controlling the geochemical distribution of arsenic and selenium are reviewed to address the key questions proposed by this work. The questions to be answered are: (i) what chemical reactions control the geochemical distribution of the two oxidation states of both arsenic and selenium in aquatic systems, (ii) how does the distribution vary as the chemical and physical conditions of the system vary, and (iii) what is the role of metal oxides in aquatic systems that contain arsenic and selenium. In order to answer these questions, a summary of previous investigations has been undertaken. The topics to be discussed in this chapter include the aqueous properties of the various oxidation states based on thermodynamic relationships, adsorption of arsenic and selenium oxyanions on mineral surfaces, surface complexation modeling, and homogeneous and heterogeneous redox transformations between oxidation states. Also, the reductive dissolution of redox-active metal oxides is reviewed to provide a mechanistic framework that describes reactions between the reduced species and a metal oxide surface.

2.2 Aqueous Chemistry of Arsenic

2.2.1 General Chemistry

Arsenic belongs to group VB (N, P, As, Sb, Bi) of the periodic table, is a non-metallic element with the elemental electronic structure $[Ar]3d^{10}4s^{2}4p^{3}$, and is known to be toxic to plants and animals. There are four oxidation states in which arsenic forms inorganic compounds: V, III, 0, -III. The acid-base equilibria and redox half reactions between the oxidation states of inorganic arsenic are summarized in Table 2.1. Figure 2.1 is a pE-pH diagram for inorganic arsenic.

There are several literature reviews of the natural aquatic chemistry of arsenic. Ferguson and Gavis (1972) provide a general review of the inorganic arsenic cycle in natural waters. Cherry et al. (1979) review the thermodynamics of inorganic arsenic as a basis for the use of arsenic as an indicator of the redox status in groundwater. The National Research Council (1977) thoroughly examines the chemistry, distribution, and biological effects of the element on plants, animals, and man. Cullen and Reimer (1989) review the interactions of arsenic compounds with individual organisms ranging from *Methanobacteria* to man and also discuss the flux of arsenic compounds between the atmosphere, aquatic systems, soils, sediments, and fossil fuels.

2.2.2 Arsenate

Arsenic in the V oxidation state forms the triprotic acid of the oxyanion arsenate, AsO_4^{3-}, which has similar acid-base chemistry to phosphate. Figure 2.2a shows the relative importance of each arsenate species as a function of pH. For

Table 2.1: Energetic Data for Inorganic Arsenic Reactions

Acid-Base Equilibria

Arsenic Acid - As(V)

$H_3AsO_4 \leftrightarrow H_2AsO_4^- + H^+$	$pK_{a1} = 2.24$
$H_2AsO_4^- \leftrightarrow HAsO_4^{2-} + H^+$	$pK_{a2} = 6.96$
$HAsO_4^{2-} \leftrightarrow AsO_4^{3-} + H^+$	$pK_{a3} = 11.50$

Arsenious Acid - As(III)

$H_3AsO_3 \leftrightarrow H_2AsO_3^- + H^+$	$pK_{a1} = 9.29$
$H_2AsO_3^- \leftrightarrow HAsO_3^{2-} + H^+$	$pK_{a2} = 12.10$

Reduction Half Reactions

As(V) - As(III)	pE°	$E_H°$(v)
$H_3AsO_4 + 2\,H^+ + 2\,e^- \leftrightarrow H_3AsO_3 + H_2O$	9.85	0.58
$H_2AsO_4^- + 3\,H^+ + 2\,e^- \leftrightarrow H_3AsO_3 + H_2O$	10.85	0.64
$HAsO_4^{2-} + 4\,H^+ + 2\,e^- \leftrightarrow H_3AsO_3 + H_2O$	14.5	0.86
$HAsO_4^{2-} + 3\,H^+ + 2\,e^- \leftrightarrow H_2AsO_3^- + H_2O$	9.9	0.58
As(III) - As(0)		
$H_3AsO_3 + 3\,H^+ + 3\,e^- \leftrightarrow As(s) + 3\,H_2O$	3.9	0.23
$H_2AsO_3^- + 4\,H^+ + 3\,e^- \leftrightarrow As(s) + 3\,H_2O$	7.0	0.41
As(0) - As(-III)		
$As(s) + 3\,H^+ + 3\,e^- \leftrightarrow AsH_3 + H_2O$	-10.28	-0.61

$E_H° = (2.3RT/F)pE°$

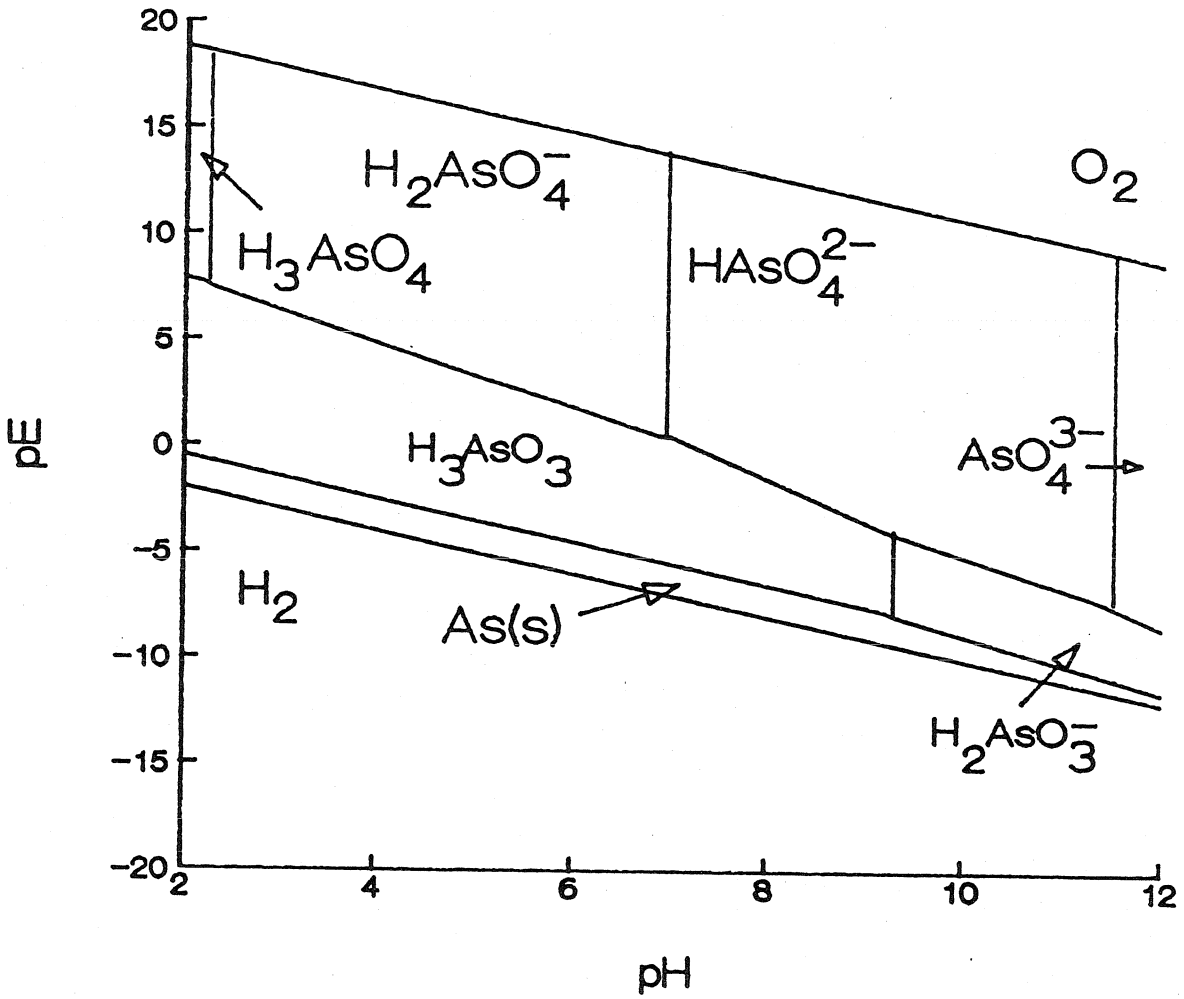

Figure 2.1: pE-pH diagram for the system As-H_2O for conditions 25 °C and As_T = 10 μM.

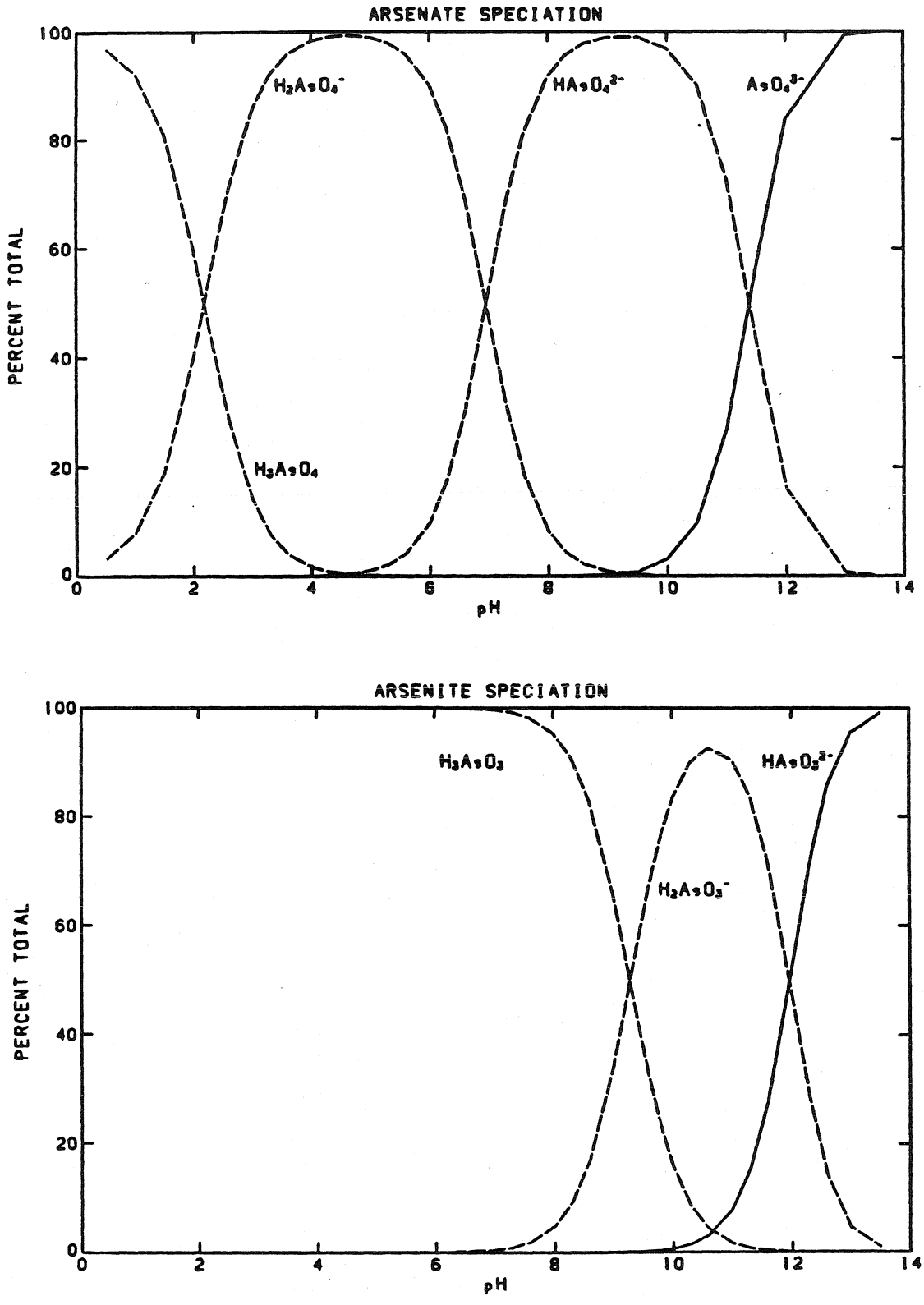

Figure 2.2: a) As(V) and b) As(III) speciation as a function of pH.

natural waters with a pH less than neutral, $H_2AsO_4^-$ is the predominant species, while in slightly alkaline natural waters $HAsO_4^{2-}$ is the major species. Iron forms the only stable complex with arsenate; ferric arsenate (pK_{s0} = 20.24) is stable in solution at pH less than 2.3 and pE above +12.5 (E_H above +0.74 volts) (Ferguson and Gavis, 1972).

2.2.3 Arsenite

Arsenic in the III oxidation state forms the triprotic acid of the oxyanion arsenite, AsO_3^{3-}. The acid-base equilibria (Table 2.1) indicate that arsenious acid H_3AsO_3, is a weak acid. Figure 2.2b illustrates that H_3AsO_3 is the predominant arsenite species in most natural water. $H_2AsO_3^-$ is the major species only in natural systems of pH greater than 9.3.

2.2.4 Elemental Arsenic and Arsenide

Elemental arsenic is very insoluble and is found in certain types of mineral deposits. Arsenic in the -III oxidation state is present as gaseous arsine, AsH_3, and is only stable at extremely low pE values. Under conditions where sulfide is present and stable, arsenic complexes with sulfur. AsS(s) (realgar) and As_2S_3(s) (orpiment) are found as stable solids. The aqueous species $HAsS_2$ is the major species at low pH in the presence of sulfide and AsS_2^-(aq) predominates at pH above 5.5.

2.2.5 Organic Arsenic

Arsenic also forms a variety of organic compounds, primarily through biological methylation. The chemistry of these compounds is reviewed by Lemmo et al. (1983). The most commonly found organic arsenic species are methylarsonic

acid ($CH_3AsO_3H_2$), dimethylarsinic acid ($(CH_3)_2AsOOH$), and trimethylarsine oxide ($(CH_3)_3AsO$). These compounds are derived from arsenic acid by replacing one or more of the hydroxyl groups with a methyl group.

2.3 Aqueous Chemistry of Selenium

2.3.1 General Chemistry

Selenium belongs to group VIB (O, S, Se, Te, Po) of the periodic table and is a non-metallic element with the elemental structure $[Ar]3d^{10}4s^24p^4$. Selenium has strong chemical similarities to sulfur, with oxidation states VI, IV, 0, and -II being important in natural systems under different redox conditions. The acid-base equilibria and the redox relationships of selenium are summarized in Table 2.2. Figure 2.3 is a pE-pH diagram for inorganic selenium.

The environmental distribution and chemistry of selenium have received extensive review since the discovery of the selenium contamination at the Kesterson National Wildlife Refuge. Previously, the only reviews were those of Rosenfeld and Beath (1964), which provided a general review of the geological distribution of selenium, and the National Research Council (1976), which reviewed the chemistry, distribution, and biological effects of the element as it pertained to plants, animals and man. Recently, there has been a plethora of selenium geochemical reviews; among the most complete reviews are those of the National Research Council (1989), which uses the Kesterson selenium accumulation for discussion of irrigation-induced water quality problems in general, and the Soil Science Society of America (Jacobs, 1989), which discusses selenium in the agriculturical environment.

Table 2.2: Energetic Data for Inorganic Selenium Reactions

Acid-Base Equilibria

Selenic Acid - Se(VI)

$H_2SeO_4 \leftrightarrow HSeO_4^- + H^+$	$pK_{a1} = -3$
$HSeO_4^- \leftrightarrow SeO_4^{2-} + H^+$	$pK_{a2} = 1.7$

Selenious Acid - Se(IV)

$H_2SeO_3 \leftrightarrow HSeO_3^- + H^+$	$pK_{a1} = 2.4$
$HSeO_3^- \leftrightarrow SeO_3^{2-} + H^+$	$pK_{a2} = 7.9$

Reduction Half Reactions

Se(VI) - Se(IV)	pE°	E_H°(v)
$SeO_4^{2-} + 4\,H^+ + 2\,e^- \leftrightarrow H_2SeO_3 + H_2O$	19.44	1.15
$SeO_4^{2-} + 3\,H^+ + 2\,e^- \leftrightarrow HSeO_3^- + H_2O$	18.24	1.08
$SeO_4^{2-} + 2\,H^+ + 2\,e^- \leftrightarrow SeO_3^{2-} + H_2O$	14.54	0.86
Se(IV) - Se(0)		
$H_2SeO_3 + 4\,H^+ + 4\,e^- \leftrightarrow Se(s) + 3\,H_2O$	12.50	0.74
$HSeO_3^- + 5\,H^+ + 4\,e^- \leftrightarrow Se(s) + 3\,H_2O$	13.10	0.77
$SeO_3^{2-} + 6\,H^+ + 4\,e^- \leftrightarrow Se(s) + 3\,H_2O$	15.08	0.89
Se(0) - Se(-II)		
$Se(s) + 2\,H^+ + 2\,e^- \leftrightarrow H_2Se$	-6.70	-0.40

$E_H° = (2.3RT/F)pE°$

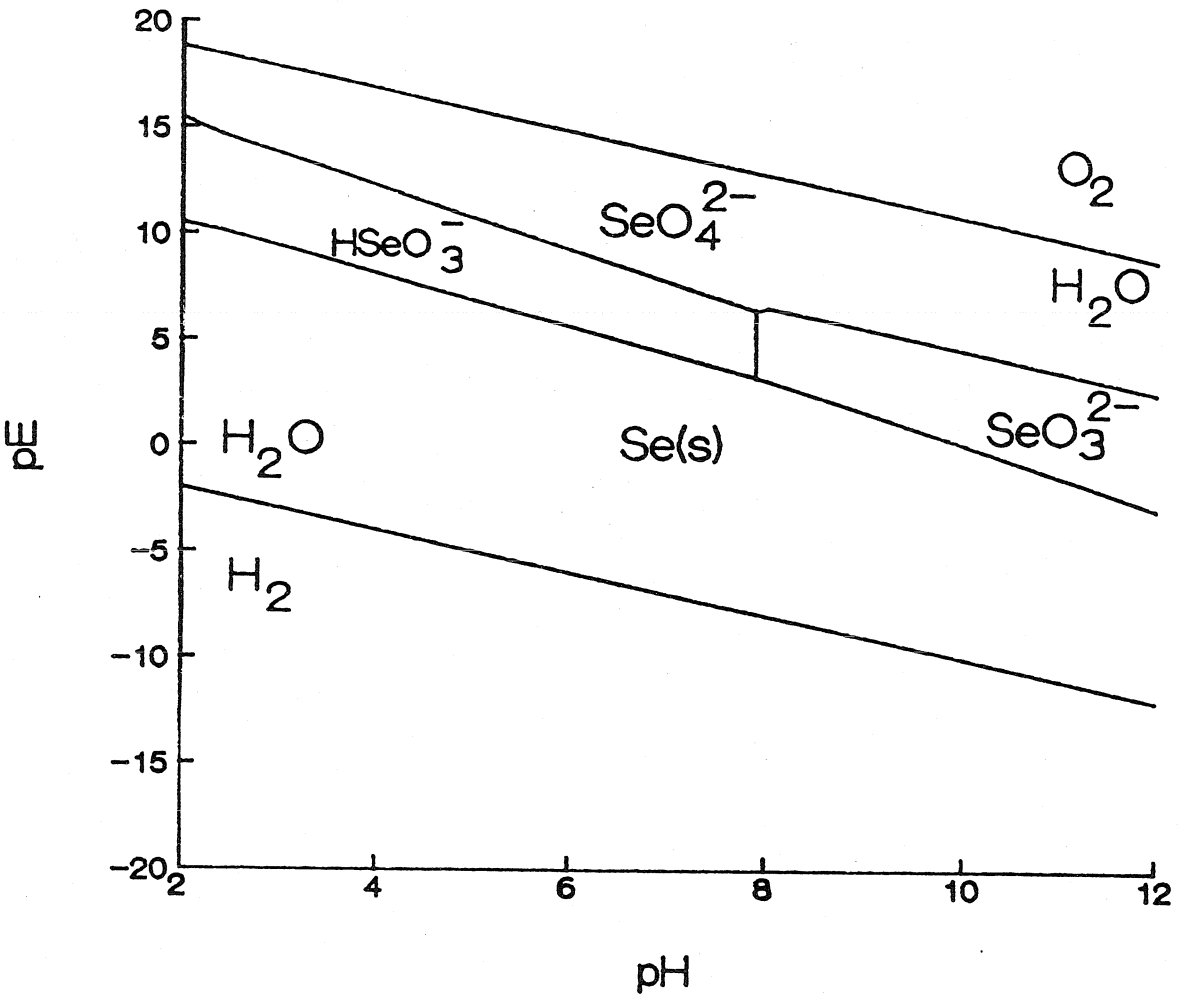

Figure 2.3: pE-pH diagram for the system Se-H_2O for conditions 25 °C and Se_T = 10 μM.

2.3.2 Selenate

Selenium in the VI oxidation state forms the diprotic acid of the oxyanion selenate, SeO_4^{2-}, and like sulfate, selenate is the predominant Se(VI) species in natural systems. Figure 2.4a indicates that selenic acid is a strong acid, much like sulfuric acid. Selenate exhibits similar solubilities to those of sulfate with the same metals (Rosenfeld and Beath, 1964) and under natural levels forms no solid with any metal.

2.3.3 Selenite

Selenium in the IV oxidation state forms the diprotic acid of the oxyanion selenite, SeO_3^{2-}. Selenious acid is a weak acid and, as indicated in Figure 2.4b, biselenite is the major dissolved selenite species between pH 3 and 7.5. Most selenite salts are less soluble than the corresponding selenates (NRC, 1976). Selenite forms several salts of low solubility with ferric iron. Chukhlantsev and Tomashevsky (1957) report that ferric selenite, $Fe_2(SeO_3)_3$ has a solubility product of 2×10^{-31} at 20 C. Williams and Byers (1936) report the formation of a basic ferric selenite, $Fe_2(OH)_4SeO_3$ (pK_{s0} = 61.7) in dilute aqueous solutions of ferric chloride and sodium selenite. However, Geering et al. (1968) and Howard (1977) conclude that neither salt is responsible for controlling the selenite concentration in natural waters. The concentration of selenite and ferric iron are far below the amounts expected from the equilibrium dissociation, at any pH, of either $Fe_2(SeO_3)_3$ or $Fe_2(OH)_4SeO_3$. Both investigators conclude that the control of selenite by iron is the adsorption onto ferric hydroxides.

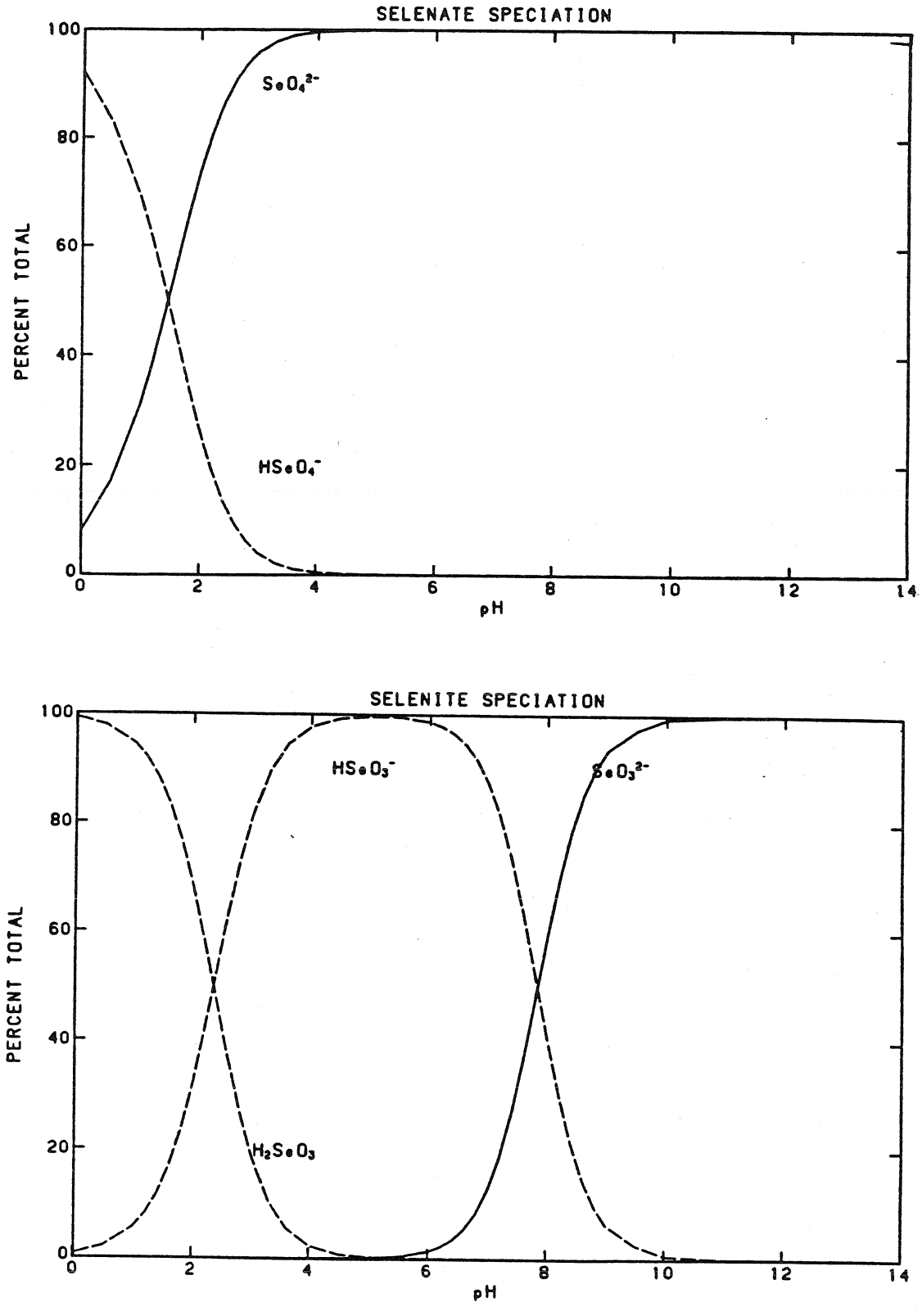

Figure 2.4: a) Se(VI) and Se(IV) speciation as a function of pH.

2.3.4 Elemental Selenium and Selenide

Elemental selenium is extremely insoluble and inert, and is a major sink for selenium in the aquatic environment. Selenide(Se(-II)) exists in reducing environments as hydrogen selenide (H_2Se), a foul-smelling poisonous gas, and as metal selenides. When dissolved in water, hydrogen selenide is a weak acid and easily oxidized to elemental Se. Metal selenides are typically found in metal sulfide ores (e.g., Fe, Cu, Pb), and tend to be very insoluble.

2.3.5 Organic Selenium

The organic chemistry of selenium is analogous to that of sulfur. Organic forms of selenium include seleno amino acids and their derivatives, methyl selenides, methyl selenic esters, methyl selenones, and methyl selenonium ions. The pathways for the bio-transformation of inorganic Se to the various organic forms and the interconversion between these different molecular species of selenium are not well understood (Cooke and Bruland, 1987).

2.4 Arsenic Anion Adsorption on Metal Oxide Surfaces

2.4.1 Previous Studies

One of the main mechanisms affecting the distribution of arsenic in natural systems is adsorption from the solution phase to sediments. Faust et al. (1987a,b,c) studied the distribution of arsenic in the bottom sediments and waters of a contaminated New Jersey watershed. The distribution coefficient, defined as the ratio of total arsenic in the sediments to the total arsenic of the water column, ranged from 53 to 22700, indicating that most of the arsenic in the system is bound

to the sediments. They observed that organic sediments had substantially higher total arsenic than sandy sediments but there was a low correlation between arsenic and TOC ($r = 0.42$). However, a high correlation was found between arsenic and iron ($r = 0.94$) and manganese ($r = 0.84$) in all sediments.

Previous investigations have studied the adsorption of arsenate and arsenite on aluminum oxides and hydroxides (Hingston et al., 1971; Ferguson and Anderson, 1974; Anderson et al., 1976; Malotky and Anderson, 1976; Anderson and Malotky, 1979), iron oxides and hydroxides (Hingston, 1970; Hingston et al., 1971; Ferguson and Anderson, 1974; Yoshida et al., 1976, 1978; Pierce and Moore, 1980, 1982; Leckie et al., 1980; Harrison and Berkheiser, 1982; Lumsdon et al., 1984), kaolinite and montmorillonite (Frost and Griffin, 1977), activated alumina, bauxite, and carbon (Gupta and Chen, 1978; Ghosh and Yuan, 1987), sand columns (Gulens et al., 1979), river sediments (Holm et al., 1979) and manganese oxides and hydroxides (Oscarson et al., 1983a,b; Thanabalasingam and Pickering, 1986).

2.4.2 pH Dependency

Oxyanions of arsenic are strongly adsorbed to most mineral surfaces but the degree of adsorption is highly dependent on pH. Arsenate adsorption on goethite, gibbsite, amorphous aluminum hydroxide, and activated carbon exhibited a maximum in the pH range 3 to 5 followed by a gradual decline with increasing pH (Hingston, 1970; Hingston et al., 1971; Anderson et al., 1976; Gupta and Chen, 1978). Arsenite adsorption on mineral surfaces exhibits a different pH dependence. Frost and Griffin (1977) found As(III) adsorption on clays to increase with increasing pH. On

activated alumina and bauxite, Gupta and Chen (1978) observed slight variations in arsenite adsorption over the pH range of 4 to 9 but adsorption decreased markedly above pH 9. Ghosh and Yuan (1987) noticed a maximum adsorption peak on alumina between pH 7 and 8 for varying As(III) concentrations. Pierce and Moore (1980) also observed a peak of arsenite adsorption on amorphous iron hydroxide at pH 7 for low initial concentrations of arsenite (0.667-13.3 μM), but for higher initial arsenite concentrations (33-667 μM), the amount of arsenite taken up increased with decreasing pH. The adsorption of arsenite on various manganese dioxides at pH 7 was studied by Oscarson et al. (1983b) and affinity for the anion by the oxides was: cryptomelane > birnessite >> pyrolusite.

2.4.3 Effect of Redox Status

In addition to being dependent on pH and the type of mineral surface, adsorption of arsenic species is also greatly influenced by the redox status of the system. Faust et al. (1987a,b) found in laboratory experiments using organic and sandy lake sediments under aerobic conditions that the order of species occurrence in the sediment phase was: As(V) > As(III) > methylarsonic acid (MAA) > dimethylarsinic acid (DMAA). In the aqueous phase, the order was As(V) > As(III) with no MAA or DMAA present. Under anaerobic conditions, the order of species occurrence in the sediment phase and in the aqueous phase was: As(III) > As(V) > MAA, DMAA. Under aerobic conditions, the total arsenic distribution coefficients for organic sediments were a magnitude greater than under anaerobic conditions. The observations from the field and laboratory suggest that arsenic is

largely bound by iron and manganese oxides that are present in aerobic, but not anaerobic, sediments.

The importance of the redox environment on arsenic mobility has also been investigated by Gulens et al. (1979). As(III) and As(V) were eluted through sand columns with waters of different redox characteristics. The elution behavior of As(III) was significantly different from that of As(V). In an oxidizing environment (pH 5.4, E_H = 580 mV), As(III) was detected in the column eluent 5-6 times sooner than As(V), and the amount of As(III) eluted (about 60% of loading) was about 8 times larger than that of As(V). In a neutral environment (pH 6.9, E_H = 140 mV), the relative amounts of both species eluted were unchanged. As(V) moved through the column more rapidly than in an oxidizing environment but it was still retarded with respect to As(III). In a reducing environment (pH 8.3, E_H = 75 mV), the mobility of As(V) was accelerated to that of As(III) and both species were also eluted almost quantitatively (about 100% for As(III) and 80% for As(V)). From these observations alone, it was not possible to elucidate whether pH or the redox environment controls the mobility. Strong retention of As(V) in the oxidizing environment can be attributed to its adsorption to iron oxide coatings on the sand particles. However, the increase in mobility of As(V) in more reducing environments may be due to the increase in pH of the eluting water or to the reduction in the column of Fe(III) to Fe(II) and, perhaps, As(V) to As(III).

2.5 Selenium Anion Adsorption on Metal Oxide Surfaces

2.5.1 Previous Studies

Adsorption of selenium has not been as extensively studied as that of arsenic. The adsorption of selenite has been studied on goethite (Hingston et al., 1968, 1972; Goldberg, 1985; Balistrieri and Chao, 1987; Hayes et al., 1987), amorphous iron oxyhydroxide (Leckie et al., 1980), gibbsite (Hingston et al., 1972), hydrous alumina (Rajan, 1979), and alluvial soils (Neal et al., 1987). Selenate adsorption has only been studied on an amorphous iron oxyhydroxide (Davis and Leckie, 1980; Leckie et al., 1980) and goethite (Balistrieri and Chao, 1987; Hayes et al., 1987). There are no literature reports of selenite or selenate adsorption on manganese oxides.

2.5.2 Selenite Adsorption

The adsorption behavior of selenite is similar to that of arsenate. Hingston et al. (1968) found the maximum adsorption of selenite on goethite at low pH and as pH increased, adsorption decreased. Similar results were found for all of the mineral surfaces that have been studied. Balistrieri and Chao (1987) examined the influence of additional anions on selenite adsorption. It was found that the competition depends on the relative affinity of the anions for the surface and the relative concentrations of the anions. For a given anion concentration ratio, the competition sequence with selenite is phosphate > silicate ≥ citrate > molybdate > bicarbonate/carbonate > oxalate. A phosphate to selenite concentration ratio greater than 10 is necessary before selenite adsorption is affected; however, for the other anions, the concentration ratio must be greater than 100 to affect the selenite

adsorption. Some anions, fluoride and sulfate, do not affect the adsorption at all, even at concentration ratios of 10^5. Neal et al. (1987) looked at the uptake of Se(IV) on alluvial soils from the San Joaquin Valley (CA). A pH dependence similar to that of hydrous metal oxides was found and adsorption of selenite could be correlated with the amounts of solubilized Al, Fe, and Mn in the soils.

2.5.3 Selenate Adsorption

Adsorption of selenate on iron oxides is considerably different from that of selenite. In the range of most natural waters (pH 6-8) there is little or no adsorption of selenate, whereas selenite is completely adsorbed. As the pH decreases, selenate begins to adsorb, and, although there are no results that indicate this, selenate probably is only completely adsorbed at pH < 4. The percentage of selenate and sulfate adsorbed on an amorphous iron oxide as a function of pH is essentially the same (Davis and Leckie, 1980). Also, sulfate effectively competes with selenate adsorption. Systems of selenate with no sulfate partition in the same manner as equivalent mixed systems of selenate and sulfate.

2.6 Surface Chemical Modeling

Adsorption of the various anions of Se(IV), Se(VI), As(III), and As(V) is interpretable in terms of mechanisms of either inner-sphere or outer-sphere coordination to metal-ion centers in oxide structures. Specific adsorption of anions occurs as the result of inner-sphere complexation. Specific adsorption of anions involves ligand exchange reactions in which singly coordinated surface hydroxyl ions are replaced by the anions that bind directly to the central metal ions on the surface.

Adsorption of anions lowers the pH of the isoelectric point (pH_{iep}) of the adsorbent. Pierce and Moore (1980) demonstrate that the pH_{iep} of amorphous iron oxides (am-$Fe(OH)_3$) is lowered by arsenite adsorption. Lowering of the pH_{iep} has also been shown for arsenate on alumina (Ghosh and Yuan, 1987) and amorphous aluminum hydroxide (Anderson et al., 1976), and for selenite on goethite and gibbsite (Hingston et al., 1972). Rajan (1979) demonstrated that the adsorption of selenite was a ligand exchange reaction. As more selenite was adsorbed by hydrous alumina, more hydroxyl ions were released, and at maximum adsorption, a 1:1 stoichiometry existed.

Hayes et al. (1987) report that the adsorption of selenite on goethite is unaffected by changes in ionic strength while the adsorption of selenate on goethite is greatly reduced by increasing ionic strength. Respective ionic strength effects suggest that selenite is a strongly bonded ion that forms an inner-sphere coordination complex with the oxide surface hydroxyl sites and that selenate is a weakly bonded ion that forms an outer-sphere, ion-pair complex that retains the primary hydration sphere upon adsorption. Hayes et al. also performed in-situ extended x-ray absorption fine structure (EXAFS) measurements of adsorbed selenate and selenite ions at the goethite-water interface. The method provided direct structural information that confirmed selenite forms an inner-sphere complex whereas selenate adsorbs as an ion-pair, outer-sphere complex.

Infrared spectroscopy has been used to show the bonding habit of arsenate and selenate on freshly prepared hydrous iron oxides (Harrison and Berkheiser, 1982) and arsenate on goethite (Lumsdon et al., 1984). Harrison and Berkheiser

(1982) report that both arsenate and selenate coordinate directly with surface iron atoms and form bidentate bridging complexes by replacement of protonated and unprotonated hydroxyls. Lumsdon et al. (1984) confirmed that arsenate forms a bidentate bridging complex with surface iron atoms and replaces two singly coordinated surface hydroxyl groups by ligand exchange.

The ligand exchange reactions of anions at reactive sites on metal oxide surfaces can be described by surface complexation reactions (Stumm and Morgan, 1981; Dzombak and Morel, 1987). The acid-base behavior of the surface functional group, >SOH, can be expressed by

$$>SOH_2^+ \rightleftharpoons >SOH + H^+ \qquad K_{a1}^s \tag{2-1}$$

$$>SOH \rightleftharpoons >SO^- + H^+ \qquad K_{a2}^s \tag{2-2}$$

and the surface complexation reactions are defined as follows

$$>SOH + A^{z-} + H^+ \rightleftharpoons >SA^{(z-1)-} + H_2O \qquad K_{1,A}^s \tag{2-3}$$

$$>SOH + A^{z-} + 2H^+ \rightleftharpoons >SHA^{(z-2)-} + H_2O \qquad K_{2,A}^s \tag{2-4}$$

$$2>SOH + A^{z-} + 2H^+ \rightleftharpoons >S_2A^{(z-2)-} + 2H_2O \qquad \beta_{2,A}^s \tag{2-5}$$

where $>SA^{(z-1)-}$; $>SHA^{(z-2)-}$; $>S_2A^{(z-2)-}$ are possible anion surface species.

Several surface chemical models have been used to describe adsorption of solutes. The models differ in the treatment of electrostatic interactions. The similarities and differences of the models are examined by Westall and Hohl (1980). Table 2.3 is a summary of the limited modeling results for the adsorption of the

various anions of arsenic and selenium. The adsorption of As(III) has not been modeled. The adsorption of As(V), Se(IV), and Se(VI) on am-$Fe(OH)_3$ was modeled using the triple layer model (Leckie et al., 1980). Affinity of the anion for the surface is indicated by the value of the equilibrium complexation constant. As(V) has the greatest affinity for the amorphous iron surface whereas selenate forms the weakest complex. Goldberg (1985) determined selenite-goethite surface complexation constants using the constant capacitance (CC) model from the adsorption data of Hingston (1970). Arsenate surface complexation constants have been determined by Goldberg (1986) using the CC model. The data are from previous adsorption work on goethite and gibbsite (Hingston, 1970), and amorphous aluminum hydroxide (Malotky and Anderson, 1976). The values of the arsenate constants are similar to those of phosphate.

As a test of the applicability of surface complexation models to predict anion adsorption in natural systems, Belzile and Tessier (1990) calculated apparent adsorption constants of As(V) onto natural Fe oxyhydroxides from the concentrations of total As and Fe determined in leachates of surficial lake sediments and the *in situ* measurement of dissolved total As in their respective overlying waters. A simplified version of the surface complexation model was used, in which the electrostatic corrections were ignored. The binding intensity values derived from field measurements agreed well with those obtained from laboratory experiments performed with amorphous Fe oxyhydroxides (Pierce and Moore, 1982), but did not

Table 2.3: Surface Complexation Constants

Anion	Oxide	Complex	log K[a]	Model	Ref.
Selenite	am-$Fe(OH)_3$	$>FeSeO_3^-$	12.5	TLM	1
		$>FeHSeO_3$	18.9		
	α-FeOOH C	$>FeSeO_3^-$	15.7	CC	2
		$>FeHSeO_3$	20.3		
	α-FeOOH E	$>FeSeO_3^-$	16.1	CC	2
		$>FeHSeO_3$	21.4		
Selenate	am-$Fe(OH)_3$	$>FeSeO_4^-$	9.9	TLM	1
		$>FeHSeO_4$	15.9		
Arsenate	am-$Fe(OH)_3$	$>FeHAsO_4^-$	25.9	TLM	1
		$>FeH_2AsO_4$	31.1		
	α-FeOOH A	$>FeAsO_4^{2-}$	20.1	CC	3
		$>FeHAsO_4^-$	26.5		
		$>FeH_2AsO_4$	30.8		
	α-FeOOH C	$>FeAsO_4^{2-}$	21.0	CC	3
		$>FeHAsO_4^-$	27.2		
		$>FeH_2AsO_4$	31.6		
	$Al(OH)_3$	$>AlAsO_4^{2-}$	17.1	CC	3
		$>AlHAsO_4^-$	24.1		
		$>AlH_2AsO_4$	30.4		
	am-$Al(OH)_3$	$>AlAsO_4^{2-}$	16.2	CC	3
		$>AlHAsO_4^-$	24.0		
		$>AlH_2AsO_4$	30.6		

[a] log K(intr) for Constant Capacitance Model; log K(app) for Triple Layer Model
(1) Leckie et al., 1980; (2) Goldberg, 1985; (3) Goldberg, 1986

agree with those obtained from laboratory experiments performed with goethite (Hingston, 1970; Hingston et al., 1971).

2.7 Heterogeneous Oxidation and Reduction

In homogeneous oxic solutions, the oxidations of arsenite and selenite proceed very slowly. Eary and Schramke (1990) reported a half-time of one year for arsenite oxidation by oxygen. Tallman and Shaikh (1980) observed no oxidation of As(III) in distilled demineralized water after 37 days. Experiments and observations with pure systems in the laboratory indicated that the rates of transformation of selenite to selenate and vice versa are relatively sluggish (Rosenfeld and Beath, 1964).

There is considerable evidence in recent experimental studies of redox reactions that mineral surfaces can play a key role in bringing about rapid transformations. The surface can either catalyze the redox reaction or be a direct oxidant or reductant. Examples of an oxide acting as a catalyst in the oxidation by O_2 include Fe(II) and Mn(II) in the presence of γ-FeOOH (Sung and Morgan, 1980, 1981); Mn(II) in the presence of various oxides (Davies and Morgan, 1989); V(IV) in the presence of Al_2O_3 and TiO_2 (Wehrli, 1987). Systems in which the oxide surface is a direct oxidant include hydroquinone with Mn(III), Mn(IV), and Fe(III) oxides (Stone, 1983; LaKind, 1988), Co(II) with MnO_2 (Crowther et al., 1983), Cr(III) with MnO_2 (Eary and Rai, 1987), and aniline and other primary aromatic amines with MnO_2 (Laha and Luthy, 1990).

Arsenic(III) oxidation has been observed to occur in freshwater lake sediments through predominantly abiotic processes (Oscarson et al., 1980). Further studies

found that Mn(IV) oxides are effective oxidants, while there was no oxidation of As(III) after 48 hours in suspensions of illite, montmorillonite, kaolinite, vermiculite, ferruginous smectite, microcline, orthoclase, or calcite (Oscarson et al., 1981a). Three manganese dioxides (birnessite (δ-MnO_2), cryptomelane (α-MnO_2), and pyrolusite (β-MnO_2))were examined for their ability to deplete As(III) in solution. The depletion (oxidation of As(III) to As(V) and adsorption of As(III)) at pH 7 by all three Mn dioxides followed first-order kinetics. The depletion rate constants of birnessite and cryptomelane at 298 K are 7.42×10^{-5} s^{-1} and 5.25×10^{-5} s^{-1}, respectively, while the rate constant of pyrolusite is more than two orders of magnitude lower (1.22×10^{-7} s^{-1}). Thanabalasingam and Pickering (1986) studied similar systems at pH 6.5 and noticed a relatively rapid (two hours) initial reaction which was followed by a slower process. Pseudo-first order depletion rate constants of the order 3.06×10^{-5} s^{-1}, 1.56×10^{-5} s^{-1}, and 9.44×10^{-6} s^{-1} are reported for systems containing MnOOH, cryptomelane, or pyrolusite, respectively. The rate constants are experimentally determined by following the disappearance of As(III) from solution. The systems reached equilibrium with respect to total As sorption while the depletion of As(III) was still progressing. The authors conclude that after adsorption of total As has reached equilibrium, in order for the concentration of As to remain constant, there must be a one-to-one relationship between the amount of As(III) depleted and the amount of As(V) appearing in solution. The results suggest a mechanism for the depletion:

As(III) (aq) + Mn oxide surface -> Adsorbed As(III) (i)

Adsorbed As(III) -> Adsorbed As(V) (ii)

Adsorbed As(V) -> As(V) (aq) (iii)

These results on heterogeneous As(III)-As(V) kinetics need to be extended to account for pH, temperature, ionic strength, concentration of As(III), surface site concentration, and the influence of O_2 concentration.

There are no reports in the literature of As(III) oxidation by Fe(III) oxides, although under the proper conditions, the reaction is thermodynamically feasible. Figure 2.5 is a pE-pH diagram for arsenic in natural waters with the redox equilibria of MnOOH(s)/Mn^{2+} and FeOOH(s)/Fe^{2+} shown for comparison. Figure 2.5 shows that manganese oxides are capable of As(III) oxidation over a wide pH range while iron oxides are capable of As(III) oxidation only under acid conditions. Oscarson et al. (1981b) report that the oxidation of As(III) in a suspension of Fe(III) oxides at pH 7 after 72 hours does not occur. Thermodynamically, at pH 7, the reaction would not be expected to occur.

The oxidation of Se(IV) in any natural system has not been studied. Figure 2.6 is a similar pE-pH diagram for selenium and it illustrates that, strictly from a thermodynamic point-of-view, Mn(III) and Mn(IV) oxides are possible oxidants of Se(IV) while Fe(III) oxides are not.

2.8 Reductive Dissolution of Metal Oxides

pE-pH diagrams for iron and manganese indicate that the oxidized forms of the elements (Fe(III), Mn(III, IV)) exist as solid phases while the reduced forms

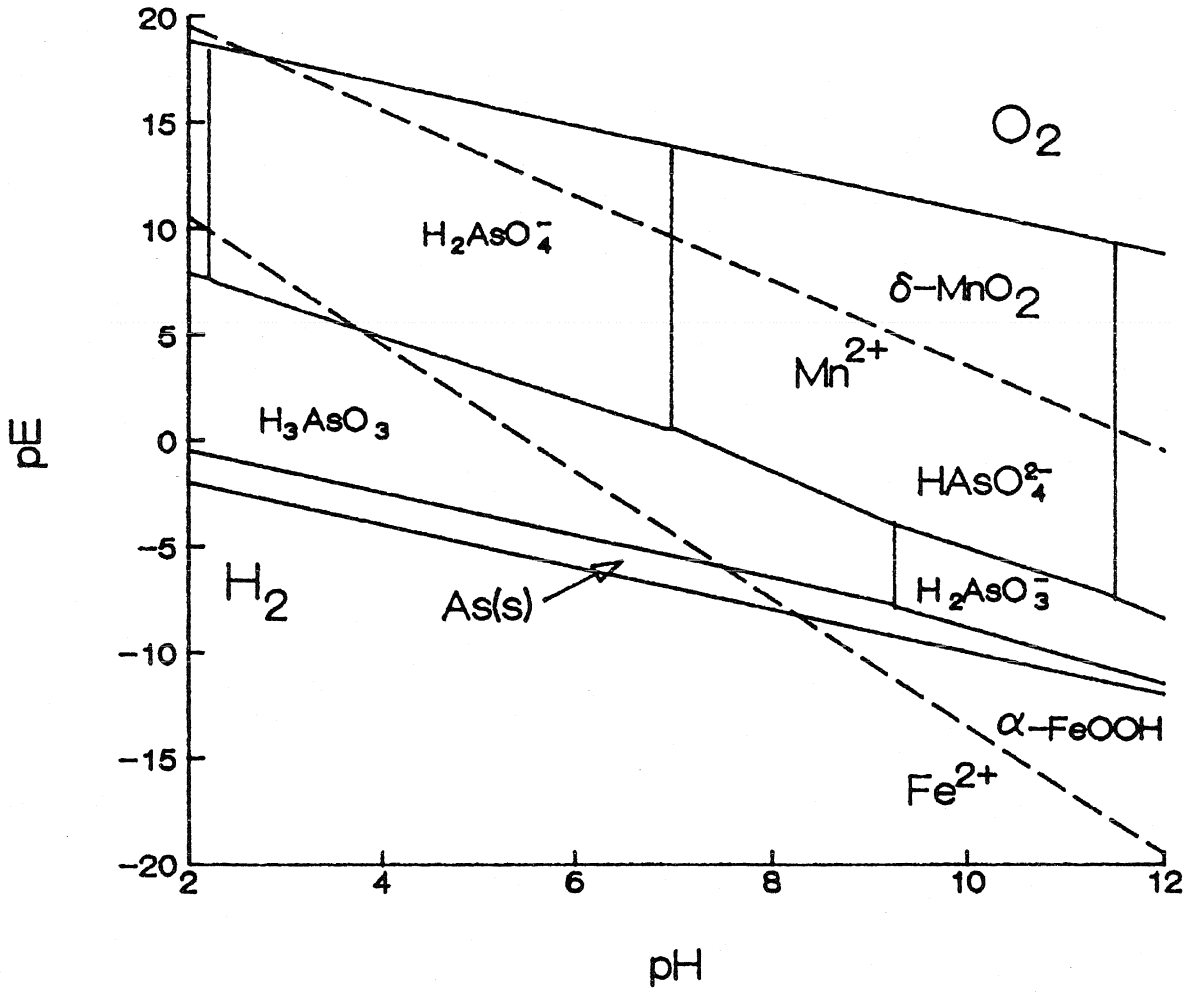

Figure 2.5: pE-pH diagram for the system As-H_2O at 25 °C and As_T = 10 μM and the pE-pH relationships for the relative Mn and Fe species for conditions Mn_T = Fe_T = 1 mM.

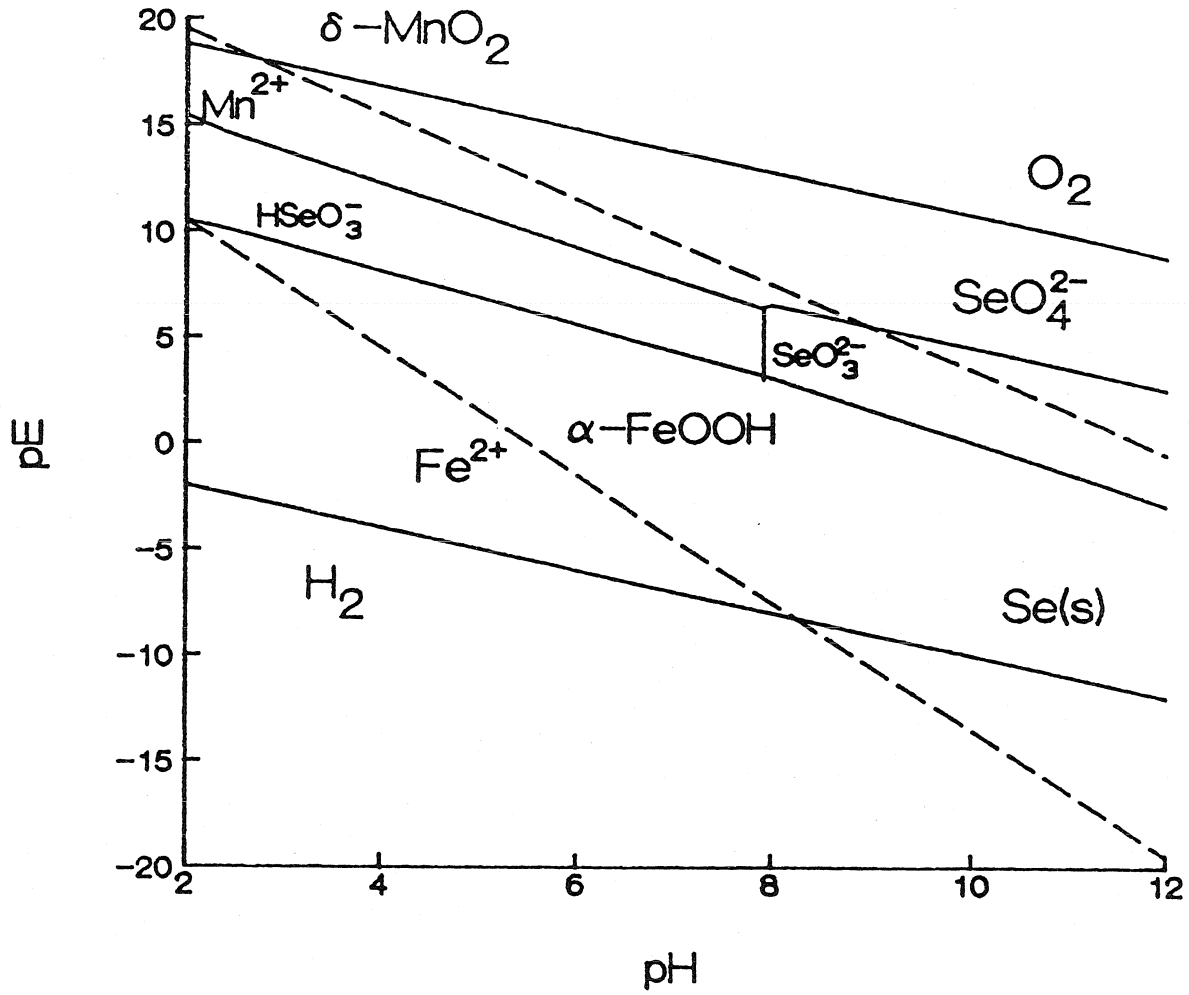

Figure 2.6: pE-pH diagram for the system Se-H_2O at 25 °C and Se_T = 10 μM and the pE-pH relationships for the relative Mn and Fe species for conditions Mn_T = Fe_T = 1 mM.

(Fe(II), Mn(II)) exist as soluble species. Thus, the reduction of the oxidized form to the reduced form of the metal results in a dramatic increase in the metal solubility. The reductive dissolution process has been studied in great detail by Stone (1983, 1986) and Stone and Morgan (1987). Reducing agents that have been studied are substitituted phenols (Stone, 1987; McBride, 1987; LaKind, 1988; Stone and Ulrich, 1989), ascorbate (Banwart et al., 1989), aniline and other aromatic amines (Laha and Luthy, 1990), cobalt(II) (Crowther et al., 1983), and chromium(III) (Eary and Rai, 1987).

The reaction mechanism of dissolution of redox-active metal oxides (i.e., Fe, Mn, Ni, Co, Cu, but not Al, Si, Ti) by a reducing agent involves (i) the transport of the reductant to the oxide surface, (ii) a surface redox reaction, and (iii) transport of the product away from the oxide surface. Transport-controlled reductive dissolution reactions are rare and most are controlled by surface chemical reactions (Stone and Morgan, 1987). Reductive dissolution of tervalent metal oxide surface sites ($>Me^{III}OH$) by phenol (HA) can be represented by the following inner-sphere process (Stone and Morgan, 1987):

Precursor Complex Formation

$$>Me^{III}OH + HA \underset{k_{-1}}{\overset{k_1}{\rightleftharpoons}} >Me^{III}A + H_2O$$

Electron Transfer

$$>Me^{III}A \underset{k_{-2}}{\overset{k_2}{\rightleftharpoons}} >Me^{II}\bullet A$$

Release of Oxidized Organic Product

$$>Me^{II}\bullet A + H_2O \underset{k_{-3}}{\overset{k_3}{\rightleftharpoons}} Me^{II}OH_2 + A\bullet$$

Release of Reduced Metal Ion

$$>Me^{II}OH_2 + 2H^+ \underset{k_{-4}}{\overset{k_4}{\rightleftharpoons}} >Me^{III}OH + Me^{2+}$$

Although only the neutral surface site is included in the process, other protonation levels ($>Me^{III}OH_2^+$ and $>MeO^-$) exist on the oxide surface and may participate in the reaction. For example, anions adsorb to a greater extent when the surface is positively charged (i.e., $[>Me^{III}OH_2^+] > [>MeO^-]$) and thus will increase the formation of the precursor complex. Likewise, the reduced metal product will adsorb to a greater extent when the surface is negatively charged (i.e., $[>MeO^-] > [>Me^{III}OH_2^+]$) and thus will decrease the number of available reactive surface sites.

Based upon this mechanism, conditions that promote increased rates of product formation are high rates of precursor complex formation (large k_1), slow desorption rates (small k_{-1}), fast electron transfer (large k_2), and fast rates of product release (large k_3 and k_4) (Stone, 1986). For a surface chemistry controlled reaction, changes in concentration of the reactants, pH, and medium composition affect overall

rates of dissolution, by modifying the rate or extent of precursor complex formation, the rate of electron transfer, the rate of release of products from the oxide surface, or the rate of product re-adsorption. The degree of adsorption of the reductant depends upon the protonation level of the reductant and the metal oxide surface sites. Also, the presence of other cations and anions that might compete with the reductant for reactive surface sites would alter the overall rate of dissolution.

2.9 Summary

The geochemical distributions of arsenic and selenium depend upon the acid-base conditions, redox status, and mineral content of the natural system. In oxic systems, arsenic should exist as As(V), which adsorbs to mineral surfaces in the acidic to neutral pH domain. As a result of slow redox kinetics As(III) has been found to persist in some oxic environments. As(III) also binds strongly to mineral surfaces in the pH of most natural systems. As the redox status of the system becomes anoxic, arsenic is first mobilized as manganese and iron oxides are reduced, and then it is reduced to elemental arsenic itself.

Selenium exists in oxic systems as selenate, which weakly adsorbs to mineral surfaces and thus, is highly mobile in aquatic systems. Under reducing conditions, selenium exists as selenite, which is immobilized by adsorption to mineral surfaces. In strongly reducing environments, selenium is reduced to the insoluble elemental form.

Kinetically-inhibited redox transformations allow both oxidation states to simultaneously exist. Homogeneous oxidation of As(III) and Se(IV) by dissolved

oxygen is extremely slow, if it occurs at all. One study has shown that manganese dioxides provide a more rapid pathway for As(III) oxidation. Studies have shown that other reduced species are also oxidized more rapidly in metal oxide systems. Based on the affinity for oxide surfaces that As(III) and Se(IV) both display, it is believed that redox-active metal oxides should provide a pathway for the redox transformations of these oxidation states.

Chapter 3

PREPARATION AND CHARACTERIZATION OF METAL OXIDES

3.1 General Remarks

Deionized distilled water (D_2H_2O) from a MILLI-Q water purification system (Millipore Corp., Bedford, MA) was used to prepare all solutions. All reagents were analytical grade and used without further treatment. All solutions were filtered through a 0.2 μm Nucleopore filter to remove possible particle contaminants. All glassware was cleaned with 4 M HNO_3 or 4 M HCl and rinsed several times with D_2H_2O.

The pH of solution was monitored in all experiments using a Radiometer glass combination electrode (Model GK2401C) and a Radiometer Model PHM84 research pH meter. The electrode was calibrated by NBS buffers.

3.2 Particle Preparation

Goethite particles were synthesized using a method similar to that of Atkinson et al. (1967). 500 ml of 1.0 N KOH was added to 50 g of $Fe(NO_3)_3 \cdot 9H_2O$ (MCB Reagents) in 500 ml of D_2H_2O in a teflon beaker. The mixture was aged for 24 hours at 60 °C. Goethite crystallizes from aqueous ferric iron via the following reaction:

$$Fe^{3+} + 3\ OH^- \rightarrow \alpha\text{-FeOOH(s)} + H_2O \qquad (3\text{-}1)$$

Birnessite particles were synthesized using a method adapted from McKenzie (1971). 16.5 ml of concentrated HCl was added dropwise to a boiling solution

(500 ml) of 0.4 M $KMnO_4$. After boiling for a further fifteen minutes, the brown precipitate was filtered and washed. Birnessite precipitates from the acid reduction of permanganate:

$$MnO_4^- + H^+ \rightarrow \delta\text{-}MnO_2(s) + \tfrac{3}{4}\, O_2(g) + \tfrac{1}{2}\, H_2O \qquad (3\text{-}2)$$

The oxide suspensions were cleaned by the following method. The suspensions were: (1) centrifuged at 5000 rpm for 30 minutes, (2) drained of supernatant, (3) resuspended with D_2H_2O, and (4) sonicated for 30 minutes. This procedure was repeated until the conductivity of the resuspended particles was that of D_2H_2O (1-2 μmhos). The oxide particles were stored as aqueous slurries (5-10 g/l), and then sonicated prior to use to ensure a uniform suspension.

3.3 Mineral Identification

3.3.1 Methods

To identify the solid phase, x-ray diffractograms were taken for each particle preparation. A Cu Kα source was used. Each suspension was filtered with a 0.2 μm Nucleopore filter, dried, and ground in a mortar and pestle.

Scanning electron microscopy was used to identify the morphology of the crystals. The samples were prepared by filtering a thousand-fold dilution of the solid stock suspension through a 0.2 μm Nucleopore filter. A portion of the filter was mounted and covered with a thin layer of gold.

Particle size distributions of the suspension were obtained from measurements using a Coulter Counter Model TA-II-L equipped with a population counting accessory PCA-II. A few drops of a sonicated particle stock suspension were added

to a 2% NaCl filtered solution and number and volume measurements were taken using a 50 μm aperture.

3.3.2 Goethite

The iron oxide particles were identified as goethite (α-FeOOH) by x-ray diffraction. Figure 3.1 is an x-ray diffractrogram of the iron oxide particles. The peaks in the diffractogram are listed in Table 3.1. The peaks for the preparation correspond closely with those expected for goethite. Lepidocrocite (γ-FeOOH) is another iron oxide hydroxide form which may be an impurity. However, no peaks in the diffractogram correspond to those of lepidocrocite.

Scanning electron microscopy was used to identify the morphology of the iron oxide particles. Figure 3.2 is a scanning electron micrograph of the preparation and shows that the goethite particles are acicular. The particles are 1-2 microns long by 0.2-0.4 microns wide.

3.3.3 Birnessite

The manganese oxide particles were identified as birnessite (δ-MnO_2) by x-ray diffraction. Figure 3.3 shows an x-ray diffractogram of the manganese oxide particles and, for comparison, a reference diffractogram for synthetic birnessite (ASTM Card 23-1046). The major peaks of the preparation correspond with the major peaks of the standard. Figure 3.4 is a scanning electron micrograph of the birnessite particles and shows that the particles are mostly aggregrated clusters of submicron-sized spheres.

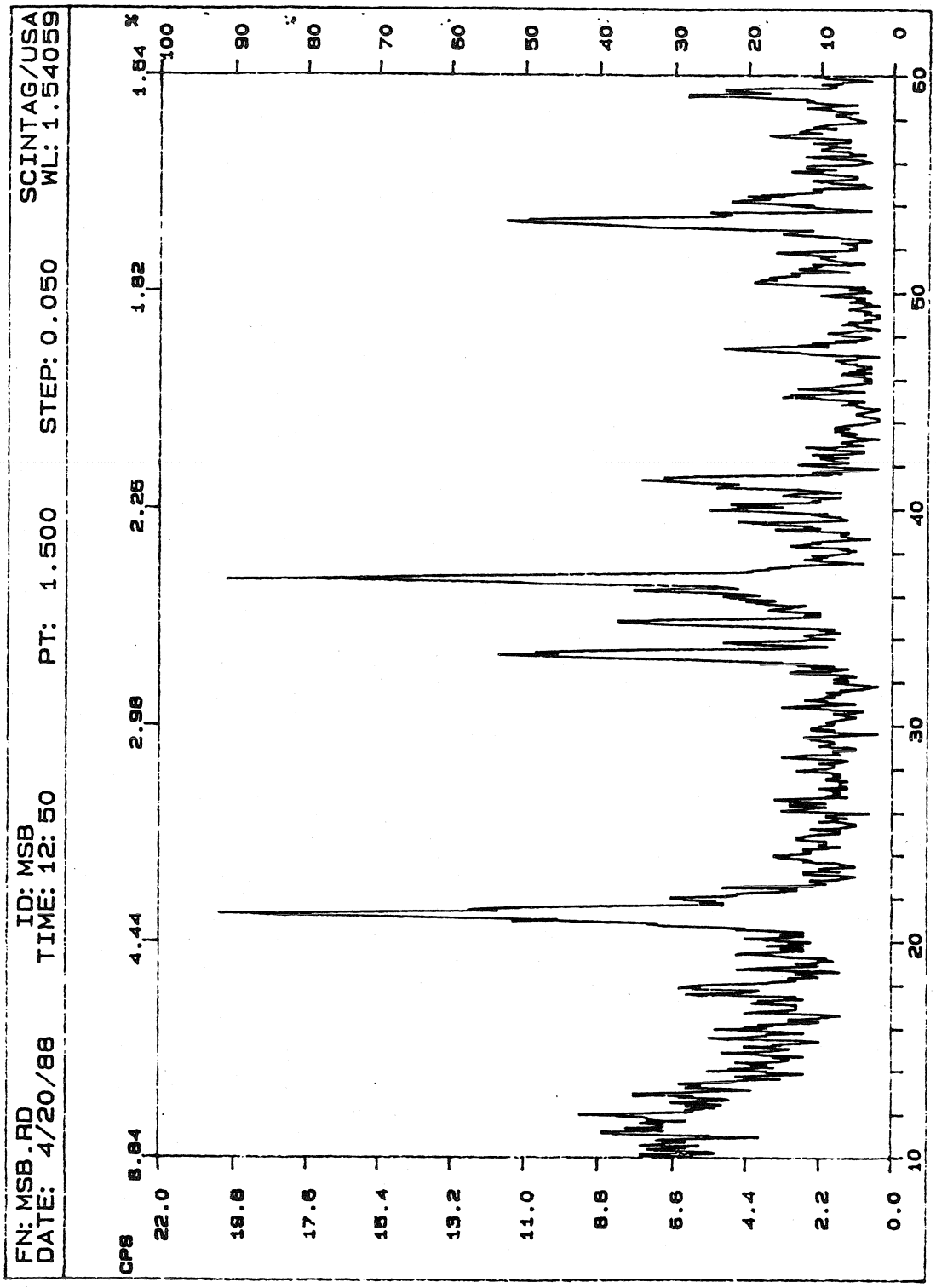

Figure 3.1: X-ray diffractogram of iron oxide particle preparation. The peaks correspond to those of goethite (α-FeOOH).

Table 3.1: Comparison of X-Ray Diffraction Peaks

Iron Oxide		Goethite		Lepidocrocite	
d(a)	Intensity	d(a)	Intensity	d(a)	Intensity
--	--	--	--	6.26	100
4.990	33	4.98	12	--	--
4.197	90	4.183	100	--	--
3.383	25	3.383	10	--	--
--	--	--	--	3.29	90
2.680	58	2.693	35	--	--
2.582	50	2.583	12	--	--
--	--	--	--	2.47	80
2.449	85	2.450	50	--	--
2.255	36	2.253	14	--	--
2.186	33	2.190	18	--	--
--	--	--	--	1.937	70
1.920	50	1.920	5	--	--
1.720	50	1.719	20	--	--
1.561	50	1.561	8	--	--

3.4 Surface Properties

3.4.1 Specific Surface Area

The specific surface areas of the oxide particles were determined by a gravimetric method based on the retention of ethylene glycol monoethyl ether (EGME) (Eltantawy and Arnold, 1973). EGME is believed to form a full unimolecular layer surface coverage of all easily accessible surfaces. An approximate 0.5 g sample of each particle preparation, which had been dried at 110 °C, was

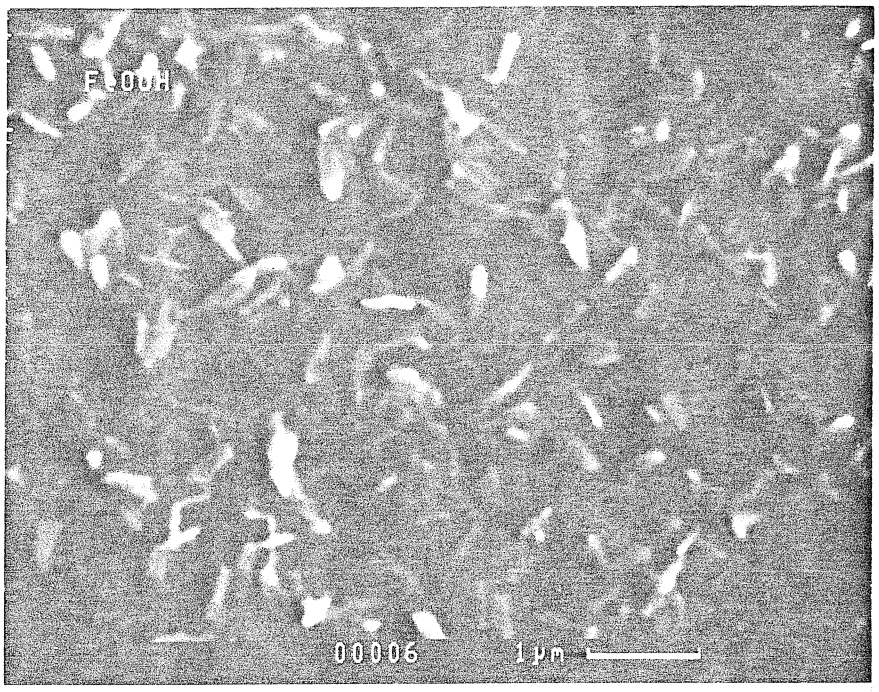

Figure 3.2: Scanning electron micrograph of goethite particles.

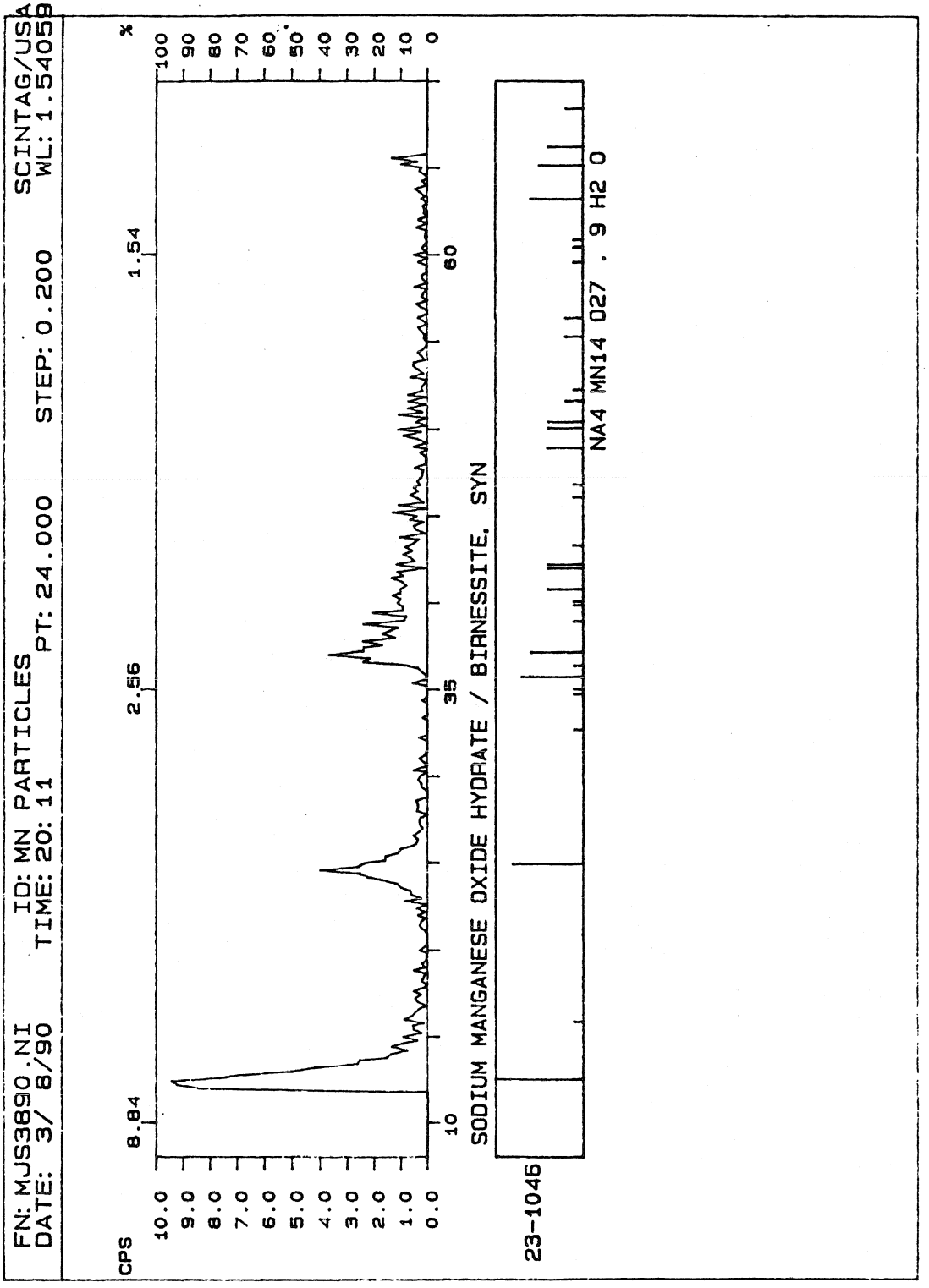

Figure 3.3: A) X-ray diffractogram of manganese oxide particles and B) matching reference diffractogram of synthetic birnessite.

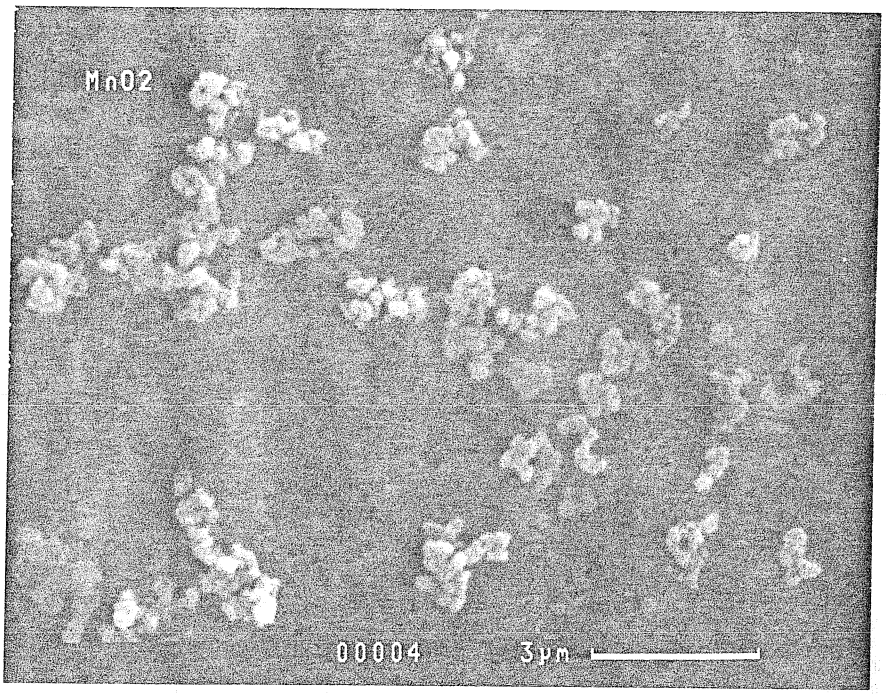

Figure 3.4: Scanning electron micrograph of birnessite particles.

wetted with 4 ml EGME in weighing bottles and the slurry allowed to stand in a dry atmosphere for 1 hour. The slurry was then placed in a dessicator which contained 100 g of dry $CaCl_2$ and a free surface of liquid EGME (approximately 40 ml). The dessicator was evacuated with a vacuum pump at room temperature until the slurry appeared to be dry and the volume of the free surface of liquid EGME had decreased by half. The sample was allowed to stand sealed for another hour before dry air was admitted. The EGME-treated particles were weighed, returned to the dessicator, and re-equilibrated for further periods of 2 hours using the same evacuation procedure. The amount of EGME retained did not change after the first evacuation. The theoretical value for complete unimolecular layer surface coverage for EGME is 3.71×10^{-4} g/m^2. Specific surface area is calculated by taking the amount of EGME retained (g/g particles) and dividing by the theoretical value.

The specific surface area of goethite was determined to be 42 m^2/g while the specific surface area of birnessite was determined to be 72 m^2/g. Table 3.2 compares these values with reported specific surface areas of other goethite and birnessite preparations.

3.4.2 Surface Exchange Capacity

Total exchange capacity of the oxide surface was determined by a back-titration method (Sigg and Stumm, 1980). A particle suspension of known concentration was equilibrated at pH 7 for goethite and pH 2.7 for birnessite. Each suspension was then adjusted to pH 11 with 0.1 M NaOH and allowed to equilibrate. The particles were removed by filtration and the filtrate titrated back to the initial

Table 3.2: Literature Values of Goethite and Birnessite Surface Properties

Reference	Surface Area (m^2/g)	Exchange Capacity (mmol/g)	pH_{zpc}
Goethite (α-FeOOH)			
Davies (1985)	34	0.734	7.5
Sigg & Stumm (1980)	29	0.2	7.8
Hayes et al. (1988)	52	0.6	8.4
Atkinson et al. (1967)	--	---	7.7
Hingston (1970)	32	0.09	8.1
Hingston et al. (1971)	60	0.16	8.1
Ainsworth et al. (1989)	34	0.92	7.5
LaKind (1988)	44	---	---
This study	42	0.326	7.6
Birnessite (δ-MnO_2)			
Morgan & Stumm (1964)	---	---	2.8 ± 0.3
Healy et al. (1966)	300	---	1.5 ± 0.5
McKenzie (1971)	32	---	---
McKenzie (1981)	93	2.31	---
Murray (1974)	270	---	2.25
Oscarson (1983b)	277	---	2.3 ± 0.1
Kanungo & Mahapatra (1989)	49	8.05	2.5
Parida et al. (1981)	71	---	---
This study	72	2.39	2.7

pH with 0.1 M $HClO_4$. The difference between the amount of base needed to raise the pH and the amount of acid needed to back titrate the filtrate is equivalent to the number of exchangeable surface sites. The surface exchange capacity of goethite was determined to be 3.26 x 10^{-4} mol/g while birnessite was found to have a surface exchange capacity of 2.39 x 10^{-3} mol/g. The birnessite value is the first to be reported for a synthetic birnessite. Comparison of other reported exchange capacities of goethite are listed in Table 3.2.

3.4.3 Surface Complexation Model

The surface chemistry of metal oxides has been discussed in detail in the literature (Schindler and Stumm, 1987; Westall, 1986, 1987; Dzombak and Morel, 1990). The metal oxide surface can be described with a coordination chemistry model which is modified to take into account electrostatic interactions. The surface groups of a metal oxide are amphoteric and can be described by surface acid-base reactions

$$>SOH_2^+ = >SOH + H^+, \quad K^s_{a1} \tag{3-3}$$

$$>SOH = >SO^- + H^+, \quad K^s_{a2} \tag{3-4}$$

where $>SOH_2^+$, $>SOH$, and $>SO^-$ represent the positively charged, neutral, and negatively charged surface species. The equilibrium constants are defined as

$$K^s_{a1} = \frac{[>SOH][H^+]}{[>SOH_2^+]}\exp(\frac{-F\Psi}{RT}) \tag{3-5}$$

$$K_{a2}^{s} = \frac{[>SO^-][H^+]}{[>SOH]}\exp(\frac{-F\Psi}{RT}) \qquad (3\text{-}6)$$

where Ψ is the surface potential (volts), R is the molar gas constant (8.314 J/mol·K), and T is the absolute temperature (K).

The surface charge and potential are a consequence of the charge species, $>SOH_2^+$ and $>SO^-$, and the surface charge density can be evaluated by applying a proton material balance relationship to titration data:

$$\sigma_o = ([>SOH_2^+] - [>SO^-])\frac{F}{A\ S_c} = (C_A - C_B + [OH^-] - [H^+]) \qquad (3\text{-}7)$$

where S_c is the solid concentration (g/L), A is the specific surface area(m^2/g), F is the Faraday constant and C_A and C_B are the resulting concentrations of acid and base added to the system. Equation (3-7) relates the surface charge density to solution pH. The pH value at which the surface proton adsorption density equals that of hydroxide ions (i.e., where proton-derived surface charge is zero) is defined as pH_{zpc}.

There are several electrostatic models that have been developed. The diffuse layer model assumes a layer of fixed charge on the surface and a diffuse layer of opposite charges in solution. A Gouy-Chapman distribution of ions is assumed for the solution side of the interface. The relationship between surface charge, σ_o, and potential, Ψ_o, is fixed by Gouy-Chapman electrical double layer theory. The surface charge density (in C/m^2) is related to the potential at the surface (in volts) by

$$\sigma_o = (8RT\epsilon\epsilon_o c \times 10^3)^{\frac{1}{2}} \sinh(ZF\Psi_o/2RT) \qquad (3\text{-}8)$$

where R is the molar gas constant (8.314 J/mol·K), T is the absolute temperature (K), ϵ is the dielectric constant of water, ϵ_o is the permittivity of free space (8.854 x 10^{-2} C/V·m), and c is the molar electrolyte concentration, and Z is the electrolyte valence.

Computer codes have been developed to solve equilibrium surface speciation calculations (e.g., SURFEQL (Faughnan, 1981)). The codes require intrinsic surface equilibrium constants and an electrostatic model to describe the surface-solid interface. The choice of the electrostatic model gives rise to a number of additional fitting parameters. Electrostatic models that have been implemented in surface chemical equilibrium computer codes are the diffuse layer model, the Stern layer model, the constant capacitance model and the triple layer model. The models differ by the treatment of the electrostatic energy associated with the charged surface. Westall and Hohl (1980) compared different surface models and concluded that the models are equivalent in their ability to fit the same titration or adsorption results, although they have different numbers of fitting parameters, such as the equilibrium constants. The diffuse layer model is chosen for this work because it is the simplest physical presentation of the interface, and thus, has the least number of fitting parameters.

3.4.4 Acid-Base Titration

3.4.4.1 Method

The surface acidity constants for goethite and birnessite surfaces were obtained by acid-base titrations. The titrations were performed in a 250 ml magnetically-stirred double-walled beaker connected to constant temperature (25 °C) water bath. N_2 gas was used to continually purge and keep the system free of CO_2. The gas was passed through a column of Ascarite II to remove any contaminant CO_2 and rehydrated through a column of D_2H_2O before being introduced into the reaction vessel. Titrations were performed on aqueous suspensions consisting of 0.1 M $NaClO_4$ and a known solid concentration. Solid concentration was determined gravimetrically by filtering 1 ml of the reaction suspension just prior to and following the titration through a 0.2 μm Nucleopore filter. For both particle preparations, the aqueous systems were adjusted to pH 4 with 1.0 M $HClO_4$ to facilitate the removal of aqueous CO_2. The goethite suspension was titrated to pH 10 by adding 10-100 μl of 0.1 M NaOH at intervals of 5 to 15 minutes. After 30 minutes at pH 4, the pH of the birnessite suspension was quickly raised to 10 with 0.1 M NaOH and equilibrated for 40 minutes. It was then titrated to pH 2 with addition of 0.1-1.0 ml of 0.1 M $HClO_4$ at intervals of 10 to 20 minutes.

3.4.4.2 Goethite

The acid-base titration data for a goethite particle suspension are plotted in Figure 3.5. Surface acidity constants were obtained by fitting the titration data with FITEQL, an iterative non-linear least squares optimization computer program

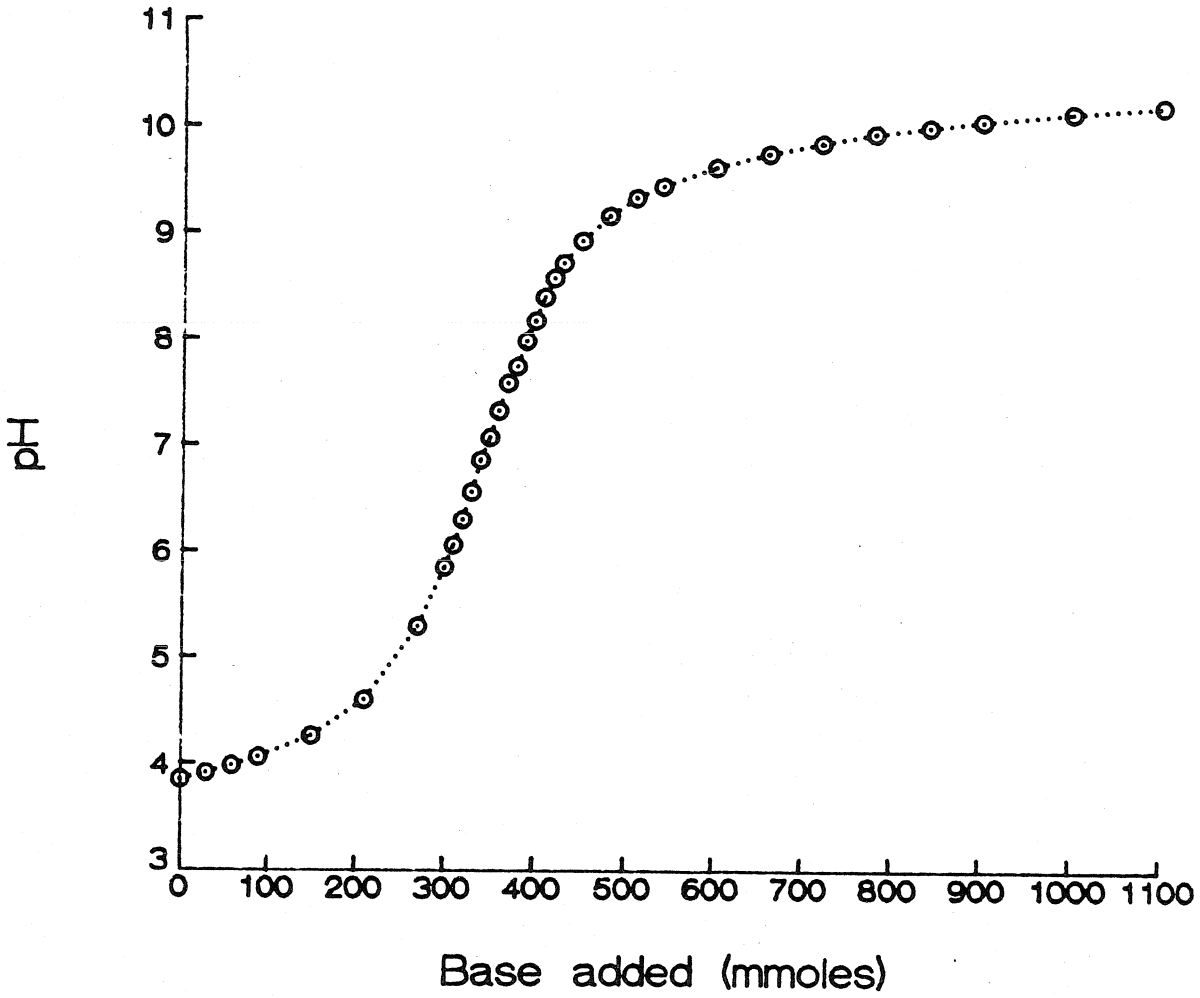

Figure 3.5: Alkalimetric titration of 1.2 g/L suspension of goethite particles at 25 °C and 0.1 M ionic strength.

(Westall, 1982). The surface acidity constants pK_{a1} and pK_{a2} for goethite were determined to be 6.4 and 8.8, respectively, and the pH_{zpc} is 7.6. These values compared well to other reported values for the goethite surface (Table 3.2).

3.4.4.3 Birnessite

The acid-base titration data are plotted in Figure 3.6. The first surface acidity constant could not be calculated using the titration data. Problems arise with the low pH data from the dissolution of the solid phase and the dilution of the sample from the large quantities of acid needed to lower the pH further. As a result of being unable to calculate pK^s_{a1} from the acid-base titration, another method was needed to independently determine the pH_{zpc} of the birnessite particles in order to calculate pK^s_{a1}. A coagulation-subsidence method was used and is discussed in the next section.

It is possible to use the titration data to calculate the second surface acidity constant. From the titration data, the surface charge at each point on the titration curve can be calculated using the charge balance equation (3-7). $[H^+]$ and $[OH^-]$ are calculated from the pH measurement using activity corrections calculated from the Davies equation ($\gamma_+ = \gamma_- = 0.774$). The total concentration of surface sites S_T is the product of the solid concentration and the exchange capacity.

$$S_T = [>SOH] + [>SOH_2^+] + [>SO^-] \qquad (3\text{-}9)$$

The pH_{zpc} is the pH at which $[>SOH_2^+] = [>SO^-]$. At $pH \ll pH_{zpc}$, $\sigma_o \approx [>SOH_2^+]$, and thus,

$$[>SOH] = S_T - \sigma_o \qquad (3\text{-}10)$$

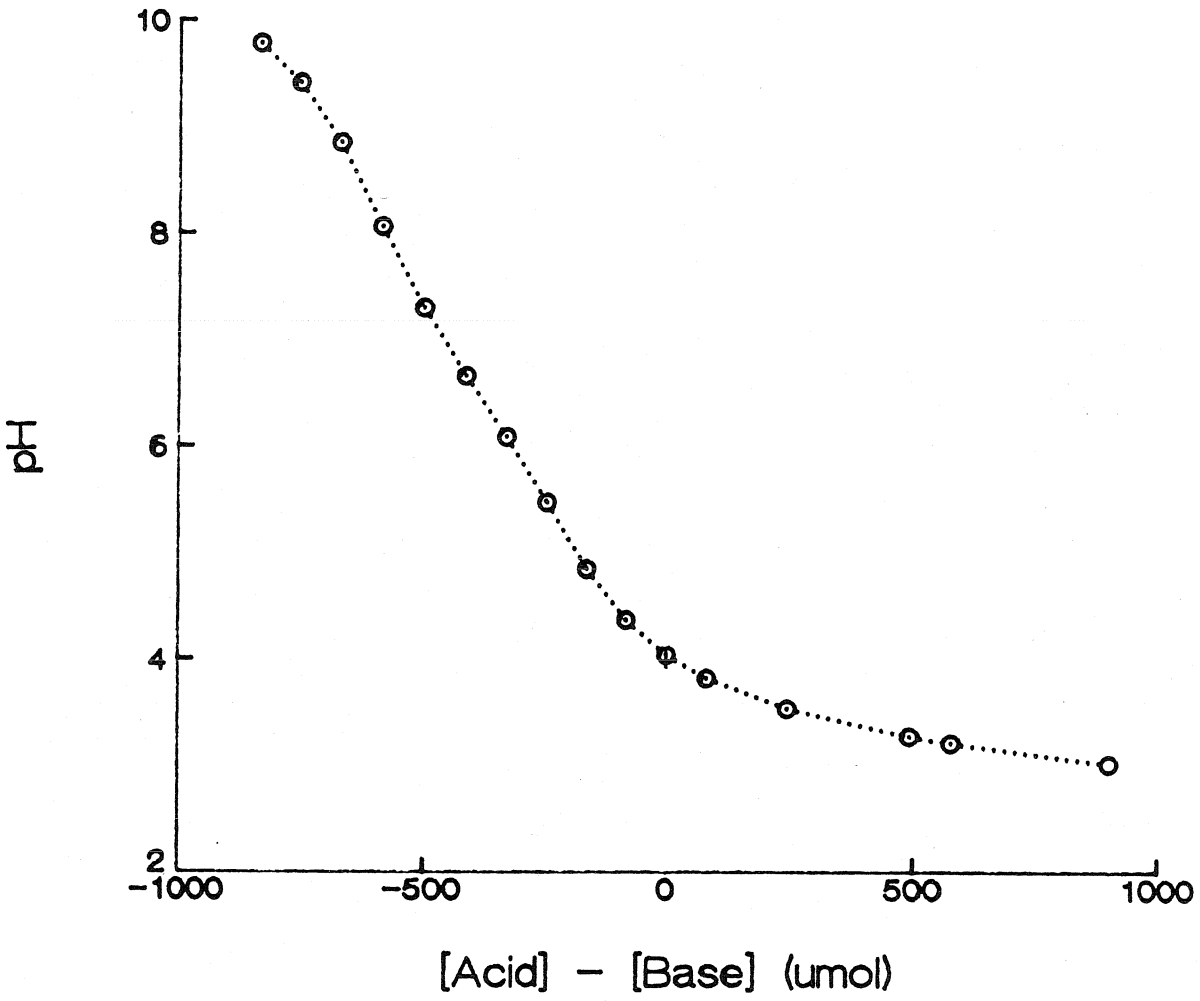

Figure 3.6: Acidimetric titration of 0.8 g/L suspension of birnessite particles at 25 °C and 0.1 M ionic strength.

At pH » pH_{zpc}, $\sigma_o \cong -[>SO^-]$, and

$$[>SOH] = S_T + \sigma_o \qquad (3\text{-}11)$$

Using these approximations, the apparent surface acidity constants can be calculated from equations (3-5) and (3-6). A plot of apparent pK^s_{ai} against surface charge is linear except near pH_{zpc}. By extrapolating the linear portion of this plot to zero surface charge, the value of the intrinsic surface acidity constant can be obtained. Figure 3.7 is a plot of apparent pK^s_{a2} against surface charge calculated from the titration data. Extrapolation of the data gives an intrinsic second surface acidity constant $pK^s_{a2} = 4.9$.

3.4.5 Determination of Birnessite pH_{zpc}

The pH of zero point of charge of the birnessite preparation was determined by adapting a coagulation-subsidence method of Healy et al. (1966). In the coagulation-subsidence method, the pH at which the coagulation-subsidence rate of a particle dispersion is a maximum corresponds to the pH_{zpc}. This is verified by independent electrophoretic measurements. Rates of coagulation and subsidence are followed by measuring the transmittance of a particle suspension over time. Particle suspensions were prepared at various pH values (1.5-4.0) and ionic strengths (0.01 M and 0.1 M NaCl) by mixing pH and ionic strength buffer solutions with the stock particle suspension. The stock particle suspension was sonicated for at least 10 minutes before being mixed with the buffer solutions. Immediately upon mixing the particle and buffer solutions, the sample was transferred to a 1 cm quartz cell, placed

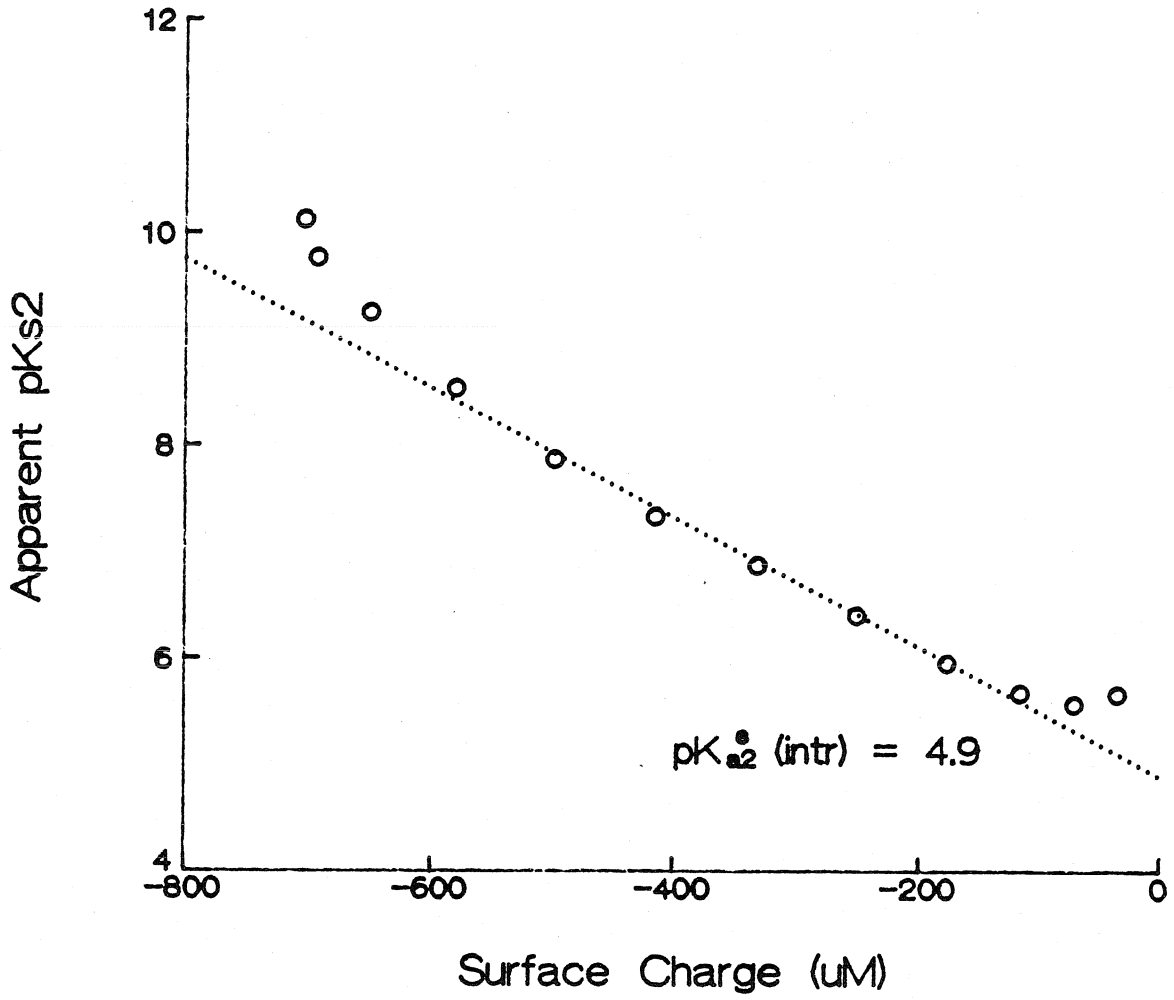

Figure 3.7: A plot of the second apparent surface acidity constant as a function of surface charge σ_o. Extrapolation to zero surface charge gives the intrinsic acidity constant.

in the spectrophotometer (Hewlett Packard 8451A Diode Array Spectrophotometer) and transmittance was measured at λ = 600 nm over a time period of 120 minutes.

The transmittance of birnessite suspensions at several pH values as a function of time is plotted in Figure 3.8. At all pH values, the transmittance is initially constant. The slopes of the curves appear to increase after approximately 1200 seconds. The rates of coagulation-subsidence were determined by linear regression of the data from 1440 to 3600 seconds. Figure 3.9 is a plot of the rate of coagulation-subsidence against pH at two different ionic strengths. The maximum rate corresponding to the pH_{zpc} occurs at pH 2.7 for both ionic strengths.

This value compares well with other reported values for the pH_{zpc} of birnessite (Table 3.2). With this independent determination of the pH_{zpc}, a value for pK^s_{a1} can be calculated, and this value is 0.5.

3.4.6 Oxide Surface Speciation

The surface acidity constants can be used with SURFEQL to determine the surface speciation at a given pH. Figures 3.10 and 3.11 show the distribution of protonated, neutral, and deprotonated surface sites of goethite and birnessite, respectively, over the pH range 2-11. The neutral sites dominate the distribution over the pH range of most natural waters.

3.4.7 Summary of Surface Characterization

The surface properties determined for goethite and birnessite are summarized in Table 3.3. The goethite surface properties compare well with those of previous

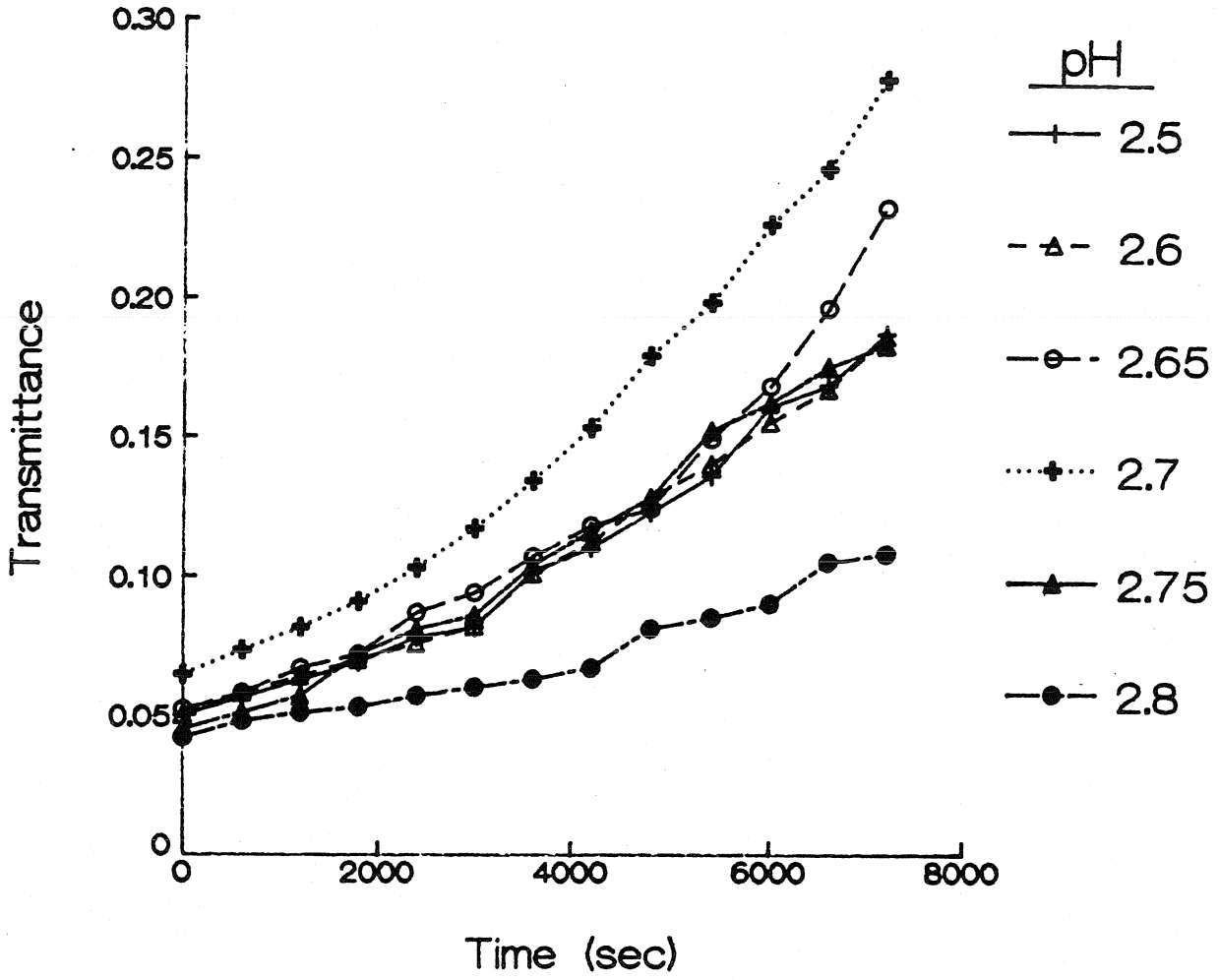

Figure 3.8: The transmittance of birnessite suspensions as a function of time at several pH values and an ionic strength of 0.01 M.

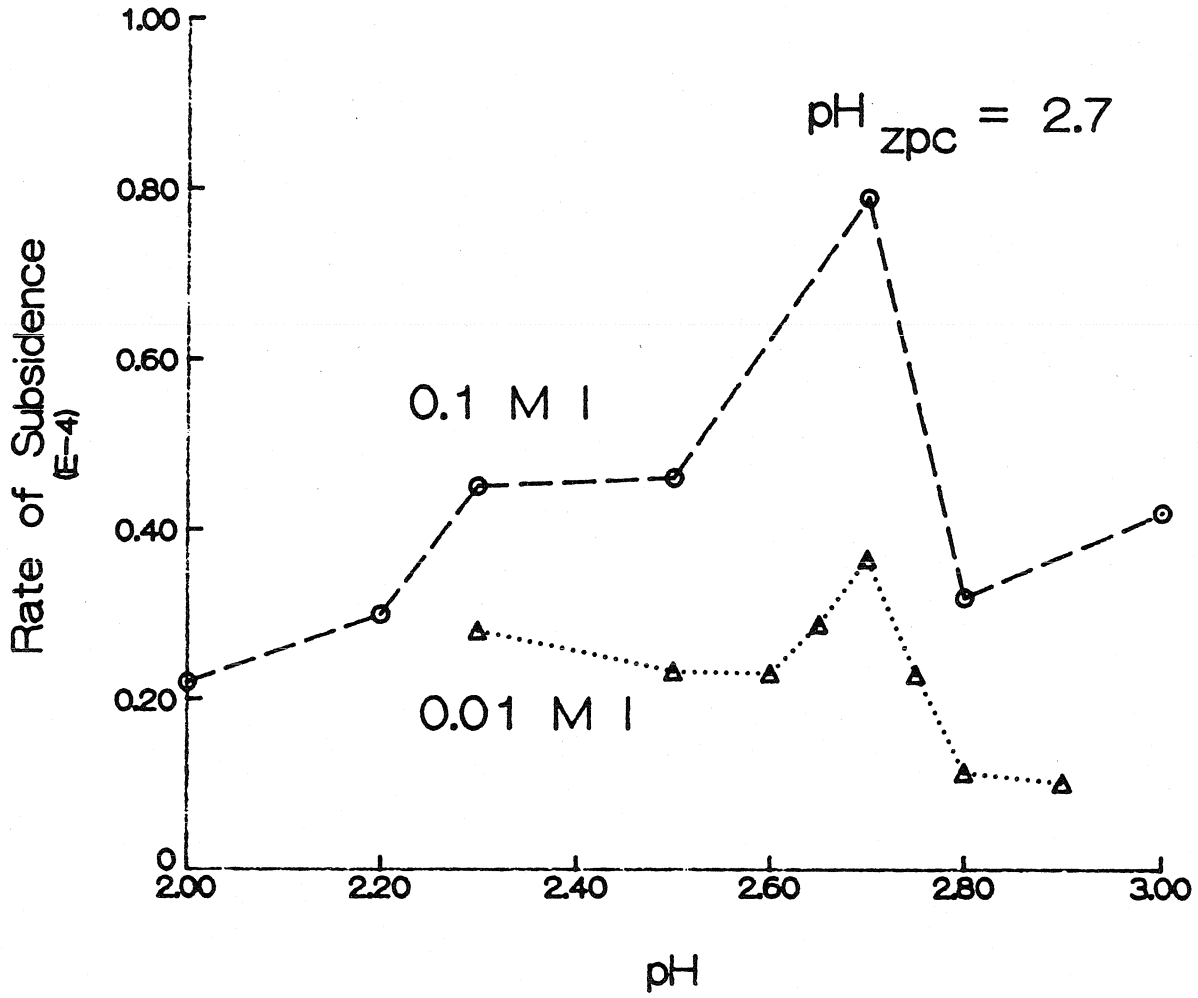

Figure 3.9: The rate of coagulation and subsidence of a birnessite suspension as a function of pH at an ionic strength of 0.01 and 0.1 M. The maximum rate corresponds to the pH_{zpc} of the oxide.

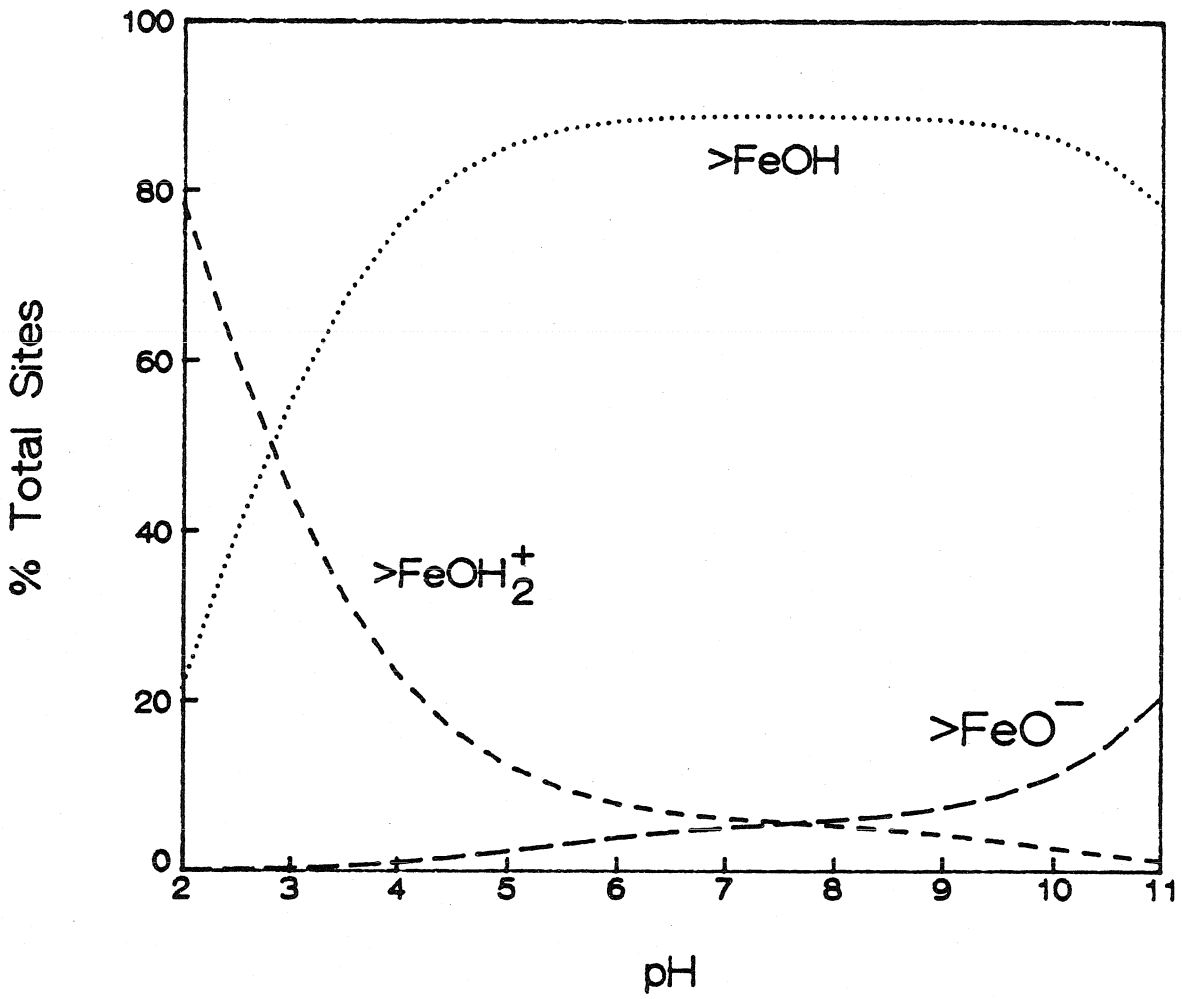

Figure 3.10: Surface speciation of goethite from pH 2-11 at an ionic strength of 0.1 M. Calculations made by SURFEQL with diffuse layer model.

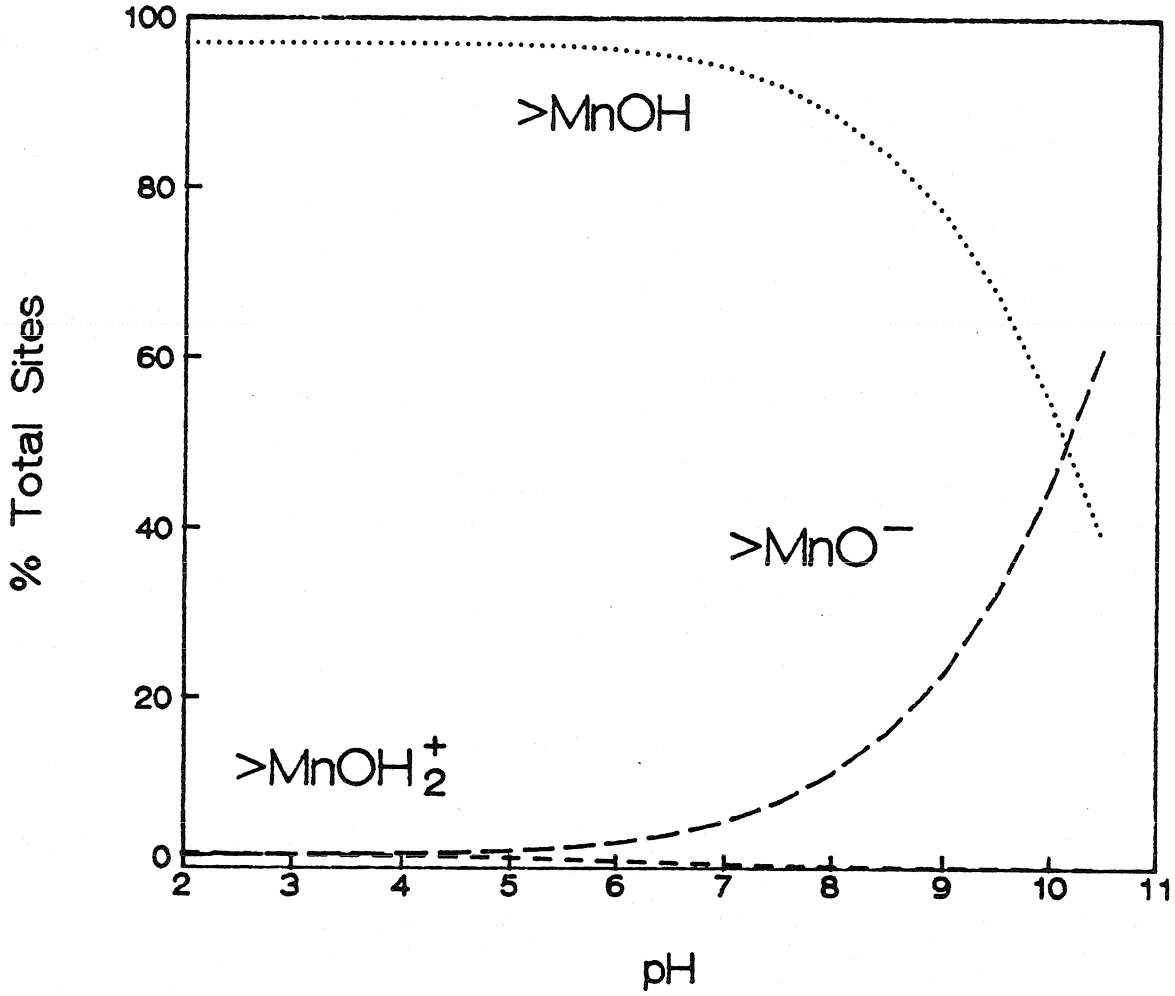

Figure 3.11: Surface speciation of birnessite from pH 2-11 at an ionic strength of 0.1 M. Calculations made by SURFEQL with diffuse layer model.

Table 3.3: Surface Properties of Metal Oxides

Mineral	Goethite	Birnessite
Formula	α-FeOOH	δ-MnO_2
Synthesis Method	Atkinson, 1967	McKenzie, 1977
Specific Surface Area (m^2/g)	42	72
Exchange Capacity (mmoles/g)	0.326	2.39
Site Density ($\#/nm^2$)	4.7	20
Surface Acidity Constants (Diffuse Layer Model)		
pK^s_{a1}	6.4	0.5
pK^s_{a2}	8.8	4.9
pH_{zpc}	7.6	2.7

investigators (Table 3.2). The values of the intrinsic surface acidity constants for birnessite are the first to be reported.

Chapter 4

ANION ADSORPTION KINETICS AND EQUILIBRIA WITH GOETHITE AND BIRNESSITE

4.1 Introduction

This chapter presents experimental results and discusses the rates and mechanisms of adsorption and desorption of arsenic and selenium oxyanions on goethite (α-FeOOH) and birnessite (δ-MnO_2). Anion adsorption involves a ligand exchange between the anion and a surface hydroxyl group in which the anion binds directly to a surface metal center. The general adsorption-desorption reaction between an anion (A^-) and an oxide surface (>SOH) can be described as:

$$>SOH + HA \underset{k_d}{\overset{k_a}{\rightleftharpoons}} >SA + H_2O \qquad (4\text{-}1)$$

where k_a and k_d are the rate constants for the adsorption and desorption reactions.

The reactions are monitored by measuring the aqueous concentration of the adsorbing species as a function of time. The initial rates of the adsorption of As(III), As(V), Se(IV), and Se(VI) on goethite and birnessite were studied and compared with the initial rates of adsorption of Mn(II), a cation, on birnessite. The kinetics and equilibria of As(III) adsorption on goethite were examined in greater detail by investigating the influence of pH and temperature.

The experimental results are interpreted with a kinetic model that accounts for both adsorption and desorption. The rate of adsorption (R_a) is a function of the

concentrations of the adsorbing species and the reactive surface sites while the rate of desorption (R_d) is a function of the concentration of adsorbed species:

$$R_a = k_a[>SOH][HA] \quad (4\text{-}2)$$

$$R_d = k_d[>SA] \quad (4\text{-}3)$$

The total concentration of the reactive surface sites is determined by the product of the exchange capacity of the oxide surface and the solid concentration of the particle suspension.

The change in the aqueous concentration of the anion is found by accounting for both adsorption and desorption:

$$-\frac{d[A^-]}{dt} = R_a - R_d \quad (4\text{-}4)$$

The expression is solved numerically using the Forward Euler Method (Forsythe et al., 1977). The Fortran computer code used to generate the model values is listed in Appendix B. Values of the rate constants are obtained from the best fit of the kinetic model to the observed aqueous profiles.

The adsorption of As(V), Se(IV), and Se(VI) on goethite has been described earlier with a surface complexation model (Chapter 2, Section 3.3). The adsorption equilibrium of As(III) on goethite is interpreted with a surface complexation model in order to fill a void in surface chemical modeling data.

4.2 Experimental Methods

4.2.1 Adsorption Kinetic Experiments

The kinetics of adsorption and desorption of aqueous As(III), As(V), Se(IV),

and Mn(II) onto metal oxide surfaces were studied by following the disappearance of the solute over time intervals of minutes to hours. Metal oxide suspensions of constant ionic strength (0.1 M $NaClO_4$ for As and Mn(II) and 0.001 M $NaNO_3$ for Se) and constant pH (4-10) were prepared in a 250 ml magnetically-stirred double-walled beaker connected to a constant temperature water bath. N_2 gas was used to purge the system of CO_2. The gas was passed through a column of Ascarite II to remove any contaminant CO_2 and rehydrated through a column of D_2H_2O before being introduced into the reaction vessel. Solid concentration was determined gravimetrically just prior to and following the experiment by filtering 1-3 ml of the reaction suspension through a 0.2 μm Uniflo filter unit. Solid concentrations of 1-2 g/L goethite and 0.2-0.3 g/L birnessite were used in order to have a surface site concentration of approximately 500 μM in each experiment. The aqueous systems were adjusted to pH 4 with 1.0 M $HClO_4$ to facilitate the removal of aqueous CO_2. After at least 3 hours and usually overnight, the pH was readjusted with 0.1 M $HClO_4$ or NaOH to the planned pH value of the experiment. pH was kept constant during an experiment with small additions of 0.1 M $HClO_4$ or NaOH when the pH had drifted ±0.05 pH units from the initial pH. The oxide suspensions were allowed to equilibrate for at least two hours at the new pH before a known concentration of the solute of interest was added to the system and mixed thoroughly. The reaction was followed by periodically withdrawing and filtering a few milliliters through a 0.2 μm Uniflo filter unit for analysis. The Mn(II) samples were acidified with concentrated HCl to pH 1 to prevent any oxidation. The effect of temperature on

the rate and extent of the As(III) reactions with goethite was studied by conducting a series of experiments at 15, 25, and 35 °C.

4.2.2 Adsorption Equilibrium Experiments

Adsorption equilibrium of arsenite onto goethite was studied at various pH values and an ionic strength of 0.1 M. Goethite suspensions were prepared as described in Section 4.2.1. The system pH was initially 4 and adjusted with 0.1 M $HClO_4$ or 0.1 M NaOH when a different pH value was being studied.

For the adsorption isotherm experiments conducted at a constant pH, a known amount of arsenite was added to the system and the pH re-adjusted with 0.1 M $HClO_4$. After a sufficient equilibrium time (3-16 hours), 2.5 ml of the suspension was withdrawn and filtered through a 0.2 μm pre-rinsed Uniflo filter disk. The filtrate was analyzed for As(III) in solution. More arsenite was then added to the system and the process repeated until the adsorption of As(III) reached a maximum.

The effect of pH on arsenite adsorption was studied by serial titration of a goethite suspension amended with 50 μM arsenite. With the system initially equilibrated at pH 3.2, arsenite was added and the system re-equilibrated before a subsample of 3 ml was withdrawn and filtered. The pH of the system was then raised with 0.1 M NaOH and the system re-equilibrated before another subsample was withdrawn and filtered. The process continued until the pH reached 11.5. The filtered subsamples were analyzed for As(III).

4.2.3 Chemical Analysis

4.2.3.1. As(III): Differential Pulse Polarography

As(III) in filtered samples was determined by a differential pulse polarography method using a Princeton Applied Research Model 174A polarographic analyzer with a EG&G PARC Model 303 Static Mercury Drop Electrode (SMDE) unit (Princeton Applied Research, 1976). The instrument settings and operation conditions are listed in Table 4.1. A procedure for a typical analysis was as follows: (i) add blank (9.0-9.8 ml 1 M HCl) and purge for 4-6 minutes to remove any dissolved oxygen and then scan between -0.25 and -0.50 volts; (ii) add unknown to bring volume to 10 ml, purge for 2 minutes to remove any dissolved oxygen and to thoroughly mix sample, and scan; (iii) add 100 µl 10^{-4} M As(III) as a standard, purge for 2 minutes, and scan; and (iv) add another 100 µl 10^{-4} M As(III) and repeat purge and scan. Concentration of As(III) in solution is calculated from the following equation:

$$[As(III)] = \frac{i_u \, v \, C_s \, D_f}{(i_u - i_s)V} \qquad (4\text{-}5)$$

where i_u is the peak height of the unknown from the blank

i_s is the peak height of the standard addition from the blank

v is the volume of the standard addition

C_s is the concentration of the standard addition

V is the initial total volume (before any standard addition)

D_f is the dilution factor (Volume of blank/Volume of unknown).

As(III) values from repeated standard additions were averaged and reported.

Table 4.1: DPP Instrument Settings for As(III) Analysis

M303	Electrode Mode:	Dropping Mercury
	Drop Size:	Small
M174A	Scan Rate:	2 mV/sec
	Direction:	Negative
	Range:	0.75 volts
	Initial Potential:	-0.25 volts
	Modulation Amplitude:	100 mV (PP)
	Operating Mode:	Differential Pulse
	Current Range:	1 μA Full Scale
	Drop Time:	2 sec
	Offset:	Off
	Display Direction:	+
	Low Pass Filter:	Off

Detection limits for As(III) using the standard addition method were 0.5 μM and the precision of duplicate samples was within 5 percent.

4.2.3.2 As(V): Molybdate Blue Spectrophotometry

A spectrophotometric method for the determination of As(V) was adopted from Johnson and Pilson (1972) and Oscarson et al. (1980). The method is similar to the classical molybdate blue method for phosphate determination and is based on the fact that As(V), like phosphate, forms a blue complex with molybdate, but As(III) does not. For each sample, 1 ml was mixed with 0.4 ml of a color reagent (mixing ratio 10:1:3:6 of 5 N sulfuric acid, 0.74 M potassium antimony tartrate, 0.22 M ammonium molybdate, and 0.01 M ascorbic acid) and diluted to 5 ml. Samples containing low amounts of As(V) were spiked with an As(V) standard. After 75 minutes of color development, the absorbance was measured on a Hewlett Packard HP8451 Diode Array Spectrophotometer in a 1 cm quartz cell. The

As(V)-molybdate complex has a broad maximum absorbance with the peak at 865 nm and a second broad absorbance peak at 724 nm. The absorbance of the complex was measured at 724 nm.

4.2.3.3 Mn(II): DCP Emission Spectrometry

Mn(II) was determined using a Beckman Spectra Span VB Direct Current Plasma (DCP) Emission Spectrometer. Filtered samples were acidified with concentrated HCl and diluted before analysis. Standards were made by dilution of a 1000 ppm Mn standard solution (VWR). Detection limits were less than 0.3 μM and the precision of replicate runs was 2 percent.

4.2.3.4 Se(IV) and Se(VI): Ion Chromatography

Se(IV) and Se(VI) were determined simultaneously using a Dionex 2020i ion chromatographic analyzer with a ASA4 anion column and a bicarbonate/carbonate eluent. 25 μl eluent stock was added to each 2.5 ml sample before injection. Se(IV) has a retention time of 1.7 minutes while Se(VI) elutes at 4.7 minutes. Detection limits for both oxidation states were 1 μM and the precision of replicate runs was less than 1 percent.

4.3 Kinetics of Adsorption

4.3.1 Initial Rate of Adsorption

The initial behavior of As and Se anions following addition to aqueous suspensions of goethite and birnessite particles was monitored in a set of experiments at pH 4 and 25 °C. The initial behavior of Mn^{2+}(aq) in a birnessite particle suspension was also monitored at 25 °C and pH values of 4 and 6. The reaction

conditions of each initial rate experiment are listed in Table 4.2 and the experimental data are listed in Appendix A. Figure 4.1 illustrates the disappearance of the aqueous species with time at pH 4, 25 °C, and ionic strength 0.1 M for the As and Mn experiments and 0.001 M for the Se experiments. The ionic strength of the Se experiments is lower than in the other experiments as a result of analytical problems in the determination of Se(IV) and Se(VI) at high salt concentrations. Even though the experiments were run at different ionic strengths, the Se(IV) results can still be compared with the As results. Hayes et al. (1987) reported that the adsorption of Se(IV) on goethite does not change with ionic strength. They attributed the observation to the formation of an inner sphere complex with Se(IV) and the goethite surface. Se(VI) forms an outer sphere complex with the surface and no Se(VI) adsorption was observed in preliminary experiments under similar conditions.

In the goethite suspension, the initial rate of adsorption is nearly identical for As(V) and Se(IV) with the initial rate of As(III) adsorption slightly slower. However, As(V) is adsorbed to the greatest extent, with only 40 percent of the initial concentration remaining in solution after 60 minutes. After the same reaction period, 50 percent of the initial Se(IV) and 65 percent of the initial As(III) still remains in solution.

In the birnessite suspension, the initial rate of adsorption appears to be the greatest for Mn(II), followed by As(III) and Se(IV). There was no As(V) adsorption on the birnessite surface at pH 4 over a time period of 120 minutes. The initial rates can be qualitatively linked to the effect of the electrostatic charge on the birnessite

Table 4.2: Reaction conditions of adsorption kinetics experiments

Expt.	Solute	Conc. (μM)	Oxide	[SOH] (μM)	pH
G4AS3	As(III)	100	G	541	4
B4AS3	As(III)	100	B	478	4
G4AS5	As(V)	50.1	G	619	4
B4AS5	As(V)	100	B	478	4
G4SE4	Se(IV)	100	G	490	4
B4SE4	Se(IV)	100	B	478	4
B4MN2	Mn(II)	98.9	B	478	4
B6MN2	Mn(II)	98.8	B	478	6

G = Goethite, B = Birnessite, SOH = Surface metal group; T = 25 °C, N_2(g) purge

surface. At pH 4, the birnessite surface is slightly negatively charged (pH_{zpc} = 2.7), Mn(II) is a bivalent cation (Mn^{2+}), As(III) is a neutral species (H_3AsO_3), and Se(IV) is an anion ($HSeO_3^-$). The observations suggest that under the experimental conditions, the more positive the charge of the species is, the faster the initial rate of adsorption of the species on birnessite.

After 60 minutes of reaction, Mn(II) and Se(IV) are approaching equilibrium with the surface. Seventy percent of the initial Mn(II) and 82 percent of the initial Se(IV) remain in solution, whereas only 2 percent of the initial As(III) remains in solution. The rapid depletion of As(III) from solution is the result of additional processes affecting the As(III) concentration. A fast redox reaction between adsorbed As(III) and surface Mn(IV) and a rapid release of the products As(V) and

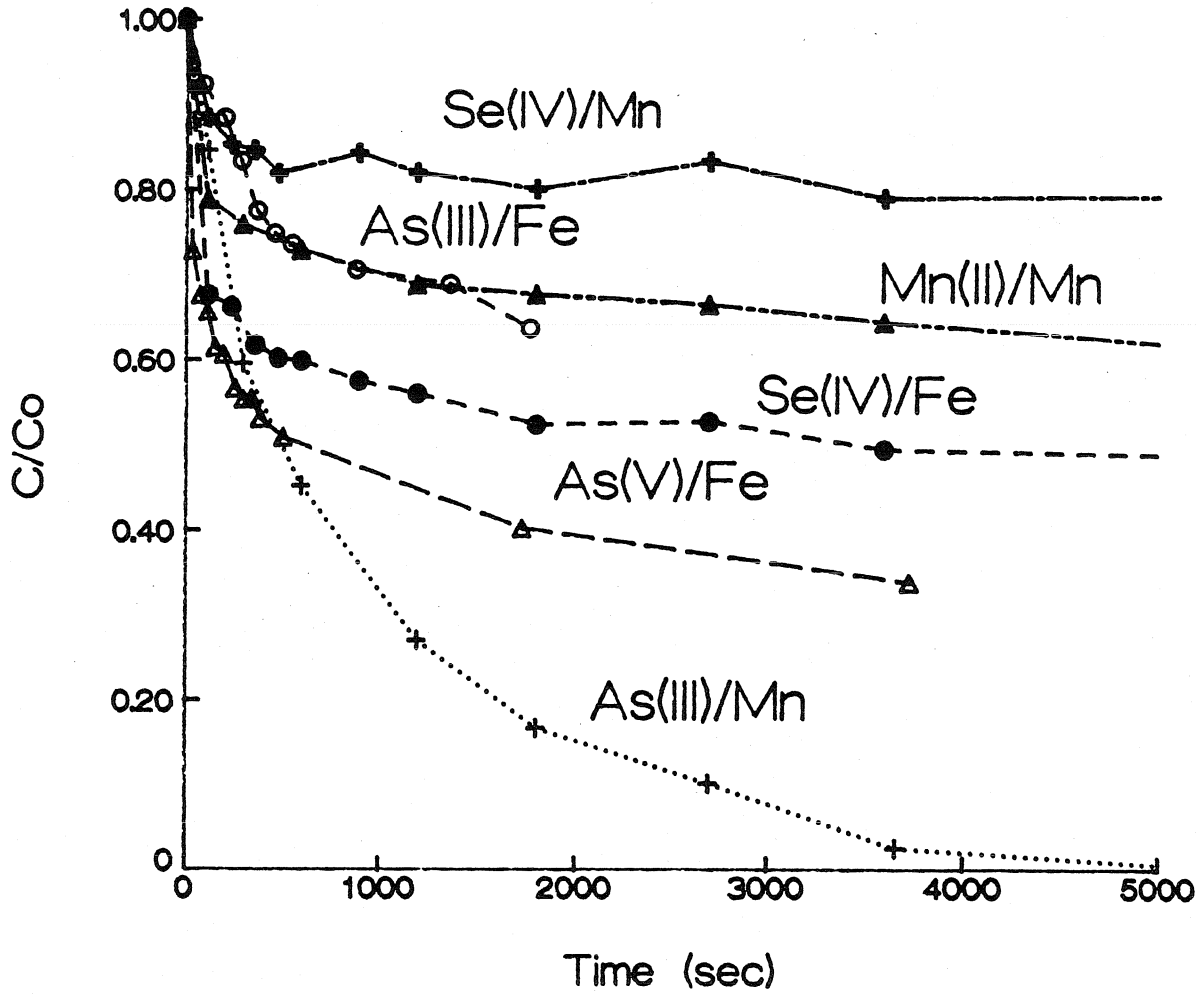

Figure 4.1: Observed rates of disappearance from solution of As(III), As(V), Se(IV), and Mn(II) in aqueous suspension of goethite and birnessite at pH 4 and 25 °C.

Mn(II) allows additional As(III) to be absorbed. Reactions between As(III) and birnessite are discussed in Chapter 5.

The initial rate of As(V) and Se(IV) adsorption on birnessite is slower than on goethite at pH 4. The results suggest an apparent electrostatic effect between the oxide surface and the solutes. At the pH of the experiments, the goethite surface is positively charged, the birnessite surface is slightly negatively charged, and As(V) and Se(IV) are both negatively charged species. Thus, the rate of adsorption on goethite is enhanced by the electrostatic attraction between the surface and the anion, while the rate of adsorption on birnessite is hindered by a small electrostatic repulsion.

The experimental data were interpreted with the kinetic model and the values of the fitted rate constants are listed in Table 4.3. The results at pH 4 indicate the rate constants for the reactions between the various solutes and oxide surfaces are approximately equivalent, ranging from 2 to 8 $M^{-1}sec^{-1}$ for k_a and 0.002 to 0.005 sec^{-1} for k_d. The only exception is the value of k_d for As(III) desorption from birnessite, which is an order of magnitude greater than the other k_d values. The values of k_a and k_d for the As(III)-birnessite data set are extracted with a more complex kinetic model which includes steps for electron transfer, release and re-adsorpion of the products As(V) and Mn(II).

4.3.2 Effect of pH on Mn(II) Adsorption on Birnessite

The extent of Mn(II) adsorption on birnessite increases with pH (Murray, 1975). The experimental results indicate that the rate of adsorption also increases with pH (Figure 4.2). The value of the rate constant k_a increases from 5 $M^{-1}sec^{-1}$ at

Table 4.3: Adsorption-Desorption Rate Constants

Solute	Oxide	pH	$k_a (M^{-1}sec^{-1})$	$k_d (sec^{-1})$	log K_1
As(III)	Goethite	4	2	0.002	3.0
As(V)	Goethite	4	8	0.004	3.3
Se(IV)	Goethite	4	6	0.003	3.3
As(III)	Birnessite	4	5	0.02	2.4
Se(IV)	Birnessite	4	2.5	0.005	2.7
Mn(II)	Birnessite	4	5	0.005	3.0
Mn(II)	Birnessite	6	12	0.0003	4.6

pH 4 to 12 $M^{-1}sec^{-1}$ at pH 6. The rate of Mn(II) desorption decreases when pH increases from 4 to 6. The value of the rate constant k_d decreases from 0.005 sec^{-1} at pH 4 to 0.0003 sec^{-1} at pH 6. The combined effects result in an increase in the value of the apparent equilibrium constant K_1; the value increases from 10^3 at pH 4 to $10^{4.6}$ at pH 6. The results compare well with rate constants obtained from pressure-jump kinetic studies for Mn(II) adsorption on γ-Al_2O_3 (Yasunaga and Ikeda, 1987). A value of approximately 40 $M^{-1}sec^{-1}$ is reported for the adsorption rate constant and a value of $10^{4.7}$ is listed as the equilibrium constant between γ-Al_2O_3 and Mn(II). However, the authors do not indicate whether the results are from a single pH experiment or from a broad range of pH values. As our results indicate, the values of the rate constants are dependent upon the pH of the solution.

4.3.3 Sensitivity of the Kinetic Model

The sensitivity of the kinetic model was examined with the data set of As(V)

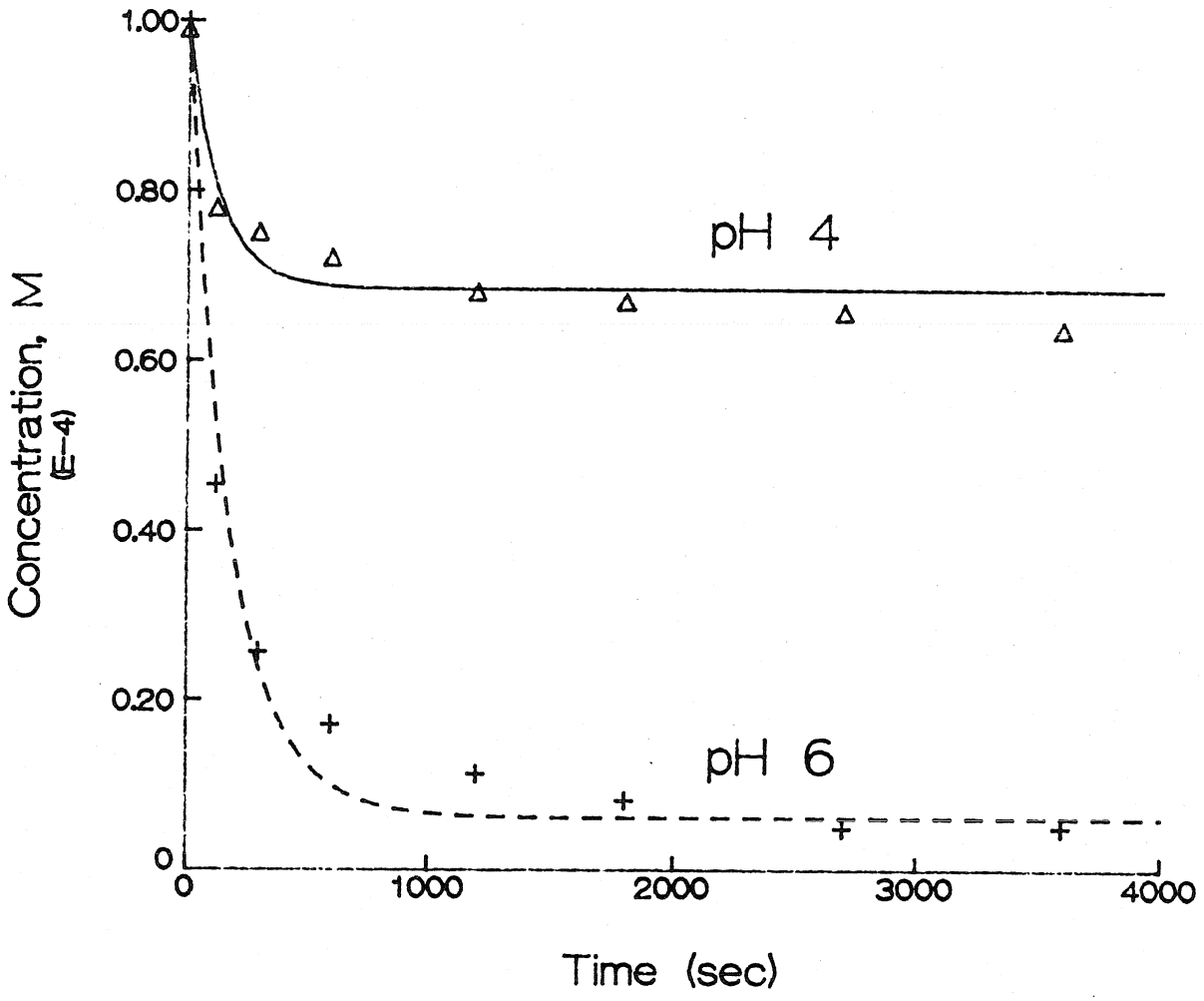

Figure 4.2: Experimental and kinetic model (lines) results of pH effect on Mn(II) adsorption on birnessite.

adsorption on goethite (experiment G4AS5) in order to get an idea of the importance of each process and size of each rate constant to the overall rate of reaction. In general, the value of k_a is determined by the initial slope of the species concentration versus time profile and the value of k_d is determined by the concentration at equilibrium. Figure 4.3 illustrates the effect of varying one of the model variables (k_a, k_d, K_1, and [>SOH]) while keeping the others constant. Figure 4.3a shows that by increasing the value of k_a from 6 to 8 and 10 $M^{-1}sec^{-1}$, both the initial rate and the amount adsorbed at equilibrium increase. Also, the time required to reach equilibrium decreases as k_a increases.

Figure 4.3a also illustrates the limitations of a simple kinetic model. The experimental data indicate that As(V) reaches equilibrium more slowly than predicted by the simple kinetic model. The initial data points are best modeled when k_a = 10 $M^{-1}sec^{-1}$, but this value overpredicts the adsorption at intermediate times (200 sec < t < 500 sec). The data points at intermediate times are best modeled when k_a = 6 $M^{-1}sec^{-1}$, but this value of k_a underpredicts both the initial data points and the data points at longer times and at equilibrium. The intermediate value of k_a = 8 $M^{-1}sec^{-1}$ gives the best fit of all of the experimental data points.

Figure 4.3b shows similar effects when k_d is varied. Increasing the value of k_d decreases the initial rate of adsorption and the amount of As(V) adsorbed at equilibrium. In addition, the time required to reach equilibrium increases with decreasing values of k_d.

Figures 4.3a and 4.3b depict the variation of the kinetic model to changing

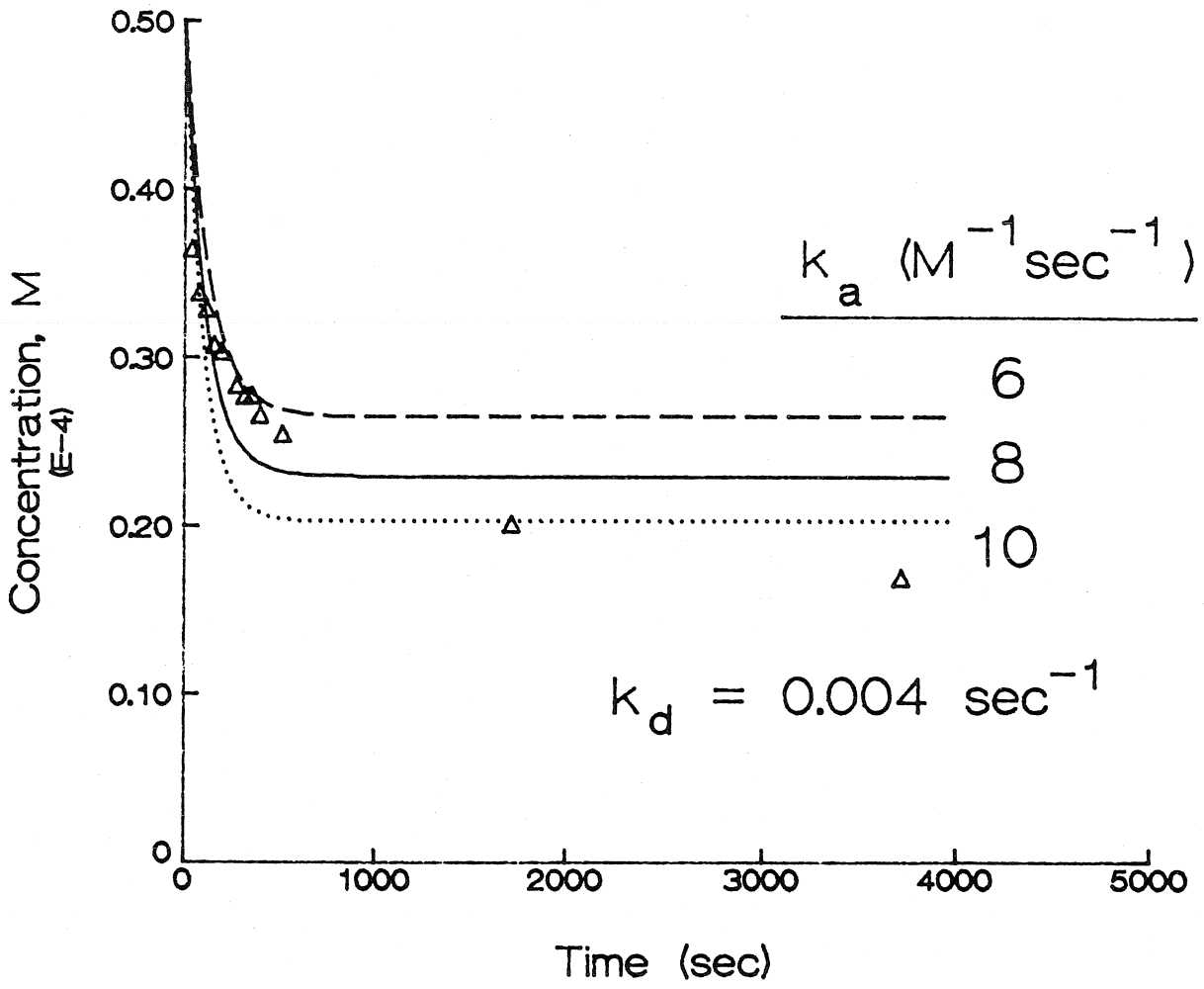

Figure 4.3: Sensitivity of kinetic model on As(V) adsorption on goethite: a) Effect of varying k_a with constant k_d.

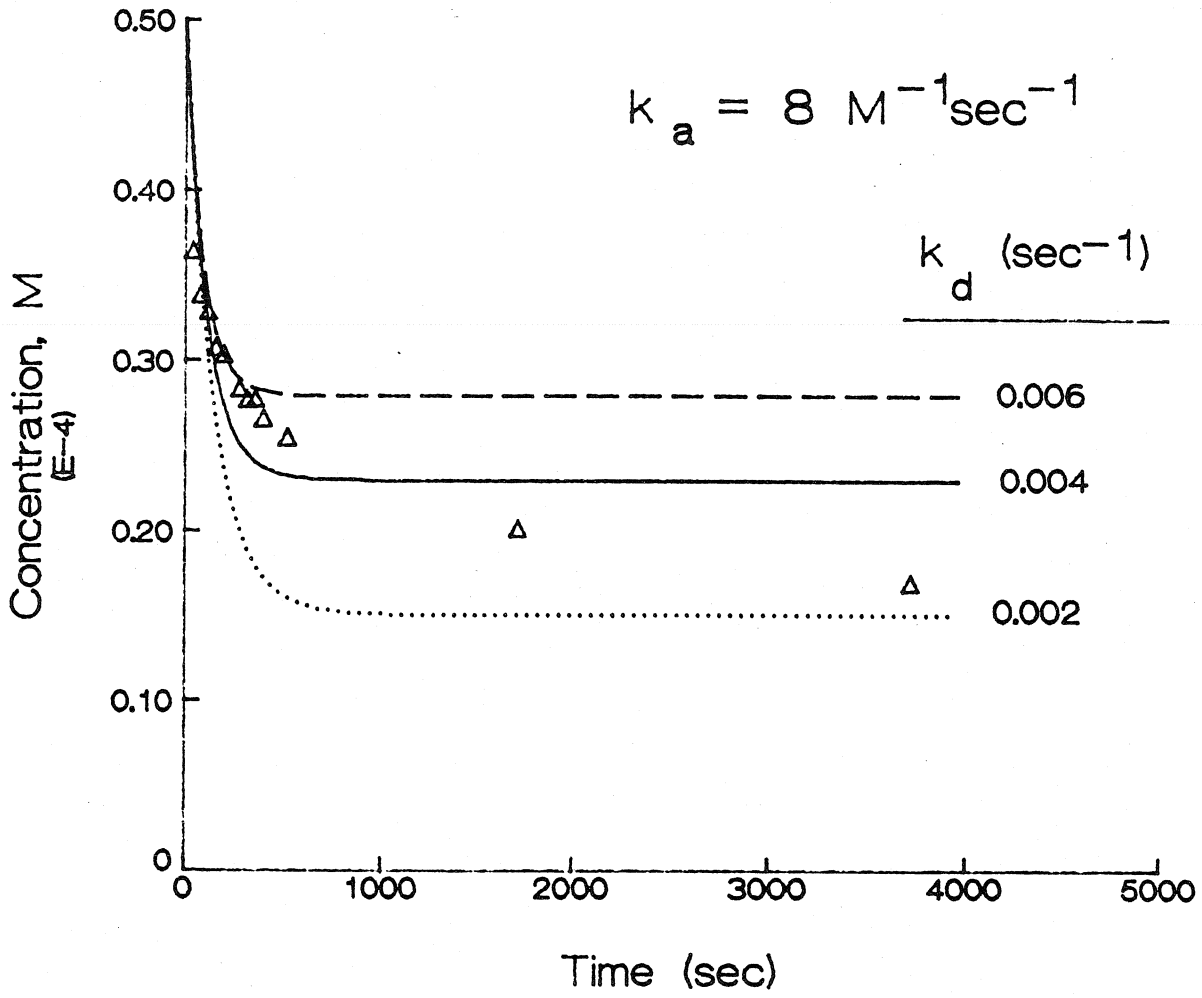

Figure 4.3: Sensitivity of kinetic model on As(V) adsorption on goethite: b) Effect of varying k_d with constant k_a.

values of the equilibrium constant. Figure 4.3c illustrates the effect of changing both rate constants but keeping the same ratio between the rate constants (i.e., the value of K_1 is not changed). The predicted equilibrium concentration does not change, but by increasing the value of the rate constants, the initial rate increases, and the time to reach equilibrium is shortened.

The influence of the initial concentration of reactive surface sites $[>SOH]_o$, is examined in Figure 4.3d. By varying $[>SOH]_o$, the initial rate, the time to equilibrium, and the equilibrium concentration are all affected. For a goethite suspension, the difference between the surface site concentrations of 520 and 720 μM is equivalent to differences in solid concentrations of 1.6 and 2.2 g/L.

The simple kinetic model may be improved by adding parallel reactions involving a range in the reactivity of the surface groups. For example, instead of considering the mineral surface to be homogeneous in reactivity, the surface can be divided into groups with varying reactivity. Infrared spectroscopic studies have indicated the existence of different types of hydroxyl sites on metal oxides (Boehm, 1971; Parfitt et al., 1977). Yates (1975) reported that the different exposed crystal planes of goethite vary in respect to the number of ionizable protons per nm^2. The surface crystal planes 100, 010, and 001 make up 60, 35 and 5 percent of the surface, respectively, and have a calculated number of ionizable protons per nm^2 of 13.4, 21.8, and 22.0, respectively, with an average of 16.6 ionizable protons per nm^2. It may be possible that the number of sites on a crystal plane influences the reactivity of the sites. Dzombak and Morel (1990) present a surface complexation model in which

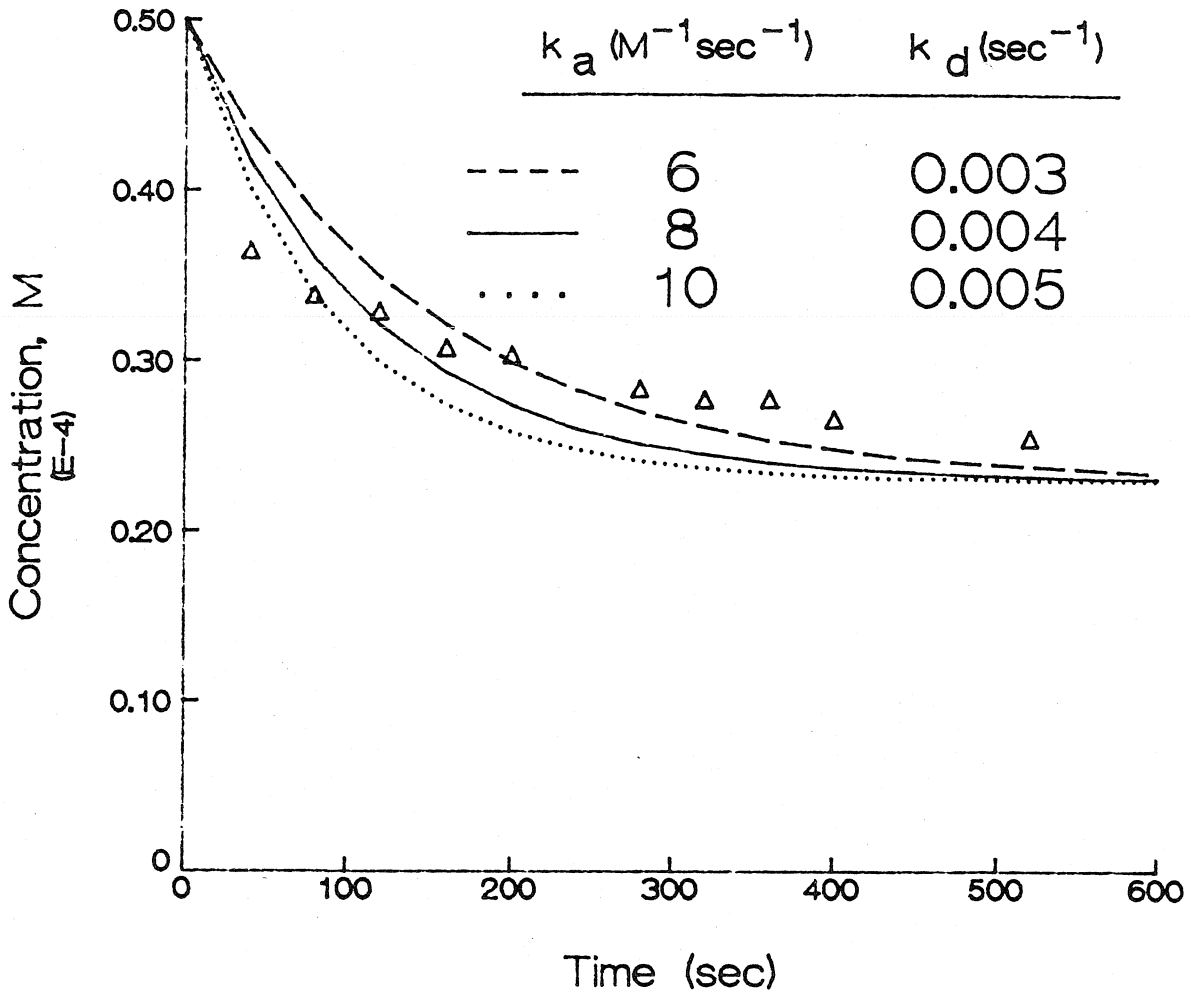

Figure 4.3: Sensitivity of kinetic model on As(V) adsorption on goethite: c) Effect of varying k_a and k_d with constant equilibrium constant K_1.

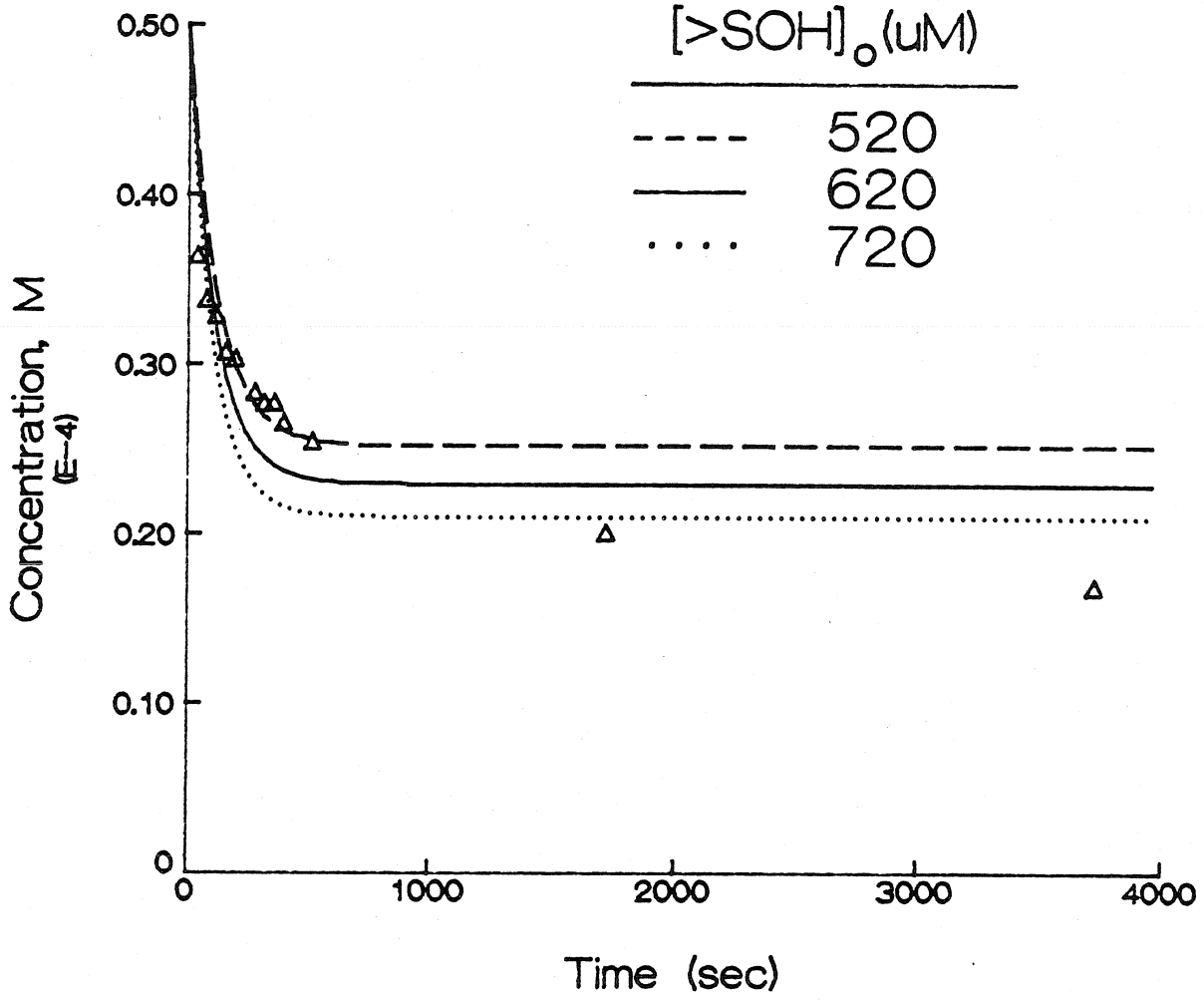

Figure 4.3: Sensitivity of kinetic model on As(V) adsorption on goethite: d) Effect of varying concentration of reactive surface groups (k_a = 8 $M^{-1}sec^{-1}$, k_d = 0.004 sec^{-1}).

two site types are required to describe cation sorption while only one site type is necessary to describe anion adsorption. For cation sorption, both site types are considered to have the same proton binding characteristics. The site types are divided into strong or high affinity bindings sites and weak or low affinity binding sites. In their model, the concentration of low affinity sites is typically much larger than the concentration of high affinity sites.

For simplicity, consider a two site model where the reactivity of $>S_AOH$ sites is greater than the reactivity of $>S_BOH$ sites. Two possible parallel reactions are described as:

$$>S_AOH + H_3AsO_4 \underset{k_{d,A}}{\overset{k_{a,A}}{\rightleftharpoons}} >S_AH_2AsO_4 + H_2O \qquad (4\text{-}6)$$

$$>S_BOH + H_3AsO_4 \underset{k_{d,B}}{\overset{k_{a,B}}{\rightleftharpoons}} >S_BH_2AsO_4 + H_2O \qquad (4\text{-}7)$$

The values of the rate constants for these reactions are of the order:

$$k_{a,A} > k_{a,B}$$

$$k_{d,A} > k_{d,B}$$

For the set of mechanisms, the overall rate of reaction of As(III) is expressed as:

$$-\frac{d[As(V)]}{dt} = (k_{a,A}[>S_AOH] + k_{a,B}[>S_BOH])[H_3AsO_4]$$

$$- k_{d,A}[>S_AH_2AsO_4] - k_{d,B}[>S_BH_2AsO_4] \qquad (4\text{-}8)$$

The numerical solution of this equation requires information about the number of each type of group on the heterogeneous surface. Spectroscopic studies may be useful in providing the necessary information for the model.

In order to illustrate improvements in the kinetic model, the assumption of an approximately equal number of "A" and "B" sites is made. Figure 4.4a shows the success of the two site model in describing the adsorption of As(V) on goethite. The two site model fits the experimental data well at all times. For comparison, the best fit of the one site model is also shown. The values of the rate constants are:

One Site Model	Two Site Model	
$k_a = 8\ M^{-1}sec^{-1}$	$k_{a,A} = 20\ M^{-1}sec^{-1}$	$k_{a,B} = 2\ M^{-1}sec^{-1}$
$k_d = 0.004\ sec^{-1}$	$k_{d,A} = 0.01\ sec^{-1}$	$k_{d,B} = 0.0003\ sec^{-1}$

Figure 4.4b illustrates the relative importance of each type of site to the overall rate of reaction. As(V) reacts rapidly with the type A sites and reaches equilibrium quickly. At the same time As(V) also reacts with type B sites although at a much slower rate. The adsorption of As(V) at type B sites affects the equilibrium at type A sites. As(V) adsorbed at type A sites begins to desorb as a consequence of less As(V) in solution. At equilibrium, the model predicts that more As(V) is adsorbed at type B sites than type A sites.

The rate constants are highly dependent upon the concentration of surface sites. In order to predict the same initial rate as the one site model, the rate constant $k_{a,A}$ had to be more than doubled that of k_1 as a result of the concentration of surface sites being almost halved. Also, the larger equilibrium constant $K_{1,B}$ is

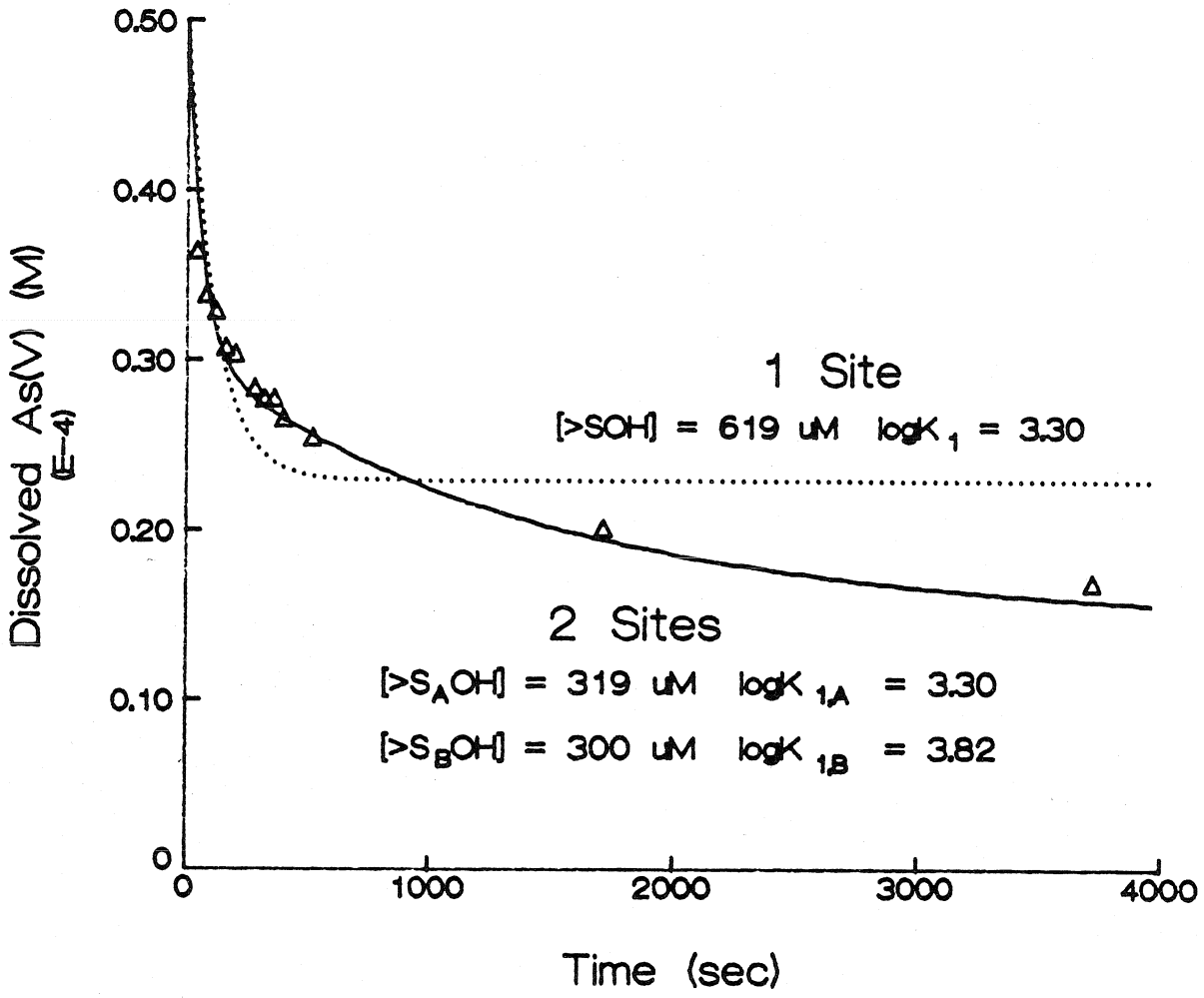

Figure 4.4: a) Comparison of the two site model with the one site model for the reaction between As(V) and goethite. Rate constants are given in the text.

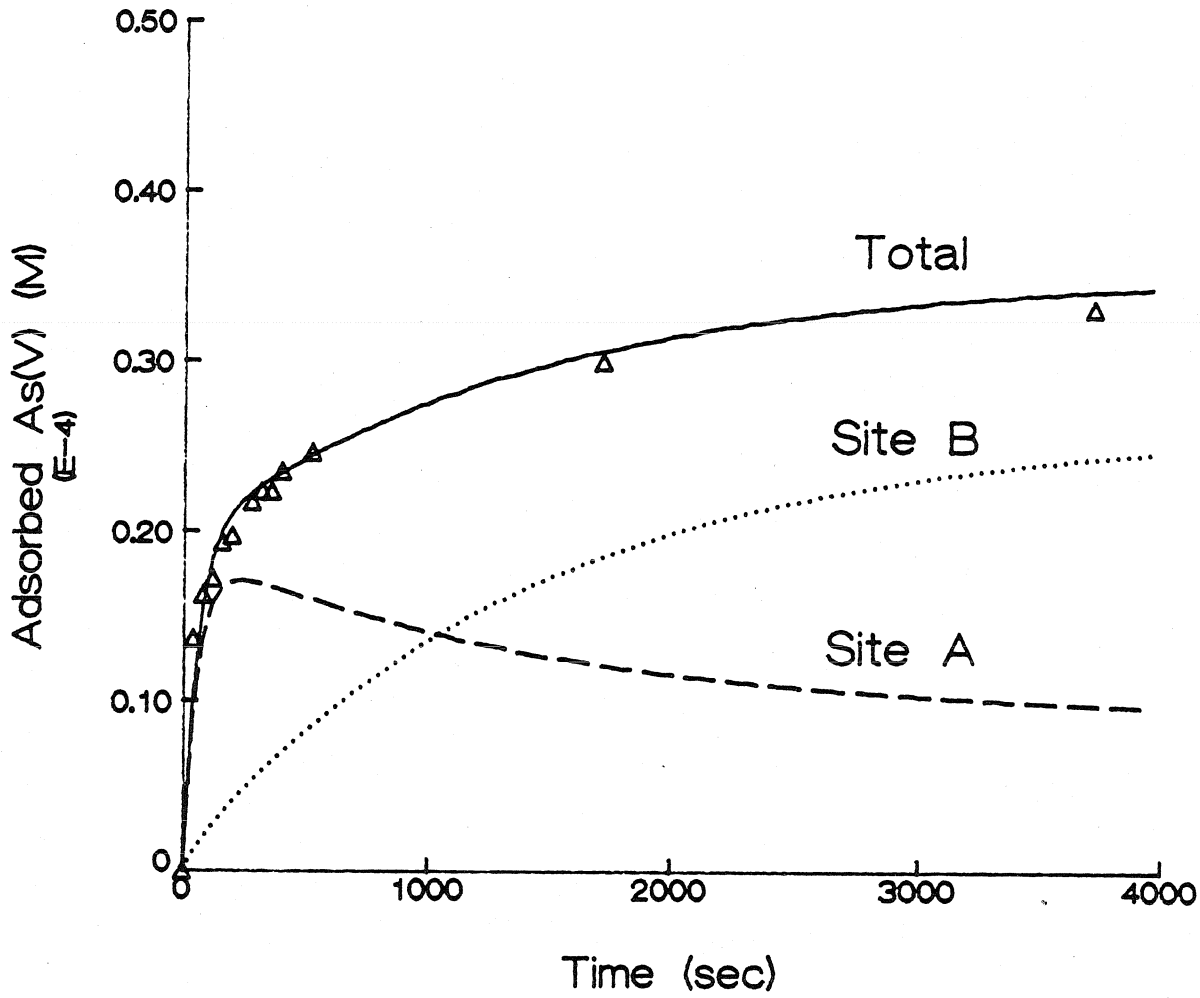

Figure 4.4: b) Two site kinetic model: dependence of the rate of adsorption of As(V) on type A and type B sites and the overall rate of As(V) adsorption on goethite.

necessary to model the experimental data at later times. If $K_{1,A}$ was larger, then the initial rate would be overpredicted.

This example of the two site model is illustrative only. The values of the rate constants and the concentrations of type A and type B sites were arbitrarily chosen. However, the good fit of the model to the data indicates the existence of more than one type of reactive surface site. But without information concerning the concentration and reactivity of different types of surface sites, too many unknowns exist to make complex kinetic modeling fruitful.

4.4 Arsenite Adsorption on Goethite

4.4.1 Effect of pH and Temperature on Kinetics

The initial rate of reaction between As(III) and goethite was studied in detail by examining the dependence of the rate on pH and temperature. The experimental results, tabulated in Appendix A, were interpreted with the kinetic model and the values of the selected rate constants are listed in Table 4.4. All of the data sets were successfully modeled by varying only the value of k_a.

Figure 4.5 displays the model results of the pH dependence at 25 °C. Within the range of pH 4 to 7, the initial rate of reaction and the equilibrium concentration of adsorbed As(III) increase with pH. The trend matches the expectation from the proposed mechanism of a reaction between two neutral species (eq. 4-1). As pH is raised from 4 to 7, the concentration of the aqueous species H_3AsO_3 remains nearly constant, but, as shown in Figure 3.10, the concentration of the neutral surface species >FeOH increases.

Table 4.4: pH and temperature dependence of As(III) adsorption-desorption on goethite

pH	Temp (°C)	[As(III)] (μM)	[SOH] (μM)	k_a ($M^{-1}sec^{-1}$)	k_d (sec^{-1})	log K_1
4	15	50.1	481	1.0	0.002	2.70
	25	50.1	397	2.0	0.002	3.00
	35	53.0	220	6.0	0.002	3.48
6	15	49.9	681	1.7	0.002	2.93
	25	50.0	292	3.0	0.002	3.18
	35	52.7	220	9.0	0.002	3.65
7	25	98.3	326	6.0	0.002	3.48

The model results of the temperature dependence of As(III) adsorption on goethite at pH 4 are shown in Figure 4.6. The results at pH 6 are similar with slightly more adsorption at each temperature. As temperature increases from 15 to 35 °C, the initial rate of reaction and the equilibrium concentration of adsorbed As(III) increases.

Knowledge of the temperature dependence of the adsorption process leads to separation of the entropic and enthalpic contributions to the process and thus provides important information on the driving forces involved. The Gibbs energy of reaction ΔG°_r is related to the equilbrium constant by

$$\Delta G^\circ_r = -RT\ln K \qquad (4\text{-}9)$$

The van't Hoff equation relates an equilibrium constant to temperature :

$$\ln K = -\Delta H_r/RT + \text{constant} \qquad (4\text{-}10)$$

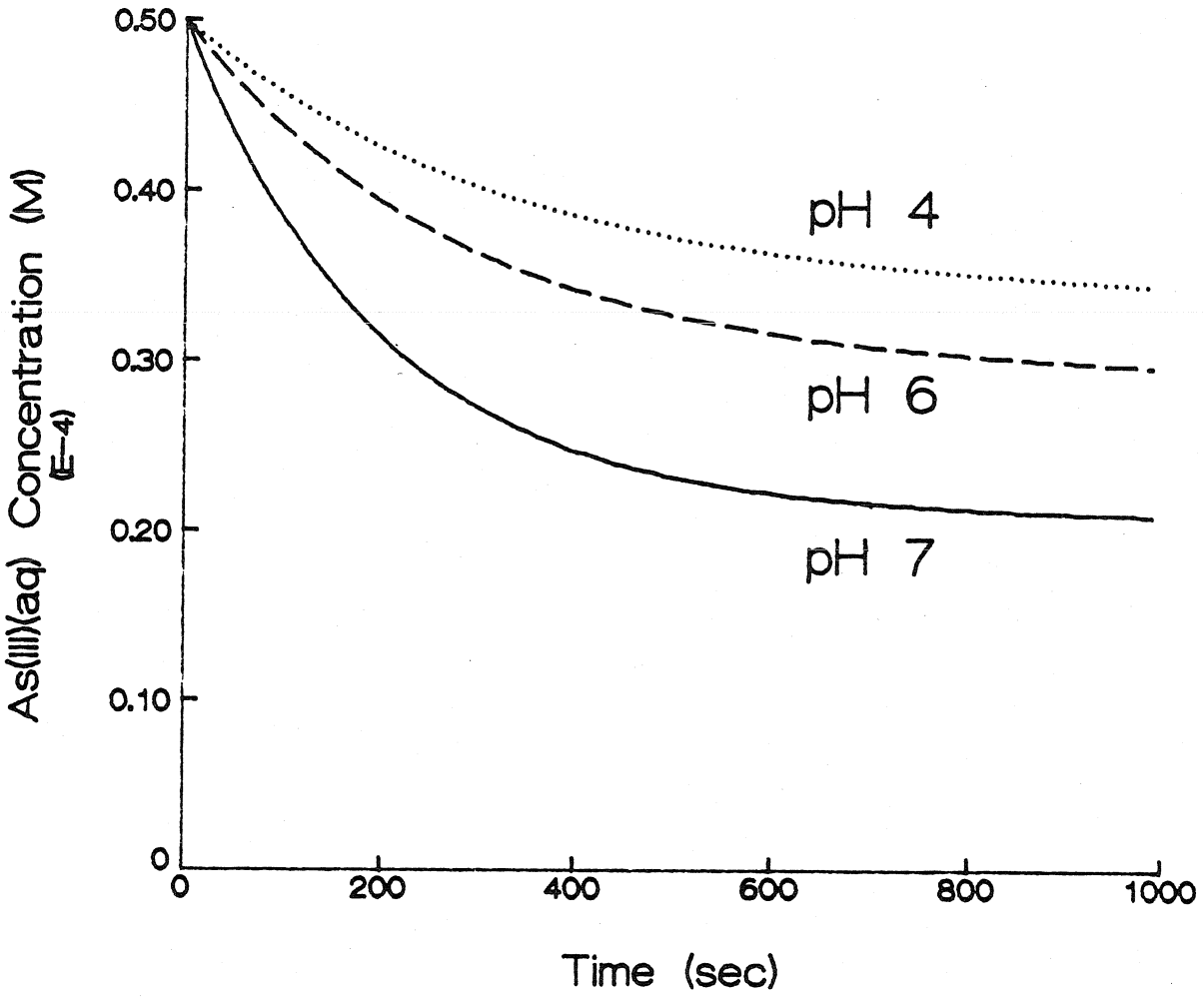

Figure 4.5: Kinetic model results of the pH dependence on As(III) adsorption on goethite at 25 °C. Initial conditions are 50 μM As(III) and 500 μM >$FeOH_T$ and the rate constants are listed in Table 4.4.

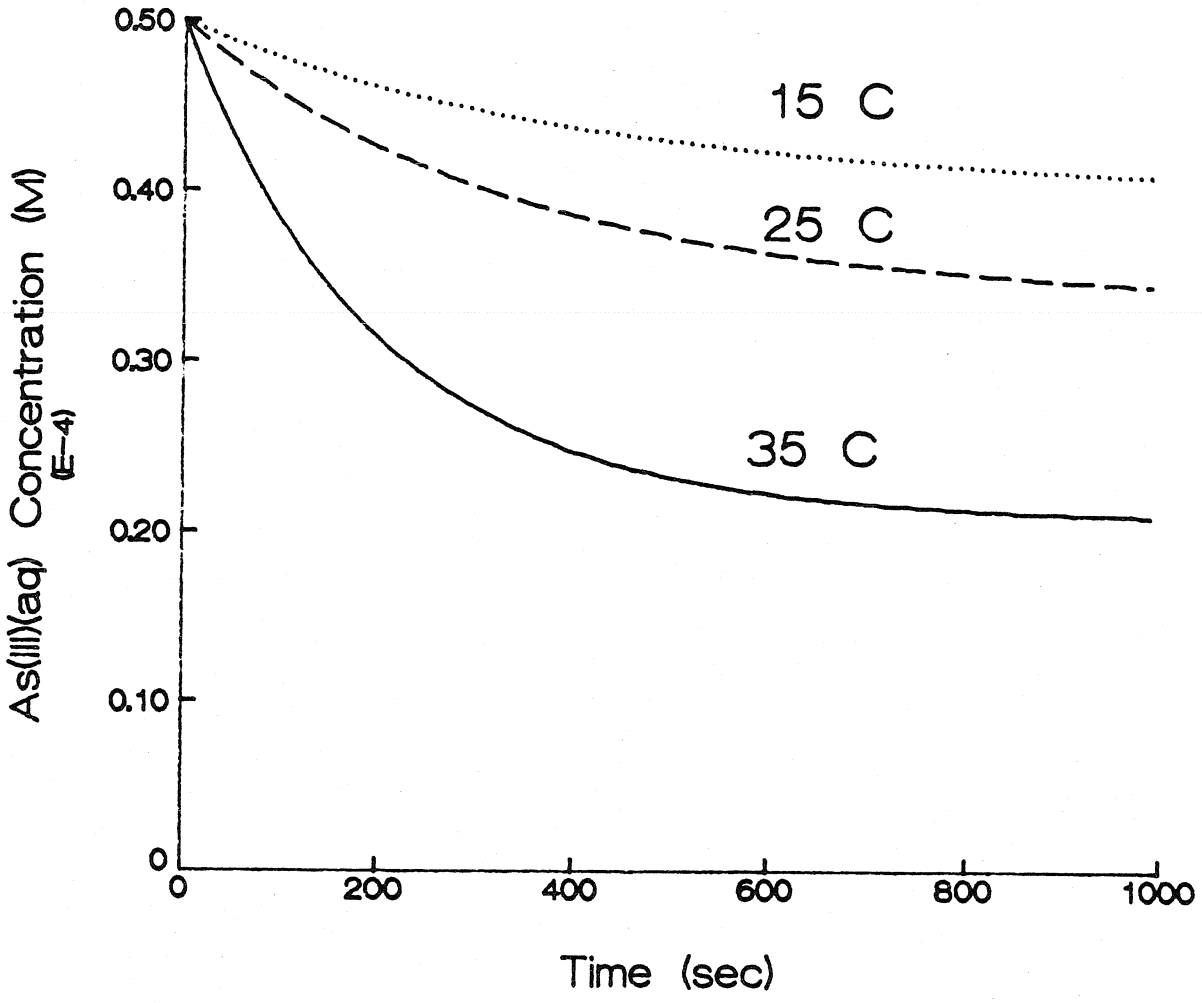

Figure 4.6: Kinetic model results of the temperature dependence on As(III) adsorption on goethite at pH 4. Initial conditions are 50 μM As(III) and 500 μM $>FeOH_T$ and the rate constants are listed in Table 4.4.

and this relationship yields information about the reaction enthalpy, ΔH_r, as long as the reaction enthalpy itself is independent of temperature. A linear plot of ln K versus 1/T indicates that the slope, $\Delta H_r/R$, is independent of temperature (Figure 4.7). The entropy, ΔS_r, is found through the equation relating the three thermodynamic functions

$$\Delta G_r = \Delta H_r - T\Delta S_r \qquad (4\text{-}11)$$

Table 4.5 gives results for the contributions to enthalpy and entropy under two pH conditions. The data indicate that As(III) adsorption is mainly driven by entropy and that the adsorption process involves a strong chemical interaction (i.e., bond formation) with the oxide surface, in the sense that the enthalpic contributions are sizable. These observations are in good agreement with the proposed adsorption mechanism: the arsenite ion replaces a hydroxyl ion that is bonded to a surface Fe.

Fokkink et al. (1990) examined the equilibrium adsorption of Cd^{2+} on rutile (TiO_2) and hematite (α-Fe_2O_3) with studies of adsorption isotherms and electrophoretic mobilities and have demonstrated that the Gibbs energy of adsorption ΔG°_{ads} is a function of the degree of surface coverage. It was also shown that ΔG°_{ads} is the sum of chemical, electrostatic, and nonelectrostatic lateral interactions. They concluded that Cd^{2+} adsorption is entropically driven.

4.4.2 Equilibrium

Aqueous As(III) was allowed to equilibrate in a goethite suspension at 25 °C and pH values of 4 and 5.5 for periods up to 150 hours. Concentrations of aqueous As(III) reached constant values after 3 hours of reaction. No measurable quantities

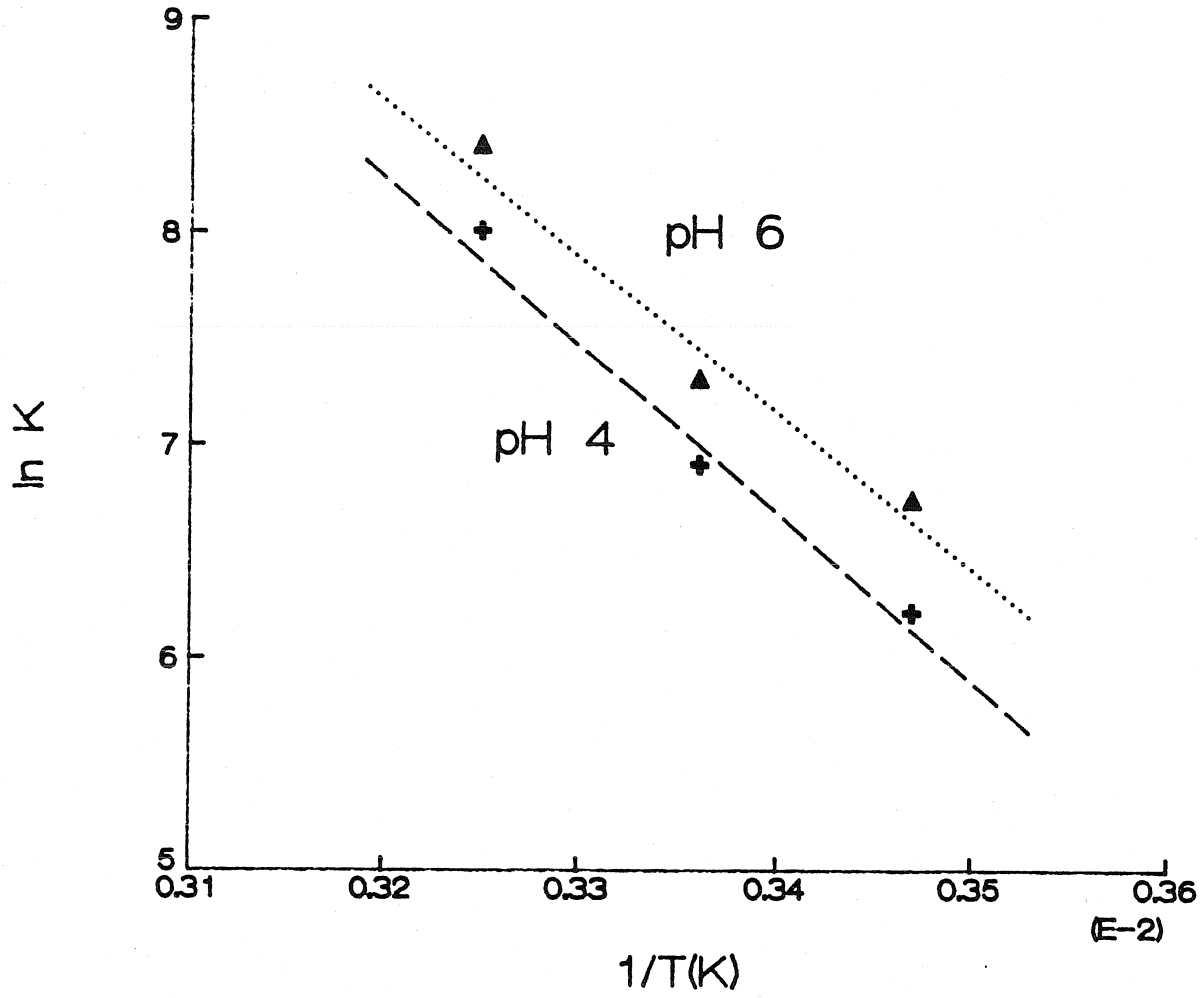

Figure 4.7: van't Hoff plot of the experimentally-derived equilibrium constants and best-fit lines for As(III) adsorption-desorption at pH 4 and pH 6. The slope of each line is equal to $-\Delta H_r/R$.

Table 4.5: Thermodynamic functions for the adsorption of As(III) on goethite derived from the equilibrium constants at pH 4 and 6

pH	ΔG_r (kJ/mole) 25 °C	ΔH_r (kJ/mole) 15-35 °C	ΔS_r (J/mole K) 25 °C
4	-17.1	65.9 ± 9.9	278.5 ± 33.2
6	-18.1	61.2 ± 12.5	266.2 ± 41.9

of As(V) or Fe(II) were detected (1 μM detection limit) throughout the experiments. These observations indicate that no electron transfer occurred between adsorbed As(III) and surface Fe(III). Oscarson et al. (1981b) reported similar findings for an As(III)-goethite system at pH 7 over a period of 72 hours. These results confirm thermodynamic calculations that do not predict a redox reaction between As(III) and Fe(III) in the pH range of study (see Figure 2.10).

The amount of As(III) adsorbed by a known concentration of goethite particles was studied at 25 °C for pH 4 and 5.5. The experimental results are plotted as adsorption isotherms in Figure 4.8. The concentration of adsorbed As(III), normalized by the solid concentration, is plotted against the concentration of dissolved As(III) at equilibrium. Figure 4.8 indicates that the adsorption isotherms at pH 4 and 5.5 are essentially identical. The maximum amount of As(III) adsorbed is 96 μmole/g. This value is nearly 5 times smaller than the maximum adsorbed on an amorphous iron hydroxide (Pierce and Moore, 1980). However, amorphous iron hydroxides have much larger surface areas than goethite, and thus would be expected

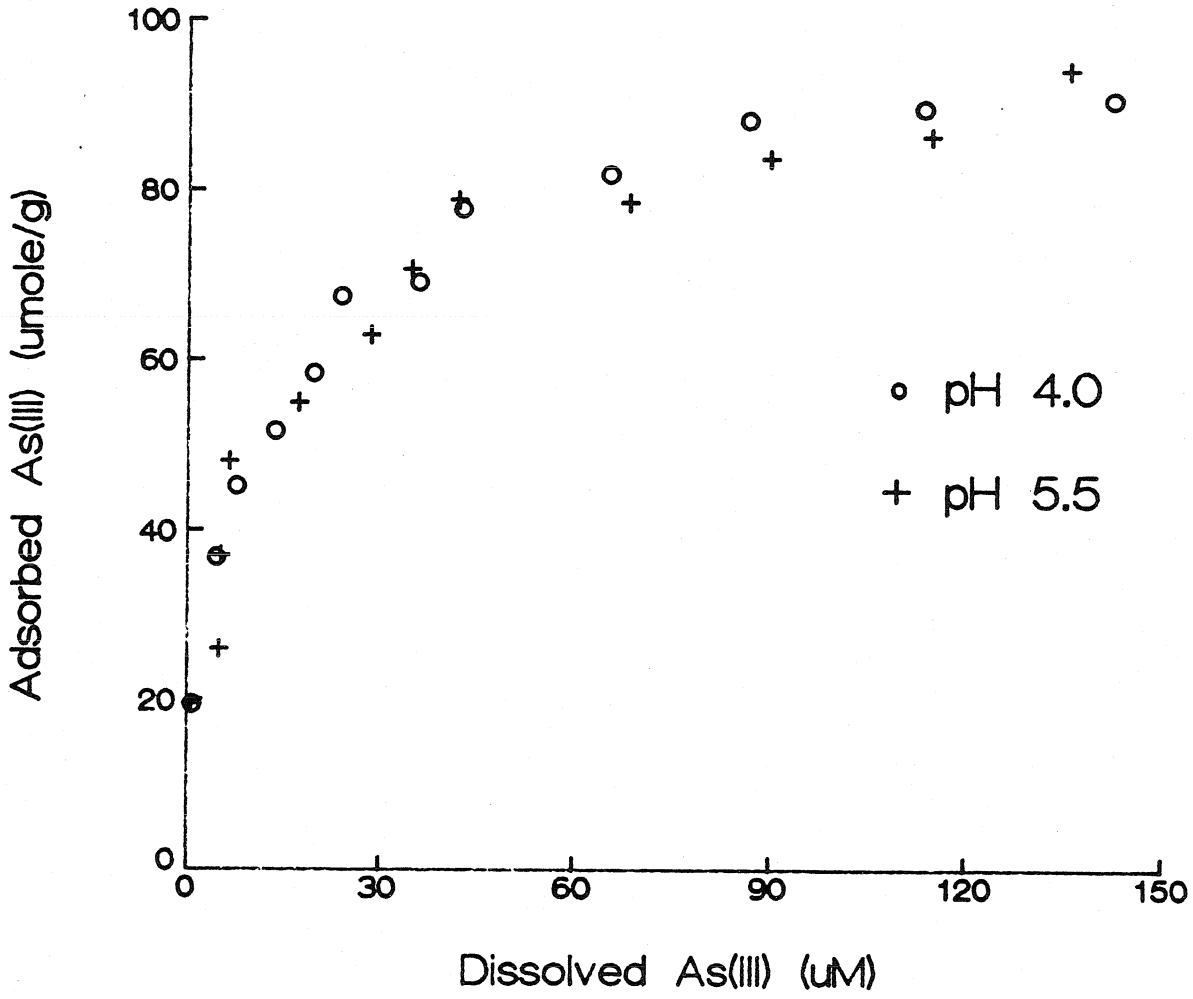

Figure 4.8: Equilibrium adsorption isotherms of As(III) on goethite at pH 4 and 5.5.

to be adsorbed more on a μmole/g basis. A surface area was not reported by Pierce and Moore, but Dzombak and Morel (1990) reported that the surface area of most amorphous iron hydroxides falls within the range of 200-840 m^2/g.

The computer program FITEQL (Westall, 1982) was used to fit the adsorption data with a surface complexation model. The formation of a single surface complex was considered and described by the following reaction:

$$H_3AsO_3 + >FeOH \overset{K_1}{\rightleftharpoons} >FeH_2AsO_3 + H_2O \qquad (4\text{-}12)$$

A value of $10^{4.2}$ for the surface complexation constant was obtained from FITEQL.

The experimental results of the pH effect of As(III) adsorption equilibrium on goethite are plotted in Figure 4.9. Adsorption reaches a maximum between pH 7 and 8 with a gradual decline in the amount adsorbed as pH is increased or decreased. Under the reaction conditions of the experiment, only 85 percent is adsorbed between pH 7 and 8 while more than 50 percent remains adsorbed at pH 3 and 10. The adsorption of As(III) appears to be correlated to the concentration of the neutral surface species >FeOH, which has a maximum concentration at the pH_{zpc} (7.6). This adsorption behavior is different from that of typical anion or cation adsorption. Typical anion adsorption (i.e., phosphate, arsenate, selenite) is greatest at pH values below the pH_{zpc} of the adsorbent and diminishes sharply as pH goes above the pH_{zpc}. Typical cation adsorption (i.e., Pb^{2+}, Mn^{2+}) displays the opposite pH dependency; adsorption is the greatest at pH values above the pH_{zpc} and

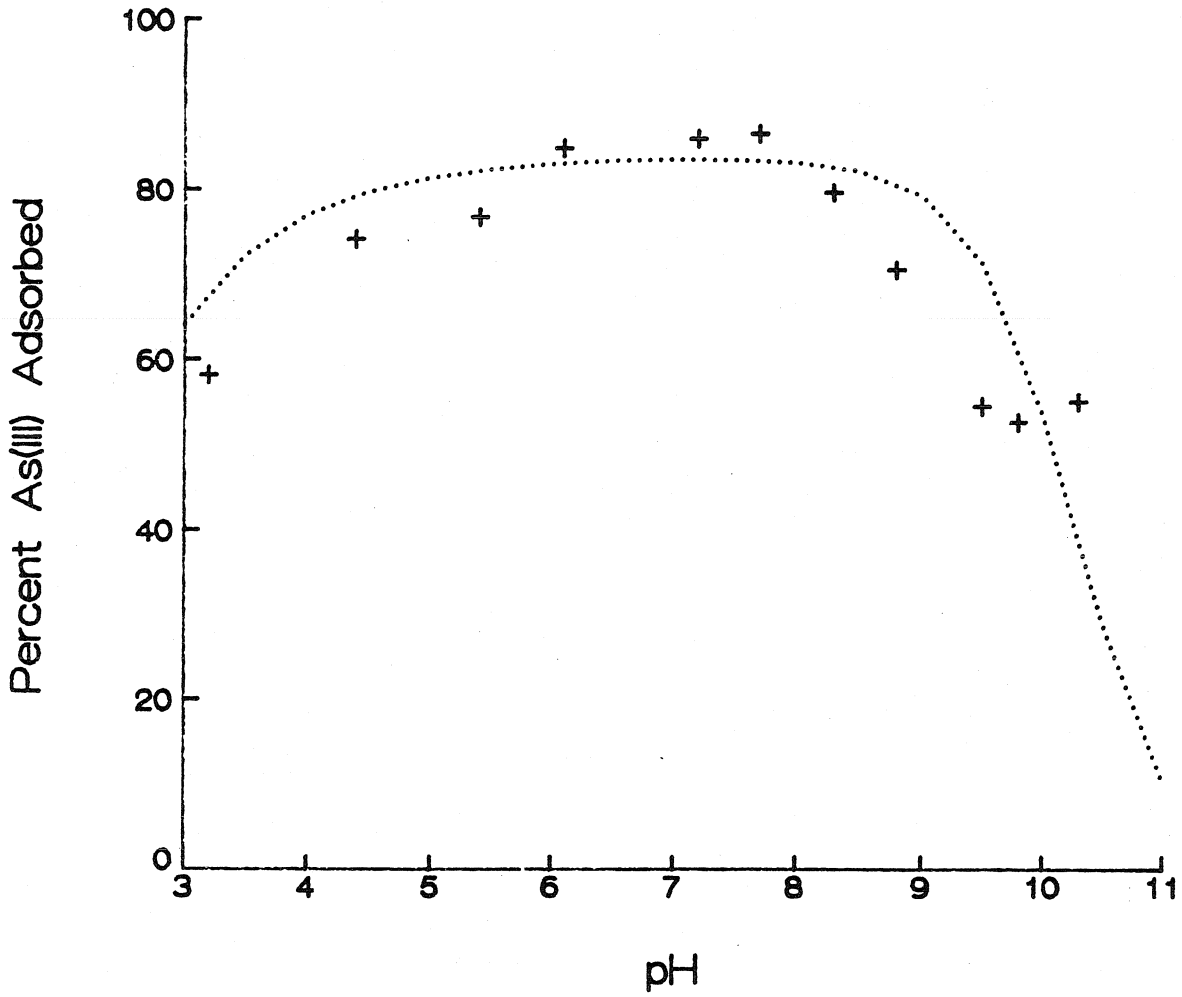

Figure 4.9: Experimental and SURFEQL diffuse layer model (lines) results of the pH effect of As(III) adsorption equilibrium on goethite.

decreases at pH values below the pH_{zpc}. As(III) adsorption on goethite is more like that of silicic acid H_4SiO_4 (Stumm and Morgan, 1981, p. 637).

The experimental results are compared with a surface complexation model using the diffuse layer model to describe the effect of the electric double layer. The single surface complex with a log K_1 value of 4.2 describes the experimental data well at pH values less than 10. Above pH 10, the single complex model predicts little adsorption while the data levels off at about 50 percent adsorption. Additional surface complexes usually improve the fit of the model at higher pH values (Sigg and Stumm, 1980), but the addition of these complexes ($>FeHAsO_3^-$, $>FeAsO_3^{2-}$) does not improve the model for these data. The surface species $>FeAsO_3^{2-}$ extends the applicability of the model to pH 11, but still decreases rapidly at greater pH values.

The value of the surface complexation constant for the reaction between As(III) and goethite is compared with those of other anions in Table 4.6. The results indicate the following relationship of favorable adsorption onto goethite:

$$H_3PO_4 > H_3AsO_3 \approx H_4SiO_4 > HAC$$

The As(III) surface complexation constant is comparable to that of the neutral silicate complex, which is reasonable since both species are fully protonated and neutral in the pH range of natural waters.

4.5 Summary

The kinetics of arsenic and selenium anion adsorption onto goethite and birnessite are similar. The experimental results indicate that the initial adsorption is relatively rapid and occurs within the first ten minutes or less following mixing.

Table 4.6: Comparison of Surface Complexation Constants for several species on goethite

REACTION	log K	Ref.
$>FeOH + H_3PO_4 = >FeH_2PO_4 + H_2O$	9.5	1
$>FeOH + H_3PO_4 = >FeHPO_4^- + H^+$	5.1	1
$>FeOH + H_3PO_4 = >FePO_4^{2-} + 2\,H^+$	-1.5	1
$>FeOH + H_3AsO_3 = >FeH_2AsO_3 + H_2O$	4.2	2
$>FeOH + H_4SiO_4 = >FeH_3SiO_4 + H_2O$	4.1	1
$>FeOH + H_4SiO_4 = >FeH_2SiO_4^- + H^+$	-3.3	1
$>FeOH + HAc = >FeAc + H_2O$	2.9	1

(1) Sigg & Stumm, 1980; (2) This study

In a goethite suspension at pH 4, the initial rate of adsorption is nearly identical for As(V) and Se(IV); for As(III), the rate is slightly slower. In a birnessite suspension at pH 4, the initial rate of adsorption follows the trend:

Mn(II) > As(III) > Se(IV)

As(V) is not adsorbed on birnessite at pH 4 and Se(VI) is not adsorbed by either oxide. It is also observed that at pH 4 the initial rate of As(V) and Se(IV) adsorption is greater on goethite than birnessite while As(III) adsorption is faster on birnessite. The extent of adsorption is qualitatively linked to the effect of the electrostatic charge on the oxide surface and the charge of the aqueous ion.

The time dependency of the adsorption and desorption processes was adequately described by a simple one-site kinetic model. It was also shown that the

kinetic description was improved by a more complex two-site model. However, the complex model requires detailed and unknown information about the number and reactivity of each type of surface site.

As(III) adsorption on goethite was investigated in greater detail with respect to pH and temperature. Both the initial rate of adsorption and the equilibrium concentration of adsorbed As(III) increase with increasing pH and temperature. As predicted from thermodynamic calculations, no redox reaction between adsorbed As(III) and surface Fe(III) was observed over an extended reaction period. At equilibrium, the maximum adsorption of As(III) occurs between pH 7 and 8 and there is a gradual decline in the quantity adsorbed as pH is increased from pH 8 or decreased from pH 7. Surface complexation modeling indicates that As(III) adsorption is less favored than phosphate adsorption, approximately equivalent to silicate adsorption, and more favored than acetate adsorption on goethite.

Chapter 5

REACTIONS AT OXIDE SURFACES: OXIDATION OF AS(III) AND SE(IV) WITH BIRNESSITE

5.1 Introduction

This chapter presents experimental results and discusses the rates and mechanisms of the reactions of As(III) and Se(IV) with the birnessite surface. The reactions obey the following overall stoichiometries:

$$(>MnO)_3MnOH + H_3AsO_3 + H^+ \rightleftharpoons 3>MnOH + Mn^{2+} + H_2AsO_4^- \qquad (5\text{-}1)$$

$$(>MnO)_3MnOH + HSeO_3^- + H^+ \rightleftharpoons 3>MnOH + Mn^{2+} + SeO_4^{2-} \qquad (5\text{-}2)$$

The reactions are monitored by measuring the aqueous concentrations of the reactants (As(III), Se(IV)) and the products (As(V), Se(VI), Mn(II)) as functions of time. For the As(III)-birnessite system, the effects of initial As(III) concentration, pH, temperature, dissolved oxygen, and competitive bivalent cations were studied. The influence of the concentration of reactants, pH, and temperature on the rate of oxidation of Se(IV) was investigated. The experimental results are interpreted with a kinetic model for the reaction sequence of adsorption, electron transfer, desorption, and dissolution.

5.2 Experimental Methods

Deionized distilled water (D_2H_2O) from a MILLI-Q water purification system (Millipore Corp., Bedford, MA) was used to prepare all solutions. All reagents were

analytical grade and used without further treatment. All solutions were filtered through a 0.2 μm Nucleopore filter to remove possible particle contaminants. All glassware was cleaned with 4 M HNO_3 or 4 M HCl and rinsed several times with D_2H_2O.

The pH of solution was monitored in all experiments using a Radiometer glass combination electrode (Model GK2401C) and a Radiometer Model PHM84 research pH meter. The electrode was calibrated with NBS buffers.

Experiments studying the reaction of As(III) with birnessite were performed in a 250 ml magnetically-stirred double-walled beaker connected to a constant temperature water bath. N_2 gas was used to purge the system of CO_2. The gas was passed through a column of Ascarite II to remove any contaminant CO_2 and rehydrated through a column of D_2H_2O before being introduced into the reaction vessel. The experiments were performed in aqueous suspensions consisting of 0.1 M $NaClO_4$ and a known solid concentration. Solid concentration was determined gravimetrically just prior to and following the experiment by filtering 1 ml of the reaction suspension through a 0.2 μm Nucleopore filter. The aqueous systems were adjusted to pH 4 with 1.0 M $HClO_4$ to facilitate the removal of aqueous CO_2. After at least 3 hours, and usually overnight, the pH was readjusted with 0.1 M $HClO_4$ or NaOH to the planned pH value of the experiment. pH was kept constant during an experiment with small additions of 0.1 M $HClO_4$ or NaOH when the pH had drifted ± 0.05 pH units from the initial pH. The oxide suspensions were allowed to equilibrate for at least two hours at the new pH before a known concentration of

As(III) as NaH_2AsO_3 was added to the system and mixed thoroughly. The reaction was followed by periodically withdrawing and filtering a few milliliters through a 0.2 μm Uniflo filter unit for analysis. The filtered samples were divided for analysis of As(III), As(V), and Mn(II). The Mn(II) subsamples were acidified with concentrated HCl to pH 1 to prevent any re-oxidation. The effects of initial As(III) concentration, temperature, pH, and dissolved oxygen were examined in a series of experiments.

Competition for reactive surface sites was studied by equilibrating the particle suspension at pH 4 with a bivalent cation (Ca^{2+}, Mn^{2+}) before adding As(III). Bivalent cations such as Ca^{2+} and Mn^{2+} bind appreciably to negatively charged surfaces and thus should compete with As(III) for reactive surface sites and reduce the rate and extent of reaction.

To study the reaction of Se(IV) with birnessite, the reaction suspension was prepared in a 125 ml polystyrene bottle to prevent evaporation of the solution during the duration of the experiment. Reaction bottles were placed in a constant temperature shaker bath. Samples were purged with CO_2-free N_2 gas prior to and for the first two hours of each experiment. Ionic strength was controlled by $NaNO_3$ instead of $NaClO_4$ or NaCl because the ClO_4^- ion contaminates the anion column of the ion chromatography unit and the Cl^- ion at high concentrations can interfere with determination of Se(IV). An ionic strength of 0.001 M was used due to similar interferences of higher concentrations of NO_3^- with Se(VI). Additions of 0.1 M HNO_3 or NaOH were made to initially adjust the pH of each solution and pH was monitored during the first two hours and then periodically over the duration of each

experiment. The reaction bottles were sampled over a period of 4 weeks. Each subsample (5 ml) was filtered through a 0.2 μm Uniflo filter unit and separated for analysis of Se(IV) and Se(VI) (together) and Mn(II). The effects of initial Se(IV) concentration, solid concentration, pH, and temperature were studied with a series of experiments.

5.3 Dynamics of As(III) and Birnessite

5.3.1 Behavior of As(III), As(V), and Mn(II) in Solution

Reaction conditions for the As(III)-birnessite experiments are listed in Table 5.1. In all experiments, total manganese and total manganese surface sites are in excess of total arsenic. Data from all of the experiments are listed in Appendix A. Figure 5.1 illustrates the behavior of aqueous arsenic and manganese species with time when aqueous As(III) is introduced into a suspension of birnessite particles under the conditions pH 4, 25 °C, and ionic strength 0.1 M.

The depletion of As(III) from solution is rapid. Fifty percent of the initial As(III) is removed from solution within 10 minutes and, after 90 minutes, the concentration is below the detection limit of 1 μM (> 99% removal). As(V) is released into solution as rapidly as As(III) is depleted and the total concentration of aqueous As is almost constant over the duration of the experiment. These observations suggest that the processes of electron transfer and release of As(V) into solution are fast when compared to adsorption of As(III). The observations also suggest that the adsorption of the released product As(V) on the birnessite surface is very limited.

Table 5.1: Reaction Conditions of Arsenite-Birnessite Experiments

Expt	Initial As(III) (μM)	Solid Conc (g/L)	Ratio Mn_T to As(III)	Ratio > Mn_T to As(III)	Temp (°C)	pH	Other
MnAs1	99.6	0.21	15.1	5.0	25	4.0	
MnAs2	199.7	0.26	9.4	3.1	25	4.0	
MnAs3	398.4	0.22	3.9	1.3	25	4.0	
MnAs4	99.6	0.42	30.5	10.1	25	4.0	pO_2 = 0.21 atm
MnAs5	0.0	0.23	---	---	25	4.0	As(V) = 100 μM
MnAs6	100.0	0.37	26.6	8.8	15	4.0	
MnAs7	106.3	0.29	19.6	6.5	35	4.0	
MnAs8	99.4	0.14	10.3	3.4	25	5.0	
MnAs9	99.4	0.36	26.3	8.7	25	5.85	
MnAs10	99.3	0.17	12.4	4.1	25	6.8	
MnAs11	99.9	0.37	26.9	8.9	25	7.7	
MnAs12	99.9	0.15	10.9	3.6	25	8.2	
MnAs13	99.8	0.30	21.8	7.2	25	4.0	Mn^{2+} = 98.9 μM
MnAs14	100.1	0.26	18.7	6.2	25	4.0	Mn^{2+} = 196 μM
MnAs15	99.8	0.24	17.2	5.7	25	4.0	Ca^{2+} = 98.9 μM
MnAs16	98.9	0.15	10.9	3.6	25	4.0	Ca^{2+} = 500 μM

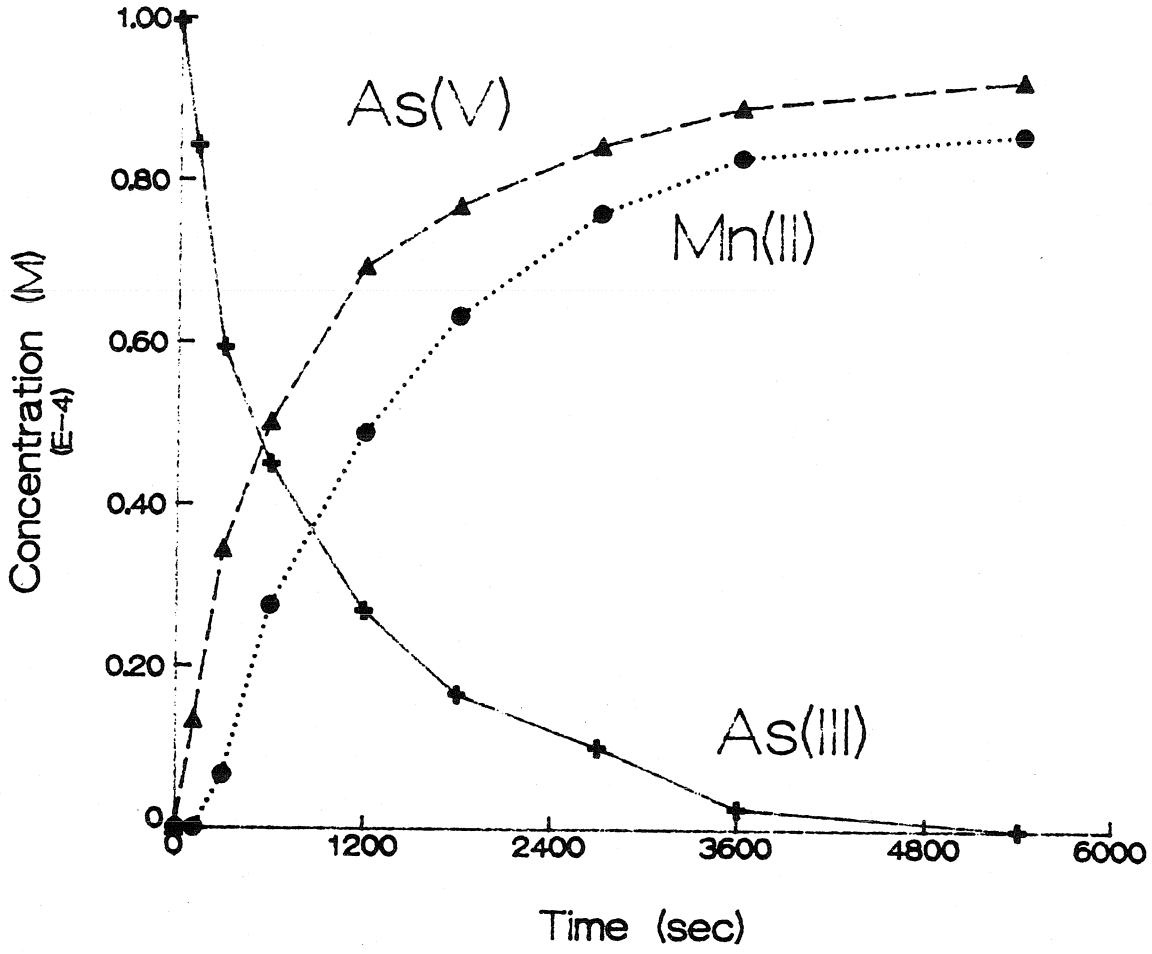

Figure 5.1: Experimental behavior of aqueous As(III), As(V), and Mn(II) following As(III) addition to a birnessite suspension. Table 5.1 lists the experimental conditions (MnAs1).

The adsorption of 100 μM As(V) on the birnessite surface was explored under the experimental conditions of pH 4 and 25 °C. No As(V) was adsorbed during the four hours of the experiment . This behavior is expected from the coulombic features of the surface chemistry of As(V) with metal oxides. The negatively-charged As(V) anion binds strongly to positively-charged oxide surfaces (i.e., when the pH of the solution is less than the pH_{zpc} of the oxide) and desorbs when the oxide surface is negatively charged (i.e., at pH values above the pH_{zpc}). The birnessite surface is negatively charged at pH 4 (Figure 3.11) and thus As(V) adsorption is not favorable under the experimental conditions.

The release of the reduced product Mn^{2+} is slower than the release of the oxidized product As(V). Also the ultimate extent of Mn^{2+} release is less than the extent of As(V) release. The ratio of Mn^{2+} /As(V) in solution as a function of time is presented in Figure 5.2. If the products both were released simultaneously into solution and neither reacted further with the surface, then the ratio should be predicted from the reaction stoichiometry, which under the experimental conditions is 1. If the reduced product is accumulating at the surface, by either not being released into solution with the oxidized product, or by being adsorbed to a greater extent, then the ratio would be less than predicted. The observed Mn^{2+} /As(V) ratio after the first two minutes of reaction is zero and then gradually increases until it reaches a maximum of 0.93 after 45 minutes of reaction. Stone and Ulrich (1989) reported similar behavior when studying the reductive dissolution of Mn(IV) dioxide and Co(III) oxide particles by hydroquinone. The behavior of reduced Mn in

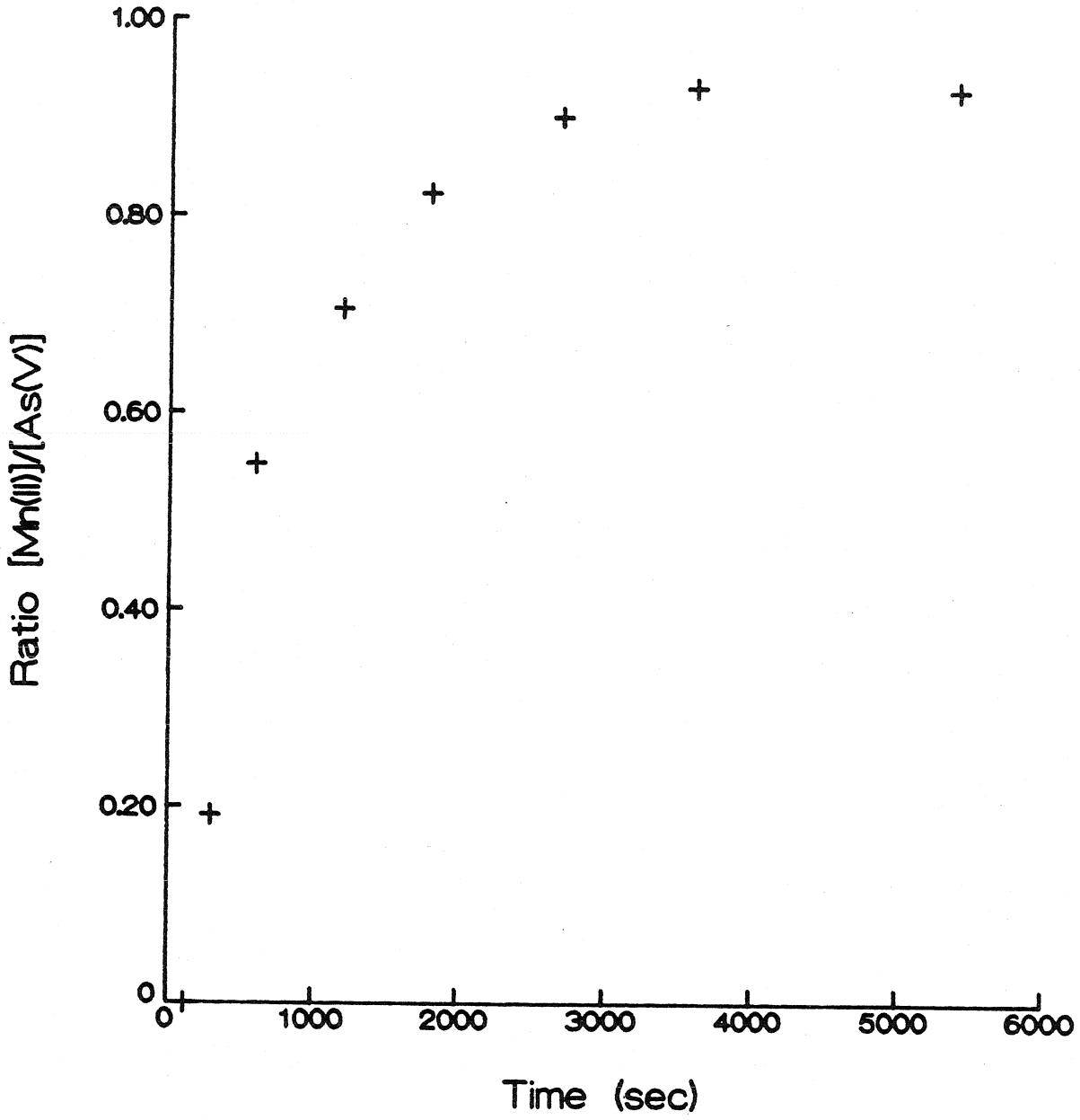

Figure 5.2: The product ratio $[Mn^{2+}(aq)]/[As(V)(aq)]$ increases as the reaction progresses and approaches 1, the value predicted from the reaction stoichiometry.

solution is probably controlled by both processes: (i) the slower release of Mn causes the ratio to be initially less than predicted and (ii) the adsorption of Mn^{2+} keeps the ratio from reaching the predicted value at longer times.

5.3.2 Kinetic Mechanisms and Expressions

A kinetic model that describes the reductive dissolution of metal oxides by organic reductants via surface reactions has been discussed in detail (Stone, 1986; Stone and Morgan, 1987; Stone and Ulrich, 1989). The general framework of the model can be used to describe the oxidation of trace reduced species by metal oxide surfaces. Surface redox reactions between reduced anions and oxidized surface metal ions occur through a multi-step mechanism, which can be best represented by four general steps. The first step is assumed to be the formation of an inner-sphere complex where the reduced anions displace surface-bound OH^- and H_2O via ligand substitution and bind directly to the oxidized metal ion. The next step represents a multi-step process that includes a transfer of two electrons from the anion to the metal ion, breaking of two Mn-O bonds, and addition of an oxygen from water to As(V). The release of the surface-bound oxidized anion and reduced metal ion constitutes the third and fourth general steps. The following equations, for reaction of As(III) with a Mn(IV) oxide, illustrate this mechanism:

$$(>MnO)_3MnOH + As(OH)_3 \underset{k_{-1}}{\overset{k_1}{\rightleftharpoons}} (>MnO)_3MnOAs(OH)_2 + H_2O \qquad (5\text{-}3)$$

$$(>MnO)_3MnOAs(OH)_2 + H_2O \underset{k_{-2}}{\overset{k_2}{\rightleftharpoons}} >MnOMnOAsO(OH)_2 + 2>MnOH \qquad (5\text{-}4)$$

$$>MnOMnOAsO(OH)_2 + H_2O \underset{k_{-3}}{\overset{k_3}{\rightleftharpoons}} >MnOMnOH + H_2AsO_4^- + H^+ \qquad (5\text{-}5)$$

$$>MnOMnOH + 2H^+ \underset{k_{-4}}{\overset{k_4}{\rightleftharpoons}} >MnOH + Mn^{2+} + H_2O \qquad (5\text{-}6)$$

The reactive surface site is represented as the species $(>MnO)_3MnOH$, a surface Mn(IV) atom bound to three MnO groups and a hydroxyl group. Figure 5.3 shows a schematic representation of the cross section of the surface layer of a Mn(IV) oxide that undergoes reductive dissolution by arsenite. In this representation, the surface Mn(IV) atom that undergoes reduction is bonded to two surface and one near-surface Mn(IV) atoms. During the electron transfer step, two Mn-O bonds are broken and each O atom is protonated. An O atom from water is added to As. The number of total surface sites remains constant as the result of the formation of a new site when the reduced Mn^{2+} is released and the near-surface MnO group is protonated.

Applying the Principle of Mass Action (Gardiner, 1969) to reactions (5-3)-(5-6) allows the rate of each reaction step to be calculated:

$$R_1 = k_1[(>MnO)_3MnOH][As(OH)_3] \qquad (5\text{-}7)$$

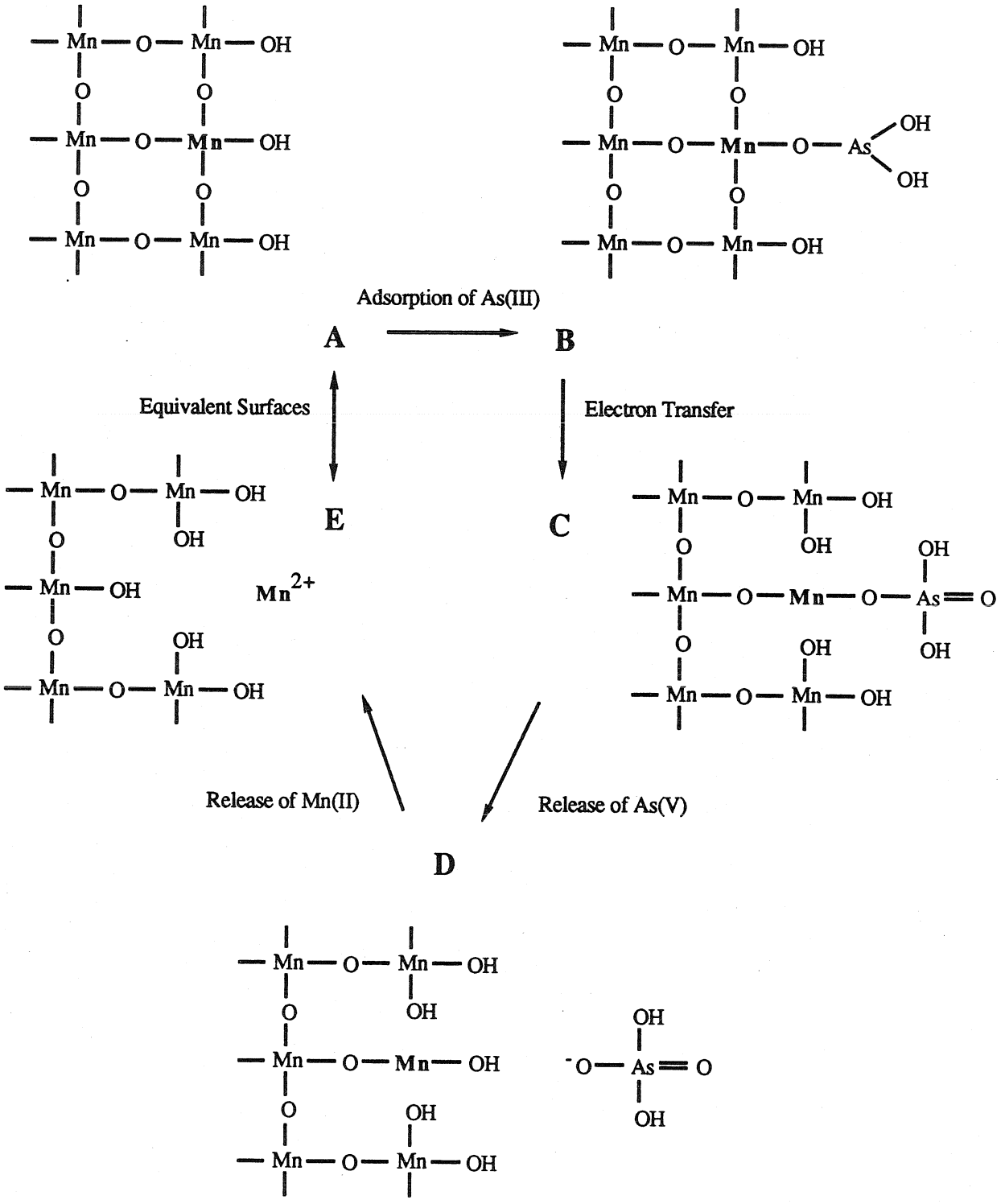

Figure 5.3: A) Schematic representation of the cross section of the surface layer of a Mn(IV) oxide and B) the resulting surface structure following arsenite adsorption, C) electron transfer, D) arsenate release and E) Mn^{2+} release.

$$R_{-1} = k_{-1}[(>MnO)_3MnOAs(OH)_2] \quad (5\text{-}8)$$

$$R_2 = k_2[(>MnO)_3MnOAs(OH)_2] \quad (5\text{-}9)$$

$$R_{-2} = k_{-2}[>MnOMnOAsO(OH)_2][>MnOH]^2 \quad (5\text{-}10)$$

$$R_3 = k_3[>MnOMnOAsO(OH)_2] \quad (5\text{-}11)$$

$$R_{-3} = k_{-3}[>MnOMnOH][HAsO_4^-][H^+] \quad (5\text{-}12)$$

$$R_4 = k_4[>MnOMnOH][H^+]^2 \quad (5\text{-}13)$$

$$R_{-4} = k_{-4}[>MnOH][Mn^{2+}] \quad (5\text{-}14)$$

Changes in the concentrations of the chemical species are found by accounting for both production and consumption:

$$-\frac{d[As(OH)_3]}{dt} = R_1 - R_{-1} \quad (5\text{-}15)$$

$$-\frac{d[(>MnO)_3MnOH]}{dt} = R_1 - R_{-1} - R_4 + R_{-4} \quad (5\text{-}16)$$

$$-\frac{d[(>MnO)_3MnOAs(OH)_2]}{dt} = -R_1 + R_{-1} + R_2 - R_{-2} \quad (5\text{-}17)$$

$$-\frac{d[>MnOMnOAsO(OH)_2]}{dt} = -R_2 + R_{-2} + R_3 - R_{-3} \quad (5\text{-}18)$$

$$-\frac{d[H_2AsO_4^-]}{dt} = -R_3 + R_{-3} \quad (5\text{-}19)$$

$$-\frac{d[>MnOMnOH]}{dt} = -R_3 + R_{-3} + R_4 - R_{-4} \quad (5\text{-}20)$$

$$-\frac{d[Mn^{2+}]}{dt} = -R_4 + R_{-4} \qquad (5\text{-}21)$$

The expressions can be solved numerically using the Forward Euler Method (Forsythe et al., 1977). The computer code used to calculate the concentrations of the chemical species as a function of time is listed in Appendix B. Experimentally observed quantities such as the aqueous concentrations of the reduced and oxidized anion and the reduced metal as functions of time provide a basis for determining values for the rate constants (k_1, k_{-1},. . ., k_4, k_{-4}). However, these values alone are not sufficient for determining unique values for all eight rate constants; although, they do limit the range of possibilities. The goodness of fit of the kinetic model was determined by minimizing the average and maximum difference between observed and predicted concentrations of each measured species at each sampling time. The general modeling procedure and sensitivity analyses of the model for MnAs and MnSe data sets are described in Appendix C. The ability of this kinetic model to describe the observed dynamic behavior of the aqueous concentrations of the reactants and products in the reactions of As(III) and Se(IV) with the birnessite surface is discussed in the following sections.

The best model fits of the three aqueous species profiles are shown with the experimental data (MnAs1) in Figure 5.4 and the values of the rate constants are listed in Table 5.2. Figure 5.5 displays the model-predicted profiles of all the proposed species, except for the reactive surface sites, $(>MnO)_3MnOH$. The model-predicted curves of the three aqueous species are repeated in the figure in order to

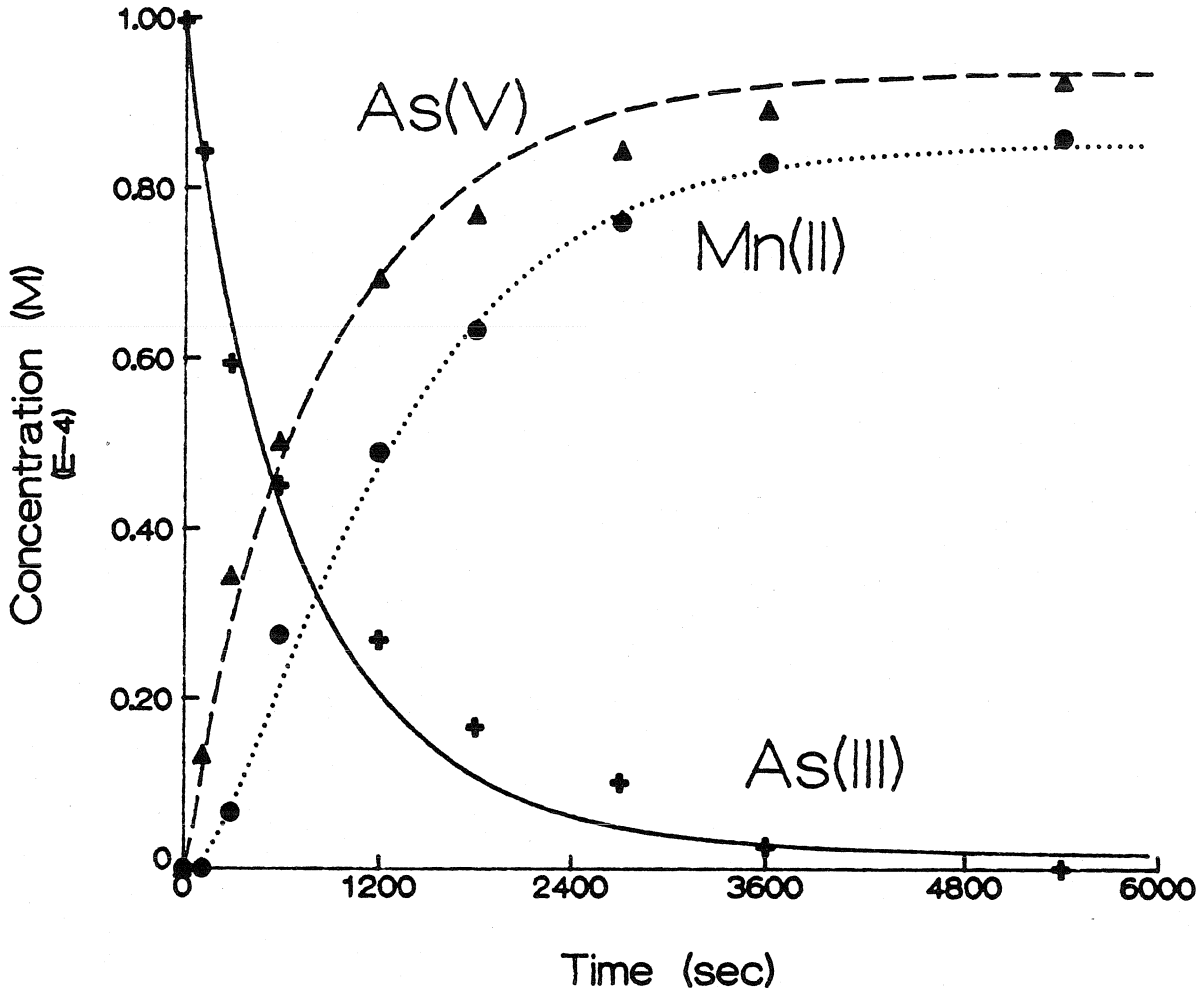

Figure 5.4: Comparison of predicted kinetic behavior (lines) with experimental data for aqueous species As(III), As(V), and Mn(II) following As(III) addition to a birnessite particle suspension (experiment MnAs1).

Table 5.2: Rate Constants and Characteristic Times for the Reaction between As(III) and Mn(IV) at pH 4, 0.1 M $NaClO_4$, and 25 °C

PROCESS	RATE CONSTANT	CHARACTERISTIC TIME Definition	τ(sec)
As(III) Adsorption	5 $M^{-1}sec^{-1}$	$1/\{k_1[(>MnO)_3MnOH]_o\}$	398
As(III) Desorption	0.02 sec^{-1}	$1/k_{-1}$	50
Electron Transfer As → Mn	0.03 sec^{-1}	$1/k_2$	33
Mn → As	0.0015 sec^{-1}	$1/k_{-2}$	667
As(V) Release	0.1 sec^{-1}	$1/k_3$	10
As(V) Adsorption	5 x10^6 $M^{-2}sec^{-1}$	---	---
Mn(II) Release	2 x10^5 $M^{-2}sec^{-1}$	$1/\{k_4[H^+]^2\}$	500
Mn(II) Adsorption	0.4 $M^{-1}sec^{-1}$	$1/\{k_{-4}[(>MnO)_3MnOH]_o\}$	4980

show the relative amounts of the other species. The surface As(III) species, $(>MnO)_3MnOAs(OH)_2$, has a maximum concentration of 4 μM after 60 seconds of reaction and slowly decays until the concentration is below the limit of detection after approximately 3000 seconds. The surface As(V) species, $>MnOMnOAsO(OH)_2$, reaches a maximum concentration of 9 μM more slowly, and after 6000 seconds, still persists at 4 μM. It is interesting to note that the surface As(V) surface species, $(>MnO)_3MnOAsO(OH)_2$, does not form when aqueous As(V) is introduced to a Mn(IV) particle suspension under similar experimental conditions (pH 4, 25 °C, 0.1 M ionic strength).

The slower release of Mn(II) into solution allows the concentration of the surface Mn(II) species to build up to a maximum of 25 μM after 600 seconds. The

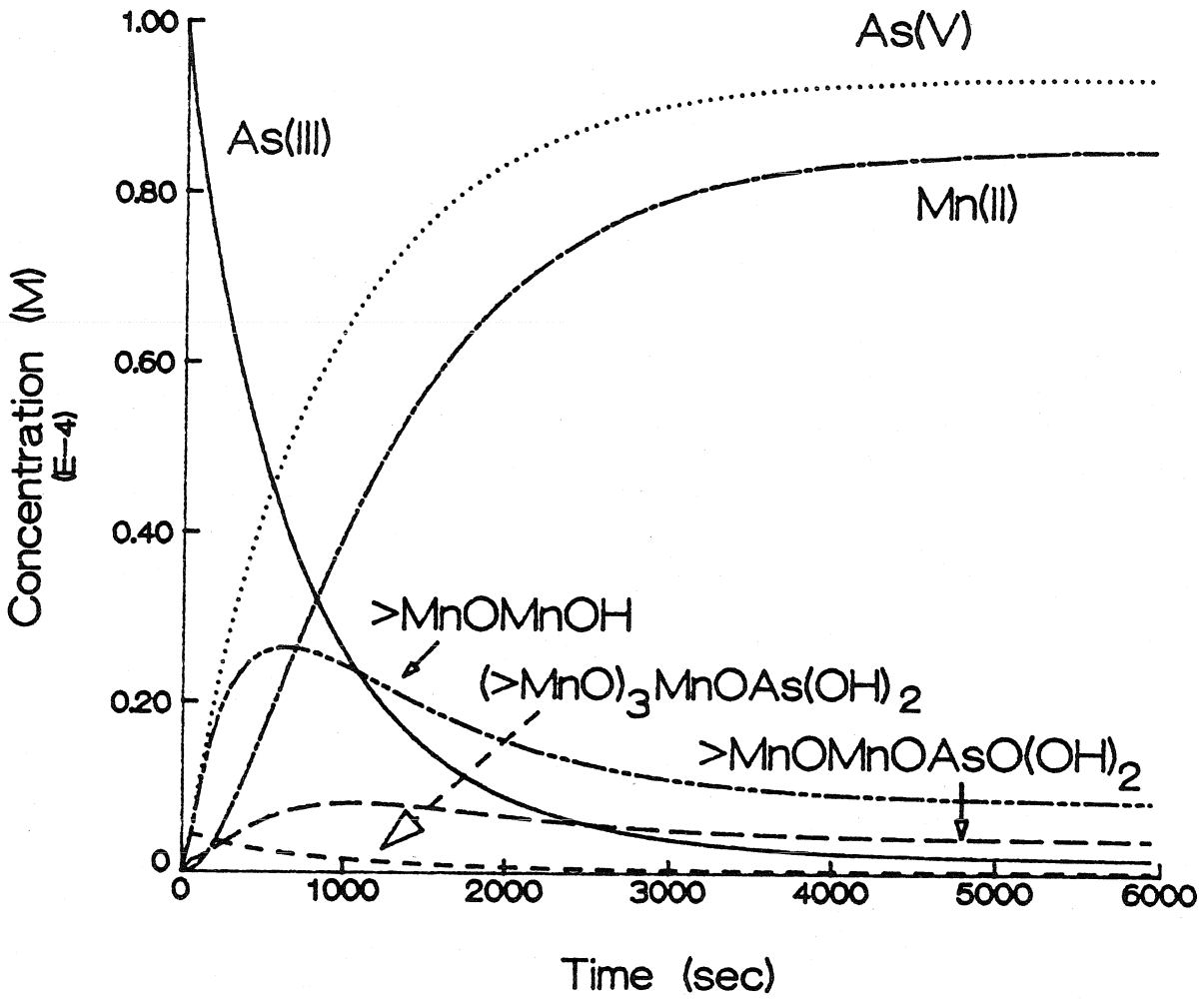

Figure 5.5: The model predicted species profiles of the As(III)-Mn(IV) reaction at pH 4 and 25 °C. Initial conditions and rate constants are listed in Table 5.2.

concentration then decreases as a result of decreased formation of precursors and coupled with continued release of Mn(II). The model indicates that after 6000 seconds about 10 percent of Mn(II) produced remains at the surface while the other 90 percent is in solution.

Overall rates of reactions in series are most influenced by the step with the longest characteristic time and the relative importance of each process to the overall rate of reaction can be determined by comparing the characteristic times for each process. The characteristic time, τ, is easily defined for first-order reaction, and is the reciprocal value of the rate constant (1/k). Half of the processes in the overall reaction are first-order reactions. The adsorption reactions (R_1, R_{-3}, R_{-4}) and the release of Mn(II) (R_4) are higher-order reactions. Defining characteristic times of higher-order reactions is more complicated. If the experimental conditions are such that the concentration of one of the reactants remains constant during the reaction, then the process can be considered a pseudo first-order reaction and the characteristic time is the reciprocal value of the product of the rate constant and the initial concentration of the reactant that remains constant. The adsorption of As(III) and Mn(II) (processes R_1 and R_{-4}) can be considered pseudo first-order reactions because the initial concentration of the reactive surface sites is much greater than the initial concentrations of As(III) and Mn(II). The release of Mn(II) can also be treated as a pseudo first-order reaction as a result of the concentration of H^+ being held constant throughout the experiment. However, the adsorption of As(V) (process

R_{-3}) cannot be simplified to a pseudo first-order reaction because the surface species, >MnOMnOH, does not remain constant.

The characteristic times for each process are listed in Table 5.2. The processes that favor the production of aqueous As(V) are the adsorption of As(III), transfer of electrons from As to Mn, and the release of As(V) from the surface. Of these three processes, the adsorption of As(III) has the longest characteristic time. The sensitivity analysis (Appendix C) indicates the reaction rate is dependent upon the rate of each process. This suggest that either the adsorption of As(III) is not slow enough or the transfer of electrons and the release of As(V) from the surface is not fast enough for there to be a rate determining step.

The rate of production of aqueous Mn(II) appears to be determined by two processes. The adsorption of aqueous As(III) and the release of Mn(II) have characteristic times of the same order of magnitude. The characteristic time for the adsorption of Mn(II) is 10 times greater than that of the release process. This indicates that the adsorption of Mn(II) under the experimental conditions is relatively unimportant for short time scales, but may become more important at longer times.

5.3.3 Effect of Initial As(III) Concentration

The effect of initial As(III) concentration was studied in a series of experiments at pH 4 and 25 °C. The ratio of total manganese surface sites to initial As(III) varied from 1.3 to 5.0. The aqueous profiles of As(III), As(V), and Mn(II) from experiments MnAs2 and MnAs3 are shown in Figure 5.6 together with the predicted curves of the kinetic model. The profiles of As(III) and As(V) keep the

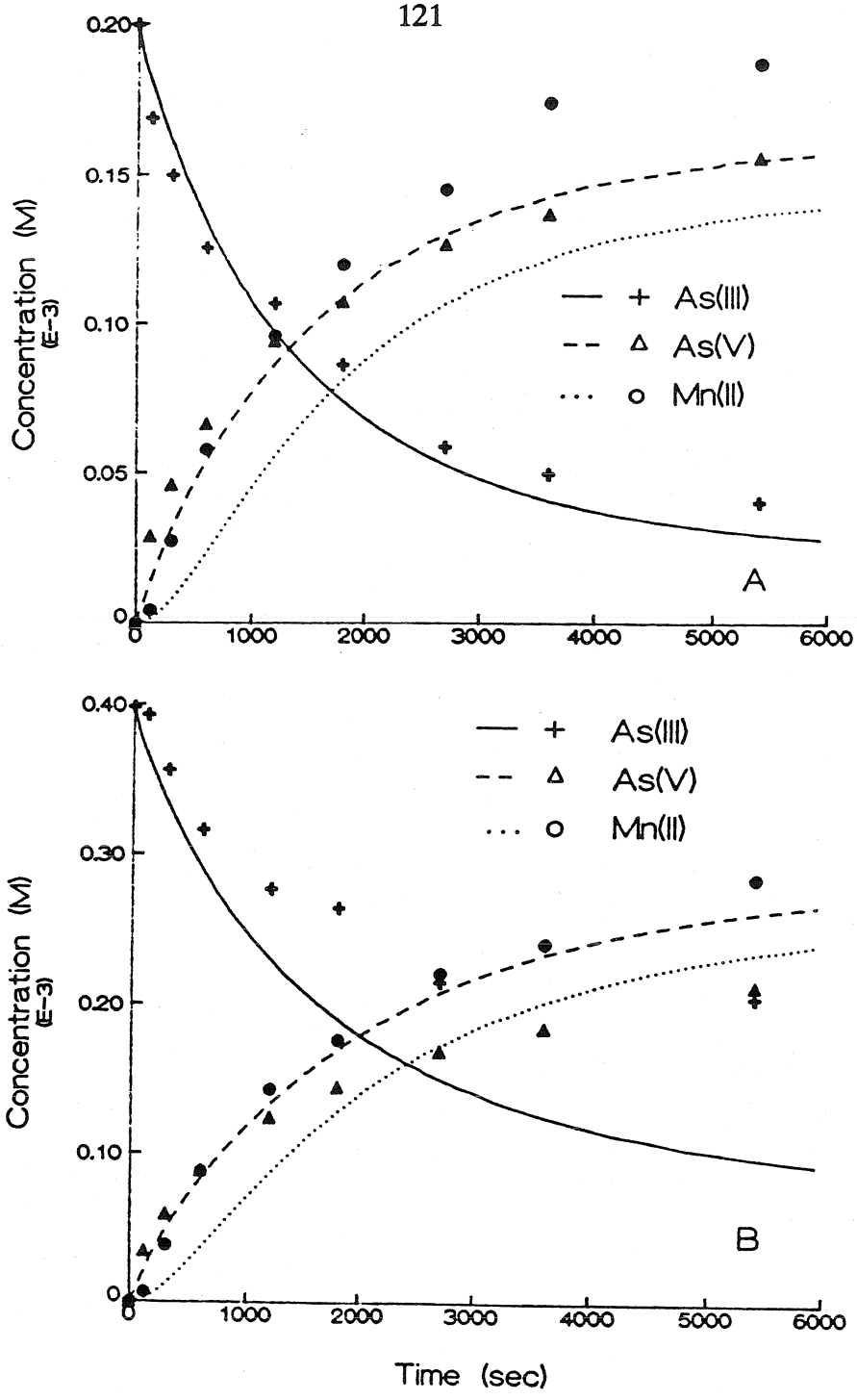

Figure 5.6: Experimental and modeled (lines) behavior of aqueous As(III), As(V), and Mn(II) in a As(III)-Mn(IV) reaction. Initial concentration of As(III) is A) 200 μM and B) 398 μM. Other reaction conditions are listed in Table 5.1.

same shape as more As(III) is added to the reaction. Initially the release of Mn(II) is slower than the release of As(V) but after a reaction period of 10-20 minutes, more Mn(II) is released than As(V). Using the same set of rate constants extracted from the data set of experiment MnAs1 ([As(III)] = 100 μM), the kinetic model was able to predict the initial behavior of As(III)(aq) and As(V)(aq). However, at longer times the model overpredicts the observed disappearance of As(III) and appearance of As(V). The disappearance of As(III) may be slowed by a greater loss of reactive surface sites than predicted by the model. The product Mn^{2+} may bind to two surface sites rather than one or the newly generated surface sites may not be as reactive as the sites they replace. It is also possible that the adsorption of As(III) becomes limited after a certain degree of surface coverage or that the electrostatic properties of the surface are altered such that adsorption of As(III) is less favored.

The model is also unable to predict the observed release of more Mn(II) than As(V). The simple model was constructed to predict Mn^{2+} concentrations that are equal to or less than the concentration of As(V). The extra Mn^{2+} may be a consequence of the difference between the true average Mn oxidation state of the oxide particles and the assumed state of +IV. If the average Mn oxidation state is less than +4, then the product ratio Mn(II)/As(V) will be greater than one. Figure 5.7 illustrates the relationship between the average Mn oxidation state in a Mn oxide and the product ratio Mn(II)/As(V). The observed product ratios from experiments MnAs2 and MnAs3 are also plotted in Figure 5.7 and indicate that the apparent Mn oxidation states are +3.6 and +3.42, respectively. The implied oxidation states are

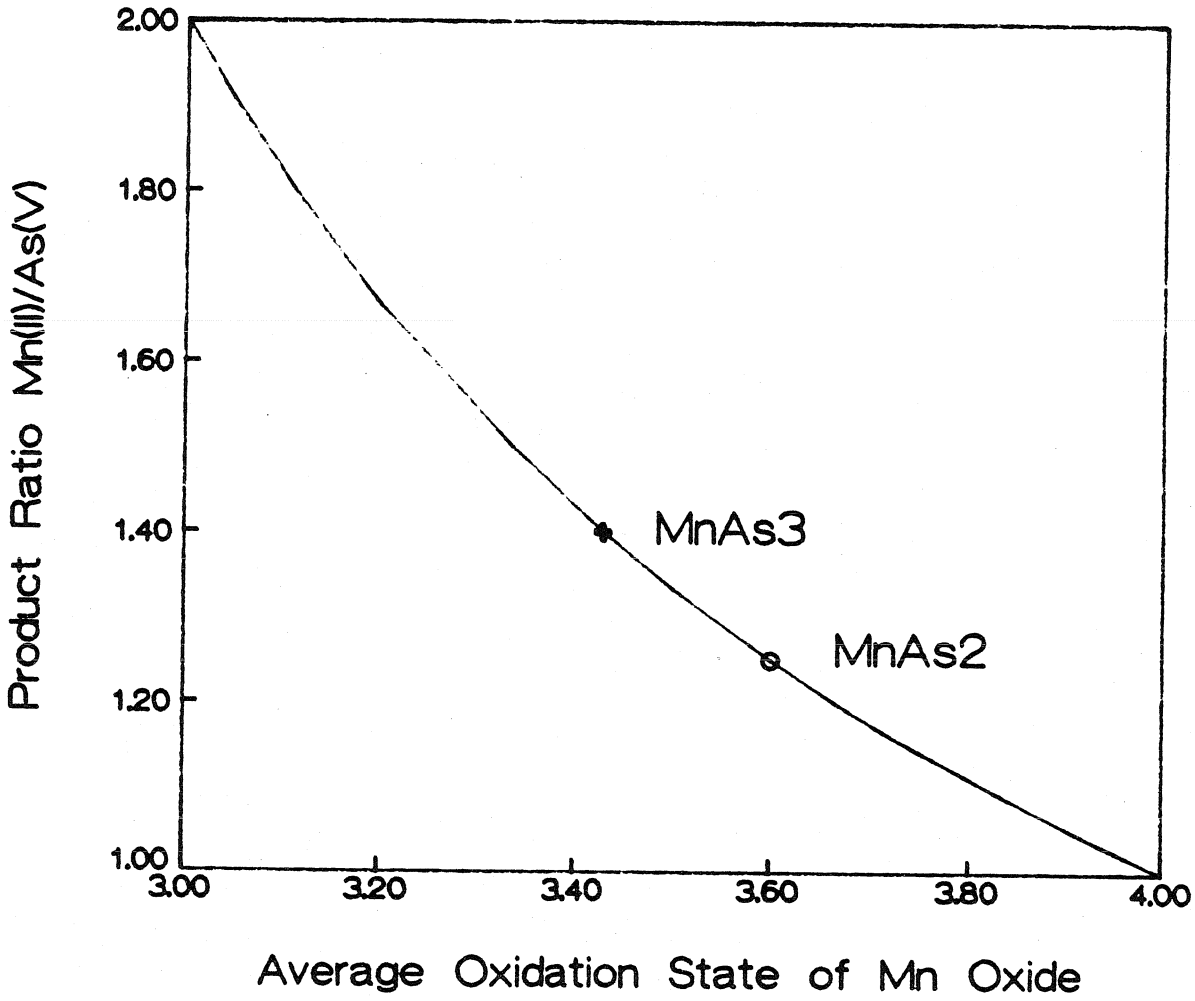

Figure 5.7: The product ratio Mn(II)/As(V) is dependent upon the average Mn oxidation state of the oxide. The observed ratios for MnAs2 and MnAs3 indicate lower oxidation states than expected for birnessite.

low compared to other reported average Mn oxidation states of synthetic birnessite particles (see Table 5.3). Also, if one considers that some of the product Mn may not be released to solution, then the average Mn oxidation state would be even lower.

Another explanation for these observations may involve the release of Mn^{2+} cations that are trapped in the lattice. Although the oxide particles were prepared by the reduction of $KMnO_4$ by HCl, some of the Mn(VII) may have been reduced past the +IV oxidation state to the +III and +II oxidation states. Mn(II) ions may have been trapped in the growing Mn(IV) crystal structure. The extent of the dissolution of the oxide structure increases as the concentration of As(III) is raised. As the oxide dissolves, the cations trapped in the bulk oxide structure are released into solution.

5.3.4 Effect of pH

The influence of pH on the reaction between aqueous As(III) and the surface of birnessite was studied in a series of experiments at 25 °C and 0.1 M ionic strength. pH values ranged from 4 to 8.2. The results of the experiments are shown in Figure 5.8.

The effect of pH on the extent of disappearance of aqueous As(III) and release of As(V) to solution is minimal. The rates are greatest at pH 4, but do not show a pronounced decline with increasing pH from 5 to 8.2. The apparent half-life of each process (i.e., the time necessary for 50 percent to disappear or to be released) is only doubled as pH is raised from 4 to 8.2. The absence of a strong

Table 5.3: Reported Values of the Average Mn Oxidation State and of x in MnO_x for Synthetic Manganese Oxides

Reference	Average Mn Oxidation State	x in MnO_x
Murray (1974)	+3.84	1.92
Murray (1975)	+3.86	1.93
Parida et. al. (1981)	+3.796	1.898
Parida et. al. (1981)	+3.936	1.918
Adams and Ghiorse (1988)	+3.86	1.93
Kanugo and Mahapatra (1989)	+3.62	1.811
Kanugo and Mahapatra (1989)	+3.74	1.87
Stone and Ulrich (1989)	+3.93	1.97

influence by the pH of the suspension is predicted by the acid-base chemistry of the proposed reactants. The first pK_a of arsenious acid is 9.3 and thus the concentration of the fully protonated species H_3AsO_3 remains nearly constant throughout the pH range of study. The concentration of the neutral surface species also is constant throughout the pH range (see Figure 3.8). The small effect of increasing pH may be due to the dissociation of a fraction of the neutral surface species. Also, as pH is raised the birnessite surface becomes increasingly negative. The adsorption of As(III) may decrease as the result of electrostatic repulsion. (As(III) adsorption on goethite decreases at pH values greater than the pH_{zpc}.)

The pH of the particle suspension does affect the release of Mn(II) considerably. At pH 4, Mn(II) is released only slightly less than stoichiometric with

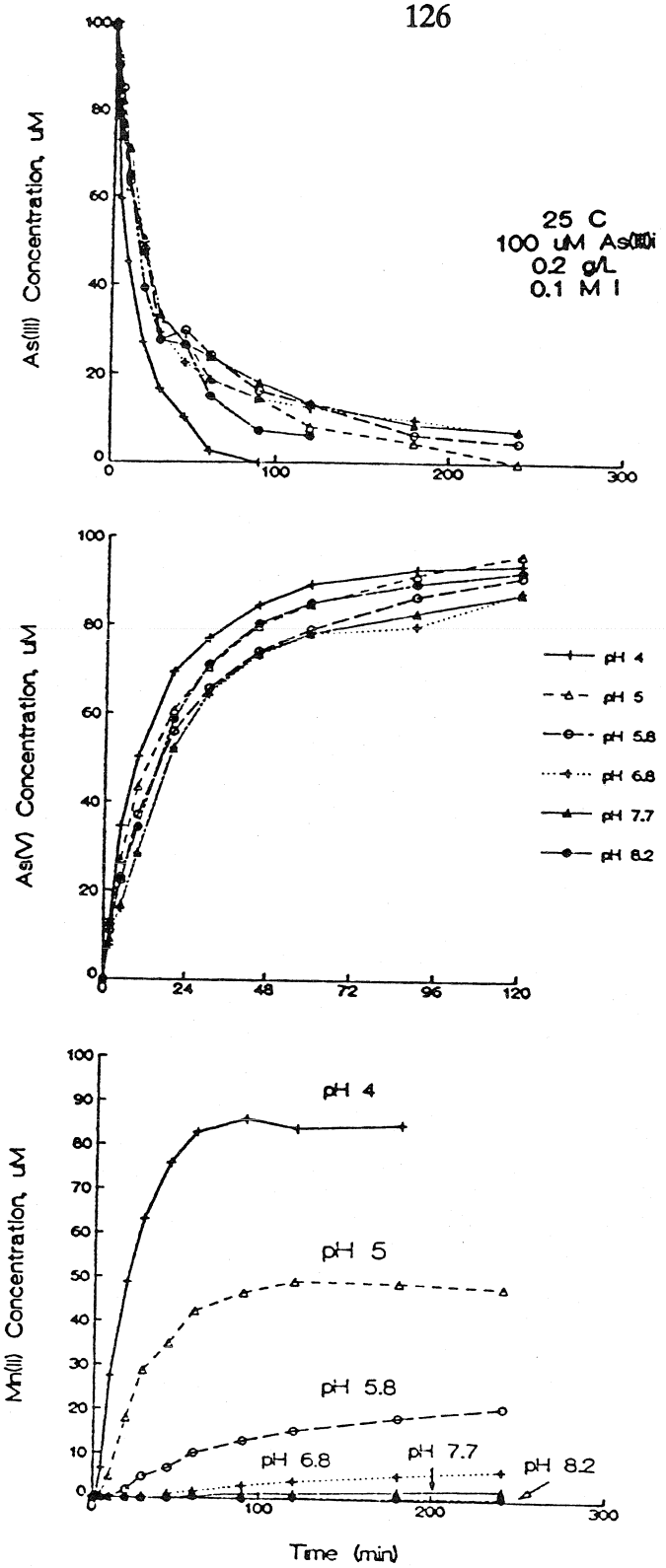

Figure 5.8: The influence of the pH of the particle suspension on the aqueous profiles of As(III), As(V), and Mn(II). Reaction conditions are listed in Table 5.1.

As(V). As the pH of the particle suspension is raised, less Mn(II) is released. After 90 minutes of reaction, the aqueous concentration of Mn(II) decreases from 3 μM to 1 μM to less than 0.4 μM as the pH of the system increases from 6.8 to 7.7 to 8.2. Stone and Ulrich (1989) report similar behavior of Mn(II) in aqueous suspensions of synthetic birnessite particles. They found for similar ratios of total Mn to Mn(II) that 20 % of Mn(II) adsorbed at low pH values with nearly 100 % adsorption at pH values greater than 6.

The reaction rate constants extracted from the numerical modeling of the three aqueous species concentration profiles as a function of pH are listed in Table 5.4. The first rate constant, k_1, varies slightly as pH is changed. Rate constants k_{-1}, k_2, k_{-2}, and k_3 do not vary with pH.

Another effect of pH on the reaction was observed during the experimental runs. The reaction suspensions were weakly buffered by a small amount of strong acid (or base) and by the oxide particle surface. In order to maintain a constant pH throughout the experiment, small amounts of strong acid or base were added periodically. At pH values less than 6, the pH of the suspension increased during the reaction and strong acid was added. At pH values greater than 6.6, the pH of the suspension decreased as the reaction progressed and a strong base was needed to maintain the initial pH. These observations suggest that the overall reaction stoichiometry changes at a pH between 6 and 6.6. For pH values less than 6 the stoichiometry of equation (5-1) is followed, in which a proton is consumed for every As(III) reacted. As pH increases, both $H_2AsO_4^-$ and the surface species release a

Table 5.4: Influence of pH on As(III)-Mn(IV) Reaction Rate Constants

pH	4	5	5.85	6.7	7.7	8.2
As_T (μM)	99.6	99.4	99.4	99.3	99.9	99.9
S_T (μM)	502	502	502	502	502	502
k_1 ($M^{-1}sec^{-1}$)	5	3	2.6	2.5	2.3	2.8
k_{-1} (sec^{-1})	0.02	0.02	0.02	0.02	0.02	0.02
k_2 (sec^{-1})	0.03	0.03	0.03	0.03	0.03	0.03
k_{-2} (sec^{-1})	0.0015	0.0015	0.0015	0.0015	0.0015	0.0015
k_3 (sec^{-1})	0.1	0.1	0.1	0.1	0.1	0.1
k_{-3} ($M^{-2}sec^{-1}$)	5×10^6	1×10^7	7×10^7	6.3×10^8	4×10^9	8×10^9
k_4 ($M^{-2}sec^{-1}$)	2.5×10^6	6.3×10^7	4×10^8	4.8×10^9	7.7×10^{10}	1.5×10^{10}
k_{-4} ($M^{-1}sec^{-1}$)	5	10	12	12	12	12
log K_1	2.40	2.18	2.11	2.10	2.06	2.15
log K_2	1.3	1.3	1.3	1.3	1.3	1.3
log K_3	-7.7	-8.0	-8.85	-9.7	-10.6	-10.9
log K_4	5.7	6.8	7.52	8.6	9.81	10.1

proton. This results in an overall net production of protons causing the pH of the suspension to decrease.

5.3.5 Effect of Temperature

The effect of temperature on the overall reaction between aqueous As(III) and birnessite was studied in a set of experiments at pH 4 and 0.1 M ionic strength. The temperature of the particle suspension was varied from 15 to 35 °C. The resulting aqueous profiles of As(III), As(V), and Mn(II) are plotted in Figure 5.9.

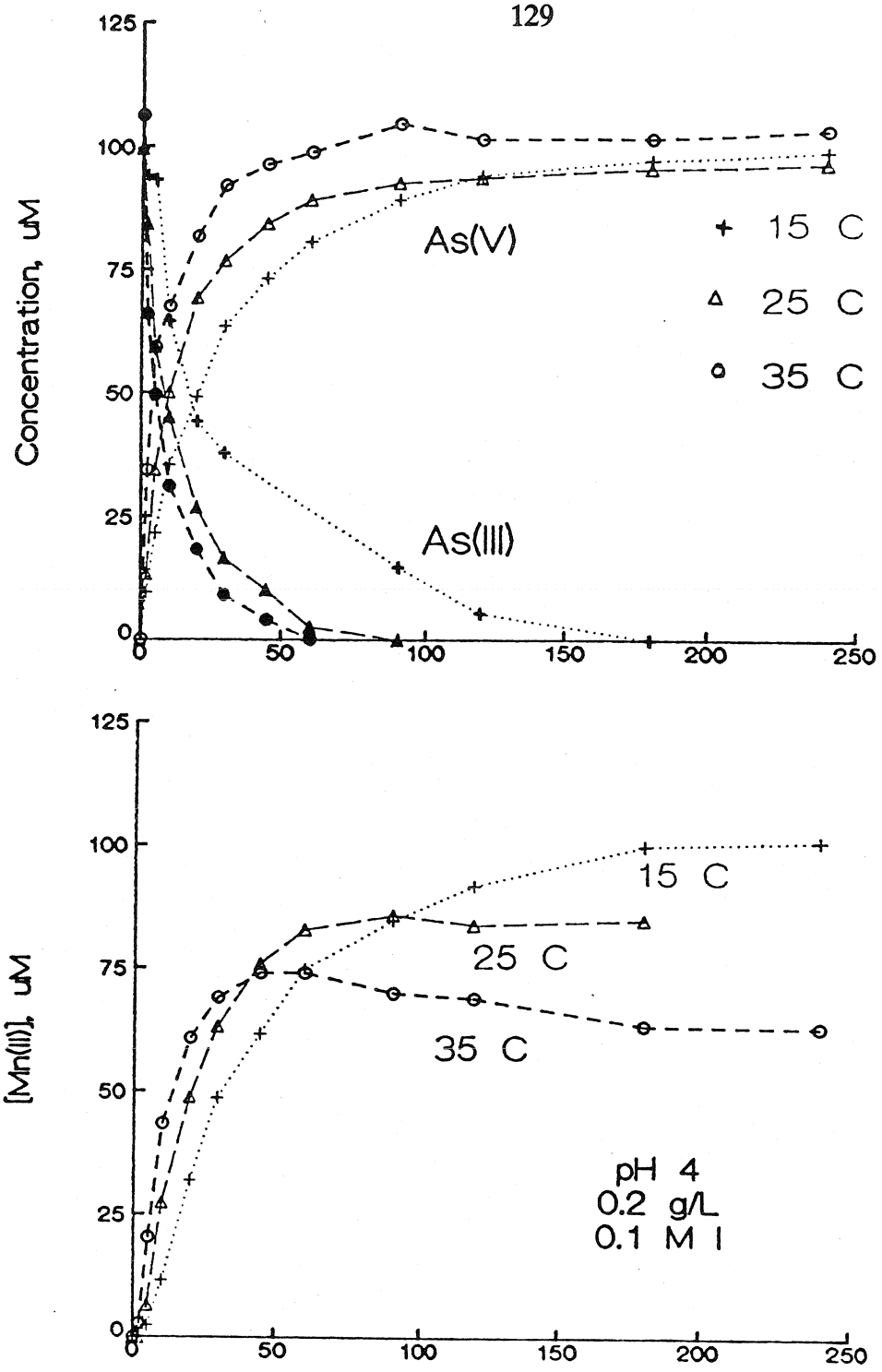

Figure 5.9: The effect of temperature on the disappearance of As(III)(aq) and the release of As(V)(aq) and Mn(II)(aq) in a 0.2 g/L birnessite suspension at pH 4 and 0.1 M $NaClO_4$.

The rates of As(III) disappearance and release of As(V) and Mn(II) increase as temperature is raised. The extent of Mn(II) release decreases with increasing temperature. At 15 °C, approximately equivalent amounts of Mn(II) and As(V) are released into solution. When the temperature is 25 °C, there is seven percent less Mn(II) in solution than As(V) and the difference is even greater (25 %) at 35 °C. Additionally, at 35 °C, the concentration of Mn^{2+}(aq) decreases after all of the As(III) has reacted. Machesky (1990) reported that metal cation adsorption increases with increasing temperature. A partial explanation of this effect is that the pH_{zpc} of the oxide surface decreases as temperature increases and a decrease in pH_{zpc} promotes cation adsorption.

The kinetic model was able to predict accurately all species profiles except for the decrease in the Mn^{2+} concentration at later times. The set of rate constants used to provide the fits and the resulting equilibrium constants are listed in Table 5.5. The kinetic modeling indicates that the adsorption-desorption processes for As(III) and Mn(II) are influenced by changes in temperature, while there is no temperature dependence on As(V) release and adsorption. The fitted rate constant for the transfer of electrons from As(III) to Mn(IV) (k_2) remains constant from 15 to 25 °C, but its value is halved at 35 °C.

The Arrhenius equation relates a rate constant to temperature:

$$\ln k_i = E_a/RT + \text{constant} \qquad (5\text{-}22)$$

and this relationship yields information about the activation energy of the reaction

Table 5.5: Influence of Temperature on As(III)-Mn(IV) Reaction Rate Constants and Equilibrium Constants

Temperature (°C)	15	25	35
As_T (μM)	100.0	99.4	106.3
S_T (μM)	502	502	502
k_1 ($M^{-1}sec^{-1}$)	2.5	5	7.5
k_{-1} (sec^{-1})	0.02	0.02	0.02
k_2 (sec^{-1})	0.03	0.03	0.015
k_{-2} (sec^{-1})	0.0015	0.0015	0.0015
k_3 (sec^{-1})	0.1	0.1	0.1
k_{-3} ($M^{-2}sec^{-1}$)	5×10^6	5×10^6	5×10^6
k_4 ($M^{-2}sec^{-1}$)	2.5×10^6	2.5×10^6	9×10^6
k_{-4} ($M^{-1}sec^{-1}$)	2.5	5	35
log K_1	2.10	2.40	2.57
log K_2	1.3	1.3	1.0
log K_3	-7.7	-7.7	-7.7
log K_4	6.0	5.7	5.4

step, E_a. Arrhenius treatment of the data gives the activation energies of the process whose rate is affected by changes in temperature.

Process and Rate Constant	E_a ± Std Error (kJ/mole)	r^2
$As(OH)_3$ Adsorption, k_1	40.6 ± 5.3	0.983
Mn^{2+} Release, k_4	45.7 ± 27.5	0.733
Mn^{2+} Adsorption, k_{-4}	99.3 ± 30.1	0.916

The values of the activation energies of these processes indicate that each of the

processes are controlled by chemical reactions rather than diffusion limited. Diffusion limited reactions have activation energies of about 15 to 21 kJ/mole. The goodness of fit of the data to the Arrhenius equation is indicated by the value of r^2. The value of the standard error is also an indicator of goodness of fit. The goodness of fit is best for the $As(OH)_3$ adsorption activation energy, poorest for the Mn^{2+} release activation energy.

The van't Hoff equation relates an equilibrium constant to temperature:

$$\ln K = - \Delta H_r/RT + \text{constant} \qquad (5\text{-}23)$$

and this relationship yields information about the reaction enthalpy ΔH_r as long as the reaction enthalpy is independent of temperature. A linear plot of ln K versus 1/T indicates that the slope, ΔH_r, is independent of temperature. Figure 5.10 is a linear van't Hoff plot of the equilibrium constants K_1 and K_4. The resulting values of the reaction enthalpies are given below.

PROCESS	ΔH_r (kJ/mole)
$As(OH)_3$ Adsorption-Desorption (K_1)	41 ± 5
Mn^{2+} Release-Adsorption (K_4)	-54 ± 3

Machesky (1990) reported that anion adsorption is exothermic ($\Delta H_r < 0$) while cation adsorption is endothermic ($\Delta H_r > 0$). The data indicate that the adsorption of both As(III) and Mn(II) is endothermic. Machesky (1990) also reported that the reaction enthalpies of cadmium, zinc, and nickel adsorption on hematite (α-Fe_2O_3) at pH 6 are, respectively, +13, +49, and +30 kJ/mole. In comparison with the

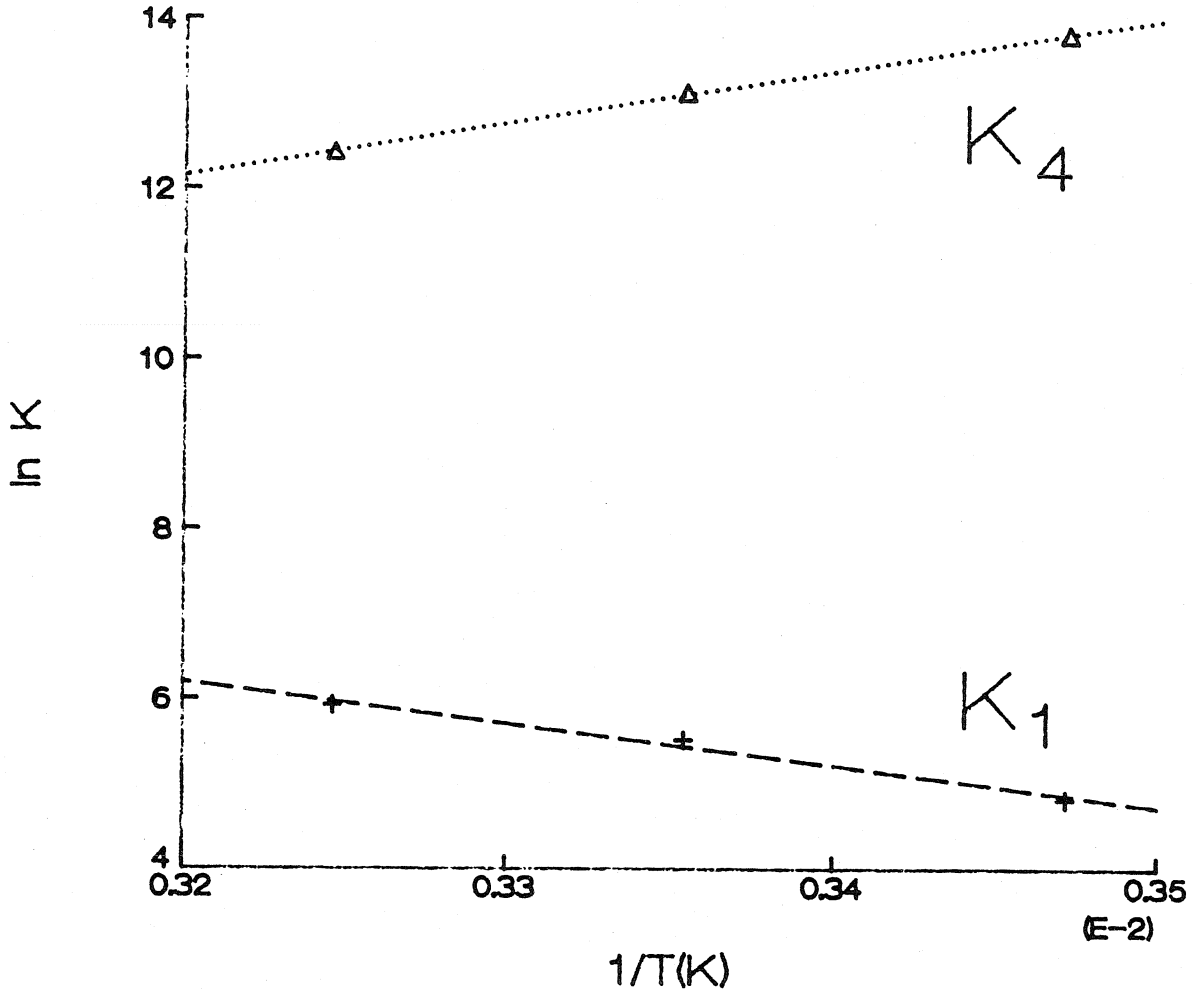

Figure 5.10: van't Hoff plot of the equilibrium constants and linear regression lines for As(III) adsorption-desorption (K_1) and Mn(II) release-adsorption (K_4). The slope of each line is $-\Delta H_r/R$.

reaction enthalpy of Mn(II), the data indicate that the affinity of the bivalent cations for the surface followed the order:

$$Mn(II) > Zn(II) > Ni(II) > Cd(II)$$

and this is the same order of affinity that Murray (1975) described for the interaction of metal ions at the manganese dioxide-solution interface.

The reaction enthalpy of an individual reaction and the activation energies of the forward and reverse steps are related by the expression

$$\Delta H_r(K_i) = E_a(k_i) - E_a(k_{-i})$$

which follows from the Arrhenius and van't Hoff equations and the definitions $K_i = k_i/k_{-i}$ and $\ln(K_i) = \ln(k_i) - \ln(k_{-i})$. We can compare temperature dependences of equilibria and kinetics on this basis.

5.3.6 Effect of Dissolved Oxygen

Dissolved oxygen is a stronger oxidant than Mn(IV). However, the reaction between dissolved oxygen and As(III) is very slow. Eary and Schramke (1990) showed that the oxygenation of As(III) in freshwater had a half-life in the range of one to three years. In our laboratory, standard arsenite solutions remained constant over a period of several days to a week.

The reaction suspension was purged with air (pO_2 = 0.21 atm) instead of $N_2(g)$ to study the effect of dissolved oxygen on the reaction between the birnessite surface and As(III). Figure 5.11 shows that there is no difference in the rate of As(V) release to solution at pH 4 and 25 °C when dissolved oxygen is present or not.

This observation confirms that the surface Mn(IV) is the oxidant in the reaction and is not just a catalyst in the oxygenation of As(III).

Another effect of dissolved oxygen is the oxidation of the product Mn(II). The homogeneous oxygenation of Mn(II) below pH values of 8 is very slow. Davies and Morgan (1989) have shown that the oxidation of Mn(II) is more rapid in metal oxide suspensions although the reaction rates are much slower than the rate of adsorption. For the short reaction time and pH conditions of this experiment, the fate of the product Mn(II) is probably controlled by adsorption and not oxidation by dissolved oxygen.

5.3.7 Effect of Bivalent Cations Ca^{2+} and Mn^{2+}

The effect of an additional adsorbing aqueous species on the rate of reaction between As(III) and Mn(IV) was examined in a set of experiments at pH 4, 25 °C, 0.2 g/L solid concentration, and 0.1 M ionic strength. The effect was studied by pre-equilibrating the particle suspension with various concentrations of Ca^{2+}(aq) and Mn^{2+}(aq) and by monitoring the appearance of As(V)(aq). Mn^{2+}(aq) appearance also was monitored in the Mn addition experiments. Previous studies (Murray, 1975; Loganathan et. al., 1977; Stone and Ulrich, 1989) report that both cations bind specifically to the surface, with Mn^{2+} binding to a much greater extent. The reaction between the particle surface and the bivalent cation can be expressed by the following equations:

$$>MnOH + Ca^{2+} \rightleftharpoons >MnOCa^{+} + H^{+} \qquad (5\text{-}24)$$

$$>MnOH + Mn^{2+} \rightleftharpoons >MnOMn^{+} + H^{+} \qquad (5\text{-}25)$$

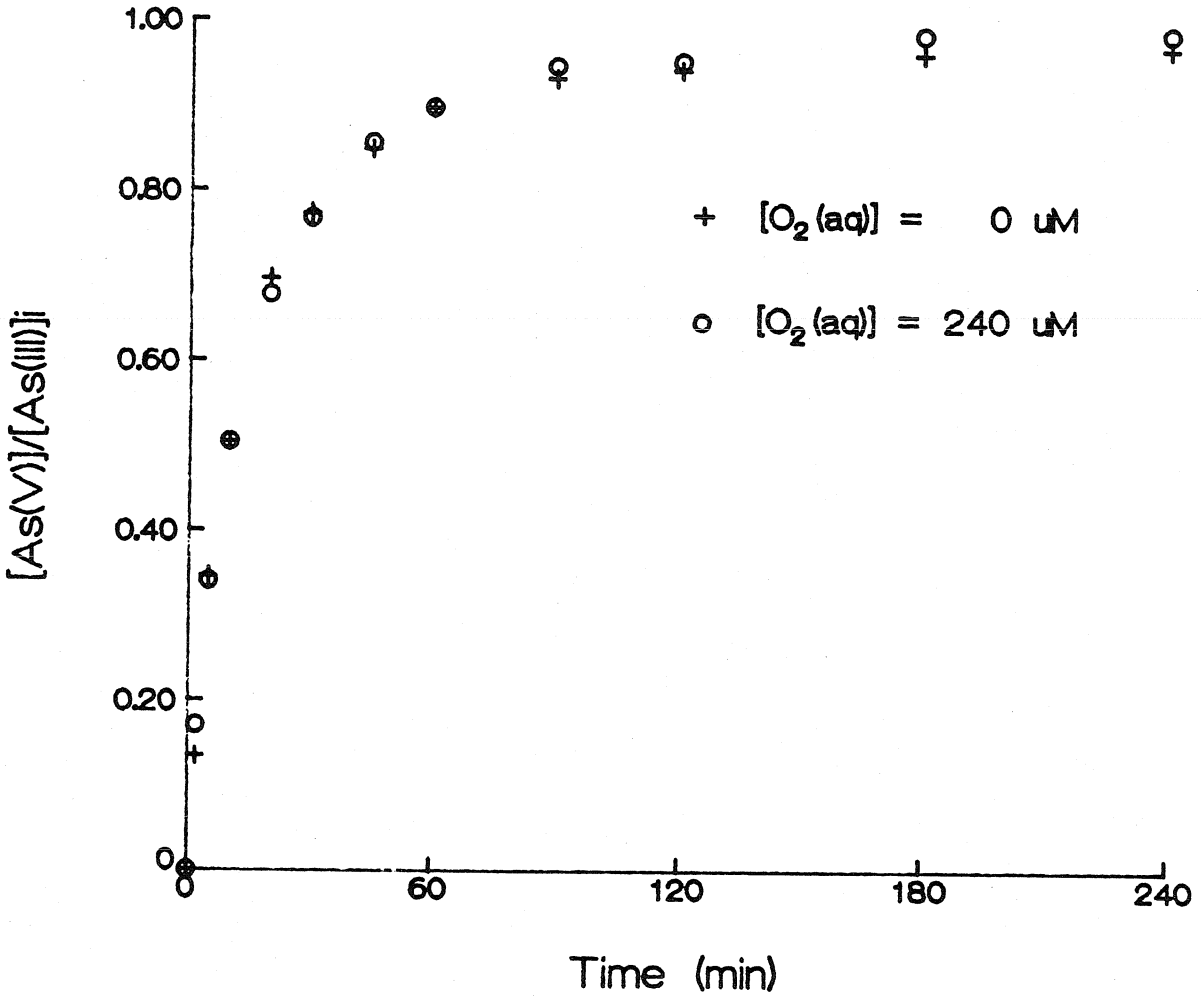

Figure 5.11: The presence of dissolved oxygen in a birnessite suspension at pH 4 and 25 °C has no effect on the rate of As(V) release to solution.

By allowing cations to pre-equilibrate with the surface before adding As(III)(aq), the number of reactive surface sites is reduced.

The effects of pre-equilibrating the particle suspension with 99 or 500 μM Ca^{2+} and 99 or 196 μM Mn^{2+} before addition of 100 μM As(III) are shown in Figure 5.12 (the results of adding no cations to the suspension are shown for comparison). The addition of Mn^{2+}(aq) caused a greater decrease in the rate of As(V) release than did the addition of Ca^{2+}(aq). Increasing the concentration of either cation decreased the rate of reaction.

For the Mn^{2+} addition experiments, the concentration of Mn^{2+}(aq) as a function of time was also determined and the data are plotted in Figure 5.13. Values for the Mn^{2+} concentrations have been adjusted to account for the Mn^{2+} in solution prior to the addition of As(III). At both concentrations of added Mn^{2+}, more Mn^{2+} is released than As(V). The opposite is observed when there is no addition of Mn^{2+}. Also, the rate of Mn^{2+} release is greater at the smaller concentration of added Mn^{2+}. These effects are the result of two processes: (i) more of the produced Mn^{2+} is released into solution as there are less surface sites for binding, and, (ii) portions of the added Mn^{2+} that adsorbed to the surface prior to the As(III) addition are released as the oxide is dissolved.

Because there is a greater release of Mn^{2+}(aq) than As(V)(aq), the simple kinetic model is unable to predict the Mn^{2+} profile. The As(V) profiles can still be modeled. The hypothesis of this set of experiments is that the addition of other species that will adsorb to the surface will decrease the rate of reaction. For

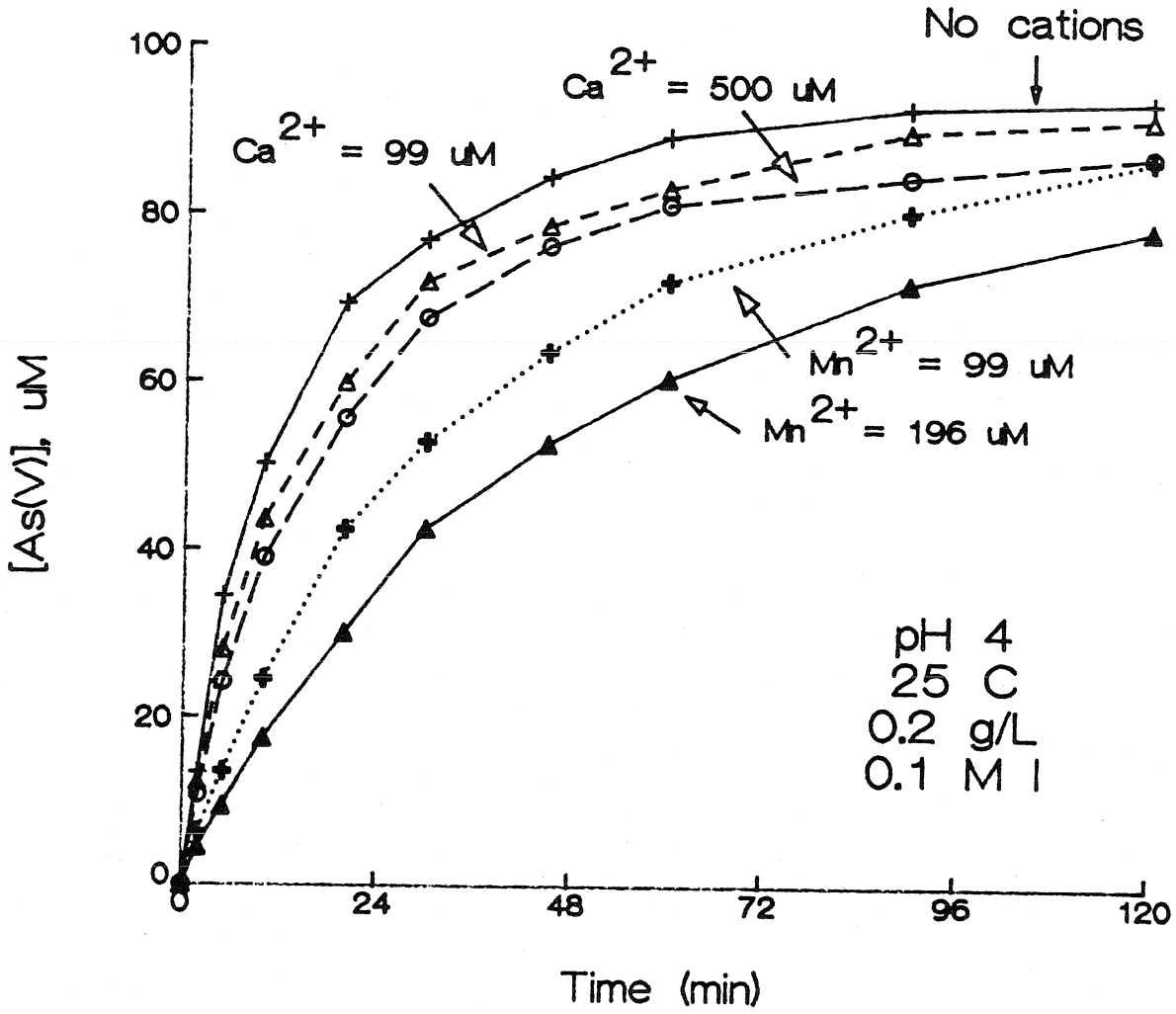

Figure 5.12: The addition of bivalent cations decreases the rate of As(V) release, with Mn^{2+} (aq) having a greater effect than Ca^{2+} (aq). Initial [As(III)] = 100 μM.

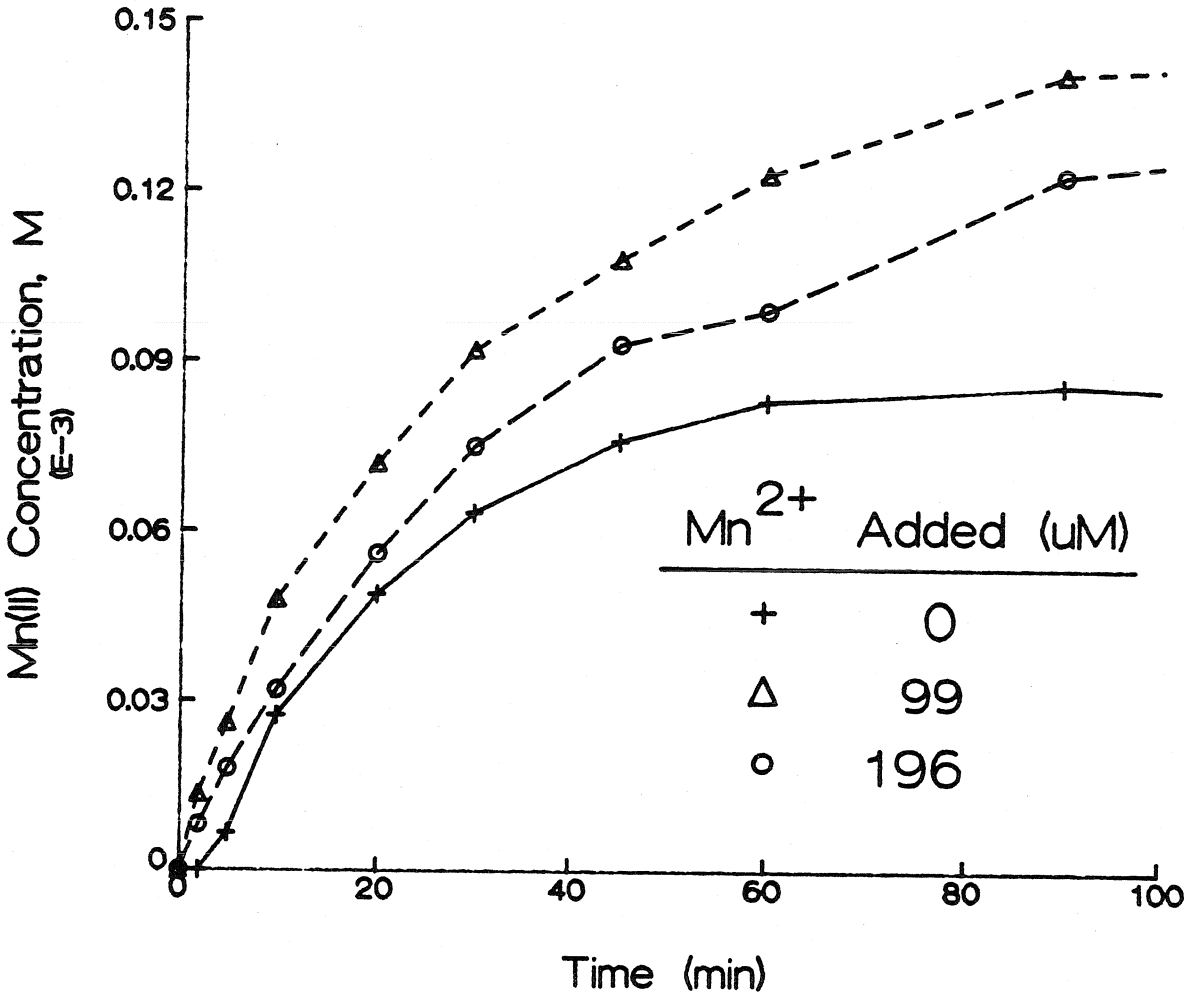

Figure 5.13: The addition of Mn^{2+} to a birnessite suspension prior to reaction with As(III) results in the release of greater amounts of Mn^{2+} (aq) during the reaction.

example, if the total concentration of sites is reduced from 502 μM to 200 μM, the As(V) profiles can be predicted from the set of rate constants derived from the experimental data in absence of cation addition. However, such a loss of reactive surface sites is much greater than predicted from the amount of Mn adsorbed. In the experiment where 99 μM Mn^{2+} is equilibrated with the oxide surface, 54 μM Mn^{2+} was adsorbed when the As(III) was added. If each Mn atom bonded with one surface site, then the total concentration of reactive surface sites would only be reduced to 448 μM. Likewise, if each Mn atom formed a bidentate complex with two surface sites, then the total concentration of reactive surface sites would be 394 μM, which is still much greater than the concentration needed to model the data.

Another approach to modeling the As(V) data would be, first, to assume that the total concentration of reactive surface sites is only reduced by the concentration of adsorbed Mn^{2+}, and second, to vary the rate constant, k_1. This approach results in a good prediction of the As(V) data when k_1 is reduced from 5 to 2 $M^{-1}sec^{-1}$. Both approaches imply that the adsorbed Mn influences the reactivity of more than one surface site.

5.3.8 Summary of the Dynamics of As(III) and Birnessite

The experiments involving aqueous As(III) and birnessite at pH 4 and 25 °C indicate that the depletion of As(III) from solution is rapid with a time scale of minutes. The oxidation product As(V) is released almost as quickly, while the release of the reduction product Mn(II) is slightly slower. The results also show that the concentration of dissolved oxygen has no effect on the rate of reaction. These

observations suggest (i) birnessite directly oxidizes As(III) through a surface mechanism, (ii) the adsorption of As(III) is the slowest step in the production of As(V), and (iii) the reaction products As(V) and Mn(II) are released by different mechanisms.

The effect of increasing pH from 4 to 8.2 has a small influence on the rate and extent of As(III) uptake and As(V) release, but it greatly reduces the rate and amount of Mn(II). Near-equivalent quantities of As(V) and Mn(II) are released at pH 4, while very little Mn(II) is released at pH values above 7.

Increasing the temperature of the birnessite suspension from 15 to 35 °C results in increased rates of reaction for all species. The extent of As(III) depletion and As(V) release is equivalent for all temperatures, but the extent of Mn(II) release decreases with increasing temperature. This is consistent with equilibrium observations of metal cation adsorption by Machesky (1990).

It is also observed that the rates of reaction decrease when adsorption competitive bivalent cations (Mn^{2+}, Ca^{2+}) are added to and equilibrated with the particle suspension. All of the observations are consistent with the surface reaction hypothesis.

The proposed four-step reversible kinetic model is successful in describing the time-dependent behavior of the aqueous reactants and products over a pH range from 4 to 8.2 and a temperature range from 15 to 35 °C. The kinetic description allows the reaction to be described in terms of specific aqueous and surface processes.

5.4 Dynamics of Se(IV) and Birnessite

5.4.1 Behavior of Se(IV), Se(VI), and Mn(II)

Reaction conditions for the Se(IV)-birnessite experiments are listed in Table 5.6. In all experiments, total manganese and total manganese surface groups are in excess of total selenium. Data from all of the experiments are listed in Appendix A. The experiments were run for a time period of nearly a month and the reactions had not yet reached completion. With the extended time period of the experiment, other reactions than those proposed were possible. Two experiments were run to assess the possibility and extent of the additional reactions.

One possible reaction pathway in the transformation of Se(IV) to Se(VI) is the homogeneous oxidation of Se(IV) by dissolved oxygen. This pathway was explored by monitoring the Se(IV) concentration in a birnessite-free solution at pH 4 and 25 °C (experiment MnSe4). For the duration of the experiment (673 hours), no changes in the concentration of Se(IV) were observed and no Se(VI) appeared, indicating that the homogeneous oxidation of Se(IV) under the experimental conditions either does not occur or is extremely slow.

Another possible reaction that is independent of the proposed mechanism is the acidic dissolution of the oxide phase. Eary and Rai (1987) had observed the appearance of 20 to 50 μM Mn^{2+}(aq) in a suspension of pyrolusite (β-MnO_2(s)) at pH values between 3.0 and 4.0 on time scales of hundreds of hours. In our laboratory, birnessite particles were suspended in a Se(IV)-free solution at pH 4 and 25 °C for 673 hours and the solution was sampled periodically for Mn^{2+}(aq)

Table 5.6: Reaction Conditions of Selenite-Birnessite Experiments

Expt	Initial [Se(IV)] (μM)	Solid Conc (g/L)	Mn_T to Se(IV)	$>Mn_T$ to Se(IV)	Temp (°C)	pH	Expt. Time(hr)
MnSe1	101.2	0.20	14.5	4.8	25	4.0	673
MnSe2	0.0	0.20	--	--	25	4.0	673
MnSe3	50.9	0.20	29	9.6	25	4.0	673
MnSe4	98.7	0.00	0	0	25	4.0	673
MnSe5	101.3	0.40	29	9.6	25	4.0	670
MnSe6	101.3	0.20	14.5	4.8	25	5.0	670
MnSe7	101.3	0.20	14.5	4.8	25	7.0	670
MnSe8	101.4	0.20	14.5	4.8	31	4.0	460
MnSe9	101.4	0.21	14.5	4.8	36	4.0	460
MnSe10	100.0	0.20	14.5	4.8	25	4.0	24

(experiment MnSe2). No Mn^{2+} (aq) was observed in solution throughout the duration of the experiment. It is possible that some dissolution of the oxide occurred, but then the released Mn^{2+} was quickly re-adsorbed to the surface. Re-adsorption would not be probable in a β-MnO_2 suspension under the experimental conditions of Eary and Rai's study. β-MnO_2 has a pH_{zpc} of 7 (Oscarson et al., 1983b) and thus, at pH values less than 7, and especially at pH values of 4 and below, Mn^{2+} (aq) would not adsorb on the β-MnO_2 surface.

Figure 5.14 illustrates the observed behavior of aqueous and adsorbed selenium species with time after aqueous Se(IV) is introduced into a suspension of

birnessite particles under the conditions pH 4, 25 °C, and ionic strength 0.001 M (experiment MnSe1). The aqueous concentration of Se(IV) decreases rapidly over the first 15 minutes. This is followed by a slower rate of depletion that continues for the duration of the experiment. Aqueous Se(VI) appears in measurable concentrations (> 1 μM) after 12 hours and is produced at a constant rate for the duration of the experiment (28 days). Mass balance of total selenium in the system indicates the adsorbed selenium (Se_{ads} = $Se(IV)_{ads}$ + $Se(VI)_{ads}$ = Se_{init} - Se(IV)(aq) - Se(VI)(aq)) remains constant for the duration of the experiment.

Mn^{2+}(aq) is not detected throughout the run of the experiment. The lack of Mn^{2+}(aq) appearance is a bit surprising since it appeared in solution during the arsenite-birnessite experiments. There are several possible reasons for the lack of aqueous Mn(II) appearance during the reactions:

(a) Mn(II) is either not released or it is totally re-adsorbed by the surface. At higher pH values (above pH 6) little or no Mn(II) is released during the arsenite experiments and it may be possible that in the selenite experiments there are no species that effectively compete with Mn(II) for the surface at the low pH values. Also, reaction conditions are such that Mn^{2+} adsorption is slightly favored (i.e., negative surface charge) and there is an abundance of surface sites to which the Mn^{2+} can adsorb. The time scales of the selenite experiments are much greater than the arsenite experiments. The longer experiments may give time for the Mn(II) to completely re-adsorb to the surface but this gives different values of the equilibrium constant K_4 for the As and Se experiments.

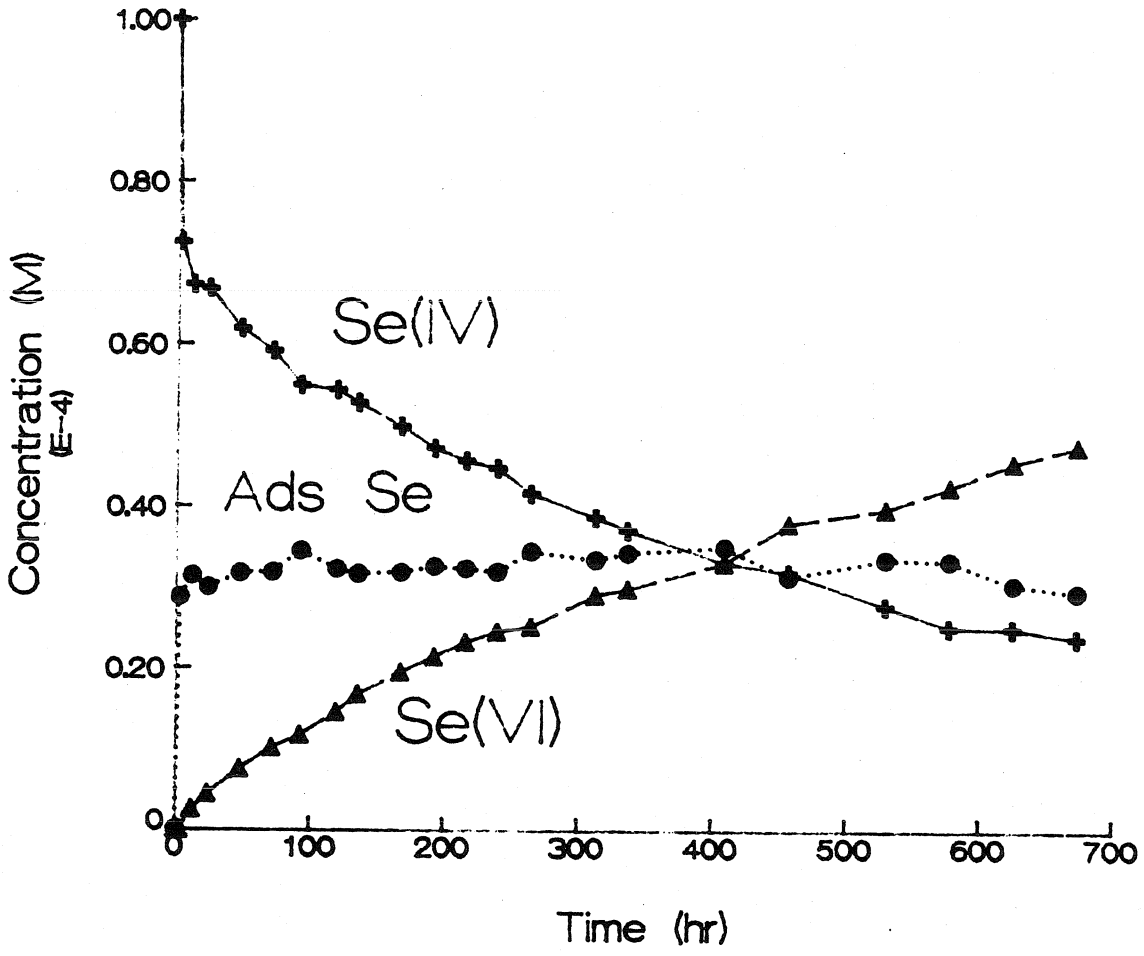

Figure 5.14: Experimental behavior of aqueous and adsorbed Se species in a 0.2 g/L birnessite suspension at pH 4, 25 °C, and 0.001 M $NaNO_3$. Initial concentration of Se(IV) is 100 μM.

(b) Other reactions which have not been identified either tied up Mn(II) on the surface in the Se experiments or kept Mn(II) in solution at low pH values in the As experiments. Possible explanations are that in the Se experiments the time scale is long enough for Mn(II) to be oxidized to either Mn(III) or Mn(IV) forming a solid, or Mn(II) forms an aqueous complex with As(V) that keeps it in solution.

(c) Mn(II) is not produced during the reaction of birnessite with selenite. Instead of transferring both electrons to on Mn(IV) atom, two Mn(IV) atoms each receive one electron and form Mn(III) atoms on the surface which would not be as likely to desorb or be released into solution. Assuming that the energetics of a surface reaction is approximated by the energetics of a bulk solid reaction, the energetics of Mn(IV)-Mn(III) redox reactions are estimated from

$$MnO_2(s) + H^+ + e^- = MnOOH(s) \qquad E_H^\circ = 1.04 \text{ volts}$$

At pH 4, $\Delta E_H^\circ = 0.083$ volts for the 2Mn(IV) + Se(IV) = 2Mn(III) + Se(VI) reaction. This value is less than the value of $\Delta E_H^\circ = 0.092$ volts for the Mn(IV) + Se(IV) = Mn(II) + Se(VI) reaction. Thus, energetics are lower for this type of reaction, but they are still favorable. Another observation that might support a mechanism of this type is the conclusion of an EXAFS spectroscopic analysis for the occurrence of a Se(IV)-Fe(III) bidentate surface species when selenite is added to a goethite suspension and then dried (Hayes et al., 1987). If it was assumed that Se(IV) also formed a bidentate surface species with birnessite, then spreading the electrons to two Mn(IV) atom might be more plausible. However, in the EXAFS study, the experimental conditions where such that Se(IV) adsorption was highly

favorable (anion and positive surface charge), whereas, in the Se-Mn system, the adsorption process was not as favored (anion and neutral to slightly negative surface charge).

5.4.2 Kinetic Mechanisms and Expressions

A set of equations similar to those that describe the reaction of As(III) with birnessite can be used for the reaction mechanism of Se(IV) with birnessite:

$$(>MnO)_3MnOH + HSeO_3^- + H^+ \underset{k_{-1}}{\overset{k_1}{\rightleftharpoons}} (>MnO)_3MnOSeOOH + H_2O \quad (5\text{-}26)$$

$$(>MnO)_3MnOSeOOH + H_2O \underset{k_{-2}}{\overset{k_2}{\rightleftharpoons}} >MnOMnOSeO_2OH + 2>MnOH \quad (5\text{-}27)$$

$$>MnOMnOSeO_2OH + H_2O \underset{k_{-3}}{\overset{k_3}{\rightleftharpoons}} >MnOMnOH + SeO_4^{2-} + 2H^+ \quad (5\text{-}28)$$

$$>MnOMnOH + 2H^+ \underset{k_{-4}}{\overset{k_4}{\rightleftharpoons}} >MnOH + Mn^{2+} + H_2O \quad (5\text{-}29)$$

The overall reaction (5-2) consumes a proton and generates the aqueous species Mn^{2+} and SeO_4^{2-} and a new surface site. Figure 5.15 shows a schematic of the cross-sections of the surface layer of a Mn(IV) oxide undergoing reductive dissolution by selenite. In this representation, the surface Mn(IV) atom that undergoes reduction is bonded to two surface and one near-surface Mn(IV) atoms. During the electron transfer step, two Mn-O bonds are broken and each O atom is protonated. The

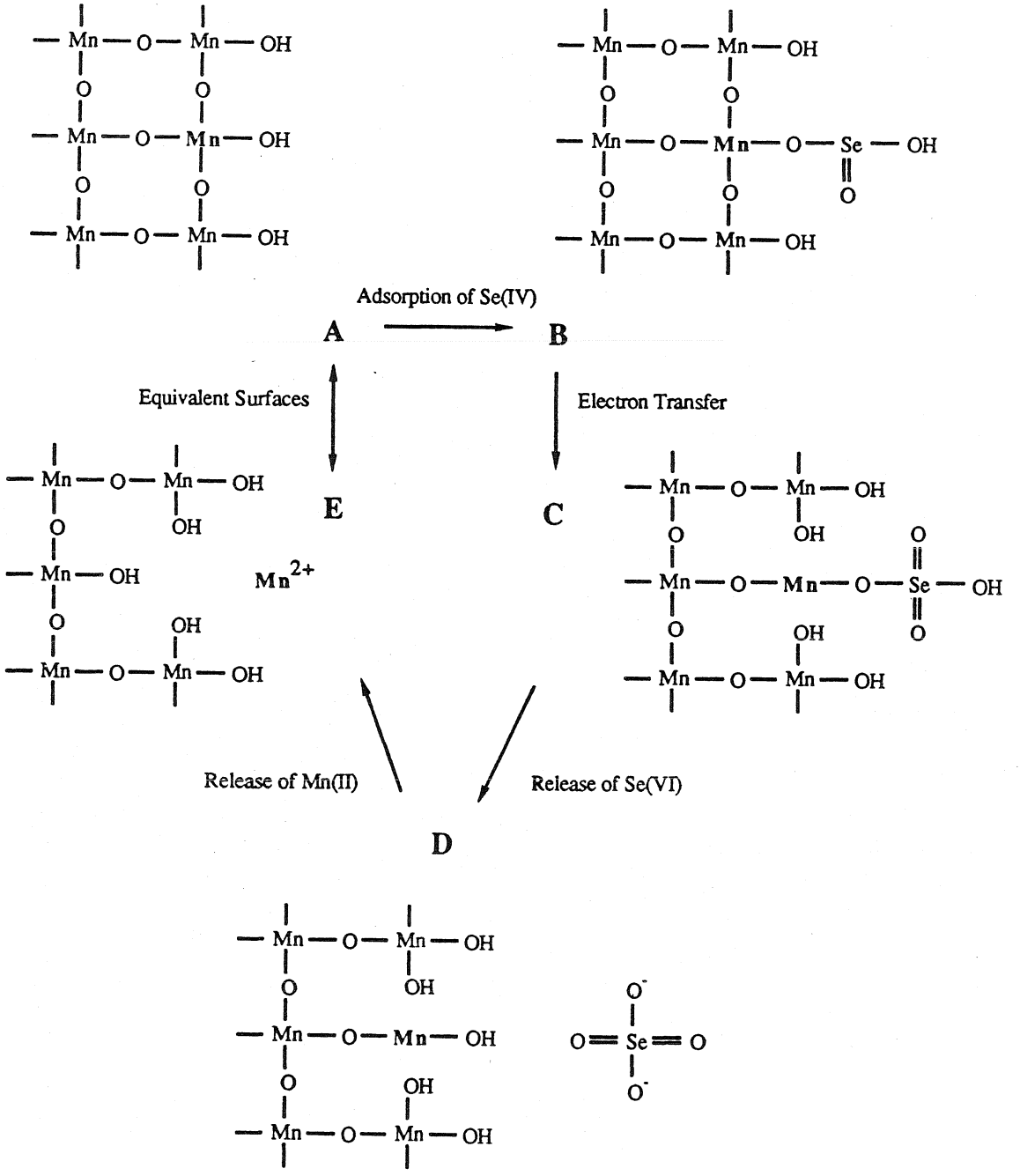

Figure 5.15 A) Schematic of the cross section of the surface layer of a Mn(IV) oxide and B) the resulting surface structure following selenite adsorption, C) electron transfer, D) selenate release, and E) Mn^{2+} release.

number of total surface sites remains constant as the result of the formation of a new site when the reduced Mn^{2+} is released and the near-surface MnO group is protonated.

As with the arsenic reaction, the rate of each elementary reaction step can be calculated:

$$R_1 = k_1[(>MnO)_3MnOH][HSeO_3^-][H^+] \quad (5\text{-}30)$$

$$R_{-1} = k_{-1}[(>MnO)_3MnOSeOOH] \quad (5\text{-}31)$$

$$R_2 = k_2[(>MnO)_3MnOSeOOH] \quad (5\text{-}32)$$

$$R_{-2} = k_{-2}[>MnOMnOSeO_2OH][>MnOH]^2 \quad (5\text{-}33)$$

$$R_3 = k_3[>MnOMnOSeO_2OH] \quad (5\text{-}34)$$

$$R_{-3} = k_{-3}[>MnOMnOH][SeO_4^{2-}][H^+]^2 \quad (5\text{-}35)$$

$$R_4 = k_4[>MnOMnOH][H^+]^2 \quad (5\text{-}36)$$

$$R_{-4} = k_{-4}[>MnOH][Mn^{2+}] \quad (5\text{-}37)$$

Changes in the concentrations of the chemical species are found by accounting for both production and consumption:

$$-\frac{d[HSeO_3^-]}{dt} = R_1 - R_{-1} \quad (5\text{-}38)$$

$$-\frac{d[(>MnO)_3MnOH]}{dt} = R_1 - R_{-1} - R_4 + R_{-4} \quad (5\text{-}39)$$

$$-\frac{d[(>MnO)_3MnOSeOOH]}{dt} = -R_1 + R_{-1} + R_2 - R_{-2} \quad (5\text{-}40)$$

$$-\frac{d[>MnOMnOSeO_2OH]}{dt} = -R_2 + R_{-2} + R_3 - R_{-3} \quad (5\text{-}41)$$

$$-\frac{d[SeO_4^{2-}]}{dt} = -R_3 + R_{-3} \quad (5\text{-}42)$$

$$-\frac{d[>MnOMnOH]}{dt} = -R_3 + R_{-3} + R_4 - R_{-4} \quad (5\text{-}43)$$

$$-\frac{d[Mn^{2+}]}{dt} = -R_4 + R_{-4} \quad (5\text{-}44)$$

Again, the expressions can be solved numerically using the Forward Euler Method (Forsythe et al., 1977). Rate constants are chosen to provide the optimal fit of the kinetic model to the observed concentration profiles of the aqueous species.

The optimal model fits obtained for the aqueous and adsorbed Se species are shown along with the experimental data (MnSe1) in Figure 5.16 and the values of the rate constants are listed in Table 5.7. Appendix C gives a sensitiviy analysis for the variation of the individual rate constants on the model fit. The model curve of the adsorbed Se species is the sum of the concentrations of the surface species $(>MnO)_3MnOSeOOH$ and $>MnOMnOSeO_2OH$. The value of the rate constant k_1 is identical to the rate constant extracted from the initial rate of adsorption data (Chapter 4.3). The rate constant chosen here for desorption of Se(IV), k_{-1}, is 2.5 times smaller than a similar rate constant obtained from the initial rate experiment. The use of the value of k_{-1} from Chapter 4 with this data set resulted in an underprediction of the disapperance of Se(IV)(aq). A smaller k_{-1} was necessary to

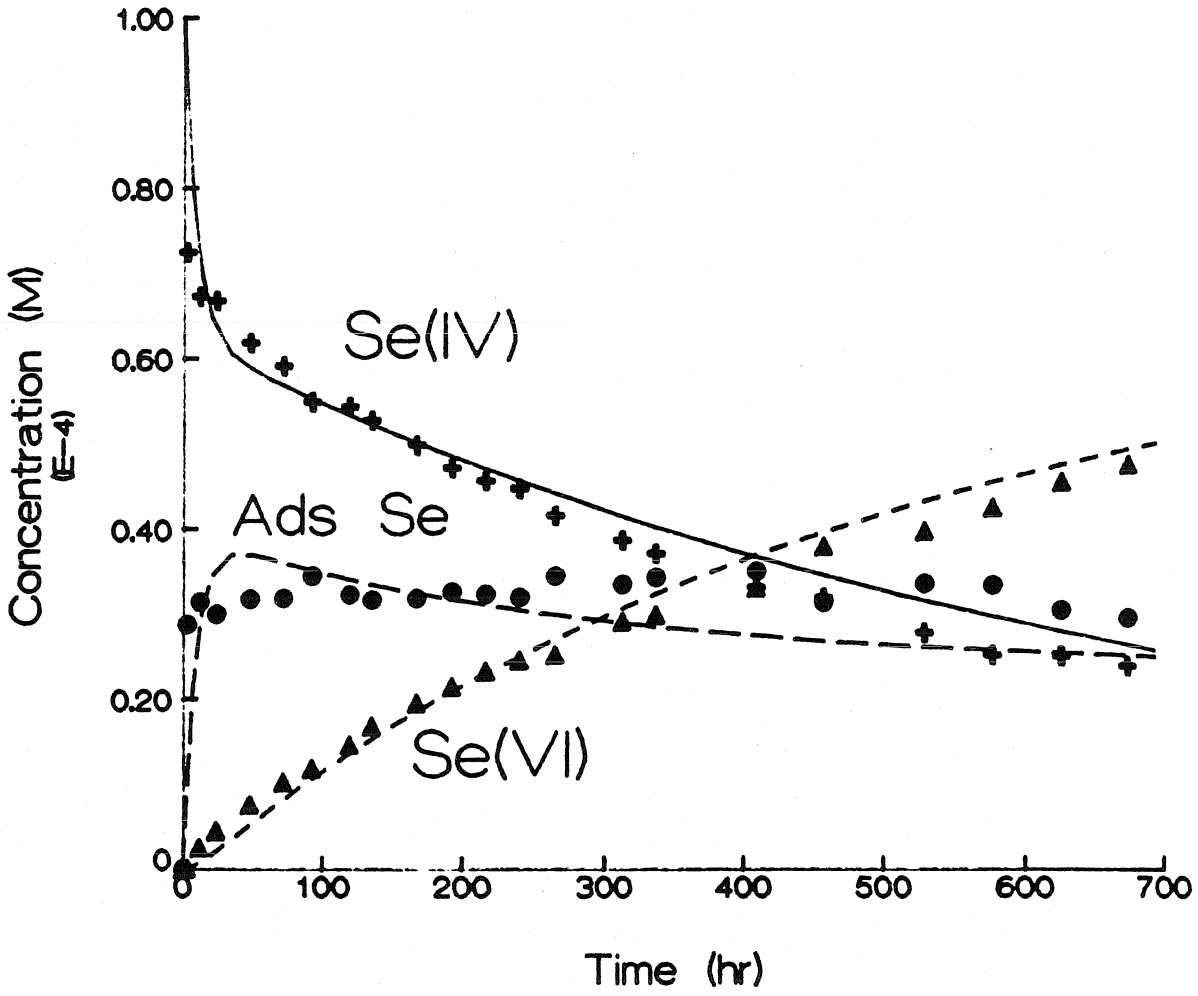

Figure 5.16: Comparison of predicted kinetic behavior (lines) and experimental data of aqueous and adsorbed Se species in a birnessite particle suspension (experiment MnSe1).

Table 5.7: Rate Constants and Characteristic Times for the Reaction between Se(IV) and Mn(IV) at pH 4, 1 mM $NaClO_4$, and 25°C

PROCESS	RATE CONSTANT	CHARACTERISTIC TIME Definition	τ (sec)
Se(IV) Adsorption	2.5×10^{4} $M^{-2}sec^{-1}$	$1/\{k_1[H^+][(>MnO)_3MnOH]_b\}$	840
Se(IV) Desorption	2.0×10^{-3} sec^{-1}	$1/k_{-1}$	480
Electron Transfer Se → Mn	1.3×10^{-6} sec^{-1}	$1/k_2$	$10^{5.9}$
Mn → Se	1.3×10^{-7} sec^{-1}	$1/k_{-2}$	$10^{6.9}$
Se(VI) Release	8.3×10^{-4} sec^{-1}	---	---
Se(VI) Adsorption	6.7×10^{8} $M^{-3}sec^{-1}$	---	---
Mn(II) Release	1.7×10^{8} $M^{-2}sec^{-1}$	---	---
Mn(II) Adsorption	3.3 $M^{-1}sec^{-1}$	---	---

predict greater adsorption of Se(IV)(aq). The difference is probably due to (i) the consideration of additional reactions affecting the Se(IV) concentration and/or (ii) the extended length of the experiment, which allows fast reactions to be described by a wider range of rate constants without much loss in goodness of fit.

Figure 5.17 displays the model predicted profiles of the two Se surface species and the two Se aqueous species. The surface Se(IV) species reaches a maximum

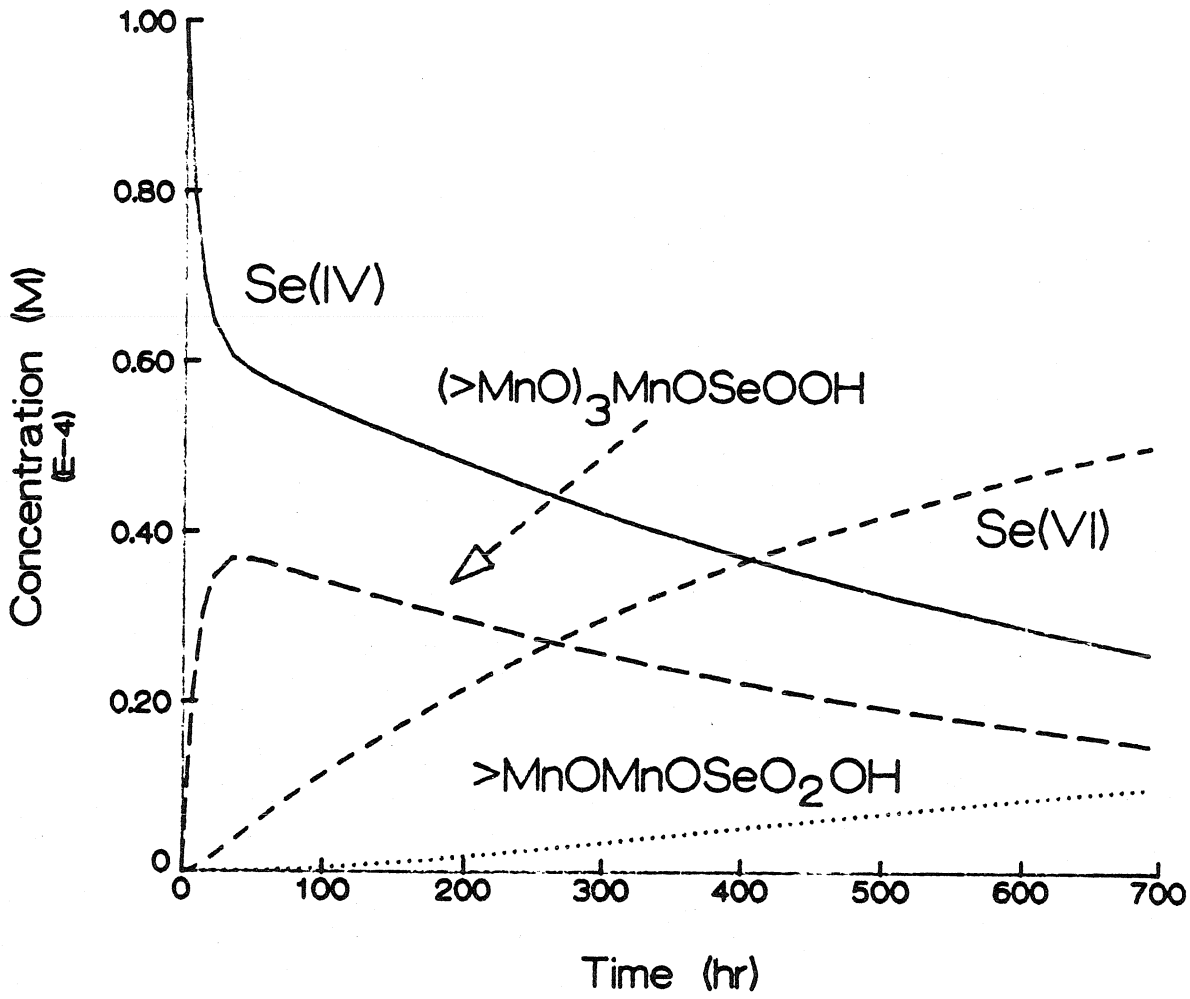

Figure 5.17: The model predicted species profiles of the Se(IV)-Mn(IV) reaction under the reaction conditions of experiment MnSe1. Rate constants are listed in Table 5.7.

concentration of 36 μM after 40 hours and then slowly decays at about the same rate of the decay of aqueous Se(IV). The surface Se(VI) species begins to appear after approximately 100 hours, and at the end of the experiment is only ten percent of the total selenium in the system. This is a result of a larger rate of Se(VI) release than rate of electron transfer. Once the surface Se(VI) species is formed from electron transfer, the complex is immediately released into solution. The increase in the concentration of the surface species at later times is the result of re-adsorption of aqueous Se(VI). The re-adsorption is not highly favored and only occurs once the concentration of Se(VI)(aq) is relatively large.

The concentration of Se(IV)(aq) is controlled initially by the adsorption and desorption processes, but at longer times is controlled by the transfer of electrons. There appears to be a limit to the total amount of Se (Se(IV) and Se(VI)) that will adsorb to the surface. The surface is quickly filled with Se(IV). The adsorption of Se(IV) only continues after Se(IV) on the surface has been transformed and Se(VI) has been released. Se(VI) does not compete well with Se(IV) for surface sites and is only adsorbed after the concentration of Se(IV)(aq) has been greatly reduced.

The forward processes that favor the production of aqueous Se(VI) are the adsorption of Se(IV), transfer of electrons from Se(IV) to Mn(IV), and the release of Se(VI) from the surface. Of these three processes, the transfer of electrons from Se(IV) to Mn(IV) has the longest characteristic time and is thus the rate-determining step in the production of Se(VI). The characteristic times for those steps that occurred prior to the rate limiting step are listed in Table 5.7. Also, the sensitivity

analyses in Appendix C indicate that only the ratios of k_3/k_{-3} and k_4/k_{-4} are obtainable from the data since no kinetic information of individual steps (e.g., values of individual rate constants) is available from steps that occurs after the rate limiting step. Data for reaction processes that occur after the rate limiting step can only be described by equilibrium constants.

5.4.3 Effect of Initial Concentrations of Se(IV) and δ-MnO_2

The applicability of the kinetic model is tested by varying the initial concentrations of the reactants. The same set of rate constants should be able to model a range of initial concentrations. The effect of initial concentration of the reactants on the rate of reaction was studied in a series of experiments at pH 4 and 25 °C. Figure 5.18 details the behavior of aqueous Se(IV) and Se(VI). Increasing the relative amount of Mn to Se in a system promotes the depletion of Se(IV) from solution and the release of aqueous Se(VI). Doubling the initial concentration of both reactants produces the same relative rates of Se(IV) depletion and Se(VI) release.

The kinetic model describes the experimental data well. The predicted behavior of the aqueous concentrations of Se(IV) and Se(VI) are plotted together with the experimental data points in Figure 5.18. The set of rate constants and equilibrium constants for each experiment are listed in Table 5.8. The rate constants from experiment MnSe1 were used to describe the other data sets, and it was necessary to adjust only the values of the rate constants k_1, k_{-1}, and k_{-3} to provide a more accurate fit. The rate constants k_1 and k_{-1} are the smallest for the data set with

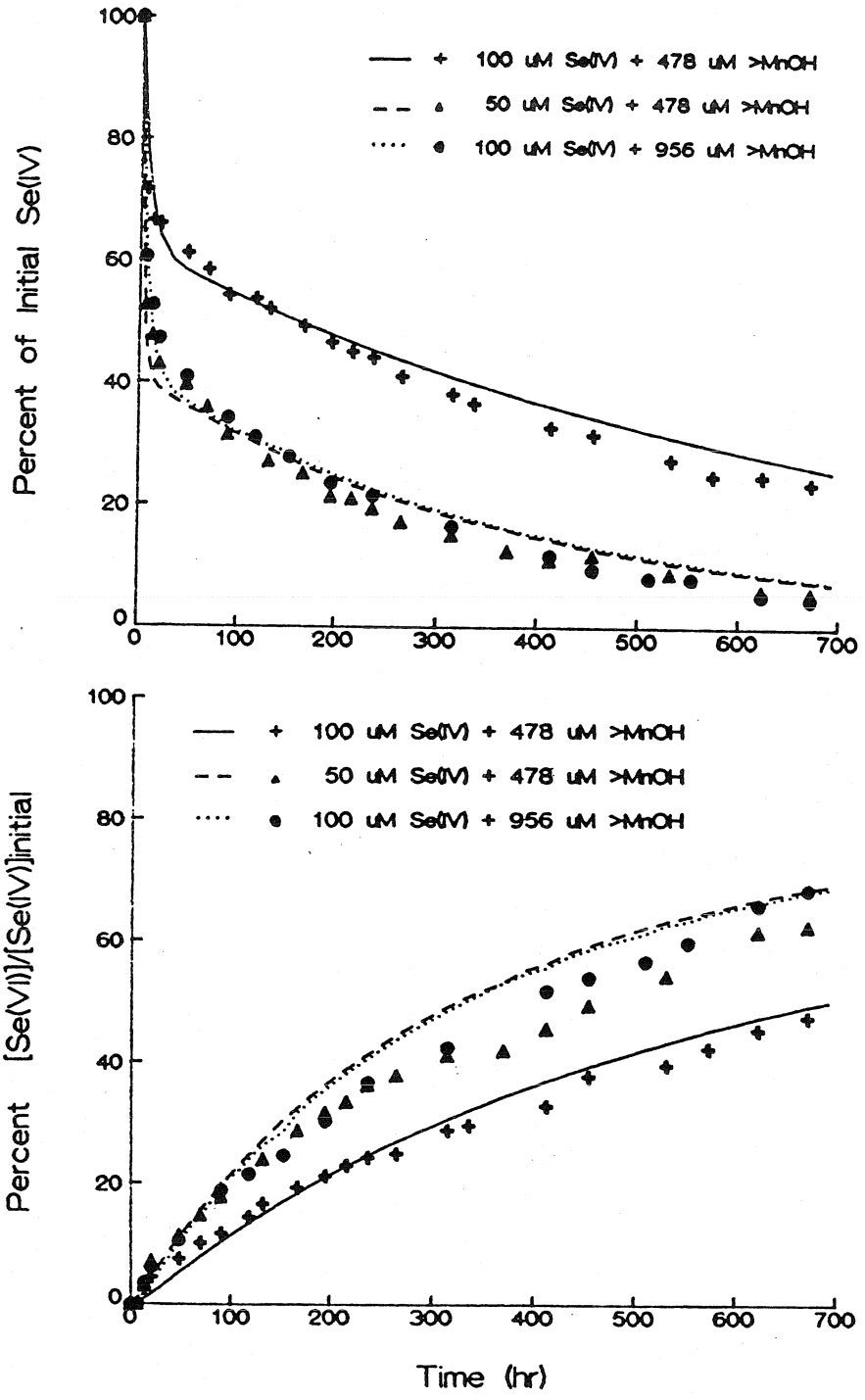

Figure 5.18: Experimental and modeled (lines) profiles of aqueous Se(IV) and Se(VI) in a birnessite suspension with varying initial concentrations of Se(IV) and δ-MnO_2.

the highest total concentration of reactants (MnSe5), but the equilibrium constant K_1 is the same for the data set with the same initial Se(IV) concentration (MnSe1). The first equilibrium constant for the data set with the lowest total concentration of reactants (MnSe3) is larger by a factor of two (+0.3 log units). Although some of the rate constants for the experiments with the same initial Mn/Se ratio are different, the overall equilibrium constant, K^*, is the same. These experiments give a small range of values for the rate constants and equilibrium constants and thus provide a good test for the applicability of the kinetic model.

5.4.4 Effect of pH

The reaction between selenite and birnessite was studied as a function of pH and the resulting concentration profiles of aqueous Se(IV) and Se(VI) are plotted in Figures 5.19 and 5.20, respectively. Aqueous Se(IV) depletion initially is rapid with the extent of depletion increasing with decreasing pH. At pH 4, the removal of aqueous Se(IV) continues until only 25 percent of the initial Se(IV) remains after 670 hours. At pH 5, the data indicate that the concentration of aqueous Se(IV) decreases for the first 150 hours of the experiment, reaching about 60 percent of the initial Se(IV). For the next 250 hours of the experiment the concentration is constant but then begins to decrease again. After 670 hours, 50 percent of the initial Se(IV) remains in solution. At pH 7, the removal of aqueous Se(IV) stops after 48 hours at about 70 percent and then increases to about 75 percent after 300 hours and remains constant for the duration of the experiment. The observed increases in Se(IV) concentration may be due to experimental uncertainties or a result of

Table 5.8: Variation of Reaction Rate Constants and Equilibrium Constants with Initial Concentrations of Reactants

Experiment	MnSe1	MnSe3	MnSe5
Se_T (μM)	101.0	50.1	101.2
S_T (μM)	478	478	956
k_1 ($M^{-2}sec^{-1}$)	2.5×10^4	6.7×10^4	1.7×10^4
k_{-1} (sec^{-1})	2.0×10^{-3}	2.7×10^{-3}	1.3×10^{-3}
k_2 (sec^{-1})	1.3×10^{-6}	1.3×10^{-6}	1.3×10^{-6}
k_{-2} (sec^{-1})	1.3×10^{-7}	1.3×10^{-7}	1.3×10^{-7}
k_3 (sec^{-1})	8.3×10^{-4}	8.3×10^{-4}	8.3×10^{-4}
k_{-3} ($M^{-3}sec^{-1}$)	6.7×10^8	6.7×10^8	3.3×10^8
k_4 ($M^{-2}sec^{-1}$)	1.7×10^3	1.7×10^3	1.7×10^3
k_{-4} ($M^{-1}sec^{-1}$)	3.3	3.3	3.3
log K_1	7.10	7.40	7.10
log K_2	1.00	1.00	1.00
log K_3	-11.90	-11.90	-11.60
log K_4	2.70	2.70	2.70
$\sum \log K_i = \log K^*$	-1.10	-0.80	-0.80

desorption caused by competition for surface sites by Mn(II). As shown in Chapter 4, Mn(II) adsorption increases with increasing pH. If Se(IV) is only weakly adsorbed at pH values 5 and above, then it may be possible for a stronger absorbate, such as Mn(II), to displace Se(IV) at the surface.

The release of Se(VI) is greatly affected by the pH of the solution. The rate of release increases with decreasing pH. At pH 4 and 5, aqueous Se(VI) is detected

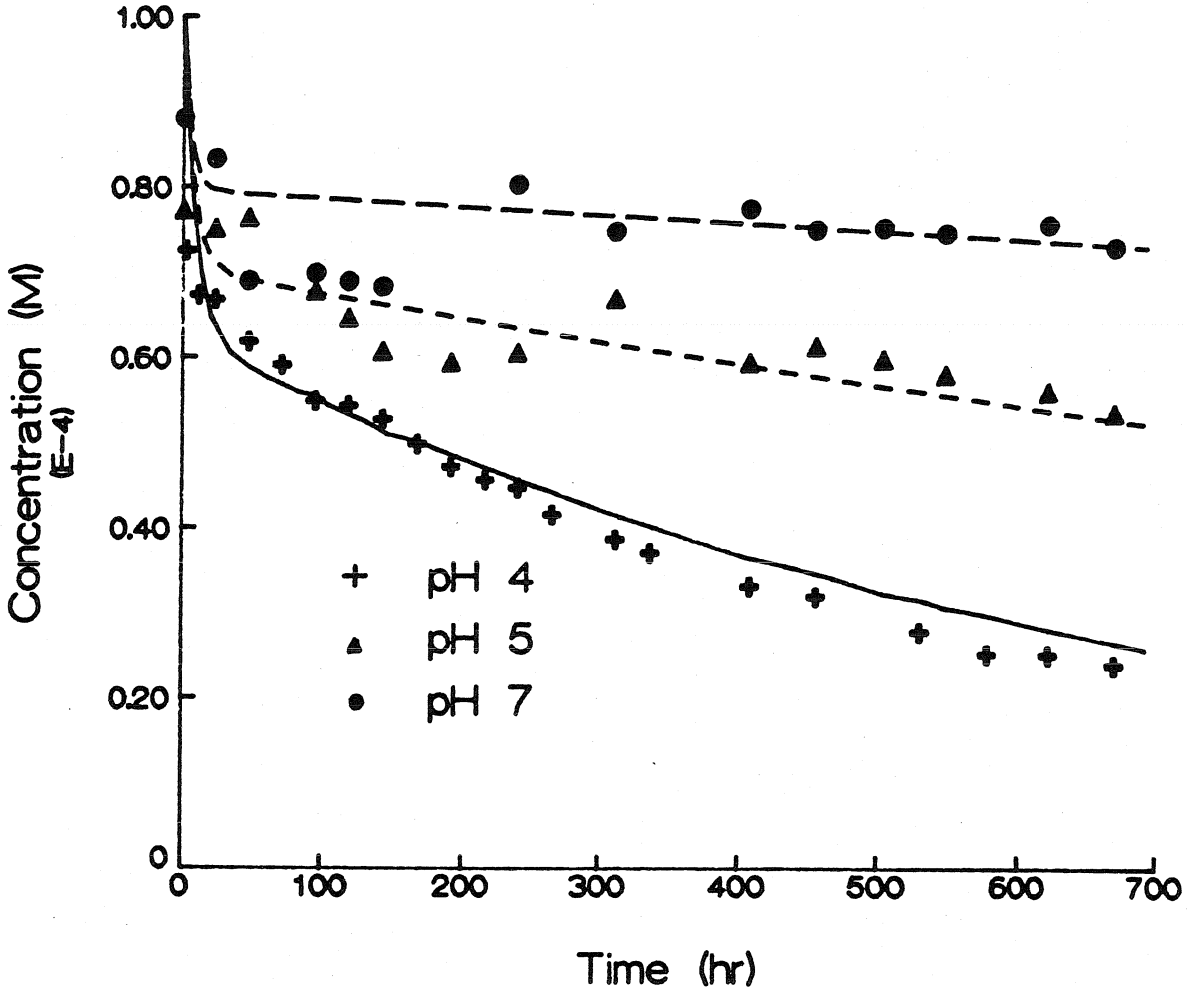

Figure 5.19: Effect of pH on the experimental and modeled (lines) profiles of Se(IV)(aq) in a 0.2 g/L birnessite suspension at 25 °C. Initial concentration of Se(IV) is 101 μM.

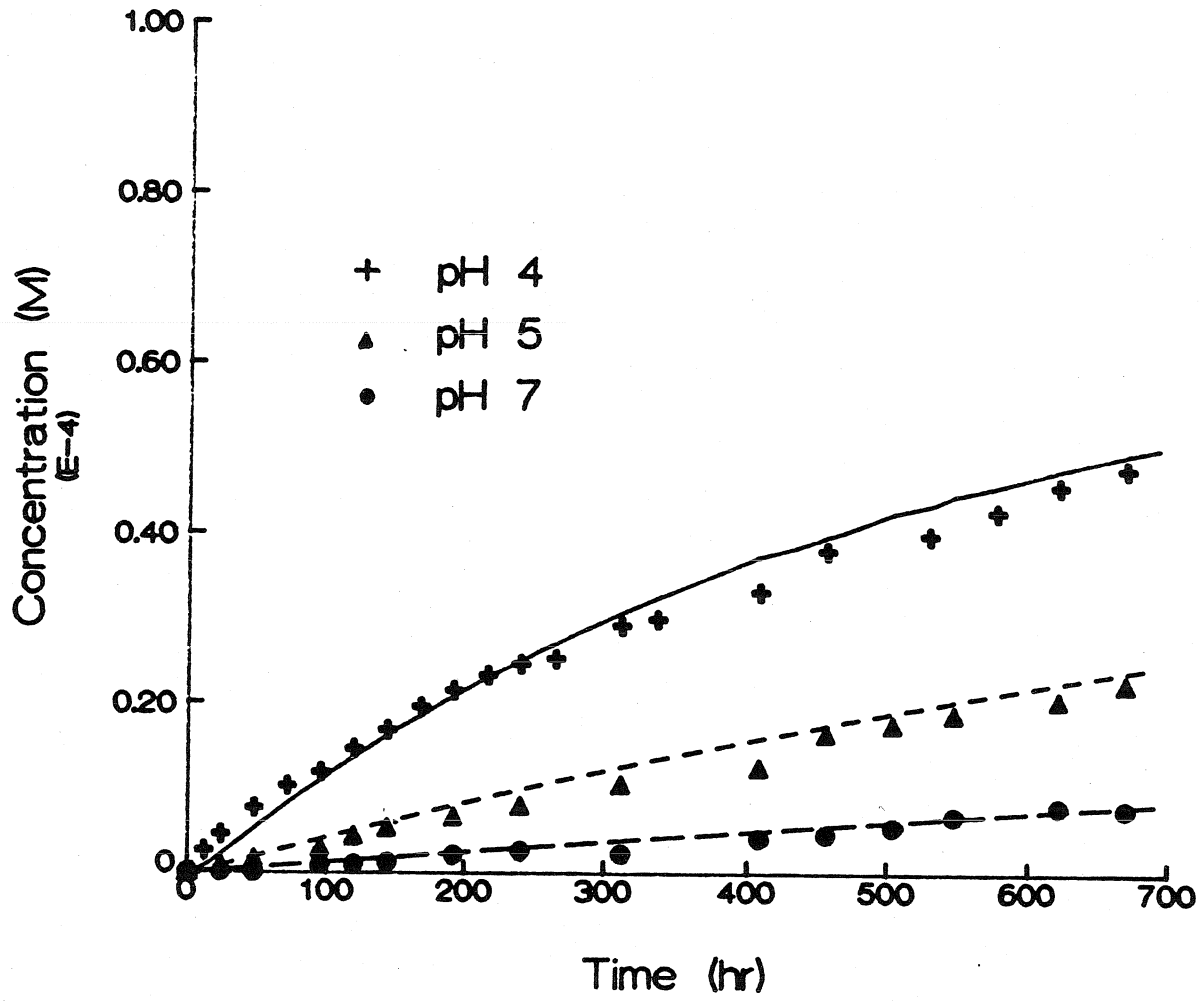

Figure 5.20: Effect of pH on the experimental and modeled (lines) profiles of Se(VI)(aq) in a 0.2 g/L birnessite suspension at 25 °C. Initial concentration of Se(IV) is 101 μM.

after 12 hours and continues to increase with time. After 670 hours, 48 percent and 22 percent of the initial Se(IV) has been oxidized to Se(VI) at pH 4 and 5, respectively. At pH 7, measurable quantities of Se(VI) are not detected until 96 hours and only 8 percent of the initial Se(IV) is oxidized to Se(VI) after 670 hours.

The best model fits of the concentration profiles of the aqueous Se species are also shown in Figures 5.19 and 5.20 and the values of the selected rate constants are listed in Table 5.9. For the Se(IV) profiles, the best overall fit was obtained at pH 4. The model was unable to accurately describe the observed increase in Se(IV) concentration at later times at pH 5 and 7. The best modeled results for the data sets at pH 5 and 7 were obtained by fitting the initial data points and the linear set of data points after approximately 250 hours. The maximum difference between the observed and predicted data points for this approach was less than ten percent.

On the other hand, the agreement between the observed and predicted concentration curves of aqueous Se(VI) is excellent for all pH values. The observed variations with pH were easily modeled by adjusting the values of only two rate constants, k_{-1} and k_2. The intrinsic values of k_1, k_{-3}, and k_4 vary considerably with pH but the product of the rate constant and $[H^+]$ is the same at each pH (i.e., $k_1' = k_1[H^+] = 1.5\ M^{-1}min^{-1}$ at all pH values). The fitted rate constant for the desorption of Se(IV), k_{-1}, increases with increasing pH. This result agrees in principle with the observations that, as pH is increased, the surface charge of the birnessite particles becomes more negative, thus promoting desorption of Se(IV).

Table 5.9: Influence of pH on the Se(IV)-Mn(IV) Reaction Rate Constants and Equilibrium Constants

pH	4	5	7
Se_T (μM)	101.0	101.3	101.3
S_T (μM)	478	478	478
k_1 ($M^{-2}sec^{-1}$)	2.5×10^{4}	2.5×10^{5}	2.5×10^{7}
k_{-1} (sec^{-1})	2.0×10^{-3}	3.0×10^{-3}	5.0×10^{-3}
k_2 (sec^{-1})	1.3×10^{-6}	5.0×10^{-7}	2.0×10^{-7}
k_{-2} (sec^{-1})	1.3×10^{-7}	1.3×10^{-7}	1.3×10^{-7}
k_3 (sec^{-1})	8.3×10^{-4}	8.3×10^{-4}	8.3×10^{-4}
k_{-3} ($M^{-3}sec^{-1}$)	6.7×10^{8}	6.7×10^{10}	6.7×10^{14}
k_4 ($M^{-2}sec^{-1}$)	1.7×10^{3}	1.7×10^{5}	1.7×10^{9}
k_{-4} ($M^{-1}sec^{-1}$)	3.3	3.3	3.3
log K_1	7.10	7.92	9.70
log K_2	1.00	0.57	0.18
log K_3	-11.90	-13.90	-17.90
log K_4	2.70	4.70	8.70

The value of the rate constant for the transfer of electrons from Se(IV) to Mn(IV) decreases with increasing pH. This result is consistent with the decline in the thermodynamic driving force (ΔpE or ΔE_H, Table 5.10) of the redox reaction between $HSeO_3^-$ and δ-MnO_2(s) with increasing pH. At pH 7, the small driving force of the reaction makes it barely thermodynamically possible ($\Delta E_H = +0.004$ volts) and the corresponding rate of Se(VI) release is extremely slow (2×10^{-10} M Se/min). The driving force increases to 0.092 volts at pH 4. In contrast, the driving force of the

Table 5.10 Thermodynamic Driving Forces for the Se(IV)-Mn(IV) Redox Reaction at Various pH Values

pH	ΔpE	ΔE_H (volts)
4	+1.56	+0.092
5	+1.06	+0.063
7	+0.06	+0.004

redox reaction between H_3AsO_3(aq) and δ-MnO_2(s) reaction is much larger (ΔE_H = 0.529 volts at pH 4) and the rate of As(V) release is over 4 orders of magnitude faster (5 x 10^{-6} M As/min).

5.4.5 Effect of Temperature

The effect of temperature on the reaction between selenite and birnessite at pH 4 was studied. Experiments were run at 25, 31, and 35 °C, and the resulting profiles of aqueous Se(IV) and Se(VI) are plotted in Figures 5.21 and 5.22. Lower temperatures that may be more typical of some aquatic environments (e.g., lake sediments, aquifers) were not studied because of the slow rate of reaction at 25 °C. Temperature has little effect on the aqueous Se(IV) profiles during the initial 100 hours of the reaction. After 100 hours, the 35 °C profile decreases more rapidly than the lower-temperature profiles. After 460 hours, only 14 percent of the initial Se(IV) at 35 °C remains in solution, compared to 32 percent at 25 °C after 450 hours.

While temperature has little apparent effect on the depletion of aqueous Se(IV), it has a considerable effect on the release of Se(VI) in solution. Increasing

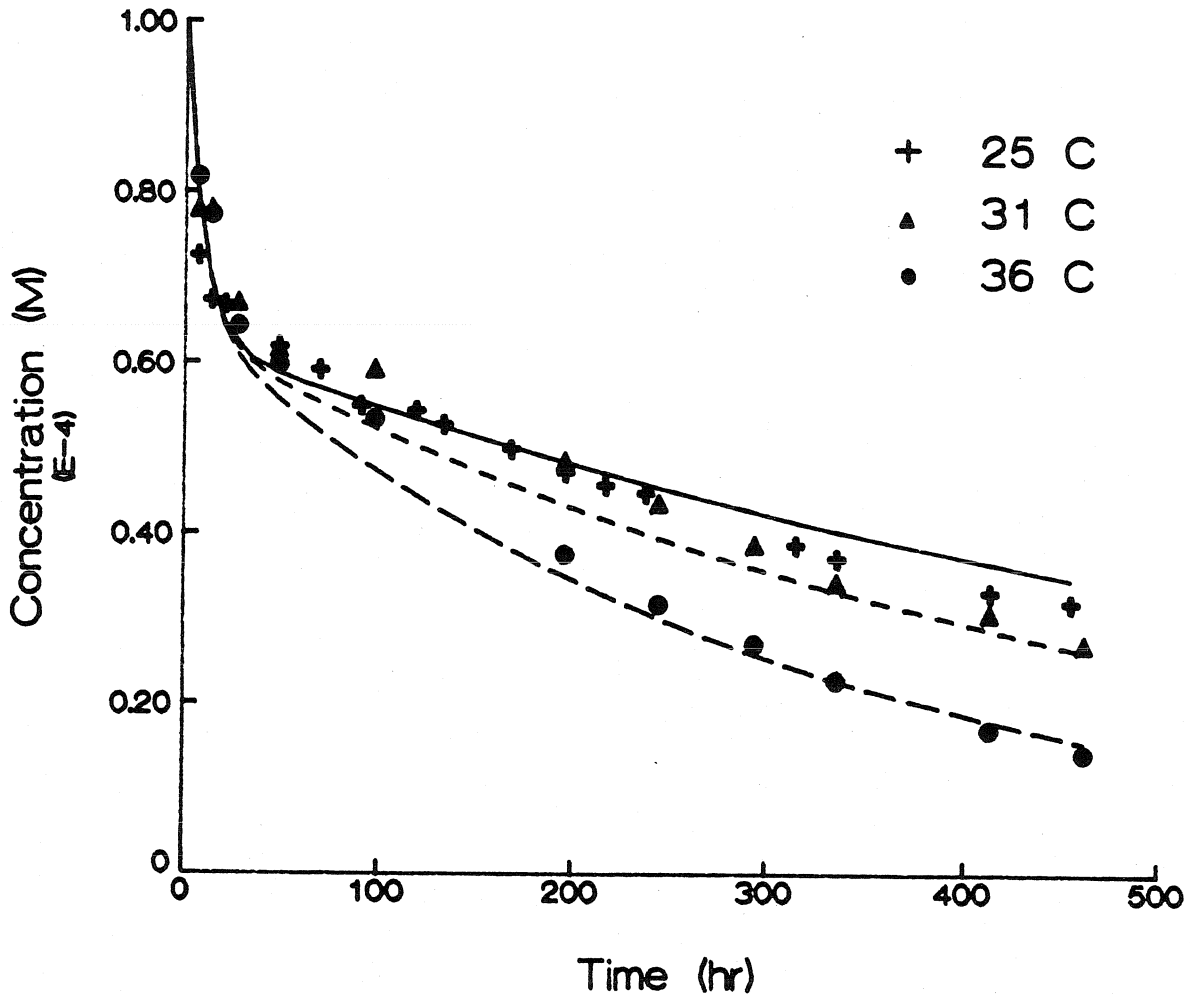

Figure 5.21: Effect of temperature on the experimental and modeled (lines) profiles of Se(IV)(aq) in a 0.2 g/L birnessite suspension at pH 4. Initial concentration of Se(IV) is 101 μM.

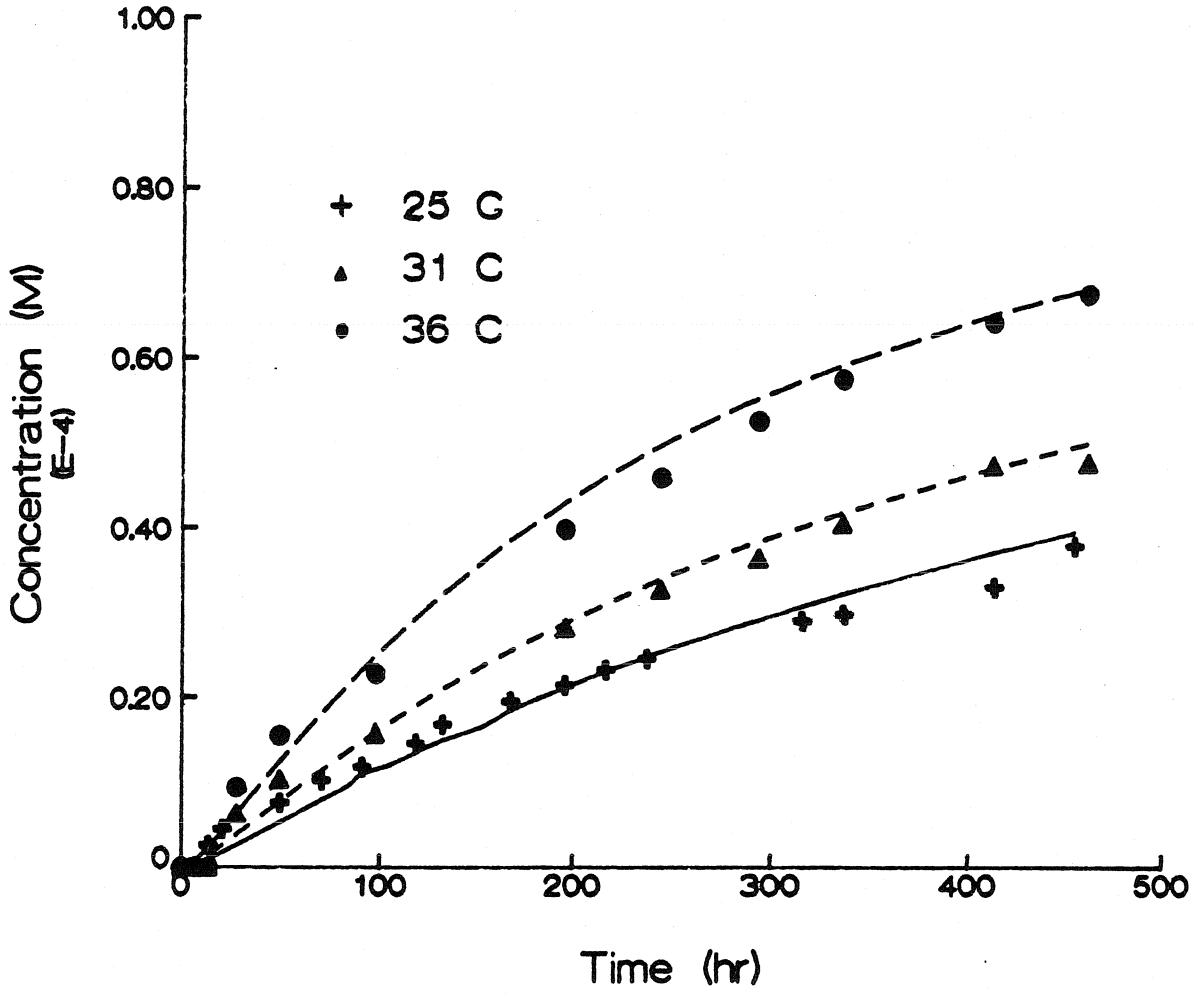

Figure 5.22: Effect of temperature on the experimental and modeled (lines) profiles of Se(VI)(aq) in a 0.2 g/L birnessite suspension at pH 4. Initial concentration of Se(IV) is 101 μM.

temperature increases the amount and rate of Se(VI) release to solution. After 460 hours, 68 percent of the initial Se(IV) at 35 °C is oxidized to Se(VI) while only 38 and 48 percent is oxidized at 25 and 31 °C, respectively.

The kinetic model was able to predict accurately the concentration profiles of the aqueous Se species. The model curves are shown in Figures 5.21 and 5.22 with the experimental data at each temperature, and the corresponding sets of the rate constants used to provide the best fits are listed in Table 5.11. The three modeled curves representing the concentration of Se(IV)(aq) initially lie on top of each other, and as a consequence the rate constants for adsorption and desorption of Se(IV) are identical for each temperature data set. The time scales for adsorption and desorption of the various species are much shorter than the time scale of electron transfer and the time scale of our observations. Any differences in the rate of adsorption and desorption due to temperature are not observed at time scales greater than a few hours. As in the As(III)-Mn(IV) system, only the rate of reaction varied with temperature; after a few hours, the extent of the reaction was the same for the range of studied temperatures. At the time scales necessary to observe the redox transformations between Se(IV) and Mn(IV), the variation of adsorption and desorption with temperature is too small to notice an effect of temperature on the adsorption and desorption of aqueous Se(IV).

The model curves for Se(IV)(aq) begin to differ after 24 hours as a consequence of different rates of electron transfer. The rate constant for the transfer of electrons from Se(IV) to Mn(IV) increases with increasing temperature. Even

Table 5.11: Influence of Temperature on the Se(IV)-Mn(IV) Reaction Rate Constants and Equilibrium Constants

Temperature (°C)	25	31	36
Se_T (μM)	101.0	101.4	101.4
S_T (μM)	478	478	478
k_1 ($M^{-2}sec^{-1}$)	2.5×10^4	2.5×10^4	2.5×10^4
k_{-1} (sec^{-1})	2.0×10^{-3}	2.0×10^{-3}	2.0×10^{-3}
k_2 (sec^{-1})	1.3×10^{-6}	1.7×10^{-6}	3.0×10^{-6}
k_{-2} (sec^{-1})	1.3×10^{-7}	1.3×10^{-7}	1.3×10^{-7}
k_3 (sec^{-1})	8.3×10^{-4}	8.3×10^{-4}	8.3×10^{-4}
k_{-3} ($M^{-3}sec^{-1}$)	6.7×10^8	3.3×10^8	3.3×10^8
k_4 ($M^{-2}sec^{-1}$)	1.7×10^3	1.7×10^3	1.7×10^3
k_{-4} ($M^{-1}sec^{-1}$)	3.3	3.3	3.3
log K_1	7.10	7.10	7.10
log K_2	1.00	1.10	1.35
log K_3	-11.90	-11.60	-11.60
log K_4	2.70	2.70	2.70

though the Se(IV) data sets for the experiments run at 25 and 31 °C appear to be nearly equivalent, the kinetic model predicts a faster rate of disappearance at 31 °C. This is the result of modeling the Se(IV) data together with the Se(VI) data. The appearance of Se(VI) in solution is faster at higher temperatures, and larger rate constants for electron transfer are necessary to predict this increased rate of appearance with temperature. The Se(IV) concentration profiles are also a function of the value of the rate constants of electron transfer.

The model curves plotted in Figures 5.21 and 5.22 essentially illustrate the variation of the model with changes in the value of k_2, the rate constant for the transfer of electrons from Se(IV) to Mn(IV). With the other reaction parameters held constant, increasing k_2 increases the disappearance of Se(IV) from solution at long times and the appearance of Se(VI) into the aqueous phase.

5.4.6 Summary of the Dynamics of Se(IV) and Birnessite

The experiments between Se(IV) and birnessite indicate that the initial disappearance of Se(IV) from solution is rapid with a time scale of minutes. At pH 4 and 25 °C, aqueous Se(VI) appears after 12 hours of reaction and is slowly produced at a constant rate throughout the duration of the experiments (28 days). The extended reaction period results in most of the product Mn(II) being adsorbed by the oxide surface. The lack of oxidation of Se(IV) in a oxygenated homogeneous solution and the appearance of aqueous Se(VI) in an O_2-free birnessite suspension is evidence for the redox reaction between Se(IV) and Mn(IV).

Increasing the pH of the particle suspension from 4 to 7 decreases the initial uptake of Se(IV) and production of Se(VI). Increasing the temperature of the particle suspension from 25 °C to 35 °C has little effect on the rate of disappearance of aqueous Se(IV) during the initial 100 hours, but after this time period, higher temperatures increase the rate of Se(IV) depletion. Increasing the temperature of the solution does increase the rate and amount of Se(VI) that is released into solution.

The four-step reversible kinetic model is successful in describing the time

dependent behavior of the aqueous species Se(IV) and Se(VI) over a pH range from 4 to 7 and a temperature range from 25 to 35 °C. The kinetic data suggest that the electron transfer step is the rate determining process for the production of Se(VI).

Chapter 6

IMPLICATIONS FOR GEOCHEMICAL SYSTEMS

6.1 Introduction

With insight into the rates and mechanisms of arsenic and selenium transformations derived from controlled experiments in simple heterogeneous systems, a better understanding of the geochemical cycles of arsenic and selenium is possible. The purpose of this concluding chapter is to explore the larger geochemical implications of the experimental results. Four topics are discussed in detail: (i) a practical use of the kinetic data; (ii) the important role that metal oxide surfaces play in the overall arsenic and selenium geochemical cycles; (iii) a comparison of oxidation rates and mechanisms of various inorganic reduced metal species with manganese oxides; and, (iv) the kinetic estimation of redox potentials of metal oxide surfaces. A few ideas for future research exploring the geochemistry of trace elements are also presented.

6.2 Practical Use of Kinetic Data

Despite the success of the kinetic model, it will be rare that future problems concerning the adsorption and oxidation of arsenic and selenium species will be as well characterized as the experimental systems presented in this thesis. Given this, the following exercise is presented to indicate the practical use of the kinetic data.

Let us imagine an industrial environmental engineer who is faced with designing waste treatment processes for two new waste streams: one which contains 10^{-4} M As(III) and one with 10^{-4} M Se(IV) as the only toxic and redox-active

constituents. The plant already has the ability to handle As(V) and Se(VI) wastes, but a new product synthesis now produces As(III) and Se(IV) and the current waste treatment process does not reduce the concentrations of As(III) and Se(IV) to regulatory discharge level of 10^{-6}M. The engineer has heard of a new single technology consisting a manganese dioxide columns that will convert As(III) and Se(IV) to As(V) and Se(VI). She needs to estimate what retention times are necessary to reduce the concentrations of As(III) and Se(IV) to regulatory discharge levels.

In the arsenic case, the rate of As(III) disappearance is described by

$$-\frac{d[As(III)]}{dt} = k_1[>MnOH][As(III)] - k_{-1}[>MnAs(III)] \qquad (6\text{-}1)$$

Figure 5.5 indicates that the species >MnAs(III) occurs in only small concentrations (4 % is the maximum percentage of the initial As(III) added) which allows the rate equation to be simplified to

$$-\frac{d[As(III)]}{dt} = k_1[>MnOH][As(III)] \qquad (6\text{-}2)$$

The manufacturer of the column supplies the following information:

Solid Manganese Concentration, S_c = 0.5 g/L

Column Exchange Capacity, X_{cpt} = 0.000326 moles/g

With this information, the concentration of surface sites can be determined:

$$[>MnOH] = S_c X_{cpt} = 1.63 \times 10^{-4}\ M$$

Manganese in the column is also in excess of both Se(IV) and As(III) in the waste

stream. Thus the rate expression becomes a simple first-order equation

$$-\frac{d[As(III)]}{dt} = k_1 S_c X_{cpt}[As(III)] = k_1^*[As(III)] \qquad (6\text{-}3)$$

Integrating the equation we get an expression for the time of reaction

$$t = \frac{-\ln([As(III)]_t/[As(III)]_o)}{k_1^*} \qquad (6\text{-}4)$$

For a 99% reduction in As(III) concentration, the retention time would be about 95 minutes.

In the selenite case, the rate of total Se(IV) transformation is described by

$$-\frac{d(Se(IV)_T)}{dt} = -\frac{d[Se(IV)]}{dt} - \frac{d[>MnSe(IV)]}{dt} \qquad (6\text{-}5)$$

The rates of change of Se(IV) and >MnSe(IV) are given in Equations 5-38 and 5-40, respectively. Substituting these equations into Equation 6-5 gives

$$-\frac{d(Se(IV)_T)}{dt} = k_2[>MnSe(IV)] - k_{-2}[>MnSe(VI)] \qquad (6\text{-}6)$$

Figure 5.17 shows that the concentration of >MnSe(VI) remains very small as compared to the concentration of >MnSe(IV) over the duration of the experiment which allows the following approximation to be made:

$$-\frac{d(Se(IV)_T)}{dt} = k_2[>MnSe(IV)] \qquad (6\text{-}7)$$

Figure 5.17 also illustrates that the adsorption-desorption reactions of Se(IV) with

the birnessite surface is at equilibrium shortly after the beginning of the experiment. Therefore, one additional approximation can be made with the equilibrium relationship to get a simple first-order equation:

$$[>MnSe(IV)] = K_1[H^+][>MnOH][Se(IV)] \qquad \text{and}$$

$$-\frac{d(Se(IV)_T)}{dt} = k_2K_1[H^+][>MnOH][Se(IV)] = k_2^*[Se(IV)] \qquad (6\text{-}8)$$

Integrating as before, a similar expression for the time of reaction is obtained. Thus, assuming the same values as before with pH = 4, $K_1 = 10^{7.1}$, and $k_2 = 1.3 \times 10^{-6} sec^{-1}$, the retention time for a 99% reduction in Se(IV) concentration is 200 days. This retention time is too long for an industrial process, but the clever engineer redesigns her plans to increase the solid concentration to 50 g/L which decreases the retention time to 2 days.

6.3 Rates of Redox Transformations in Aquatic Systems

A good indicator for comparison of rates of redox transformations is the half-life of the reaction, the time required for fifty percent reaction. In the following, the observed half-lives of As(III) oxidation in natural systems and inorganic redox reactions with manganese dioxides are reviewed and compared.

6.3.1 As(III) Oxidation

The results presented in Chapter 5 indicate that As(III) has a half-life of approximately 10-20 minutes in a 0.2 g/L suspension of birnessite particles. The rates of As(III) oxidation in seawater, estuarine water, and lake sediments are approximately equivalent, with half-lives ranging between 5 and 17 hours (Scudlark

and Johnson, 1982; Knox et al., 1984; Oscarson et al., 1980). Table 6.1 compares several reported half-lives of As(III) oxidation in natural and laboratory systems with the results of this study. Oxidation of As(III) occurs at slower rates in natural systems, yet the natural rates are more than two orders of magnitude faster than the rate of homogeneous oxygenation. One of the factors that affects slower oxidation rates in natural systems is the competition for surface sites among adsorbing species.

In another laboratory study, Oscarson et al. (1983a,b) isolated manganese dioxides as the oxidizing component of their lake sediments. They observed half-lives of 27 to 203 hours for As(III) oxidation by synthetic birnessite particles, which were prepared according to the same chemical recipe used for the birnessite particles in this study. Their results are based on the observation of As(III) disappearance from solution only. The authors observed two rates of reaction with the added concentration of As(III) in excess of the concentration of Mn(IV) under reaction conditions at pH 7 and 25 °C. A rapid disappearance of As(III) from solution occurred in the first thirty minutes, and was followed for several hours by a slower decrease in aqueous As(III) concentration. The initial rate corresponded to the rate of As(III) adsorption on the oxide surface, and the second slower rate was attributed to the rate of As(III) oxidation by the surface. The half-lives were obtained from kinetic treatment of the second rate data. The authors concluded that As(III) reached adsorption equilibrium with the oxide surface within the first 30 minutes, and that the slower decrease in aqueous As(III) concentration at longer times was the result of further adsorption to new surface sites exposed by the slow oxidation of

Table 6.1: Comparison of As(III) Oxidation Half-Lives

STUDY	HALF-LIFE (hr)
Seawater--Microbial Oxidation (Scudlark and Johnson, 1982)	8-13
Lake Sediments (Oscarson et al., 1980)	10-17 (5 °C) 5.1-6.7 (25 °C)
Estuary (Knox et al., 1984)	8.6
Oxygenation (Eary and Schramke, 1990)	8760
Synthetic Birnessite, pH 7 (Oscarson et al., 1983b)	27-203[1]
Synthetic Birnessite (This Study) pH 4 pH 6.8 pH 4, 100 μM Mn^{2+}	 0.15[2] 0.33 0.35

[1]derived from secondary rate data (t > 30 minutes)
[2]derived from initial rate data (0 < t < 90 minutes)

adsorbed As(III) and subsequent rapid release of As(V).

The results of the present work suggest a different interpretation of these rate data. According to the current study, As(III) is oxidized immediately and produces Mn(II), and, at pH 7, adsorption/retention of Mn(II) is highly favored on the birnessite surface. Rather than the slower rate of As(III) depletion being a result of slow oxidation kinetics, as concluded by Oscarson et al., the slower rate is actually the result of Mn(II) occupying the newly generated surface sites, thus blocking the adsorption and oxidation of As(III). By taking into account the behavior of the reaction products, a clearer mechanistic picture is possible.

6.3.2 Inorganic Redox Reactions with Manganese Dioxides

Until the present study, Cr(III) was the only reduced inorganic species whose kinetics of oxidation by direct reaction with a manganese dioxide surface had been studied. Cr(III) oxidation by pyrolusite (β-MnO_2) particles was examined at pH values between 3.0 and 4.7 (Eary and Rai, 1987). Pyrolusite is a highly crystalline form of manganese dioxide with a low surface area (5.7 m^2/g) and a neutral pH_{zpc} (7.3). Now, the Cr(III) data can be compared to the results of our As(III) and Se(IV) work. The observed time required to oxidize fifty percent of the initial concentration of each of the reduced species is listed in Table 6.2. Also listed in Table 6.2 are the values of the thermodynamic driving force (ΔE_H) at pH 4 for the redox reactions. The observed "half-lives" of the redox transformation correlate with driving force. The Cr(III) redox transformation on pyrolusite is the slowest of the three, the combined result of unfavorable adsorption conditions (i.e., positively charged surface and positively charged aqueous species) and a small thermodynamic driving force. In addition, transfer of three electrons from Cr(III) to Mn(IV) requires the involvement of more than one Mn(IV) per Cr(III). Eary and Rai (1987) found the rate of oxidation to be proportional to the surface area of the oxide particles. This suggests that birnessite may oxidize Cr(III) more rapidly as a result of its larger surface area and acidic pH_{zpc}. Also, the redox potential of birnessite (E°_H = +1.29 volts) is slightly larger than that of pyrolusite (E°_H = +1.23 volts). These observations indicate that inorganic redox reactions involving manganese

Table 6.2: Inorganic Redox Reactions with Manganese Dioxides

SYSTEM	TIME TO OXIDIZE 50%	DRIVING FORCE AT pH 4 ΔE_H (volts)
δ-MnO_2: As(III) → As(V) pH 4, 25 °C, 14 m^2/L	10 minutes	+ 0.529
δ-MnO_2: Se(IV) → Se(VI) pH 4, 35 °C, 14 m^2/L pH 4, 25 °C, 28 m^2/L pH 4, 25 °C, 14 m^2/L	 10 days 16 days 30 days	 + 0.092
β-MnO_2: Cr(III) → Cr(VI) pH 4, 25 °C, 71 m^2/L (Eary and Rai, 1987)	95 days	+ 0.011

dioxides depend upon (i) the surface area of the mineral form, (ii) the surface chemistry, and (iii) the energetics of the reactions.

6.4 Role of Metal Oxides in the Geochemical Distribution of Arsenic and Selenium

In most heterogeneous aquatic systems, adsorption to metal oxide surfaces is the major chemical reaction controlling the distribution and fate of arsenic and selenium. Selenate is the only mobile anion in most natural systems as a result of the low affinity it displays for metal oxide surfaces. Selenite and both oxidation states of arsenic are immobilized in aquatic systems by adsorption to mineral surfaces. The abundance in natural systems and favorable aquatic surface chemistry (i.e., high pH_{zpc}) of iron and aluminum minerals results in most of arsenate, arsenite, and selenite being adsorbed to these minerals. Arsenite and selenite are directly

oxidized by manganese dioxides, but the redox transformation is limited by unfavorable adsorption conditions in most natural environments.

6.5 Redox Potential of Manganese Dioxide Surfaces

Manganese dioxide surfaces have been shown to be oxidants for several reduced species. A question arises whether the redox potential of the surface/aqueous redox couple $(>MnO)_3MnOH/Mn^{2+}$ is the same as the redox potential of the solid/aqueous couple δ-MnO_2/Mn^{2+}. The redox potential of Mn(IV) surface species can be calculated from the experimental data and compared with tabulated values of the bulk phase.

The kinetic model describes the reaction between As(III) and birnessite surface species with a set of basic and distinct reactions and provides rate constants for each forward and reverse reaction. Applying the law of microscopic reversibility, an equilibrium constant K_i is defined as

$$K_i = \frac{k_{f,i}}{k_{r,i}} \qquad (6\text{-}9)$$

The overall equilibrium constant, K^*, is the product of equilibrium constants of the reactions that comprise the overall reaction. For the four-step kinetic model, the overall equilibrium constant is

$$K^* = (K_1 \times K_2 \times K_3 \times K_4) \qquad (6\text{-}10a)$$

or

$$\log K^* = \log K_1 + \log K_2 + \log K_3 + \log K_4 \qquad (6\text{-}10b)$$

If the overall reaction is a redox reaction, then an overall redox potential can be calculated from

$$E_H(overall) = \frac{2.3RT}{nF} logK^* \qquad (6\text{-}11)$$

The overall redox reaction can be divided into two half-reactions, and if one of the redox potentials is known, then the other can be calculated from the following relationship

$$E_H(\text{overall}) = E_H(\text{known}) + E_H(\text{unknown}) \qquad (6\text{-}12)$$

For example, consider the As(III)-birnessite overall reaction:

$$(>MnO)_3MnOH + H_3AsO_3 + H^+ \rightleftharpoons 3>MnOH + Mn^{2+} + H_2AsO_4^-$$

The equation can be divided into an As(III)-As(V) half-reaction with a known redox potential and a >Mn(IV)-Mn(II) half-reaction with an unknown redox potential:

$$H_3AsO_3 + H_2O \rightleftharpoons H_2AsO_4^- + 3H^+ + 2e^- \qquad E_H^o = -0.64 \text{ volts}$$

$$(>MnO)_3MnOH + 4H^+ + 2e^- \rightleftharpoons 3>MnOH + Mn^{2+} + H_2O \qquad E_H^o = ?$$

The calculated values of log K^*, E_H(overall), and E_H(surface) from the As(III)-birnessite pH experiments (Table 5.4) are listed in Table 6.3. The average redox potential for the couple $(>MnO)_3MnOH/Mn^{2+}$ from the pH experiments is +0.71 volts. The bulk oxide couple has a redox potential of +1.29 volts.

The same treatment of the Se(IV)-birnessite data results in a slightly negative overall redox potential (-0.05 volts). This implies that the redox transformation is not thermodynamically favored. However, since no aqueous Mn(II) was detected during the reaction, the value of K_4 can only be approximated. If the value of K_4 was similar to that for the As(III)-birnessite reaction (log K_4 = 5.7), then the overall

Table 6.3: Calculated Overall Equilibrium Constants and Redox Potentials for the As(III)-Mn(IV) Reaction and Redox Potentials for the >Mn(IV)-Mn(II) Redox Couple

pH	log K^*	E_H (overall) (volts)	E_H (surface) (volts)
4	1.70	+ 0.05	+ 0.69
5	2.28	+ 0.07	+ 0.71
5.85	2.08	+ 0.06	+ 0.70
6.8	2.10	+ 0.06	+ 0.70
7.7	2.57	+ 0.08	+ 0.72
8.2	2.65	+ 0.08	+ 0.72

redox potential would be +0.13 volts. Using these two values as a possible range for the overall redox potential, then the redox potential of the couple $(>MnO)_3MnOH/Mn^{2+}$ falls between +1.03 and +1.21 volts. These values are closer to the redox potential of birnessite.

Wehrli (1990) estimated the redox potential of adsorbed metal ions (Fe(II), V(IV), and Mn(II)) through the use of a linear free-energy relationship between equilibrium constants calculated from the reduction potentials of the metal ion and oxygen redox couples and rate constants from heterogeneous oxygenation experiments. His estimates for the redox potentials of Fe(II) on goethite (E° = 0.36 volts) and V(IV) on anatase (TiO_2) (E° = 0.73 volts) are close to the redox potentials for the monohydroxo complexes of iron and vanadyl (E° = 0.34 and 0.72 volts for Fe(II) and V(IV), respectively). However, the estimate of the potential for

a surface Mn(II) complex on goethite (E° = 0.41 volts) is much smaller than the value of E° = 0.9 volts for the couple $MnOH^{2+}/MnOH^{+}$. Wehrli suggests that the large discrepancy for Mn(II) indicates an inner-sphere oxygenation of the Mn(II) surface complex. This observation is in agreement with the proposed inner-sphere mechanism for the reactions between As(III) and Se(IV) with the birnessite surface.

6.6 Thoughts for Future Research

There are several areas, suggested by these results, which need further research related to the kinetics of adsorption and redox processes on metal oxide surfaces. Some of these are listed below:

1. The various mineral forms of manganese dioxide have different surface chemical properties with pH_{zpc} values ranging from 2-3 for birnessite to 7.3 for pyrolusite. A more thorough investigation of the As(III) and Se(IV) redox reaction with other manganese dioxides would clarify the dependence on the surface areas, surface chemistry, and redox energetics.

2. Examination of adsorption and oxidation reactions in more complex oxide systems by using actual or simulated groundwater would yield valuable estimates for environmental reaction rates.

3. The two-site adsorption model presented in Chapter 4 illustrated that the kinetic adsorption model could be improved by the inclusion of multiple surface sites. Spectroscopic methods could assist in characterizing the heterogeneities of the surface in order to alleviate the added uncertainties of a multi-site model.

4. By using radiolabeled Mn, the fate of surface Mn can be followed

throughout the reaction to determine the mass balance of Mn in the system.

5. Competitive effects of other redox active species on reaction rates could be evaluated, for example, by adding As(III) and Se(IV) simultaneously to a particle suspension.

REFERENCES

Adams, L. F., and W. C. Ghiorse, 1988. Oxidation state of Mn in the Mn oxide produced by *Leptothrix discophora* SS-1, Geochim. Cosmochim. Acta, 52, 2073-2076.

Ainsworth, C. C., D. C. Girvin, J. M. Zachara, and S. C. Smith, 1989. Chromate adsorption on goethite: effects of aluminum substitution, Soil Sci. Soc. Am. J., 53, 411-418.

Anderson, M. A., J. F. Ferguson, and J. Gavis, 1976. Arsenate adsorption on amorphous aluminum hydroxide, J. Colloid Interface Sci., 54, 391-399.

Anderson, M. A., T. R. Holm, D. G. Iverson, and R. R. Stanforth, 1978. Mass balance and speciation of arsenic in the Menominee River, Wisconsin. Proj. Rep. 6, USEPA Environ. Res. Lab., Athens, GA.

Anderson, M. A., and D. T. Malotky, 1979. The adsorption of protolyable anions on hydrous oxides at the isoelectric pH, J. Colloid Interface Sci., 72, 413-427.

Andreae, M. O., 1979. Arsenic speciation in seawater and interstitial waters: the influence of biological-chemical interactions on the chemistry of a trace element, Limnol. Oceanogr., 24, 440-552.

Atkinson, R. J., A. M. Posner, and J. P. Quirk, 1967. Adsorption of potential-determining ions at the ferric oxide-aqueous electrolyte interface, J. Phys. Chem., 71, 550-558.

Bainbridge, D., V. Wegrzyn, and N. Albasel, 1988. Selenium in California Volume I: History, Chemistry, Biology, Uses, Management. Report no. 88-10-I-WR, California State Water Resources Control Board, Sacramento, CA.

Balistrieri, L. S., and T. T. Chao, 1987. Selenium adsorption by goethite, Soil Sci. Soc. Am. J., 51, 1145-1151.

Banwart, S., S. Davies, and W. Stumm, 1989. The role of oxalate in accelerating the reductive dissolution of hematite (α-Fe_2O_3) by ascorbate, Colloid Surfaces, 39, 303-309.

Belzile, N., and A. Tessier, 1990. Interactions between arsenic and iron oxyhydroxides in lacustrine sediments, Geochim. Cosmochim. Acta, 54, 103-109.

Boehm, P., 1971. Acidic and basic properties of hydroxylated metal oxides surfaces, Discussions Faraday Soc., 52, 264-275.

Cherry, J. A., A. U. Shaikh, D. E. Tallman, and R. V. Nicholson, 1979. Arsenic species as an indicator of redox conditions in groundwater, J. Hydrology, 43, 373-392.

Chukhlantsev, V. G., and G. P. Tomashevsky, 1957. The solubility of the selenites of certain metals, J. Anal. Chem. USSR, 12, 303-309.

Cooke, T. D., and K. W. Bruland, 1987. Aquatic chemistry of selenium: evidence of biomethylation, Environ. Sci. Technol., 21, 1214-1219.

Crecelius, E. A., M. H. Bothner, and R. Carpenter, 1975. Geochemistries of arsenic, antimony, mercury, and related elements in sediments of Puget Sound, Environ. Sci. Technol., 9, 325-333.

Crowther, D. L., J. G. Dillard, and J. W. Murray, 1983. The mechanisms of Co(II) oxidation on synthetic birnessite, Geochim. Cosmochim. Acta, 47, 1388-1403.

Cullen, W. R., and K. J. Reimer, 1989. Arsenic speciation in the environment, Chem. Rev., 89, 713-764.

Davies, S. H. R., 1985. Mn(II) oxidation in the presence of metal oxides. Ph.D. Thesis, California Institute of Technology, Pasadena.

Davies, S. H. R., and J. J. Morgan, 1989. Manganese(II) oxidation kinetics on metal oxide surfaces, J. Colloid Interface Sci., 129, 63-77.

Davis, J. A., and J. O. Leckie, 1980. Surface ionization and complexation at the oxide/water interface. 3. Adsorption of anions, J. Colloid Interface Sci., 74, 32-43.

Dzombak, D. A., and F. M. M. Morel, 1987. Adsorption of inorganic pollutants in aquatic systems, J. Hydraulic Eng., 113, 430-475.

Dzombak, D. A., and F. M. M. Morel, 1990. Surface Complexation Modeling. Hydrous Ferric Oxide. Wiley-Interscience, New York.

Eary, L. E., and G. D. Rai, 1987. Kinetics of chromium(III) oxidation to chromium(VI) by reaction with manganese dioxide, Environ. Sci. Technol., 21, 1187-1193.

Eary, L. E., and J. A. Schramke, 1990. Rates of inorganic oxidation reactions involving dissolved oxygen, in Chemical Modeling of Aqueous Systems II, D. C. Melchior and R. L. Bassett, eds., ACS Symp. Ser. 416, 379-396.

Elrashidi, M. A., D. C. Adriano, S. M. Workman, and W. L. Lindsay, 1987. Chemical equilibria of selenium in soils: a theoretical development, Soil Sci., 144, 141-152.

Eltantawy, I. M., and P. W. Arnold, 1973. Reappraisal of ethylene glycol mono-ethyl ether (EGME) method for surface area estimations of clays, J. Soil Science, 24, 232-238.

Faughnan, J., 1981. The SURFEQL/MINEQL Manual. Environmental Engineering Science, California Institute of Technology, Pasadena, CA.

Faust, S. D., A. J. Winka, and T. Belton, 1987a. An assessment of chemical and biological significance of arsenical species in the Maurice River drainage basin (N. J.). Part I: Distribution in water and river and lake sediments, J. Environ. Sci. Health, A22, 203-237.

Faust, S. D., A. J. Winka, and T. Belton, 1987b. An assessment of chemical and biological significance of arsenical species in the Maurice River drainage basin (N. J.). Part II: Partitioning of arsenic into bottom sediments, J. Environ. Sci. Health, A22, 239-262.

Faust, S. D., A. J. Winka, and T. Belton, 1987c. An assessment of chemical and biological significance of arsenical species in the Maurice River drainage basin (N. J.). Part III: Transformation in aerobic and anaerobic conditions, J. Environ. Sci. Health, A22, 263-282.

Ferguson, J. F., and J. Gavis, 1972. A review of the arsenic cycle in natural waters, Water Res., 6, 1259-1274.

Ferguson, J. F., and M. A. Anderson, 1974. Chemical form of arsenic in water supplies and their removal, In Chemistry of Water Supply, Treatment, and Distribution, Rubin, A. J., Ed., Ann Arbor Science: Ann Arbor, MI, 137-158.

Fokkink, L. G. J., A. de Keizer, and J. Lyklema, 1990. Temperature dependence of cadmium adsorption on oxides: I. Experimental observations and model analysis, J. Colloid Interface Sci., 135, 118-131.

Forsythe, G. E., M. A. Malcolm, and C. B. Moler, 1977. Computer Methods for Mathematical Computations. Prentice-Hall, Englewood Cliffs, NJ.

Frost, R. R., and R. A. Griffin, 1977. Effect of pH on adsorption of arsenic and selenium from landfill leachate by clay minerals, Soil Sci. Soc. Am. J., 41, 53-57.

Fuller, C. C., and J. A. Davis, 1989. Influence of coupling of sorption and photosynthetic processes on trace element cycles in natural waters, Nature, 340, 52-54.

Gardiner, W. C., 1969. Rates and Mechanisms of Chemical Reactions. Benjamin, Menlo Park, CA.

Geering, H. R., E. E. Cary, L. H. P. Jones, and W. H. Allaway, 1968. Solubility and redox criteria for the possible forms of selenium in soils, Proc. Soil Sci. Soc. Am., 32, 35-40.

Ghosh, M. M., and J. R. Yuan, 1987. Adsorption of inorganic arsenic and organoarsenicals on hydrous oxides, Env. Progress, 6, 150-157.

Goldberg, S., 1985. Chemical modeling of anion competition on goethite using constant capacitance model, Soil Sci. Soc. Am. J., 49, 851-856.

Goldberg, S., 1986. Chemical modeling of arsenate adsorption on aluminum and iron oxide minerals, Soil Sci. Soc. Am. J., 50, 1154-1157.

Gulens, J., D. R. Champ, and R. E. Jackson, 1979. Influence of redox environments on the mobility of arsenic in ground water, ACS Symp. Ser. 93, 711-736.

Gupta, S. K., and K. Y. Chen, 1978. Arsenic removal by adsorption, J. Water Poll. Control Fed., 50, 493-506.

Harrison, J. B., and V. E. Berkheiser, 1982. Anion interactions with freshly prepared hydrous iron oxides, Clays Clay Miner., 30, 97-102.

Hayes, K. F., A. L. Roe, G. E. Brown, Jr., K. O. Hodgson, J. O. Leckie, and G. A. Parks, 1987. In situ x-ray absorption study of surface complexes: selenium oxyanions on α-FeOOH, Science, 238, 783-786.

Healy, T. W., A. P. Herring, and D. W. Fuerstenau, 1966. The effect of crystal structure on the surface properties of a series of manganese dioxides, J. Colloid Interface Sci., 21, 435-444.

Hingston, F. J., 1970. Specific adsorption of anions on goethite and gibbsite. Ph. D. Thesis, Univ. of W. Australia, Nedlands.

Hingston, F. J., A. M. Posner, and J. P. Quirk, 1968. Adsorption of selenite by goethite, In Adsorption from aqueous solution, Weber, W. J., and E. Matijeva, Eds., Advances in Chemistry #79, Am. Chem. Soc., Washington, D. C., 82-90.

Hingston, F. J., A. M. Posner, and J. P. Quirk, 1971. Competitive adsorption of negatively charged ligands on oxide surfaces, Discussions Faraday Soc., 52, 334-342.

Hingston, F. J., A. M. Posner, and J. P. Quirk, 1972. Anion adsorption by goethite and gibbsite. I. The role of the proton in determining adsorption envelopes, J. Soil Sci., 23, 177-192.

Holm, T. R., M. A. Anderson, D. G. Iverson, and R. S. Stanforth, 1979. Heterogeneous interactions of arsenic in aquatic systems, ACS Symp. Ser. 93, 711-736.

Howard, J. H., 1977. Geochemistry of selenium: formation of ferroselite and selenium behavior in the vicinity of oxidizing sulfide and uranium deposits, Geochim. Cosmochim. Acta, 41, 1665-1678.

Jacobs, L. W., ed., 1989. Selenium in Agriculture and the Environment. SSSA Special Publication no. 23, Madison, WI: American Society of Agronomy, Inc. and Soil Science Society of America, Inc., 233 pp.

Johnson, D. L., and M. E. Q. Pilson, 1972. Spectrophotometric determination of arsenite, arsenate, and phosphate in natural waters, Anal. Chim. Acta, 58, 289-299.

Kanungo, S. B., and D. M. Mahapatra, 1989. Interfacial properties of some hydrous manganese dioxides in 1-1 electrolyte solution, J. Colloid Interface Sci., 131, 103-111.

Laha, S., and R. G. Luthy, 1990. Oxidation of aniline and other primary aromatic amines by manganese oxides, Environ. Sci. Technol., 24, 363-373.

LaKind, J. S., 1988. The reductive dissolution of goethite and hematite by phenolic reductants. Ph.D. Thesis, Johns Hopkins University, Baltimore, MD.

Leckie, J., M. Benjamin, K. Hayes, G. Kaufman, and S. Altmann, 1980. Adsorption-coprecipitation of trace elements from water with iron oxyhydroxides, EPRI RS-910-1, Electric Power Research Institute, Palo Alto, CA.

Lemmo, N., S. Faust, T. Belton, and R. Tucker, 1983. Assessment of the chemical and biological significance of arsenical compounds in a heavily contaminated watershed. Part I: The fate and speciation of arsenical compounds in aquatic environments--a literature review, J. Environ. Sci. Health, A18, 389-411.

Lindberg, R. D. and D. D. Runnells, 1984. Ground water redox reactions: an analysis of equilibrium state applied to E_H measurements and geochemical modeling, Science, 225, 925-927.

Loganathan, P., R. G. Burau, and D. W. Fuerstenau, 1977. Influence of pH on the sorption of Co^{2+}, Zn^{2+}, and Ca^{2+} by a hydrous manganese oxide, Soil Sci. Soc. Am. J., 41, 57-62.

Lumsdon, D. G., A. R. Fraser, J. D. Russell, and N. T. Livesay, 1984. New infrared band assignments for the arsenate ion adsorbed on synthetic goethite (α-FeOOH), J. Soil Sci., 35, 381-386.

Machesky, M. L., 1990. Influence of temperature on ion adsorption by hydrous metal oxides, in Chemical Modeling of Aqueous Systems II, D. C. Melchior and R. L. Bassett, eds., ACS Symp. Ser. 416, 282-292.

Malotky, D. T., and M. A. Anderson, 1976. The adsorption of the potential determining arsenate anion on oxide surfaces, In Colloid and Interface Science, 4, Kerker, M., ed., Academic Press: New York, 281-295.

McBride, M. B., 1987. Adsorption and oxidation of phenolic compounds by iron and manganese oxides, Soil Sci. Soc. Am. J., 51, 1466-1472.

McKenzie, R. M., 1971. The synthesis of birnessite, crytomelane, and some other oxides and hydroxides of manganese, Mineralogical Magazine, 38, 493-502.

McKenzie, R. M., 1981. The surface charge on manganese dioxides, Aust. J. Soil Res., 19, 41-50.

McNeal, J. M., and L. S. Balistrieri, 1989. Geochemistry and occurrence of selenium: an overview, in Selenium in Agriculture and the Environment, L. W. Jacobs, ed., SSSA Special Publication no. 23, Soil Science Society of America and American Society of Agronomy, Madison, WI, 1-13.

Mok, W. M., and C. M. Wai, 1989. Distribution and mobilization of arsenic species in the creeks around the Blackbird mining district, Idaho, Water Res., 23, 7-13.

Morgan, J. J., and W. Stumm, 1964. Colloid-chemical properties of manganese dioxide, J. Colloid Sci., 19, 347-359.

Murray, J. W., 1974. The surface chemistry of hydrous manganese dioxide, J. Colloid Interface Sci., 46, 357-371.

Murray, J. W., 1975. The interaction of metal ions at the manganese dioxide-solution interface, Geochim. Cosmochim. Acta, 39, 505-510.

National Research Council, Committee on medical and biological effects of environmental pollutants, 1976. Selenium. Washington, D. C.: National Academy of Science, 203 pp.

National Research Council, Committee on medical and biological effects of environmental pollutants, 1977. Arsenic. Washington, D. C.: National Academy of Science, 322 pp.

National Research Council, Committee on irrigation-induced water quality problems, 1989. Irrigation-induced water quality problems: what can be learned from the San Joaquin Valley experience. Washington, D. C.: National Academy of Science, 157 pp.

Neal, R. H., G. Sposito, K. M. Holtzclaw, and S. J. Traina, 1987. Selenite adsorption on alluvial soils. I. Soil composition and pH effects, Soil Sci. Soc. Am. J., 51, 1161-1165.

Oscarson, D. W., P. M. Huang, and W. K. Liaw, 1980. The oxidation of arsenite by aquatic sediment, J. Environ. Qual., 9, 700-703.

Oscarson, D. W., P. M. Huang, and W. K. Liaw, 1981a. The role of manganese in the oxidation of arsenite by freshwater lake sediments, Clays Clay Miner., 29, 219-225.

Oscarson, D. W., P. M. Huang, C. Defosse, and A. Herbillon, 1981b. Oxidative power of Mn(IV) and Fe(III) oxides with respect to As(III) in terrestrial and aquatic environments, Nature, 291, 50-51.

Oscarson, D. W., P. M. Huang, U. T. Hammer, and W. K. Liaw, 1983a. Oxidation and sorption of arsenate by manganese dioxide as influenced by surface coatings of iron and aluminum oxides and calcium carbonate, Water, Air, and Soil Poll., 20, 233-244.

Oscarson, D. W., P. M. Huang, W. K. Liaw, and U. T. Hammer, 1983b. Kinetics of oxidation of arsenite by various manganese dioxides, Soil Sci. Soc. Am. J., 47, 644-648.

Parfitt, R. L., A. R. Fraser, and V. C. Farmer, 1977. Adsorption on hydrous oxides. III. Fulvic acid and humic acid on goethite, gibbsite, and imogolite, J. Soil Sci., 28, 289-296.

Parida, K. M., S. B. Kanungo, and B. R. Sant, 1981. Studies on MnO_2--I. Chemical composition, microstructure and other characteristics of some synthetic MnO_2 of various crystalline modifications, Electrochim. Acta, 26, 435-443.

Peterson, M. L., and R. Carpenter, 1983. Biogeochemical processes affecting total arsenic and arsenic species distribution in an intermittently anoxic fjord, Marine Chem., 12, 295-321.

Pierce, M. L., and C. B. Moore, 1980. Adsorption of arsenite on amorphous iron hydroxides from dilute aqueous solutions, Environ. Sci. Technol., 14, 214-216.

Pierce, M. L., and C. B. Moore, 1982. Adsorption of arsenite and arsenate on amorphous iron hydroxide, Water Res., 16, 1247-1253.

Presser, T. S., and I. Barnes, 1984. Selenium concentrations in waters tributary to and in the vicinity of Kesterson National Wildlife Refuge, Fresno and Merced counties, California. Water Resources Invest. Rep. 84-4122. U. S. Geol. Surv., Menlo Park, CA.

Presser, T. S., and I. Barnes, 1985. Dissolved constituents including selenium in waters tributary to and in the vicinity of Kesterson National Wildlife Refuge and the West Grassland, Fresno and Merced counties, California. Water Resources Invest. Rep. 85-4220. U. S. Geol. Surv., Menlo Park, CA.

Princeton Applied Research, 1976. Application Brief A-6: Determination of arsenic by differential pulse polarography.

Rajan, S. S. S., 1979. Adsorption of selenite, phosphate, and sulfate on hydrous alumina, J. Soil Sci., 30, 709-718.

Rosenfeld, I., and O. A. Beath, 1964. Selenium. Geobotany, biochemistry, toxicity and nutrition. New York: Academic Press, 411 pp.

Schindler, P. W., and W. Stumm, 1987. The surface chemistry of oxides, hydroxides, and oxide minerals, in Aquatic Surface Chemistry, W. Stumm, ed., Wiley-Interscience, New York, 83-110.

Sigg, L., and W. Stumm, 1980. The interaction of anions and weak acids with the hydrous goethite (α-FeOOH) surface, Colloid Surf., 2, 101-117.

Stone, A. T., 1983. The reduction and dissolution of manganese(III) and (IV) oxides by organics, Ph. D. Thesis, California Institute of Technology, Pasadena, CA.

Stone, A. T., 1986. Adsorption of organic reductants and subsequent electron transfer on metal oxide surfaces, in Geochemical Processes at Mineral Surfaces, J. A. Davis and K. F. Hayes, eds., ACS Symp. Ser. 323, 446-461.

Stone, A. T., 1987. Reduction dissolution of manganese(III, IV) oxides by substituted phenols, Environ. Sci. Technol., 21, 979-988.

Stone, A. T., and J. J. Morgan, 1987. Reductive dissolution of metal oxides, in Aquatic Surface Chemistry, W. Stumm, ed., Wiley-Interscience, New York, 221-254.

Stone, A. T., and H. Ulrich, 1989. Kinetics and reaction stoichiometry in the reductive dissolution of manganese(IV) dioxide and Co(III) oxide by hydroquinone, J. Colloid Interface Sci., 132, 509-522.

Stumm, W., and J. J. Morgan, 1981. Aquatic Chemistry. New York: Wiley, 538 pp.

Sung, W., and J. J. Morgan, 1980. Kinetics and product of ferrous ion oxygenation in aqueous systems, Environ. Sci. Technol., 14, 561-567.

Sung, W., and J. J. Morgan, 1981. Oxidative removal of Mn(II) from solution catalyzed by the lepidocrocite surface, Geochim. Cosmochim. Acta, 45, 2377-2383.

Tallman, D. E., and A. U. Shaikh, 1980. Redox stability of inorganic arsenic(III) and arsenic(V) in aqueous solution, Anal. Chem., 52, 196-199.

Thanabalasingam, P., and W. F. Pickering, 1986. Effect of pH on interaction between As(III) or As(V) and manganese(IV) oxide, Water, Air, and Soil Poll., 29, 205-216.

Wehrli, B., 1987. Vanadium in the hydrosphere: surface chemistry and oxidation kinetics, Ph. D. Thesis, ETH, Zurich.

Wehrli, B., 1990. Redox reactions of metal ions at mineral surfaces, in Aquatic Chemical Kinetics, W. Stumm, ed., Wiley-Interscience, New York, 311-336.

Welch, A. H., M. S. Lico, and J. L. Hughes, 1988. Arsenic in ground water of the western United States, Groundwater, 26, 333-347.

Westall, J. C., 1982. FITEQL: a computer program for determination of chemical equilibrium constants from experimental data, Rep. 82-02, Oregon State University, Corvalis.

Westall, J. C., 1986. Reactions at the oxide-solution interface: chemical and electrostatic models, in Geochemical Processes at Mineral Surfaces, J. A. Davis and K. F. Hayes, eds., ACS Symp. Ser. 323, 54-78.

Westall, J. C., 1987. Adsorption mechanisms in aquatic surface chemistry, in Aquatic Surface Chemistry, W. Stumm, ed., Wiley-Interscience, New York, 3-32.

Westall, J., and H. Hohl, 1980. A comparison of electrostatic models for the oxide/solution interface, Adv. Colloid Interface Sci., 12, 265-294.

Williams, K. T., and H. G. Byers, 1936. Selenium compounds in soils, Ind. Eng. Chem., 28, 912-914.

Yasunga, T., and T. Ikeda, 1987. Adsorption-desorption kinetics at the metal oxide-solution interface studied by relaxation methods, in Geochemical Processes at Mineral Surfaces, J. A. Davis and K. F. Hayes, eds., ACS Symp. Ser. 323, 230-253.

Yates, D. E., 1975. The structure of the oxide-aqueous electrolyte interface. Ph.D. Thesis, University of Melbourne, Australia.

Yoshida, I., H. Kobayashi, and K. Ueno, 1976. Selective adsorption of arsenic ions on silica gel impregnated with ferric hydroxide, Anal. Lett., 9, 1125-1133.

Yoshida, I., K. Ueno, and H. Kobayashi, 1978. Selective separation of arsenic(III) and (V) ions with ferric complex of chelating ion-exchange resin, Sep. Sci., 13, 173-184.

Appendix A

EXPERIMENTAL DATA

Experiment G4AS3		Experiment G4AS5		Experiment B4AS3	
As(III) & Goethite		As(V) & Goethite		As(III) & Birnessite	
pH 4, 25 °C		pH 4, 25 °C		pH 4, 25 °C	
Time (sec)	As(III) (μM)	Time (sec)	As(V) (μM)	Time (sec)	As(III) (μM)
0	100.0	0	50.09	0	99.60
93	92.33	37	36.45	120	84.29
205	88.39	78	33.85	300	59.35
291	83.31	119	32.89	600	45.00
372	77.47	158	30.76	1200	26.88
461	74.78	201	30.36	1800	16.59
549	73.54	260	28.36	2700	10.10
886	70.54	303	27.73	3600	2.55
1363	68.83	345	27.75	5400	0.00
1766	63.64	389	26.58		
		507	25.46		
		1727	20.11		
		3730	16.91		

Experiment B4AS5		Experiment B4MN2		Experiment B6MN2	
As(V) & Birnessite		Mn(II) & Birnessite		Mn(II) & Birnessite	
pH 4, 25 °C		pH 4, 25 °C		pH 6, 25 °C	
Time (sec)	As(V) (μM)	Time (sec)	Mn(II) (μM)	Time (sec)	Mn(II) (μM)
0	100.0	0	98.9	0	98.8
120	100.0	120	78.0	120	45.4
300	100.0	300	75.1	300	25.6
600	100.0	600	72.1	600	17.1
1200	100.0	1200	68.1	1200	11.3
1800	100.0	1800	67.0	1800	8.2
2700	100.0	2700	65.8	2700	4.9
3600	100.0	3600	63.8	3600	5.0
5400	100.0	5400	60.8	5400	3.1
7200	100.0				

Experiment G4SE4		Experiment B4SE4	
Se(IV) & Goethite		Se(IV) & Birnessite	
pH 4, 25 °C		pH 4, 25 °C	
Time (sec)	As(III) (μM)	Time (sec)	As(V) (μM)
0	100.0	0	100.0
120	67.48	120	88.43
240	66.18	240	85.24
360	61.66	360	84.58
480	60.10	480	81.87
600	59.81	900	84.26
900	57.46	1200	81.99
1200	55.96	1800	80.02
1800	52.30	2700	83.28
2700	52.67	3600	79.00
3600	49.43	5400	79.44
5400	48.76	8520	80.34
7500	48.34	86400	78.66

Experiment PH4T15		Experiment PH4T25		Experiment PH4T35	
As(III) & Goethite		As(III) & Goethite		As(III) & Goethite	
pH 4, 15 °C		pH 4, 25 °C		pH 4, 35 °C	
Time (sec)	As(III) (μM)	Time (sec)	As(III) (μM)	Time (sec)	As(III) (μM)
0	50.12	0	50.14	0	53.05
63	49.24	78	47.67	75	49.23
130	49.38	155	46.52	152	43.98
196	46.57	235	43.58	217	47.97
260	45.57	306	43.8	284	44.57
322	43.19	372	44.66	348	41.99
393	44.49	435	44.23	409	44.35
457	42.11	503	39.14	550	39.25
515	41.54	569	39.86	676	36.29
580	41.39	634	40.65		
654	43.34	706	41.08		

Experiment PH6T15		Experiment PH6T25		Experiment PH6T35	
As(III) & Goethite		As(III) & Goethite		As(III) & Goethite	
pH 6, 15 °C		pH 6, 25 °C		pH 6, 35 °C	
Time (sec)	As(III) (μM)	Time (sec)	As(III) (μM)	Time (sec)	As(III) (μM)
0	49.86	0	49.98	0	52.74
59	46.32	68	47.49	84	44.28
121	43.57	141	45.95	141	42.34
179	42.30	210	42.80	212	37.30
247	41.33	271	40.45	276	35.50
311	40.07	332	40.77	330	36.00
384	38.43	405	40.93	393	37.94
437	38.73	480	38.02	446	33.91
492	37.61	545	36.97	505	37.73
550	35.75	606	33.49	588	36.10
600	34.48	668	35.52	644	34.56

Experiment PH7T25	
As(III) & Goethite	
pH 7, 25 °C	
Time (sec)	As(III) (μM)
0	98.30
240	65.89
480	56.75
600	70.40
900	48.03
1,200	53.74
1,500	52.35
1,800	43.47
2,400	45.78
3,000	39.80
3,600	47.92
4,500	44.39
5,400	39.54
6,300	42.49
7,200	42.49
10,800	48.85
14,400	49.60
27,840	41.31
86,460	35.88
176,040	34.92

ExperimentMnAs1				ExperimentMnAs2			
As(III) & Birnessite				As(III) & Birnessite			
pH 4, 25 ℃, 0.1 M I				pH 4, 25 ℃, 0.1 M I			
Time (min)	As(III) (μM)	As(V) (μM)	Mn(II) (μM)	Time (min)	As(III) (μM)	As(V) (μM)	Mn(II) (μM)
0	99.60	0	0	0	199.7	0	0
2	84.29	13.39	0	2		28.90	4.2
5	59.35	34.47	6.6	5		45.95	27.3
10	45.00	50.19	27.5	10		66.27	57.7
20	26.88	69.36	48.9	20		94.25	96
30	16.59	76.92	63.3	30		107.5	120
45	10.10	84.44	76	45		126.8	145
60	2.55	89.23	83	60		137.0	174
90	0	92.72	86	90		155.6	187
120	0	93.71	84	120		162.8	202
180	0		85	180		178.4	223
240	0			240		184.2	228
				300		186.7	234
				360		191.9	234

Experiment MnAs3				Experiment MnAs4			
As(III) & Birnessite				As(III) & Birnessite pO_2 = 0.21 atm			
pH 4, 25 °C, 0.1 M I				pH 4, 25 °C, 0.1 M I			
Time (min)	As(III) (μM)	As(V) (μM)	Mn(II) (μM)	Time (min)	As(III) (μM)	As(V) (μM)	Mn(II) (μM)
0	398.4	0	0	0	99.6	0	0
2	393.3	34.26	6.6	2	n.d.	16.97	1.0
5	357.9	59.10	38.2	5	n.d.	33.91	8.0
10	321.6	88.60	88	10	n.d.	50.20	28.0
20	281.2	124.2	143	20	n.d.	67.48	52.2
30	270.1	144.5	176	30	n.d.	76.38	68
45	217.1	168.9	221	45	n.d.	85.16	78
60	243.2	184.6	241	60	n.d.	89.27	85
90	207.0	213.3	285	90	n.d.	94.16	91
120	161.4	233.9	312	120	n.d.	94.69	88
180	124.8	261.1	369	180	n.d.	97.88	89
240	138.5	283.0	396	240	n.d.	98.15	85

n.d.= not determined

ExperimentMnAs5		ExperimentMnAs6			
As(V) & Birnessite		As(III) & Birnessite			
pH 4, 25 ℃, 0.1 M I		pH 4, 15 ℃, 0.1 M I			
Time (min)	As(V) (μM)	Time (min)	As(III) (μM)	As(V) (μM)	Mn(II) (μM)
0	100	0	99.6	0	0
2	100	2	94.13	9.62	0.4
5	100	5	93.3	21.66	2.5
10	100	10	64.68	35.46	11.7
20	100	20	44.28	49.30	32.0
30	100	30	37.84	63.64	48.8
45	100	45		73.31	61.8
60	100	60		80.78	75
90	100	90	14.81	89.32	85
120	100	120	5.46	94.21	92
180	100	180	0	97.36	100
		240	0	98.94	101

ExperimentMnAs7				ExperimentMnAs8			
As(III) & Birnessite				As(III) & Birnessite			
pH 4, 35 ℃, 0.1 M I				pH 5, 25 ℃, 0.1 M I			
Time (min)	As(III) (μM)	As(V) (μM)	Mn(II) (μM)	Time (min)	As(III) (μM)	As(V) (μM)	Mn(II) (μM)
0	106.3	0	0	0	99.4	0	0
2	65.88	34.26	2.7	2	93.24	11.33	0
5	49.44	59.20	20.3	5	73.66	26.85	0.8
10	30.96	67.51	43.4	10	62.00	43.45	4.8
20	18.22	81.70	60.8	20	50.31	60.70	18.1
30	8.92	92.05	69	30	32.24	70.42	28.9
45	3.9	96.28	74	45	27.34	79.64	35.1
60	0	98.79	74	60	18.66	84.63	42.6
90	0	104.6	70	90	14.54	91.47	46.8
120	0	101.3	69	120	8.11	95.96	49.5
180	0	101.6	63.4	180	4.52	101.6	49.3
240	0	103.1	63.1	240	0	104.4	48.2

ExperimentMnAs9				ExperimentMnAs10			
As(III) & Birnessite				As(III) & Birnessite			
pH 5.85,25 ℃, 0.1 M I				pH 6.8,25 ℃, 0.1 M I			
Time (min)	As(III) (μM)	As(V) (μM)	Mn(II) (μM)	Time (min)	As(III) (μM)	As(V) (μM)	Mn(II) (μM)
0	99.4	0	0	0	99.3	0	0
2	91.29	10.90	0	2	87.14	7.61	0
5	84.78	22.20	0	5	75.65	15.91	0
10	63.13	36.96	0	10	63.78	28.28	0
20	47.92	55.82	1.7	20	46.60	52.15	0.3
30	27.34	65.65	4.8	30	29.14	64.15	0.5
45	29.62	74.00	6.8	45	22.39	73.11	1.1
60	24.12	78.96	10.3	60	18.59	77.94	1.7
90	16.16	86.46	13.1	90	14.49	79.75	3.0
120	13.09	90.99	15.5	120	12.16	87.60	4.1
180	6.31	98.63	18.6	180	9.70	91.39	5.6
240	4.54	101.6	20.9	240	6.92	93.76	6.8

ExperimentMnAs11				ExperimentMnAs12			
As(III) & Birnessite				As(III) & Birnessite			
pH 7.7,25 ℃, 0.1 M I				pH 8.2,25 ℃, 0.1 M I			
Time (min)	As(III) (μM)	As(V) (μM)	Mn(II) (μM)	Time (min)	As(III) (μM)	As(V) (μM)	Mn(II) (μM)
0	99.9	0	0	0	99.9	0	0
2	90.69	9.14	0	2	115.8	12.22	0
5	81.89	16.77	0	5	76.34	22.83	0
10	70.87	28.33	0	10	64.70	34.18	0
20	47.77	51.95	0	20	39.15	58.64	0
30	33.24	64.77	0	30	27.38	71.01	0
45	26.36	73.39	0.3	45	26.32	80.27	0
60	23.65	78.03	0.6	60	14.91	85.03	0.4
90	18.01	82.68	1.1	90	7.23	89.38	0
120	13.30	87.13	1.3	120	6.02	92.19	0.4
180	8.56	91.53	1.9	180			0.5
240	7.26	94.33	2.3	240			0.5

ExperimentMnAs13				ExperimentMnAs14			
As(III) & Birnessite: Mn^{2+} = 98.9 μM				As(III) & Birnessite: Mn^{2+} = 196 μM			
pH 4, 25 ℃, 0.1 M I				pH 4, 25 ℃, 0.1 M I			
Time (min)	As(III) (μM)	As(V) (μM)	Mn(II) (μM)	Time (min)	As(III) (μM)	As(V) (μM)	Mn(II) (μM)
0	99.8	0	44.9	0	101.1	0	161
2	n.d.	6.21	58.4	2	n.d.	4.49	169
5	n.d.	13.51	71	5	n.d.	9.33	179
10	n.d.	24.53	93	10	n.d.	17.50	193
20	n.d.	42.36	117	20	n.d.	30.08	217
30	n.d.	52.78	137	30	n.d.	42.46	236
45	n.d.	63.56	153	45	n.d.	52.57	254
60	n.d.	71.98	168	60	n.d.	60.45	260
90	n.d.	80.34	186	90	n.d.	71.84	284
120	n.d.	86.79	189	120	n.d.	78.47	290
180	n.d.	91.83	203	180	n.d.	86.70	305
240	n.d.	94.13	203	240	n.d.	90.08	312

n.d.= not determined

ExperimentMnAs15				ExperimentMnAs16			
As(III) & Birnessite: Ca^{2+} = 98.9 μM				As(III) & Birnessite: Ca^{2+} = 500 μM			
pH 4, 25 ℃, 0.1 M I				pH 4, 25 ℃, 0.1 M I			
Time (min)	As(III) (μM)	As(V) (μM)	Mn(II) (μM)	Time (min)	As(III) (μM)	As(V) (μM)	Mn(II) (μM)
0	99.8	0	0	0	98.9	0	0
2	n.d.	12.30	n.d.	2	n.d.	10.69	n.d.
5	n.d.	28.06	n.d.	5	n.d.	24.19	n.d.
10	n.d.	43.62	n.d.	10	n.d.	39.02	n.d.
20	n.d.	59.83	n.d.	20	n.d.	55.57	n.d.
30	n.d.	71.98	n.d.	30	n.d.	67.61	n.d.
45	n.d.	78.64	n.d.	45	n.d.	76.20	n.d.
60	n.d.	83.12	n.d.	60	n.d.	81.14	n.d.
90	n.d.	89.92	n.d.	90	n.d.	84.51	n.d.
120	n.d.	91.65	n.d.	120	n.d.	87.27	n.d.
180	n.d.	89.18	57.6	180	n.d.	88.72	65.5
240	n.d.	92.66	56.9	240	n.d.	92.18	64.1

n.d.= not determined

ExperimentMnSe1				ExperimentMnSe3			
Se(IV) & Birnessite				Se(IV) & Birnessite			
pH 4, 25 ℃, 0.001M I				pH 4, 25 ℃, 0.001M I			
Time (hr)	Se(IV) (μM)	Se(VI) (μM)	Mn(II) (μM)	Time (hr)	Se(IV) (μM)	Se(VI) (μM)	Mn(II) (μM)
0	100.0	0	0	0	50.90	0	0
3	72.48	0	0	3	26.77	0	0
12	67.27	2.53	0	12	24.27	1.56	0
24	66.79	4.47	0	24	21.88	3.63	0
48	61.88	7.59	0	48	20.22	5.82	0
72	59.15	10.23	0	72	18.27	7.54	0
93	54.91	11.81	0	93	16.00	9.05	0
120	52.74	14.60	0	136	13.83	12.16	0
136	49.85	16.82	0	168	12.77	14.60	0
193	47.17	19.53	0	193	10.91	16.12	0
216.5	45.64	21.45	0	216.5	10.73	17.03	0
240	44.72	23.25	0	240	9.86	18.47	0
265	41.57	24.55	0	265	8.76	19.25	0
313	38.66	25.17	0	313	7.69	20.91	0
337	37.08	29.08	0	361	6.35	21.31	0
409	33.11	33.08	0	409	5.61	23.07	0
457	31.89	37.98	0	457	6.00	25.05	0
529	27.79	39.82	0	529	4.51	27.50	0
577	25.15	42.60	0	625	3.09	31.19	0
625	25.08	45.63	0	673	2.95	31.62	0
673	23.92	47.70	0				

Experiment MnSe5				Experiment MnSe6			
Se(IV) & Birnessite				Se(IV) & Birnessite			
pH 4, 25 °C, 0.001 M I				pH 5, 25 °C, 0.001 M I			
Time (hr)	Se(IV) (μM)	Se(VI) (μM)	Mn(II) (μM)	Time (hr)	Se(IV) (μM)	Se(VI) (μM)	Mn(II) (μM)
0	101.3	0	0	0	101.3	0	0
1	61.36	0	0	1	77.24	0	0
12	53.38	3.66	0	12	75.10	0.88	0
24	47.84	6.12	0	24	76.38	1.61	0
48	41.47	10.65	0	48	67.82	2.93	0
96	34.62	19.06	0	96	64.68	4.40	0
120	31.41	21.80	0	120	60.75	5.29	0
144	28.16	24.94	0	144	59.46	6.62	0
192	23.87	30.62	0	192	60.62	7.92	0
240	21.81	37.10	0	240	66.94	10.44	0
312	16.76	42.87	0	312	59.46	12.49	0
408	11.90	52.30	0	408	61.39	16.47	0
456	9.57	54.46	0	456	59.88	17.57	0
504	8.23	57.18	0	504	58.12	18.77	0
547	8.09	60.25	0	547	56.14	20.45	0
622	5.37	66.47	0	622	53.63	22.40	0
670	4.77	69.02	0				

Experiment MnSe7				Experiment MnSe8			
Se(IV) & Birnessite				Se(IV) & Birnessite			
pH 7, 25 °C, 0.001 M I				pH 4, 31 °C, 0.001 M I			
Time (hr)	Se(IV) (μM)	Se(VI) (μM)	Mn(II) (μM)	Time (hr)	Se(IV) (μM)	Se(VI) (μM)	Mn(II) (μM)
0	101.3	0	0	0	101.4	0	0
1	88.06	0	0	0.25	77.99	0	0
24	83.32	0	0	1	77.97	0	0
48	68.99	0	0	26	67.03	6.31	0
96	69.88	0.92	0	47	61.69	10.36	0
120	68.93	0.99	0	100	59.25	15.73	0
144	68.31	1.24	0	196	48.48	28.24	0
192		2.15	0	244	43.58	32.77	0
240	80.33	2.63	0	292	38.74	36.50	0
312	74.82	2.29	0	337	34.31	40.63	0
408	77.51	4.13	0	412	30.66	47.46	0
456	75.04	4.58	0	460	27.08	47.76	0
504	75.29	5.43	0				
547	74.70	6.72	0				
622	75.75	7.86	0				
670	73.14	7.61	0				

Experiment MnSe9				Experiment MnSe10			
Se(IV) & Birnessite				Se(IV) & Birnessite			
pH 4, 36 °C, 0.001 M I				pH 4, 25 °C, 0.001 M I			
Time (hr)	Se(IV) (μM)	Se(VI) (μM)	Mn(II) (μM)	Time (min)	Se(IV) (μM)	Se(VI) (μM)	Mn(II) (μM)
0	101.4	0	0	0	100.0	0	0
0.25	81.76	0	0	2	88.43	0	0
1	77.29	0	0	4	85.24	0	0
26	64.33	9.39	0	6	84.58	0	0
47	59.75	15.53	0	8	81.87	0	0
100	53.42	22.84	0	15	84.25	0	0
196	37.53	39.92	0	20	81.99	0	0
244	31.62	45.99	0	30	80.02	0	0
292	26.96	52.66	0	45	83.28	0	0
337	22.73	57.56	0	60	79.00	0	0
412	16.98	64.32	0	90	79.44	0	0
460	14.20	67.67	0	142	80.34	0	0
				1440	78.66	3.68	0

Appendix B

In this appendix two Fortran computer codes that were used to model the dynamics of arsenic and selenium with iron and manganese oxide surface are listed. The first code was used to model anion and cation adsorption and desorption processes that are discussed in Chapter 4. The second code was used to model the four step surface redox process that is utilized in Chapter 5. An example of the input data files used with each code is also included.

Model A: Adsorption-Desorption

```
c       Forward Euler Method, Explicit
c       Requires small time steps
c       Reaction:  a + x = b
c       Aqueous species = a
c       Surface Hydroxyl Complex = x
c       Adsorbed Anion = b
        implicit double precision (a-h,o-z)
        real*8 k1,k2
        common /param/ k1,k2,deltat
c       Input data in file called "kinput.dat"
c       Output data in file called "kinout.dat"
        open(2,file='kinput.dat',status='old')
        open(4,file='kinout.dat',status='new')
        call readin(a,b,x,nsteps,nod)
        t=0.00
        izod=1
        do 10 j=1,nsteps
        t = t + deltat
        call update(a,b,x,j)
        if (j.ne.izod) GOTO 10
        call writer(a,b,x,j,t)
        izod= izod + nod
```

```
10     continue
       close(2)
       close(4)
      stop
      end
      subroutine readin(a,b,x,nsteps,nod)
      implicit double precision (a-h,o-z)
      real*8 k1,k2
      common /param/k1,k2,deltat
      read(2,20) a,x
20     format(e9.3,1x,e9.3)
      read(2,30) ftime,nsteps,nprt
30     format(e9.3,1x,i7,1x,i5)
       nod = nsteps/nprt
      read(2,40) k1
40     format(e9.3)
       read(2,41) k2
41     format(e9.3)
       demon=nsteps - 1
      deltat=ftime/demon
      b=0.d0
      write(4,60) a
60     format('  initial value of a = ',1pe10.4,/)
      write(4,70) x
70     format('  initial value of x = ',1pe10.4,//)
       write(4,71) k1,k2
71     format(' k1 = ', 1pe10.2,5x,' k2 = ', 1pe10.2,/)
      write(4,80) ftime,nsteps,deltat
80     format(' t 0.0 to ',f9.3,' in ',i7,' steps of ', f9.3,/)
       write(4,85)
85     format(3x,'t   a   b    x ',/)
      return
      end
      subroutine update(a,b,x,j)
      implicit double precision (a-h,o-z)
      real*8 k1,k2
      common /param/k1,k2,deltat
c      Adsorption Rate = r1
```

```
c       Desorption Rate = r2
        r1 = k1*a*x
        r2 = k2*b
        a = a + deltat*(-r1 + r2)
        b = b + deltat*(r1 - r2)
        x = x + deltat*(-r1 + r2)
        return
        end
        subroutine writer(a,b,x,j,t,)
        implicit double precision (a-h, o-z)
        write(4,100)t,a,b,x
100      format(f8.2,1p3e10.2)
120      return
        end
```

Input Data File for Model A

+5.000e-5 +3.190e-4	[Initial a, Mol/L][Initial x, Mol/L]
+4.000e+3 0010000 00100	[Final t][Total Time Steps][Write every t]
+2.000e+1	[k_a]
+1.000e-2	[k_d]

Model B: Adsorption-Desorption-Electron Transfer

```
c       forward euler method, explicit, requires small times steps
c       ReactionA:  a + x = b
c       ReactionB:  b = c
c       ReactionC:  c = d + y
c       ReactionD:  y = e + x
c       Aqueous reduced anion = a
c       Surface Hydroxyl Complex = x
c       Adsorbed Anion = b
c       Surface Redox Product = c
c       Aqueous oxidized anion = d
c       Aqueous reduced metal = e
c       Surface reduced metal complex = y
c       Input data in file called "kinput.dat"
c       Output data in file called "kinout.dat"
      implicit double precision (a-h,o-z)
      real*8 k1,k2,k3,k4,k5,k6,k7,k8
      common /param/ k1,k2,k3,k4,k5,k6,k7,k8,deltat
       open(2,file='kinput.dat',status='old')
       open(4,file='kinout.dat',status='new')
      call readin(a,b,c,d,e,y,x,nsteps,nod)
      t=0.00
       izod=1
      do 10 j=1,nsteps
      t = t + deltat
      call update(a,b,c,d,e,y,x,j)
       if (j.ne.izod) GOTO 10
      call writer(a,b,c,d,e,y,x,j,t)
       izod= izod + nod
10     continue
       close(2)
       close(4)
      stop
      end
      subroutine readin(a,b,c,d,e,y,x,nsteps,nod)
      implicit double precision (a-h,o-z)
      real*8 k1,k2,k3,k4,k5,k6,k7,k8
      common /param/k1,k2,k3,k4,k5,k6,k7,k8,deltat
      read(2,20) a,x
```

```
20     format(e9.3,1x,e9.3)
      read(2,30) ftime,nsteps,nprt
30     format(e9.3,1x,i7,1x,i5)
       nod = nsteps/nprt
      read(2,40) k1,k3,k5,k7
40     format(4(e9.3,2x))
       read(2,41) k2,k4,k6,k8
41     format(4(e9.3,2x))
       demon=nsteps - 1
      deltat=ftime/demon
      b=0.d0
      c=0.d0
      d=0.d0
      e=0.d0
      y=0.d0
      write(4,60) a
60     format('  initial value of a = ',1pe10.4,/)
      write(4,70) x
70     format('  initial value of x = ',1pe10.4,//)
       write(4,71) k1,k2
71     format(' k1 = ', 1pe10.2,5x,' k2 = ', 1pe10.2,/)
       write(4,72) k3,k4
72     format(' k3 = ', 1pe10.2,5x,' k4 = ', 1pe10.2,/)
       write(4,73) k5,k6
73     format(' k5 = ', 1pe10.2,5x,' k6 = ', 1pe10.2,/)
       write(4,74) k7,k8
74     format(' k7 = ', 1pe10.2,5x,' k8 = ', 1pe10.2,//)
      write(4,80) ftime,nsteps,deltat
80     format(' t 0.0 to ',f9.3,' in ',i7,' steps of ', f9.3,/)
       write(4,85)
85     format(3x,'t   a   b   c   d   e   y   x ',/)
      return
      end
      subroutine update(a,b,c,d,e,y,x,j)
      implicit double precision (a-h,o-z)
      real*8 k1,k2,k3,k4,k5,k6,k7,k8
      common /param/k1,k2,k3,k4,k5,k6,k7,k8,deltat
      r1 = k1*a*x
      r2 = k2*b
      r3 = k3*b
      r4 = k4*c
      r5 = k5*c
      r6 = k6*y*d
      r7 = k7*y
```

```
      r8 = k8*x*e
      a = a + deltat*(-r1 + r2)
      b = b + deltat*(r1 - r2 - r3 + r4)
      c = c + deltat*(r3 - r4 - r5 + r6)
      d = d + deltat*(r5 - r6)
      e = e + deltat*(r7 - r8)
      y = y + deltat*(r5 - r6 - r7 + r8)
      x = x + deltat*(-r1 + r2 + r7 - r8)
      return
      end
      subroutine writer(a,b,c,d,e,y,x,j,t,)
      implicit double precision (a-h, o-z)
      write(4,100)t,a,b,c,d,e,y,x
100    format(f8.2,1p7e10.2)
120    return
      end
```

Input Data File for Model B

```
+9.980e-5 +4.480e-4                [Initial a, Mol/L][Initial x, Mol/L]
+6.000e+3 10000 00100              [Final t][Total Time Steps][Write every t]
+2.000e-0  +3.000e-2  +1.000e-1  +2.000e-3                    [k1,k3,k5,k7]
+2.000e-2  +1.500e-3  +5.000e+2  +4.000e-1                    [k2,k4,k6,k8]
```

Appendix C

MODELING PROCEDURES AND SENSITIVITY

In this appendix the procedures used in the kinetic modeling of the experimental data are presented and discussed with some general modeling rules of thumb. Also the sensitivity of the kinetic model used to describe the adsorption and redox processes studied in Chapter 5 is examined by varying the values of the rate constants and the equilibrium constants.

C.1 Modeling Procedures

1. Create a Lotus 1-2-3 worksheet for each experimental data set.
2. Choose a set of rate constants.
3. Run FORTRAN computer code.
4. Import output file into Lotus 1-2-3 worksheet.
5. Compare model data with experimental data (see Figure C.1):
    a. Visually by inspecting the time profiles of each set.
    b. Statistically by minimizing the average difference and maximum difference between the experimental and model data. The average difference is defined as the average of all the absolute values of the differences between the measured species concentration and the predicted species concentration at each time throughout the duration of the experiment. The maximum difference is defined as the maximum value of all the absolute values of the differences between the measured and predicted concentrations throughout the duration of each experiment.

6. Adjust the rate constants and repeat steps 2-5 until minimum difference values have been obtained.

Figure C.1 is an example of the experimental data and the optimized model curve of the As(III) data set from experiment MnAs1. Points from each sampling time of the two data sets are shown with symbols. The maximum difference occurs at 1200 seconds.

C.2 Modeling Rules of Thumb

The modeling of the experimental data was not a straight-forward exercise nor was it executed with conventional statistical practices. The complexity of the sequential reaction scheme required many iterations of the trial and error process and a good sense of chemical intuition. The value of each rate constant influences the rate and equilibrium of more than one reaction. The modeling exercise was a learning process in itself and would not have possible without a computer. Some rules of thumb for modeling complex chemical reactions are offered here for those who wish to understand the mathematics behind the chemistry and for those who are daring enough to attempt similar endeavors. The "Scott Rules of Kinetic Modeling" are:

1. **Start with what you know.** Initial guesses for k_1, k_{-1}, k_3, k_{-3}, k_4, and k_{-4} were taken from the modeling of the adsorption experiments described in Chapter 4, although the reactions are not necessarily the same. For example, the release of Mn(II) from the bulk birnessite solid structure is not necessarily the same as the desorption of Mn(II) from the hydrated manganese surface and the reactions may not

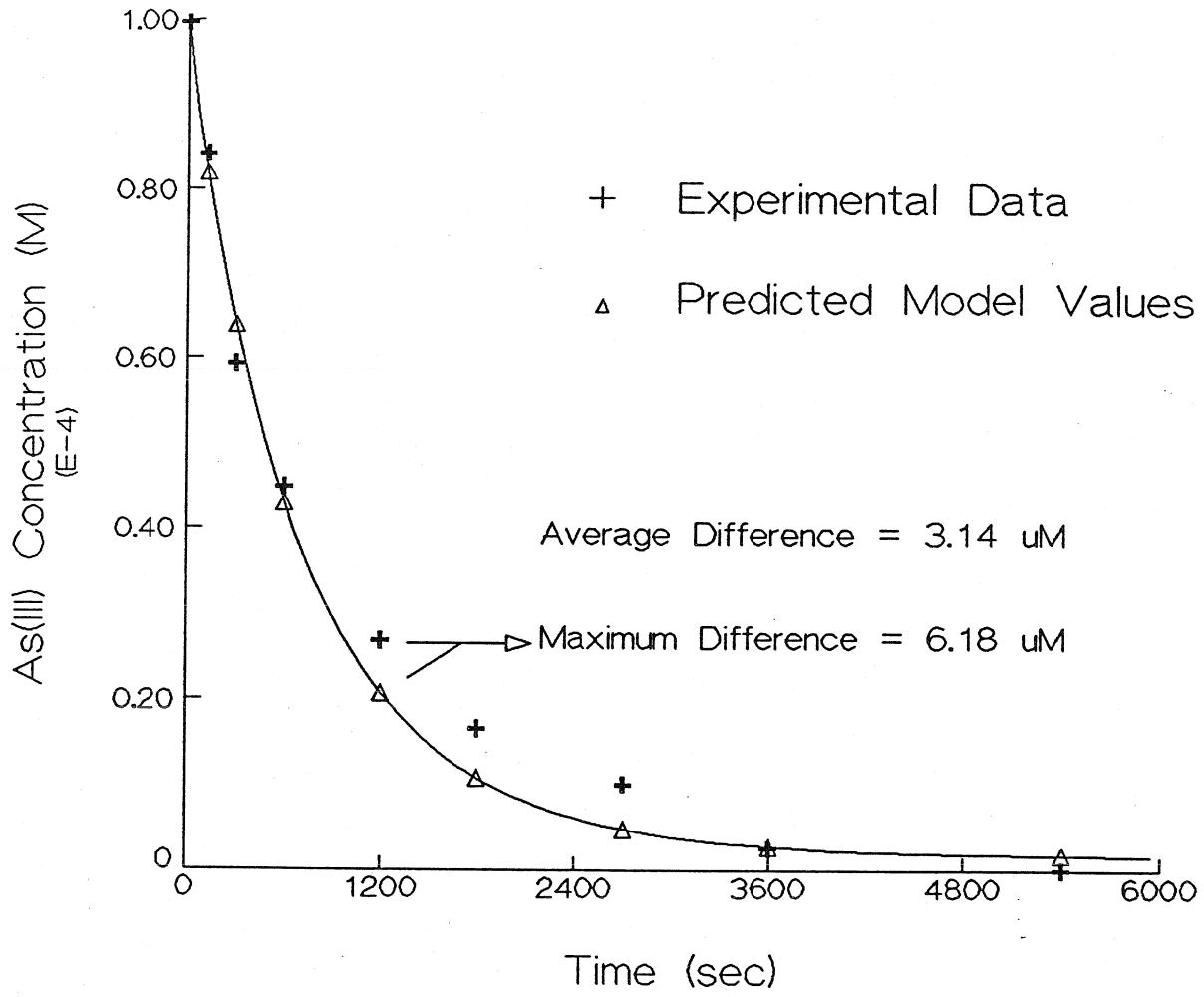

Figure C.1: Comparison of experimental data and predicted model curve of As(III) from experiment MnAs1 (Table 5.2).

proceed at the same rates. However, in order to keep the kinetic model simple, the reactions were considered similar enough to use the values of the adsorption-desorption rate constants as initial guesses.

2. **Start at the beginning.** The modeling exercise was begun by finding a value for k_1 that minimized the difference between measured and predicted As(III) or Se(IV) concentrations. Particular interest was placed on minimizing the difference for the initial data points. When the best value of k_1 was obtained, k_{-1} was then varied. Likewise, the rate constants were optimized in order, although sometimes it was necessary to readjust a previously optimized rate constant before continuing through the group of rate constants.

3. **Six of one, half dozen of the other: making choices.** Minimizing the differences for initial data points of each data set were given preference over minimizing the differences for later data points. This was done because the reaction conditions were generally better known at the beginning of each experiment than at the end.

4. **Remember the value of the rate constant is only as good as the experimentalist.** The value of each rate constant was reported to one or two significant digits. Only two significant digits were used if, for example, 3.5 was better than 3 or 4, or, as in the case of the selenium data, the rate constants were optimized in time units of minutes and then changed to seconds by dividing by 60 (e.g., 10 min^{-1} = 0.17 sec^{-1}). While it may have been possible to see a difference between rate

constants at 3 or 4 significant digits, I did not feel the experimental data was sufficient to warrant such high precision.

C.3 Sensitivity of the Adsorption-Redox Kinetic Model

The average and maximum differences between the experimental and model data for the reactions involving arsenite and selenite with birnessite are listed in Tables C.1 and C.2. In the arsenite experiments the rate constants were adjusted to minimize the differences for the experimental As(III), As(V), and Mn(II) data, while in the selenite experiments, only data for Se(IV) and Se(VI) were used in the optimization process. No Mn(II) appeared in solution during the extended selenite experiments and the rate constants were adjusted so that no Mn(II) would be predicted to appear in solution. Thus it was enough to visually compare the difference between the experimental and predicted data sets for Mn(II).

C.3.1 Sensitivity Analysis of Experiment MnAs1

The sensitivity of the kinetic model is examined by taking a closer look at the modeling of experiment MnAs1 (Figure 5.4: pH 4, 25 °C, 99.6 μM As(III), 502 μM >MnOH). The final results of the optimization processes are given in Table 5.2. In Figure C.2, the effect on the average and maximum differences of varying k_1 is presented. All other rate constants and reaction variables are held constant (Table 5.2). The figure illustrates the sensitivity of the model. The differences grow rapidly when the value of k_1 is either decreased or increased from the optimal value of 5 $M^{-1}sec^{-1}$. The maximum difference for As(III) is the most sensitive. For this data set, a value of 5 $M^{-1}sec^{-1}$ was chosen although the minimum average difference for the

Table C.1: Average and Maximum Differences between Experimental and Modeled Arsenite-Birnessite Reaction Results

EXPERIMENT	As(III)		As(V)		Mn(II)	
	AVG DIFF (μM)	MAX DIFF (μM)	AVG DIFF (μM)	MAX DIFF (μM)	AVG DIFF (μM)	MAX DIFF (μM)
MnAs1	3.14	6.18	2.56	5.87	1.48	6.40
MnAs2	8.94	12.2	6.97	16.0	30.7	52.0
MnAs3	53.9	116	22.2	49.4	36.0	56.3
MnAs6	2.25	6.20	3.12	4.86	1.74	5.50
MnAs7	3.56	6.98	4.40	10.3	2.93	7.90
MnAs8	3.13	6.10	2.79	6.44	1.51	4.70
MnAs9	3.46	9.00	2.20	4.29	1.37	3.16
MnAs10	2.84	5.82	1.50	4.10	0.29	1.08
MnAs11	3.38	9.10	1.55	3.18	0.14	0.62
MnAs12	3.00	11.1	1.62	5.06	0.04	0.10

As(III) data set occurs when k_1 is 4.5 $M^{-1}sec^{-1}$. If only the average difference was considered, then k_1 could range from 4 to 6 $M^{-1}sec^{-1}$ with little effect on the fit. However, the sensitivity of the maximum difference for As(III) clearly indicates that the best value is 5 $M^{-1}sec^{-1}$.

Figure C.3 is a similar graph examining the minimum differences for the variation of k_{-1}. This figure illustrates the point that the best fit of the experimental data occurs for a narrow range of values. Again, the average difference for As(V) and Mn(II) and the maximum difference for As(III) are at a minimum at the same

Table C.2: Average and Maximum Differences between Experimental and Modeled Selenite-Birnessite Reaction Results

EXPERIMENT	Se(IV)		Se(VI)	
	AVG DIFF (μM)	MAX DIFF (μM)	AVG DIFF (μM)	MAX DIFF (μM)
MnSe1	1.57	7.98	1.93	5.02
MnSe3	2.75	6.50	1.22	3.59
MnSe5	5.43	14.6	1.68	3.97
MnSe6	3.58	9.34	0.31	0.71
MnSe7	5.19	12.9	0.57	1.76
MnSe8	2.96	5.65	2.05	3.43
MnSe9	3.97	7.52	2.46	5.26

value of k_{-1} while the average difference for As(III) is at a minimum at a slightly higher value. The average differences allow a broader range of values to acceptably describe the data, but the maximum difference clearly suggests the best value.

By varying k_1 or k_{-1} only, as done in Figures C.2 and C.3, the equilibrium constant K_1 is also varied. For Figure C.4, the equilibrium constant K_1 is fixed while the values of k_1 and k_{-1} are varied. This is done to isolate the effect of varying the equilibrium constant and focus on the effect of the individual rate constants on the rates of reaction. Figure C.4 indicates that the optimal value of k_1 (and indirectly k_{-1}) for best describing the disappearance of As(III) and the appearance of As(V) and Mn(II) is 5 $M^{-1}sec^{-1}$.

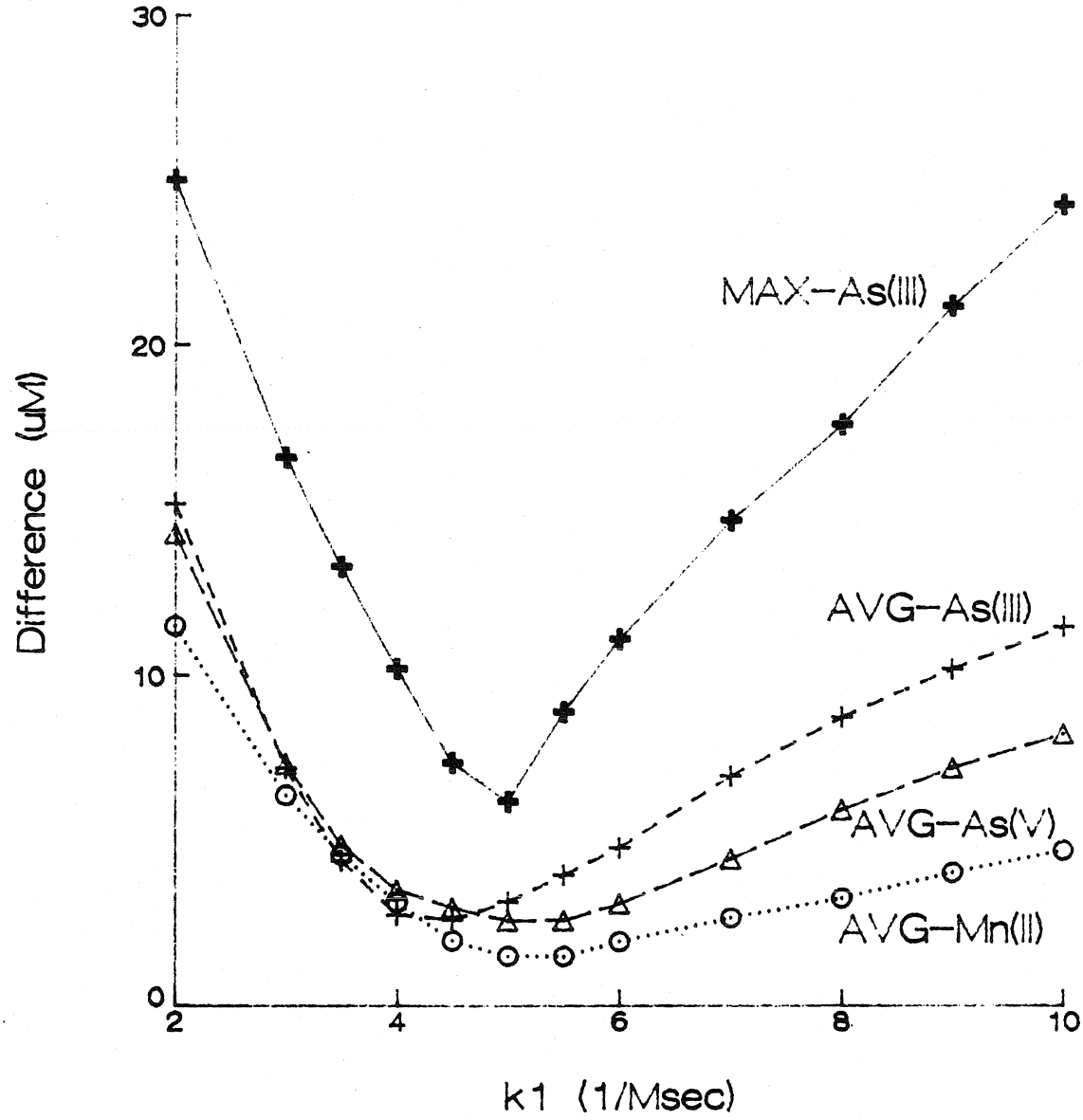

Figure C.2: Effect of k_1 on the average and maximum differences between experimental and predicted MnAs1 results.

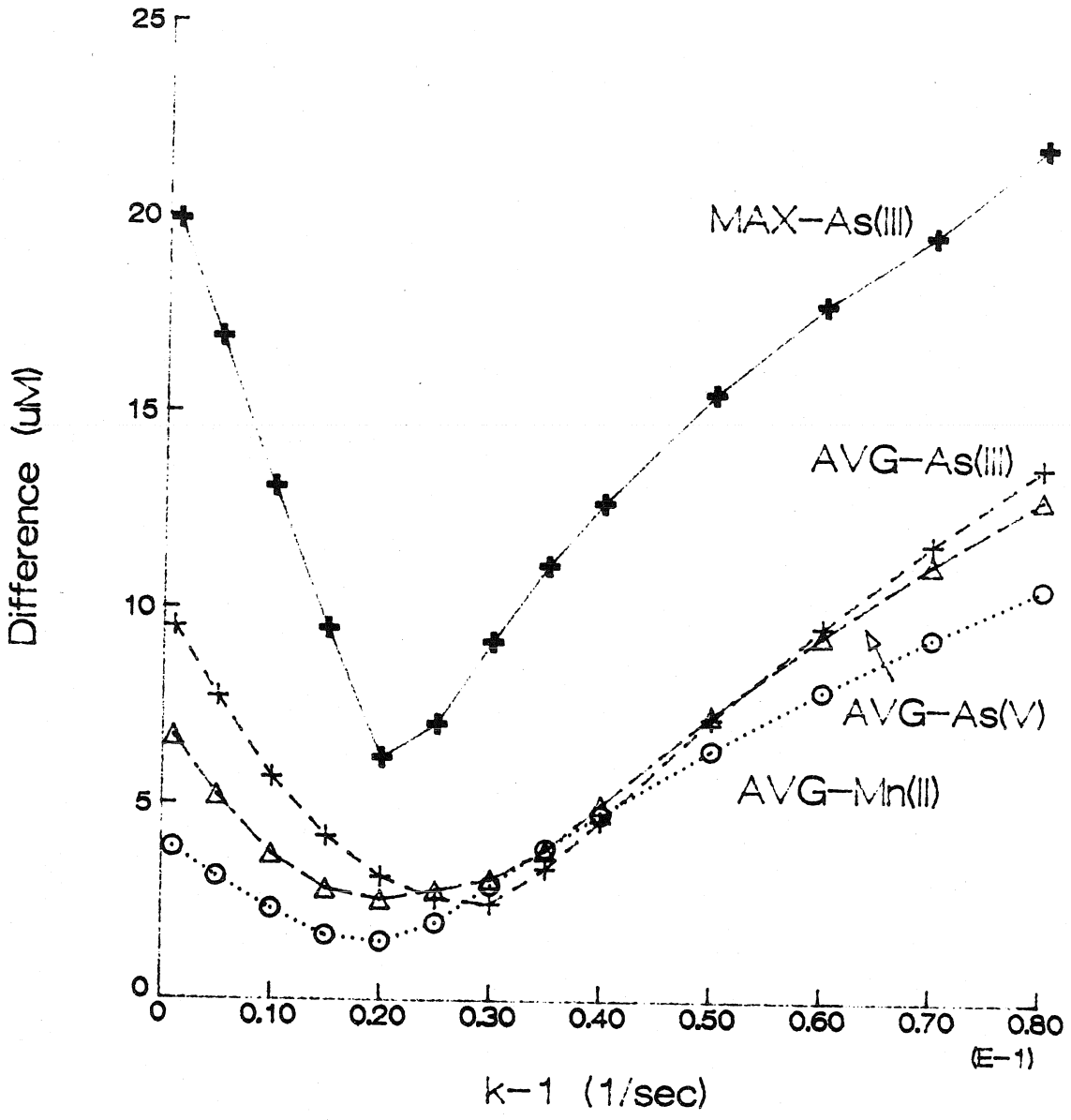

Figure C.3: Effect of k_{-1} on the average and maximum differences between experimental and predicted MnAs1 results.

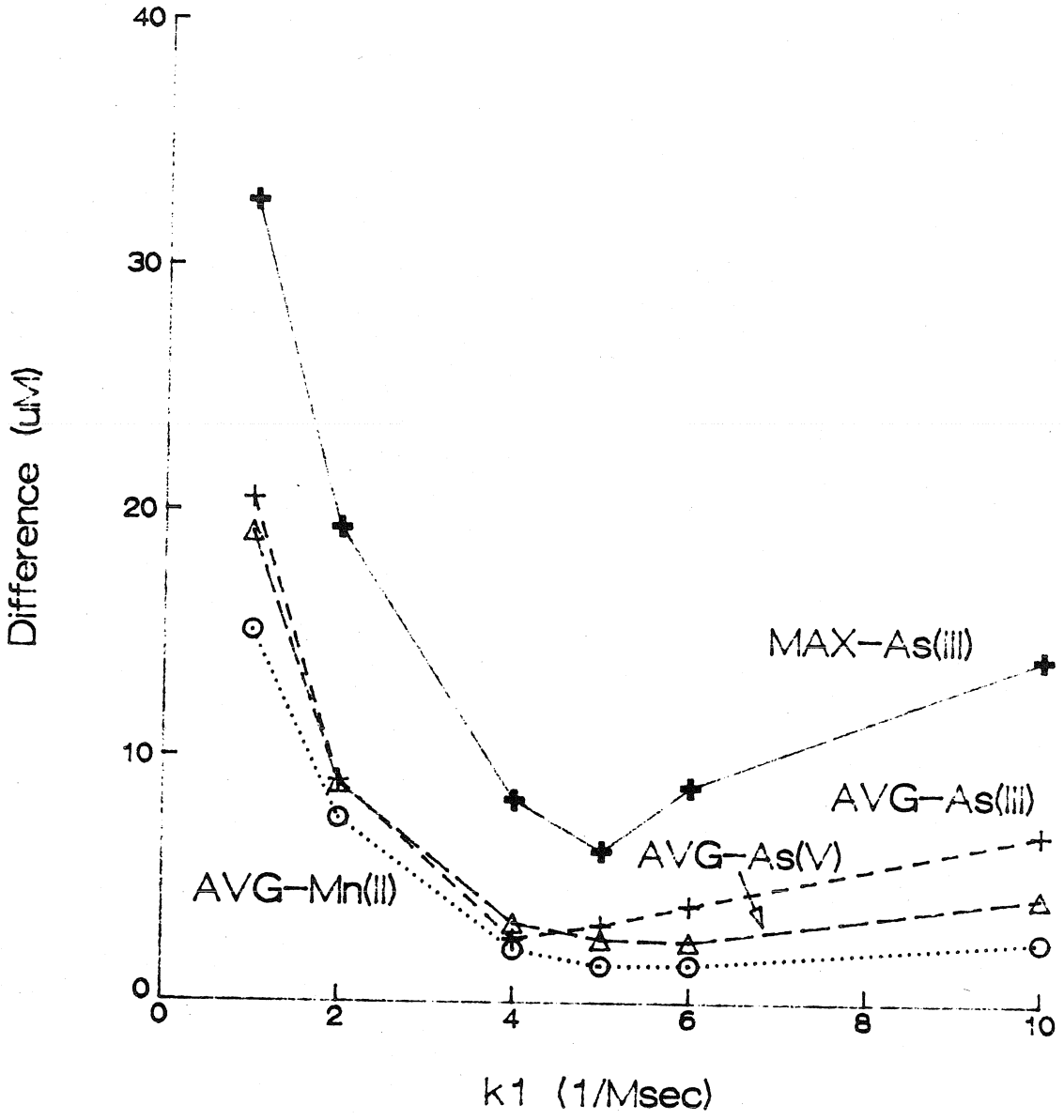

Figure C.4: Effect of varying the values of k_1 and k_{-1} while maintaining a constant value for K_1 on the average and maximum differences between experimental and predicted MnAs1 results.

Figures C.5-7 represent similar exercises for k_2 and k_{-2} as in Figures C.2-4 for k_1 and k_{-1}. There is a less dramatic effect on the differences with variations of k_{-2}. Figure C.6 shows that varying k_{-2} from 0.0005 to 0.004 sec^{-1} has only a minor effect on the fit of the model to the As(III), As(V), and Mn(II) profiles.

Figure C.8 shows that at a fixed equilibrium constant (log K_3 = -7.7) and above a certain value, variations of k_3 and k_{-3} do not affect the fit of the model. Only when the value of k_3 approaches that of k_{-1} and k_2 does the goodness of the model fit for As(V) and Mn(II) decrease. Also, As(III) is relatively unaffected by changes in the value of k_3.

The fit of the As(III) data is also unaffected by changes in k_4 and k_{-4}. Figure C.9 illustrates that at a constant K_4, variations of k_4 and k_{-4} only greatly affect the difference of Mn(II). The best values of k_4 and k_{-4} are 2 x 10^5 $M^{-2}sec^{-1}$ and 0.4 $M^{-1}sec^{-1}$, respectively.

In summary, the fit of the kinetic model to the experimental data of MnAs1 appears to be strongly dependent upon the values of the rate constant k_1, k_{-1}, k_2, and k_{-2}. The results seems to be only moderately dependent upon the values of rate constant k_3, k_{-3}, k_4, and k_{-4}.

C.3.2 Sensitivity Analysis of Experiment MnSe1

The sensitivity of the kinetic model was also examined with the MnSe1 data set (Figure 5.16: pH 4, 25 °C, 101 μM Se(IV), 478 μM >MnOH). Either a single rate constant or a pair of rate constants fixed at the same ratio (e.g., $k_1/k_{-1} = K_1$, a constant) was examined. Variations in the rate constants k_1 and k_{-1} had similar

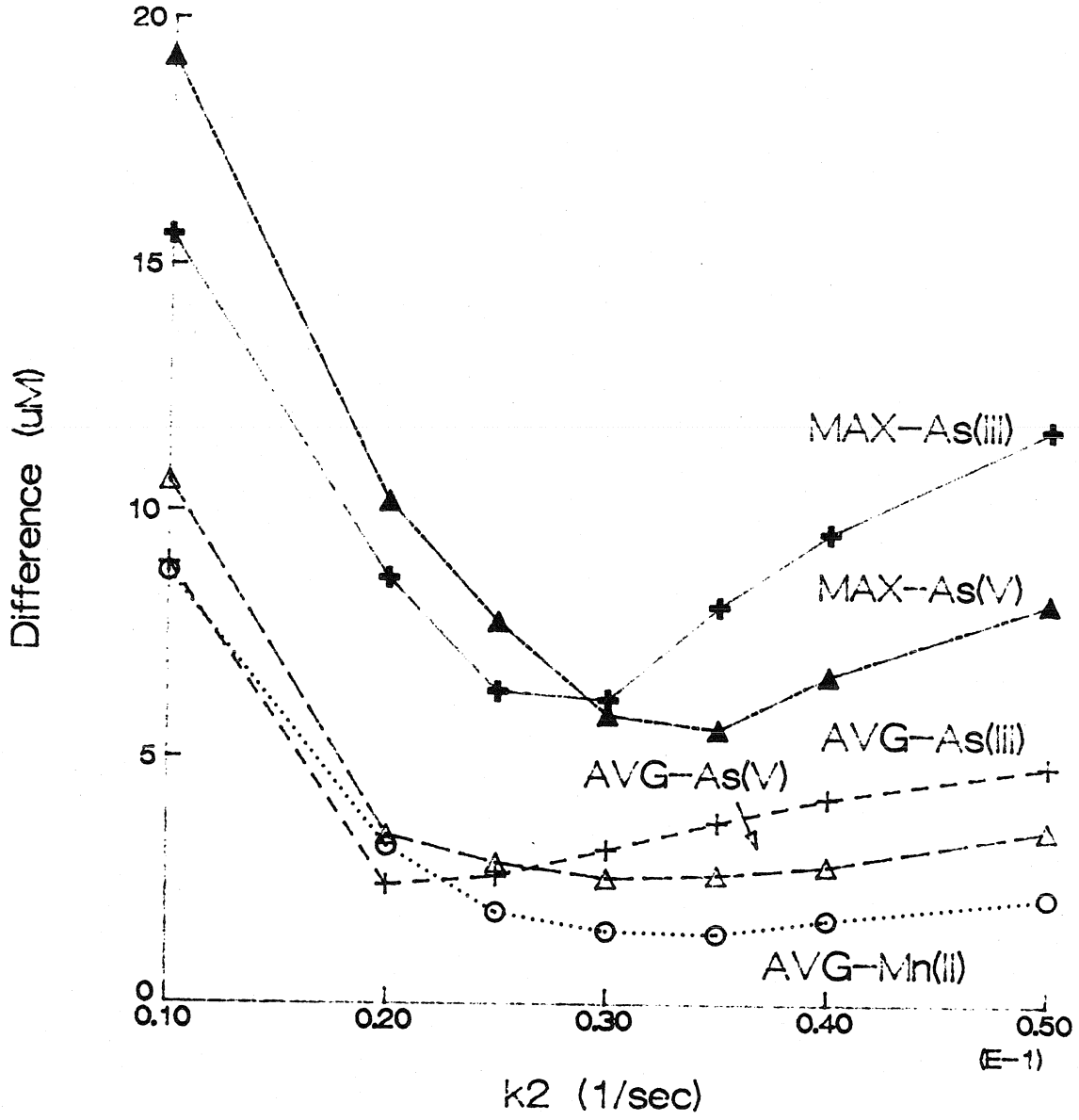

Figure C.5: Effect of k_2 on the average and maximum differences between experimental and predicted MnAs1 results.

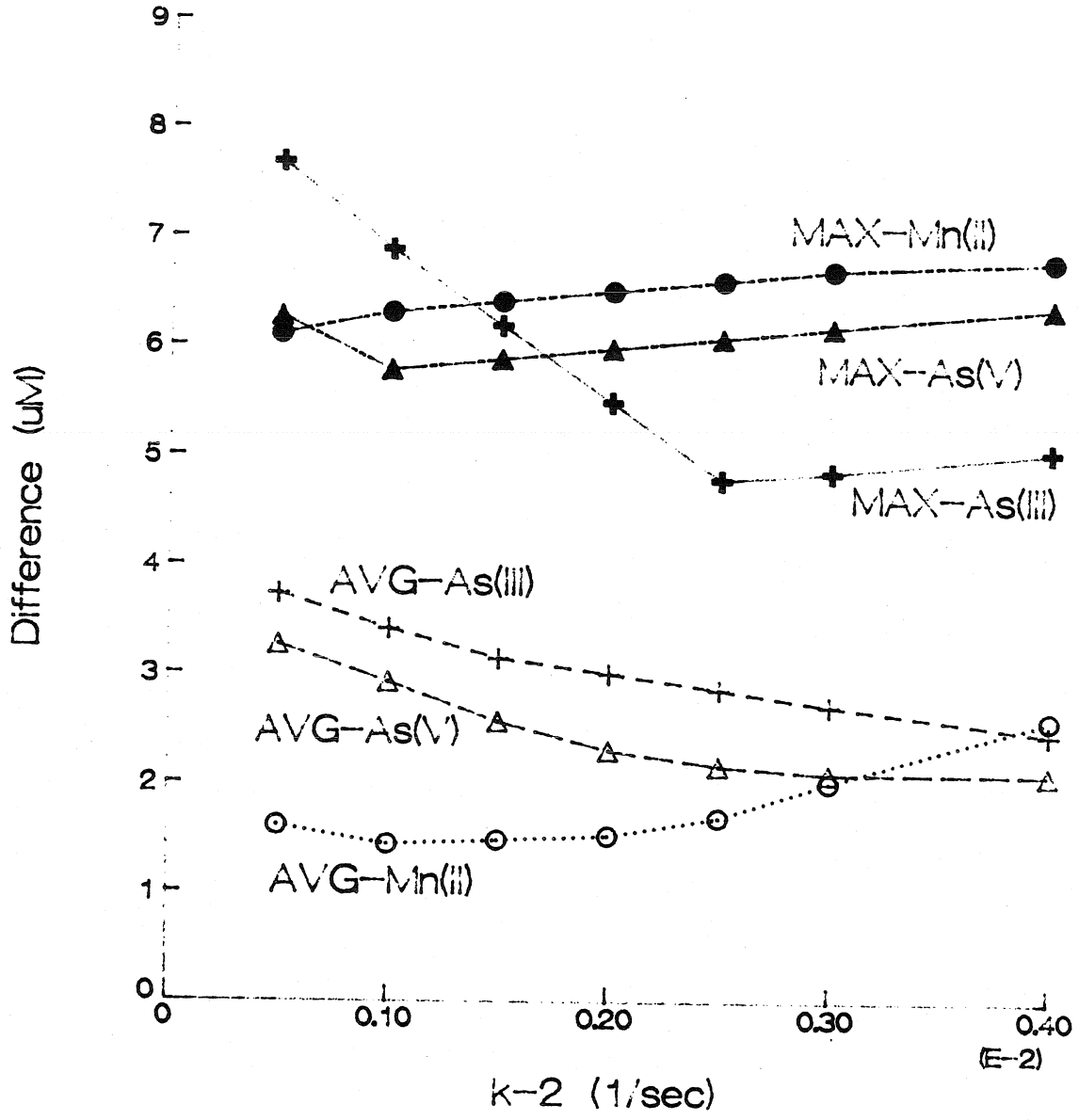

Figure C.6: Effect of k_2 on the average and maximum differences between experimental and predicted MnAs1 results.

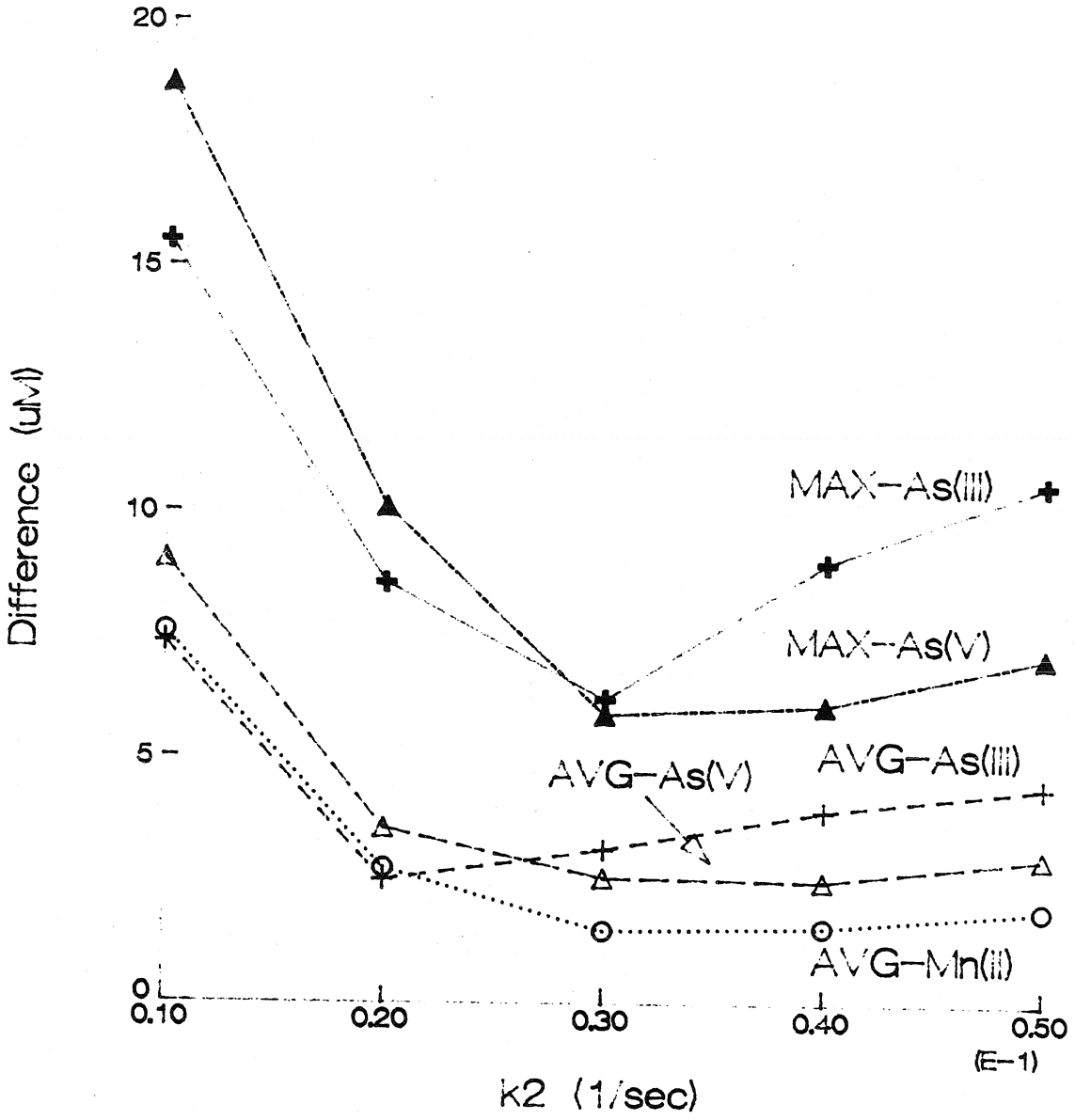

Figure C.7: Effect of varying the values of k_2 and k_{-2} while maintaining a constant value for K_2 on the average and maximum differences between experimental and predicted MnAs1 results.

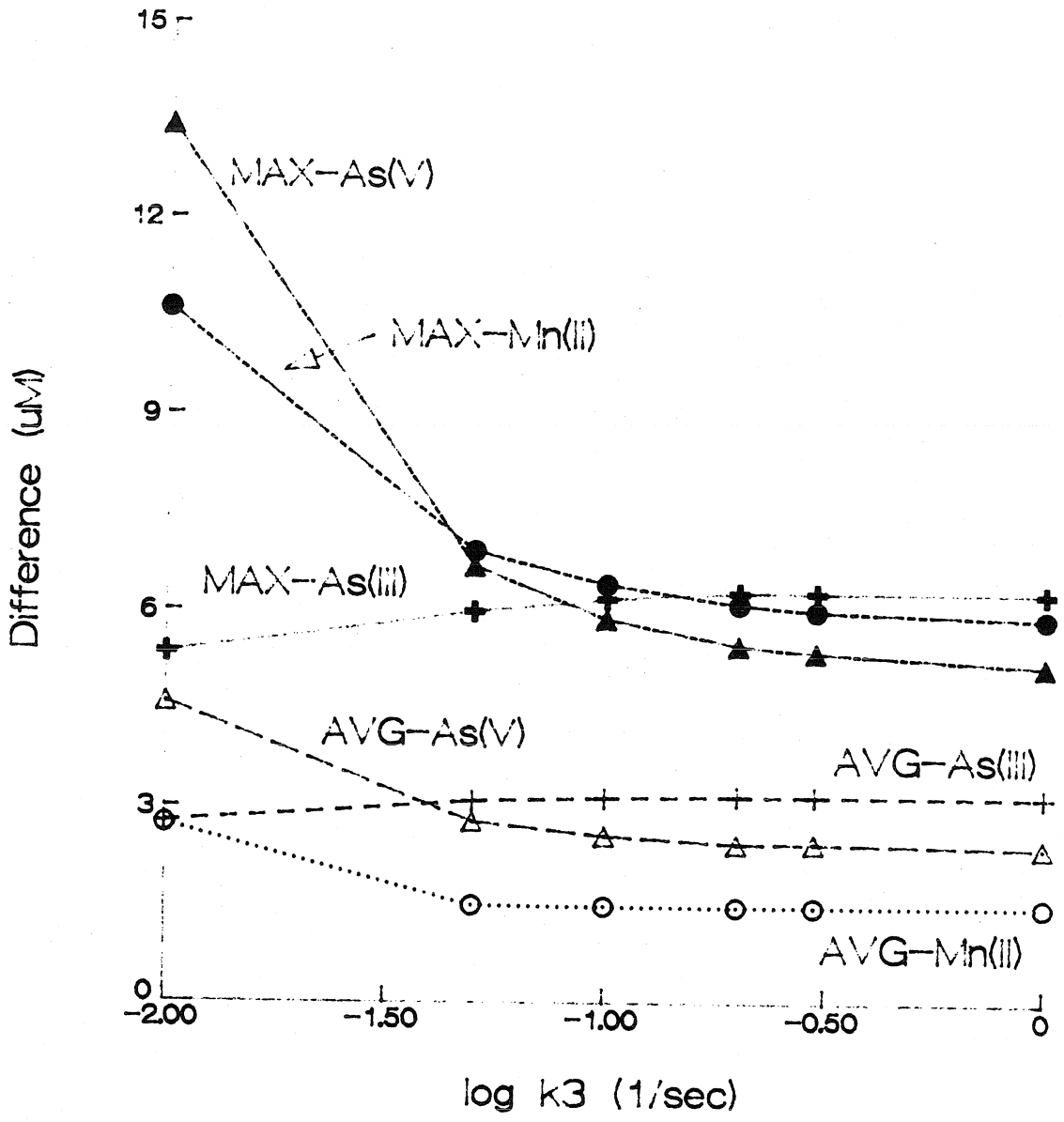

Figure C.8: Effect of varying the values of k_3 and k_{-3} while maintaining a constant value for K_3 on the average and maximum differences between experimental and predicted MnAs1 results.

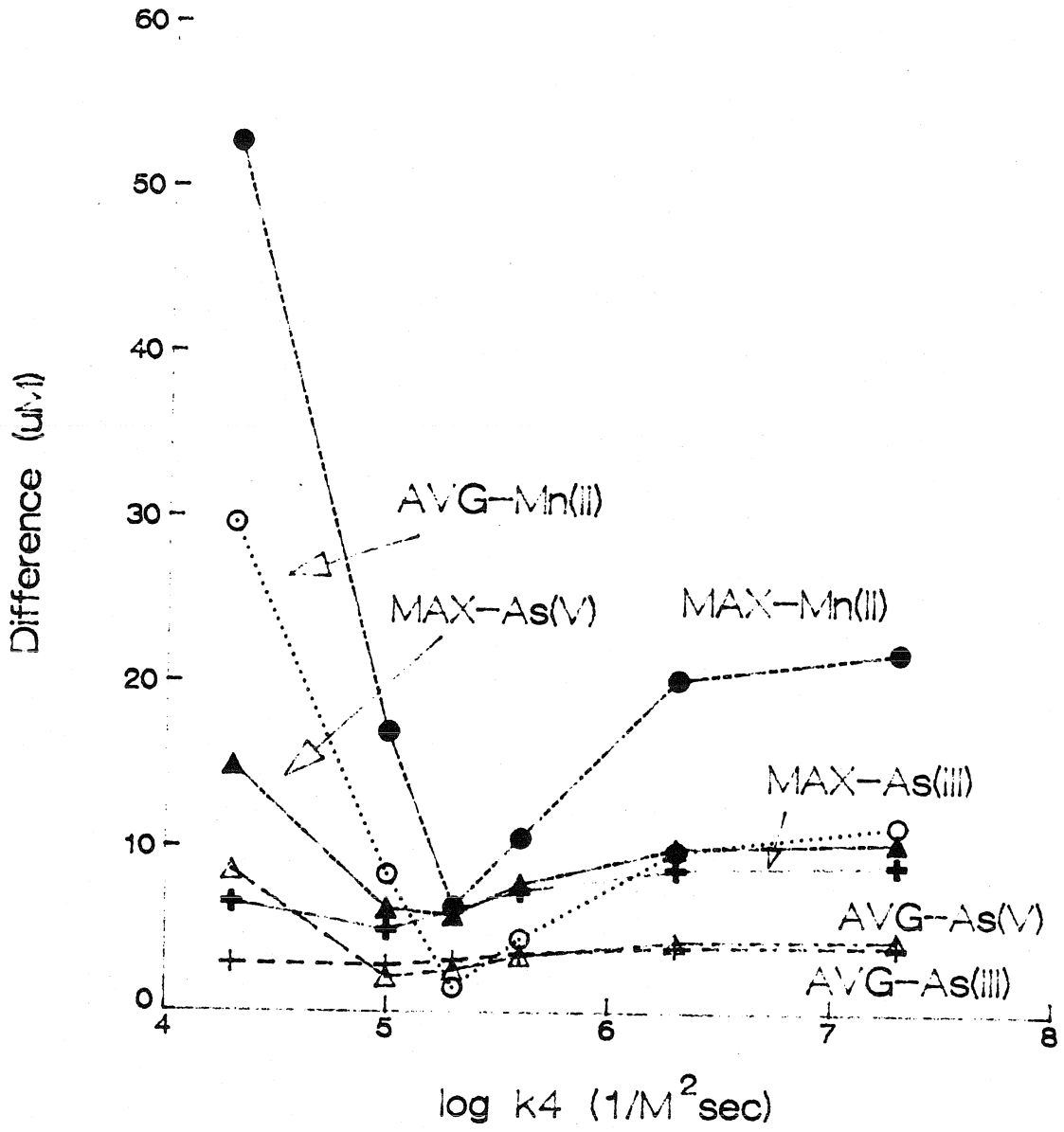

Figure C.9: Effect of varying the values of k_4 and k_{-4} while maintaining a constant value for K_4 on the average and maximum differences between experimental and predicted MnAs1 results.

effects on the model fit as did the corrresponding adsorption-desorption rate constants in the MnAs experiments (see Figures C.2-C.4) and optimal values of k_1 and k_{-1} were chosen on that basis (Table 5.7).

The influence of the equilibrium constant K_2 was examined by holding k_2 constant and varying k_{-2} several orders of magnitude. Figure C.10 illustrates that the model fit is independent of the value of k_{-2} unless it is near to that of k_2 (i.e., unless k_{-2} is greater than $0.1 \bullet k_2$). The maximum difference of Se(IV) was not affected within the range of variation of log K_2. At values of log K_2 greater than 1, there was little change in the average differences of Se(IV) and Se(VI) and the maximum difference of Se(VI). However, at values of log K_2 less than 1, the average and maximum differences of Se(VI) decreased while the average difference of Se(IV) increased. Therefore the best value of log K_2 was chosen to be 1.

The effect of the rate constant k_2 under the condition of constant K_2 is examined in Figure C.11. This rate constant clearly influences the success of the model. The minimum of each difference occurs for the value of k_2 is $1.3 \times 10^{-6} sec^{-1}$.

Figures C.12-C.14 all indicate that the rate constants k_3, k_{-3}, k_4, and k_{-4} have little or no effect on the fit of the model to the Se(IV) and Se(VI) experimental data. These figures support the conclusion that the rate determining step of the reaction process is the electron transfer step. The lack of a unique rate constant for these reaction steps that follow the rate determining step indicates that they can only be described as an equilibrium process.

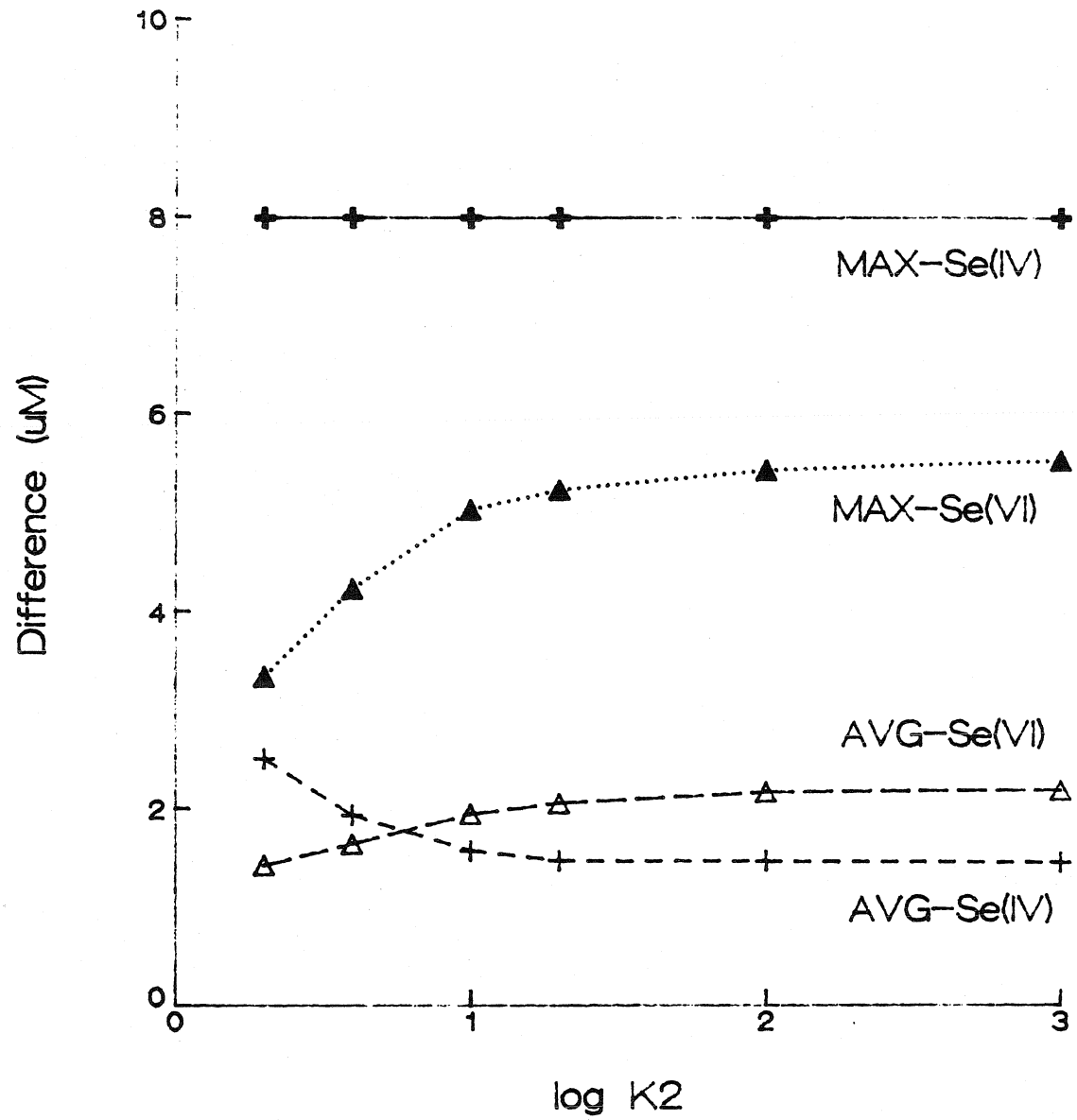

Figure C.10: Effect of varying the value of K_2 (k_2 = 1.3 x10^{-6}sec^{-1}, varying k_{-2}) on the average and maximum differences between experimental and predicted MnSe1 results.

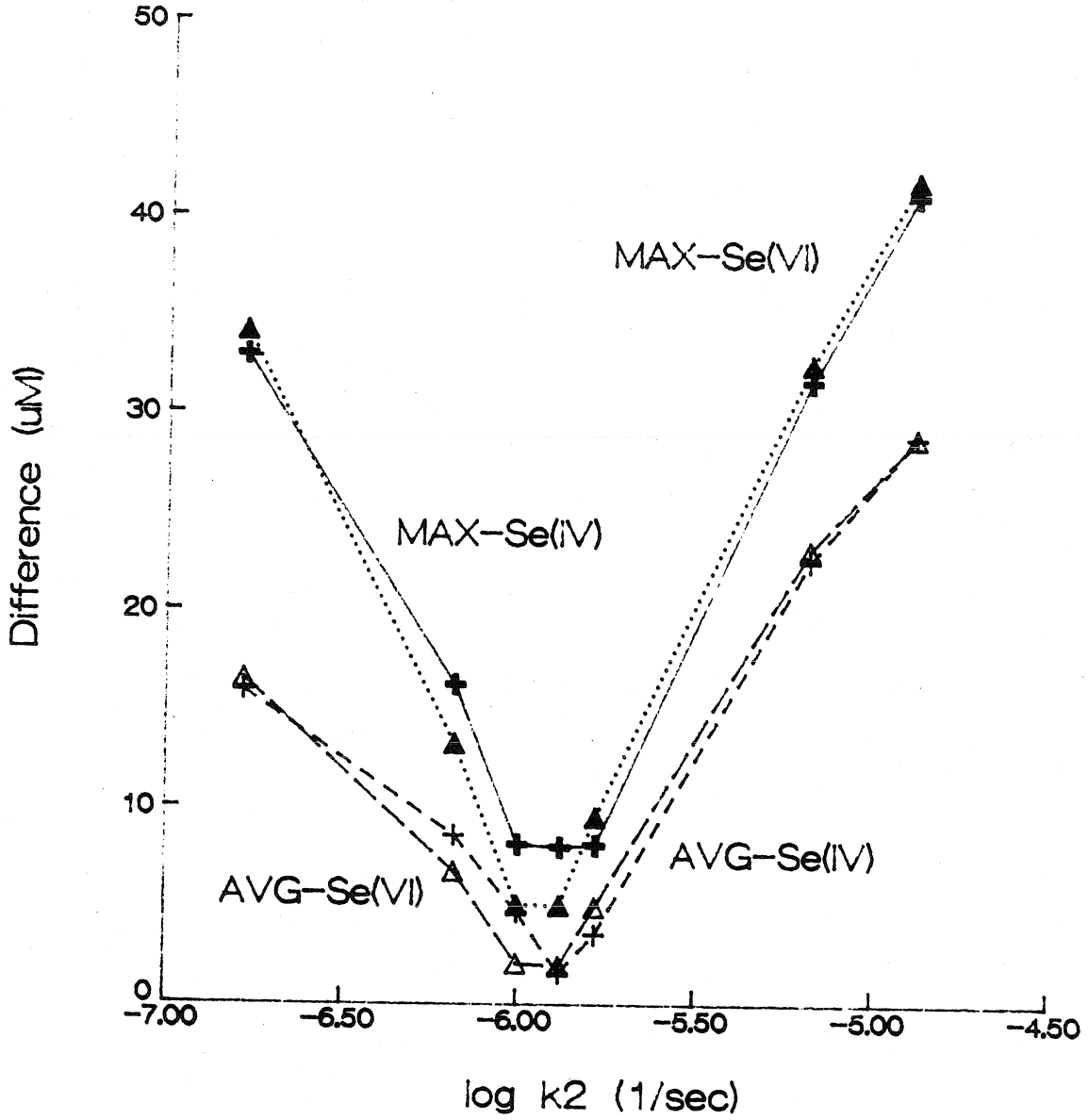

Figure C.11: Effect of varying the values of k_2 and k_{-2} while maintaining a constant value for K_2 on the average and maximum differences between experimental and predicted MnSe1 results.

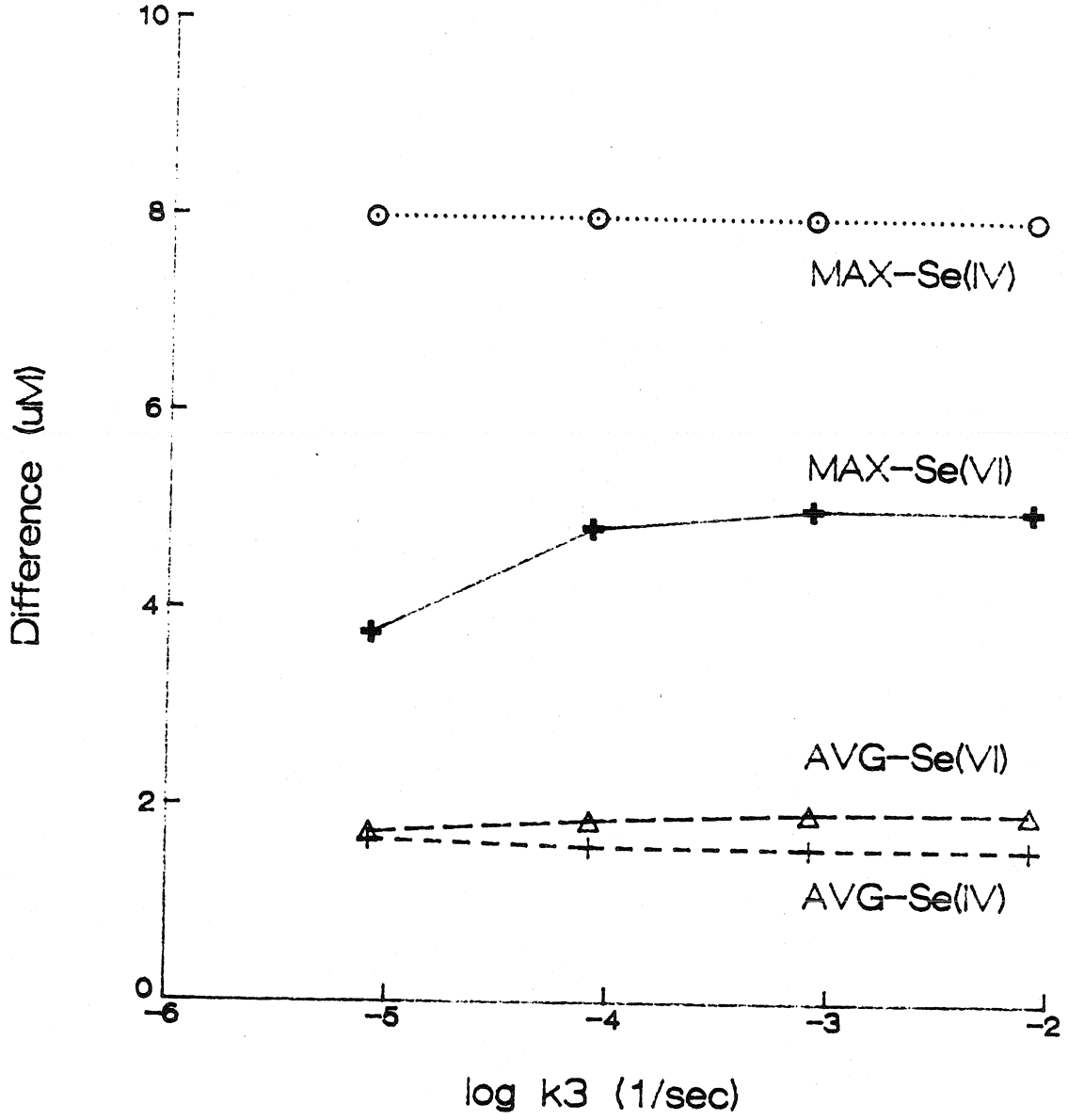

Figure C.12: Effect of varying the values of k_3 and k_{-3} while maintaining a constant value for K_3 on the average and maximum differences between experimental and predicted MnSe1 results.

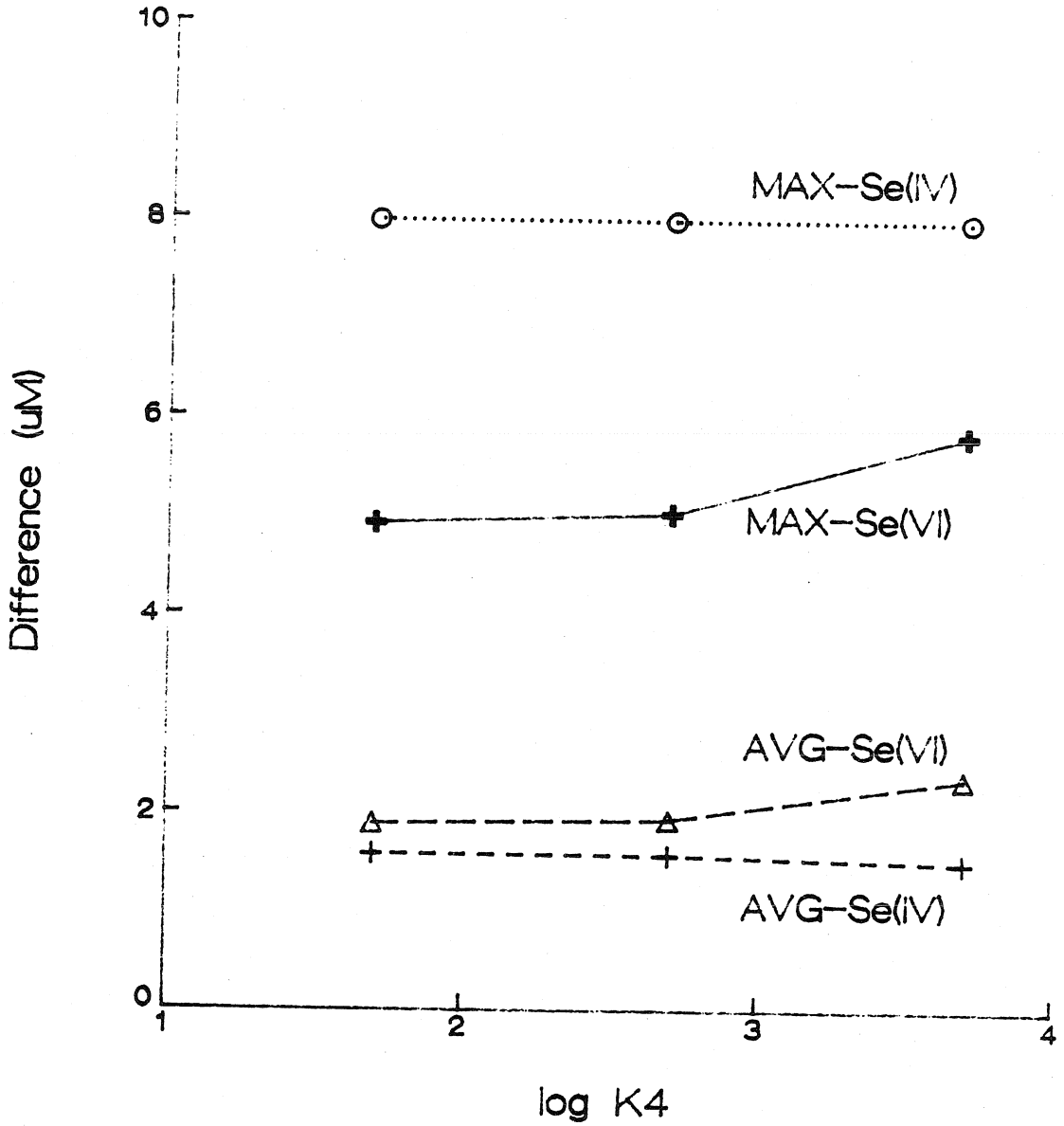

Figure C.13: Effect of varying the value of K_4 (k_{-4} = 3.3 $M^{-1}sec^{-1}$, varying k_4) on the average and maximum differences between experimental and predicted MnSe1 results.

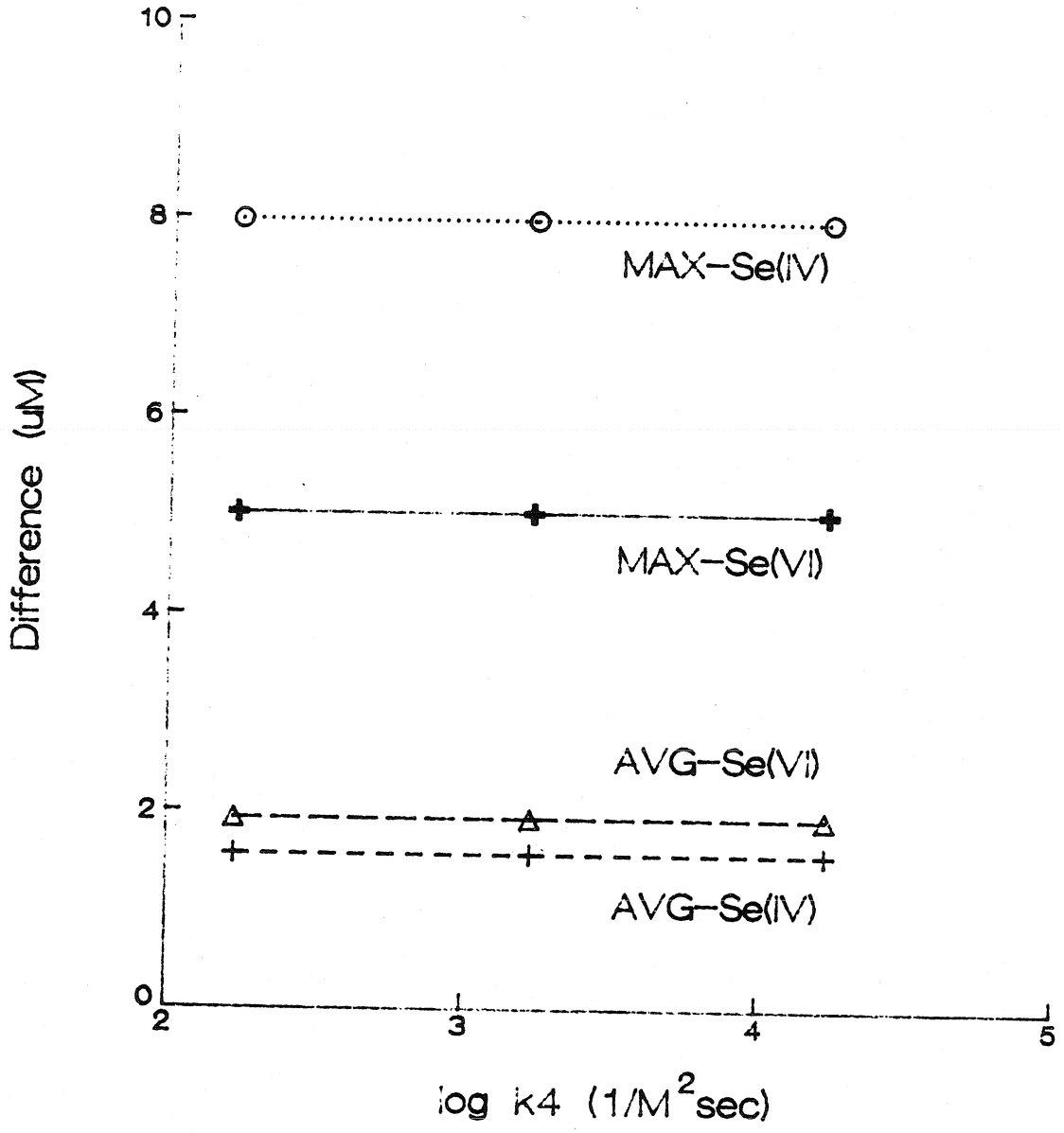

Figure C.14: Effect of varying the values of k_4 and k_{-4} while maintaining a constant value for K_4 on the average and maximum differences between experimental and predicted MnSe1 results.

In conclusion, the kinetic modeling of the selenite-birnessite system under the conditions that were studied appears to be strongly dependent upon the rate constants k_1, k_{-1}, and k_2. The results are only weakly dependent upon the rate constant k_{-2}, and moderately dependent upon the equilibrium constants K_3 and K_4.